Compte rendu de la

DIXIÈME RENCONTRE
DE MORIOND

Méribel-lès-Allues (France) 2-14 Mars 1975

VOL. I

PHÉNOMÉNOLOGIE DE LA STRUCTURE HADRONIQUE

J. TRAN THANH VAN

SOUS LE HAUT PATRONAGE DE

- INSTITUT NATIONAL DE PHYSIQUE NUCLÉAIRE ET DE PHYSIQUE DES PARTICULES
- LABORATOIRE DE L'ACCÉLÉRATEUR LINÉAIRE
- LABORATOIRE DE PHYSIQUE THÉORIQUE ET HAUTES ÉNERGIES
- LABORATOIRE DE PHYSIQUE THÉORIQUE ET PARTICULES ÉLÉMENTAIRES

PUBLICATION SUBVENTIONNÉE PAR LE CNRS

La première session de la dixième Rencontre de Moriond sur
la Phénoménologie de la Structure hadronique
était organisée par

J. Trân Thanh Vân

avec la précieuse collaboration de

A. Capella

A. Krzywicki

Barbara et F. Schrempp

Secrétariat permanent :

Rencontre de Moriond

Laboratoire de Physique Théorique et Particules Élémentaires
Bâtiment 211 - Université de Paris-Sud
91405 ORSAY (France)
Tél. 928.59.87

Proceedings of the

TENTH RENCONTRE DE MORIOND

Méribel-lès-Allues (France) March 2-14 1975

VOL. I

PHENOMENOLOGY OF HADRONIC STRUCTURE

edited by

J. TRAN THANH VAN

SPONSORED BY

- INSTITUT NATIONAL DE PHYSIQUE NUCLÉAIRE ET DE PHYSIQUE DES PARTICULES
- LABORATOIRE DE L'ACCÉLÉRATEUR LINÉAIRE
- LABORATOIRE DE PHYSIQUE THÉORIQUE ET HAUTES ÉNERGIES
- LABORATOIRE DE PHYSIQUE THÉORIQUE ET PARTICULES ÉLÉMENTAIRES

AND BY THE CNRS FOR PUBLICATION

The first Session or the Tenth Rencontre de Moriond on
Phenomenology of Hadronic Structure
was organized by

J. Trân Thanh Vân

with the active collaboration of

A. Capella
A. Krzywicki
and Barbara and F. Schrempp

Permanent Secrétariat :
Rencontre de Moriond
Laboratoire de Physique Théorique et Particules Élémentaires
Bâtiment 211 - Université de Paris-Sud
91405 ORSAY (France)
Tél. 928.59.87

FOREWORD

The Rencontre de Moriond held at Meribel-les-Allues (France) from March 2 to 14, 1975, was the tenth such meeting.

The first one was held in 1966 at Moriond in the French Alps. There, physicists - experimentalists as well as theoricians - not only shared their scientific preoccupations but also household chores. That meeting grouped essentially French physicists interested in electromagnetic interactions. At following meetings a session on high energy strong interactions was added to the electromagnetic one.

The main purpose of these meetings is to discuss recent developments of contemporary physics and to promote effective collaboration between experimentalists and theoriticians in the field of electromagnetic interactions and elementary particles. Besides, the length of the meeting coupled with the small number of participants favours better human relations as well as a more thorough and detailed discussion of the contributions.

This concern for research and experimentation of new channels of communication and dialogue which from the start animated the Moriond meetings, incited us, five years ago, to organize a simultaneous meeting of biologists on Cellular Differenciation at Meribel-les-Allues. Common seminars were organized to study to what extent analytical methods used in physics could be applied to some biological problems. This year, Professor ZICHICHI, gave an introductory talk to the High Energy Physics and the experimental methods and Professor VAN DER WALLE has presented a method of data analysis in the research on the cancer. These conferences as well as a round table discussion on the present problems of Biology gave rise to spirited and enriching discussions between biologists and physicists. They led us to hope that biological problems, at present so complex, may gave birth in the future to new analytical methods or new mathematical languages.

The first session of the tenth Rencontre de Moriond (March 2-8, 1975) is devoted to high energies hadronic interactions. A. CAPELLA, A. KRZYWICKI, Barbara and F. SCHREMPP have given me their help in setting the program of the Rencontre.

The second session (March 8-14, 1975) was devoted to high energies leptonic interactions and the coordination was assumed by M. GOURDIN and L. MONTANET. A particular attention was given on the discovery of the narrow resonances and their interpretation.

Mrs G. BEUCHEY and M.T. PILLET, Misses M.P. COTTEN and N. RIBET, all devoted much of their time and energy to the success of this meeting. On behalf of the participants I thank them as well as Mr. and Mrs. Raiberti who welcomed us in their hotel.

J. TRAN THANH VAN

P A R T I C I P A N T S

First session

ABOLINS Maris A.	Department of Physics, Michigan State University, East Lansing, Michigan 48824 (U.S.A)
AMATI Daniele	Division TH, CERN, 1211 Genève 23 (Suisse)
ANJOS Joao	Physique Théorique, C.E.N. Saclay, B.P.2, 91190 Gif sur Yvette (France)
ANTONIOU Nikos	N.R.C. "Democritos" Aghia Paraskevi Attikis, Athens (Greece)
ARNEODO Alain	Physique Théorique, Parc Valrose, 06034 Nice Cedex (France)
BALL James	Division TH, CERN, 1211 Genève 23 (Suisse)
BANNER Marcel	D.Ph.P.E., C.E.N. Saclay, B.P. 2, 91190 Gif sur Yvette (France)
BIALAS Andrezej	Department of Physics, Institute of Nuclear Physics, Mickiewicza 30, Krakow (Poland)
BORG Alan	D.Ph.P.E., C.E.N. Saclay, B.P.2, 91190 Gif sur Yvette (France)
BROLL Claude	Division NP, CERN, 1211 Genève 23 (Suisse)
BURAS Andrezej	Niels Bohr Institute, Blegdamsvej 17, 2100 Copenhagen (Denmark)
CAPELLA Alphonse	Physique Théorique et Particules Elémentaires, Bât. 211, 91405 Orsay (France)
CASTALDI Rino	Division NP, CERN, 1211 Genève 23 (Suisse)
COHEN-TANNOUDJI Gilles	D.Ph.T., C.E.N. Saclay, B.P.2, 91190 Gif sur Yvette (France)
CONTOGOURIS André	Physique Théorique et Particules Elémentaires, Bât. 211, 91405 Orsay (France)
COON Darryl	University of Pittsburgh, Department of Physics, Pittsburgh, PA 15213 (U.S.A.)

CUTTS David	Brown University. Providence, R.I. 02912 (U.S.A.)
DAR Arnon	Physics Dept. Technion Institute of Technology, Haifa, (Israel)
DARRIULAT Pierre	Division NP, CERN, 1211 Genève 23 (Suisse)
DE GROOT Henri	Division TH, CERN, 1211 Genève 23 (Suisse)
DE TAR Carleton	Division TH, CERN, 1211 Genève 23 (Suisse)
DONOHUE Jack	Physique Théorique, Univ. de Bordeaux I, Chemin du Solarium, 33170 Gradignan (France)
FARRAR Glennys	Caltech 452-48, Pasadena, Ca 91125 (U.S.A)
GODRECHE Claude	LPTHE, Tour 33, Université Paris VII, 2 Place Jussieu, 75221 Paris (France)
GOGGI Giorgi	Istituto di Fisica Nucleare, Pavia (Italie)
GOLDBERG Jacques	Physics Dept. Technion Institute of Technology, Haifa, (Israel)
HEMINGWAY Richard	Division TC, CERN, 1211 Genève 23 (Suisse)
INAMI Takeo	Physique Théorique et Particules Elémentaires, Bât. 211, Orsay 91405, (France)
ISLAM Muhammad	C.E.N. Saclay, Service de Physique, B.P. 2, 91190 Gif sur Yvette (France)
JACKSON Shirley	Division TH, CERN, 1211 Genève 23 (Suisse)
JARLSKOG Göran	Division NP, CERN, 1211 Genève (Suisse)
KANE Gordon	Physics Dept. University of Michigan, Ann Arbor, Michigan, 48104 (U.S.A)
KROLL Peter	Inst. of Theor. Kernphysik, Universität Karlsruhe, (Germany)
KRZYWICKI André	Physique Théorique et Particules Elémentaires, Bât. 211, Université de Paris-Sud, 91405 Orsay (France)
KUTI Julius	Central Research Institute for Physics, Hungarian Academy of Sciences, H - 1525 Budapest P.F. 49 (Hongrie)
LABERRIGUE Jeanne	LPNHE, Tour 32, Univ. de Paris VI, 4 Place Jussieu, 75230 Paris Cedex 05 (France)
LE BELLAC Michel	Physique Théorique, Parc Valrose - 06034 Nice Cedex (France)

LEROYER Yves	Laboratoire de Physique Théorique, Chemin du Solarium, 33170 Gradignan (France)
LETESSIER Jean	Physique Théorique, Tour 33, 1er étage, 2 Place Jussieu, Université de Paris VII, 75221 Paris 5ème (France)
LUNDBY Arne	Division NP, CERN, 1211 Genève 23 (Suisse)
MANDELLI Luciano	Division TC, CERN, 1211 Genève 23 (Suisse)
MAOR Uri	Physique Théorique, C.E.N. Saclay, B.P. 2, 91190 Gif sur Yvette (France)
MARTIN Alexander	Centre de Physique Théorique, C.N.R.S., 31 Chemin J. Aiguier, 13274 Marseille Cedex 2 (France)
MENZIONE Aldo	Istituto di Fisica, Piazza Torricelli 2, 56100 Pisa (Italie)
MEYERS Christian	Laboratoire de Physique Théorique, Université de Bordeaux I, Chemin du Solarium, 33170 Gradignan (France)
MICHAEL Christopher	Dept. of applied Maths and theoretical physics, Univ. of Liverpool, Liverpool L 69 3BX (England)
MORENO Hector	Centro de Investigation y de Estudios Avanzados del Instituto Politecnico Nacional, Apartado Postal 14-740, Mexico 14, D.F.
NAGY Elemer	Division NP, 1211 Genève 23 (Suisse)
OLSEN Steve	University of Rochester, Dep. of Physics, Rochester, N.Y. 14627 (U.S.A)
PALER Kenneth	Rutherford Lab. Chilton, Didcot, Berkshire, OX11 OQX (England)
PEOPLE John	Fermi Nal. Laboratory, P.O. Box 500, Batavia, Ill. 60510 (U.S.A)
PELAQUIER Elie	Laboratoire Physique Mathématique - USTL - 34060 Montpellier Cedex (France)
SAKAI Norisuke	Rutherford Laboratory, Chilton, Didcot, Berkshire CX11 OQX (England)
SANNES Felix	Physics Dept, Rutgers University, New Brunswick, New Jersey 08903 (U.S.A)
SAVIT Robert	Division TH, CERN, 1211 Genève 23 (Suisse)
SCHREMPP Barbara	Division TH, CERN, 1211 Genève 23 (Suisse)

SCHREMPP Friedger	Division TH, CERN, 1211 Genève 23 (Suisse)
SCHUBELIN Peter	Brookhaven National Lab. Upton, N.Y. 11973 (U.S.A)
SCOTT David	Rutherford Laboratory, Chilton, Didcot, OX11 OQX (England)
SQUIRES Euan James	Dept. of Mathematics, University of Durham, Durham, (England)
STROLIN Paolo	Division NP, CERN, 1211 Genève 23 (Suisse)
STROYNOWSKI Ryszard	Division TC, CERN, 1211 Genève 23 (Suisse)
TEPER Michael	Institute of Theoretical Science, University of Oregon, Eugene, Oregon 97403 (U.S.A)
TRAN THANH VAN Jean	Physique Théorique et Particules Elémentaires, Bât. 211, Université de Paris-Sud, 91405 Orsay (France)
VAN DE WALLE Remy	Physics Lab. Univ. of Nijmegen, Toernooiveld, Nijmegen (Netherlands)
WORDEN Robert	Division TH, CERN, 1211 Genève 23 (Suisse)
YVERT Michel	I.P.N. Division de Physique Nucléaire, Université de Paris-Sud, Bât. 100, 91400 Orsay (France)
YOKOSAWA Aki	Argonne National Laboratory, 9700 South Cass Avenue, Argonne, Ill 60439 (U.S.A)

Secrétariat :

BEUCHEY Geneviève	D.Ph.P.E./S.E.E., CEN Saclay, BP 2, 91190 Gif sur Yvette (France)
COTTEN Marie-Paule	Laboratoire de l'Accélérateur Linéaire, Bât. 200, Université de Paris-Sud, 91405 Orsay (France)
PILLET Marie-Thérèse	Laboratoire de Physique Théorique et Particules Elémentaires, Bât. 211, Université de Paris-Sud, 91405 Orsay (France)
RIBET Nicole	Laboratoire de Physique Théorique et Hautes Energies, Université de Paris-VI, Tour 16, 4 place Jussieu, 75230 Paris Cedex 05 (France)

A. MARTIN AND J. BALL

F.SCHREMMP, BARBARA SCHREMMP AND M. ISLAM

G. FARRAR, P. DARRIULAT AND G. JARLSKOG

A. CONTOGOURIS, N. ANTONIOU AND E. SQUIRES

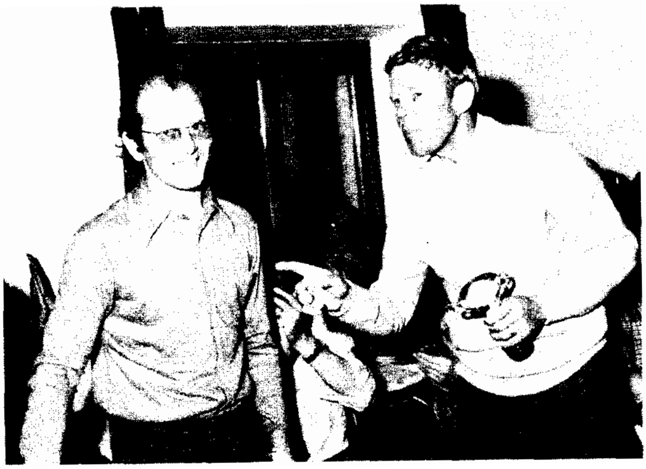

M. LE BELLAC AND A. LUNDBY

MRS. ANTONIOU, E. NAGY AND J. LABERRIGUE

T. INAMI , MRS. AND MR. KRZYWICKI

MR. AND MRS. M. ISLAM

C O N T E N T S

First Session

SINGLE AND DOUBLE DIFFRACTION DISSOCIATION AT FNAL AND ISR ENERGIES

G. Goggi

Istituto di Fisica Nucleare, Università di Pavia, Italy
Istituto Nazionale di Fisica Nucleare, Sezione di Pavia, Italy

Abstract: The present status of single and double diffraction dissociation at high energies is discussed in view of recent results and new preliminary data from FNAL and ISR on both types of processes. Some results of the Pavia-Princeton collaboration on exclusive double diffraction dissociation at the ISR are presented.

Résumé : Nous présentons une revue de la dissociation diffractive (simple et double) à hautes énergies. Quelques résultats de la collaboration Pavia-Princeton sur la double diffraction dissociative exclusive aux ISR sont aussi présentés.

1. - INTRODUCTION

High energy p-p inelastic interactions, in particular the reactions generally identified as diffractive dissociation, represent a class of processes extensively studied at the lower accelerator energies and presently under investigation up to the highest available energies at FNAL and CERN ISR.

Inclusive spectra obtained at the ISR provided the first indication of a large diffractive component in high energy p-p collisions and specifically in the inelastic part of the interaction. Soon after bubble chamber data from FNAL in the 100-400 GeV region began to fill the picture with more specific information on the different topological components of the proton diffractive dissociation with data on some specific reaction channels. Recent results obtained at the ISR on semi-inclusive and exclusive diffractive reactions extend considerably the explored energy range and are particularly important to check whether a more general definition of diffraction dissociation can emerge from data available at high energy.

In this talk I shall first try to summarize the data on inelastic diffractive reactions at high energies both from the inclusive and exclusive viewpoint. Given the many complementary aspects of the available results, high energies are defined here as the FNAL and ISR energy range. By no means a complete review, this is intended to be just a survey providing basic information, as well as indications on existing problems and limits of the presently available data. Complete reviews of diffraction have been published recently[1,3].

Our interest will be focused on the relationships between inclusive and exclusive data on single and double diffraction and on the questions that may arise from this comparison.

The general discussion on single diffraction dissociation is the obvious starting point to discuss double diffraction processes, which probably share with single diffraction a common dynamical nature. The latter processes, more easily accessible at the highest energies at least in terms of rapidity separation of the decaying systems, will be discussed in view of some recent experimental results, as yet unpublished, and as a natural extension of single diffractive reactions using the well known theoretical tool of factorization.

Although double diffraction is expected to be only a small fraction of the total diffractive cross section, it represents an exciting and so far almost unexplored field of investigation, whose dynamical connections with single diffractive processes are potentially capable of providing new insights into the general mechanisms of diffraction dissociation.

2. - DIFFRACTION DISSOCIATION

2.1 A general outlook

Before showing any data, let us review briefly the basic properties and characteristics of diffractive scattering which will be recalled in the following.

We can describe diffraction dissociation in terms of the exchange of a Pomeron ($\mathbb{P}$) in the t-channel, or identify the diffraction process by its properties observed in scattering reactions. These properties, unfortunately, do not represent a complete description of the process or of the Pomeron itself, but are just a set of phenomenological prescriptions. Basically what we do have is a set of rules that allow us to classify what is meant by diffractive reaction or $\mathbb{P}$ -exchange process:

a - energy independent cross section - or weakly dependent on energy, such as the elastic one, to factors of ln s

b - forward peak in the angular distribution - differential cross section described by an exponential parametrization

c - exchange process characterized by the quantum numbers of the vacuum in the t-channel - I=0, Q=0, S=0, B=0, C=+1, G=+1

d - spin and parity change obeying the Gribov-Morrison rule

$$\Delta P = (-1)^{\Delta J}$$

or final state quantum numbers following the natural spin-parity series

e - t-channel helicity conservation mostly obeyed

f - various branching ratio sum rules, connected with the isoscalar nature of the exchange; for example:

$$\frac{\sigma\left[pp \rightarrow p(n\pi^{+})\right]}{\sigma\left[pp \rightarrow p(p\pi^{o})\right]} = 2 \qquad (1)$$

Factorization is not explicitly included in this list since, rather than an operational criterion, it is a property which links different reactions and the theoretical assumption underlying the concept must yet be tested experimentally in detail.

Whenever a given reaction exhibits the above characteristics, or most of them, we describe it as a diffractive process and try to interpret it in terms of $\mathbb{P}$-exchange in Regge language. It has to be remembered, though, that the experimental picture is far from being satisfactorily described by the exchange of a simple Regge pole and the Pomeron must therefore be considered as a somewhat unspecified notion.

2.2 The high energy region

The presently well established examples of diffractive production are all of the single diffraction dissociation type; for an exclusive dissociated system a relevant property is that its invariant mass distribution should tend to become stable as $s \rightarrow \infty$.

Double diffraction dissociation can be related to single diffraction processes on the grounds of theoretical arguments assuming factorizability of the $\mathbb{P}$-exchange amplitudes. In this framework diffraction dissociation processes are directly related to diffraction scattering; neglecting phase space factors:

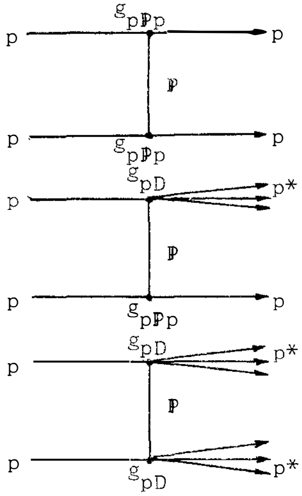

$$\sigma_{el} \sim (g^2_{p\mathbb{P}p})^2$$

$$\sigma(pp \to pp^*) \sim g^2_{p\mathbb{P}p}\, g^2_{pD}$$

$$\sigma(pp \to p^*p^*) \sim (g^2_{pD})^2$$

The simplest application of factorization is the following relationship of the three mechanisms:

$$\sigma_{DD}(pp) \cdot \sigma_{el}(pp) \sim g^4_{pD} \cdot g^4_{p\ p}$$

thus

$$\sigma_{DD}(pp) = \frac{\sigma^2_D(pp)}{\sigma_{el}(pp)} \tag{2}$$

where σ_D is the cross section corresponding to single vertex diffraction.

The total inelastic diffractive cross section is made up of three terms, namely

$$\sigma\,(\text{beam diffraction}) + \sigma(\text{target diffraction}) +$$
$$+\ \sigma(\text{double diffraction})$$

for the pp system this is just $2\sigma_D + \sigma_{DD}$.
Fig. 1 shows a summary of the data on the total inelastic cross section, as well as the elastic and the inelastic diffractive component. The main feature of this set of data is the energy dependence of the total inelastic cross section which steadily increases in the range 6 ÷ 1500 GeV. Many authors(4,5) attribute the increasing behaviour of the inelastic cross section to the diffractive component, whose energy dependence seems to be compatible with a ln s dependence. Probably a large fraction

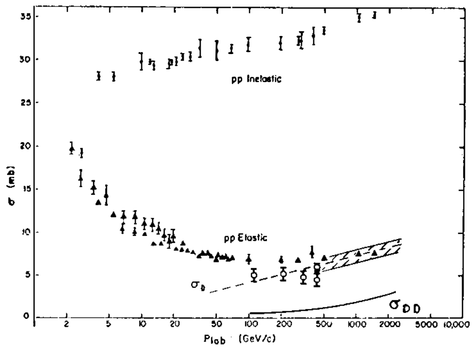

Fig. 1 - Elastic, total inelastic and diffractive inelastic cross sections. For the latter points are from ref. 9, the band represents ISR values(4,10-13) and the dotted line corresponds to $\sigma_{sD} = .7 \ln (M_p^2 + .0725\ s/1.2\ M_p^2)$mb(3a). The predicted double diffractive cross section σ_{DD} is also shown.

of the increase in inelastic cross section ($\Delta\sigma_{in} = 3.3 \pm .7$ mb) in the ISR energy range is due to this mechanism; it seems likely that the single diffractive cross section rises by $\sim 2 \pm 1$ mb in the range p_{lab} 300 to 1500 GeV(6).

The NAL and ISR data show that these diffractive processes account for ~ 20% of the total inelastic cross section and this contribution is comparable to the total elastic cross section.

$$\frac{\sigma\text{(Total diffraction cross section)}}{\sigma\text{(Diffractive elastic scattering)}} \sim 1$$

As a first consequence we can tentatively estimate the total double diffraction cross section:

$$\sigma_D(pp) \sim \frac{\sigma_{el}(pp)}{2} \qquad \sigma_{DD}(pp) \sim \frac{\sigma_{el}(pp)}{4} \sim 1.5 \text{ mb} \qquad (3)$$

The analysis of the detailed properties of the excited states appears as the obvious next step.

3. - THE INCLUSIVE AND SEMI-INCLUSIVE APPROACH

3.1 Missing mass data

Recent investigations of the recoil proton spectrum observed in p-p collisions at NAL and ISR have provided evidence for the presence of a sizeable inelastic diffractive component in the data. The energy and momentum-transfer dependence found for such inclusive processes can be considered as evidence for their diffractive nature.

As is well known we talk about exclusive or inclusive reactions depending on whether the emission of secondaries besides those detected and measured is excluded or included. From this viewpoint the single diffractive or the double diffractive cross sections give inclusive information from which we can get, at most, the energy and momentum transfer dependence.

The ISR data were first to show that the momentum spectrum of the proton is quite flat, with a peak in the invariant cross section for $x \sim 1$ (Figs. 2a,b). After substraction of elastic events the peak is attributed to a process of quasi-elastic scattering off an excited proton. This process is interpreted as diffraction excitation of the recoiling system with a missing-mass squared given by

$$M^2 \sim s(1-x)$$

Since diffraction production seems to be present for $x > .95$, masses as large as 10 GeV are excited at the top ISR energies.

Fig. 3a and 3b show the missing mass spectrum for inelastic events at 205 GeV/c as measured and FNAL[8,9] at various energies. The diffractive peak is a prominent feature of the data, extending up to 50 GeV^2.

The dominant features of these data are:

a - the large peak for low M^2

b - the relatively flat distribution at high M^2

c - the constant height of the peak between 102 and 405 GeV/c

d - the greater width of the peak with respect to the low energy data

The general picture emerging is a relatively constant cross section for low mass single diffraction in pp collisions, with a value $\sim$ 2.2 $\pm$ .5 mb from 20 GeV/c onwards into the ISR energy region. With factorization the corresponding inclusive double diffraction cross section turns out to be from (3):

$$\sigma_{DD} \sim 700 \ \mu b \qquad (4)$$

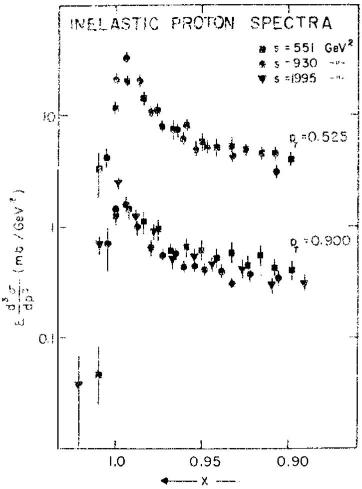

Fig. 2a – Invariant cross sections for inelastic protons in p-p collisions at $\sqrt{s}$ = 23, 31 and 45 GeV as a function of $x = 2\,p_L/\sqrt{s}$(7).

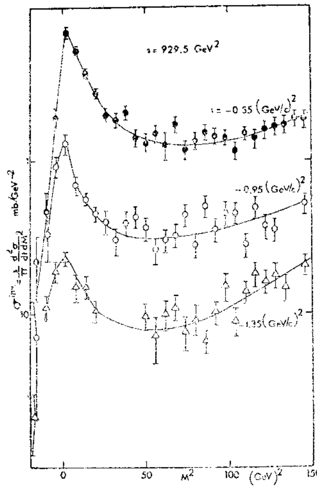

Fig. 2b – Missing mass distributions at $\sqrt{s}$ = 31 GeV at different t-values.

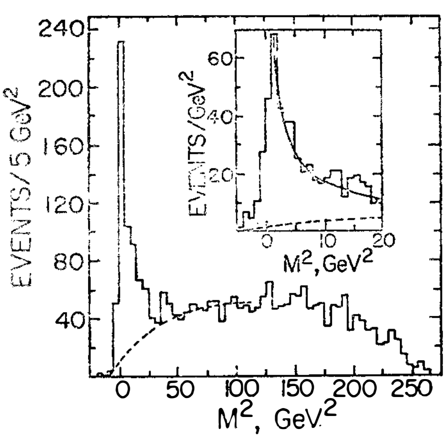

Fig. 3a – Missing mass distribution for inelastic events at 205 GeV/c. Dashed lines represent a hand-drawn background; the solid line shows background plus a $1/M^2$ dependence for the tail of the peak(8).

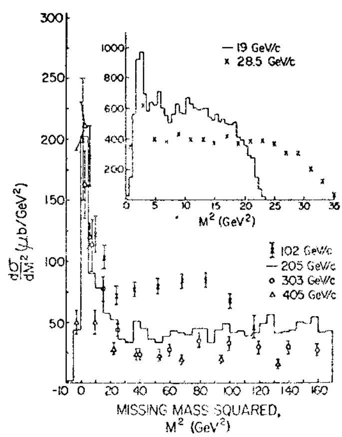

Fig. 3b – Same as in Fig. 3a at different energies between 100 and 400 GeV/c.

3.2 Topological decompositions

Many of the characteristics of very high energy reactions observed at ISR and FNAL can be interpreted in terms of two-component models[10-13] with features of both multiperipheral and fragmentation ideas. The component which is responsible for the diffractive part of the interaction can be phenomenologically defined as the one which leads to events with large rapidity gaps. In other words in an ordered rapidity distribution for an individual event there should be a large rapidity gap corresponding to Pomeron exchange; this feature is used to sharpen the selection criteria adopted to classify diffractive events into the different topological categories.

An example is given in Fig. 4 where the 205 GeV/c inelastic events are separated into topological classes. It is clearly seen that the low mass peak is associated mainly with the low-multiplicity configurations, whereas the tail receives contributions from higher topologies as the missing mass is increased. This correlation is even more evident in Fig. 5, where the average charged multiplicity of the system is plotted against the square of the missing mass.

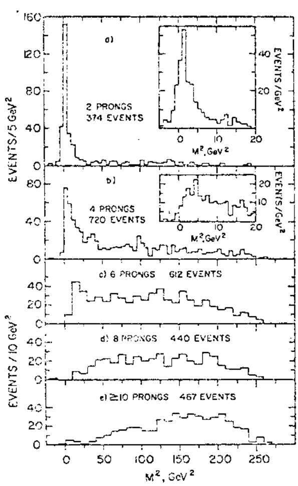

Fig. 4 - Missing mass squared distributions for various topologies for events of Fig.3a. (a) 2-prong inel.

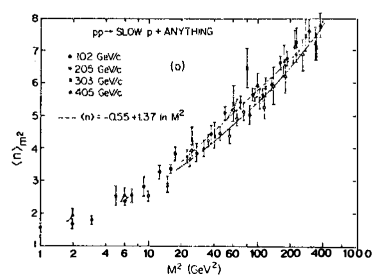

Fig. 5 - Average charged multiplicity of the system recoiling off the slow proton vs. the missing mass.

At both 100 and 200 GeV the size of the total p-p diffractive dissociation cross section into four prongs is about 2 mb[14] for a mass of the dissociating system up to 4 GeV. It is then possible to estimate the amount of double diffraction dissociation in the 6-prong topological channel with both (M_1 and M_2) $\leqslant$ 4 GeV.

$$\sigma_{DD}(pp \to 6 \text{ prongs}) \doteq \frac{(1\text{mb})^2}{\sigma_{el}} \sim 150\ \mu b \qquad (5)$$

which is only about 2% of σ (6 prongs).

3.3 Resonance excitation and differential distributions

The interesting feature emerging from the data considered so far is that at high energies there seems to appear a mechanism responsible for the excitation of high masses decaying predominantly into high-multiplicity final states. Because of kinematical limitations this aspect of diffraction was not evident at lower energies. On the other hand low energy inelastic interactions are characterized by the well known diffractive excitation of resonant states. The corresponding processes depend only weakly on energy and populate primarily low-mass, low-multiplicity channels. At high energies the low mass diffractive dissociation region ($M^2 < 10\ GeV^2$) still contributes a large fraction, about 50%, of the total diffractive dissociation cross section.

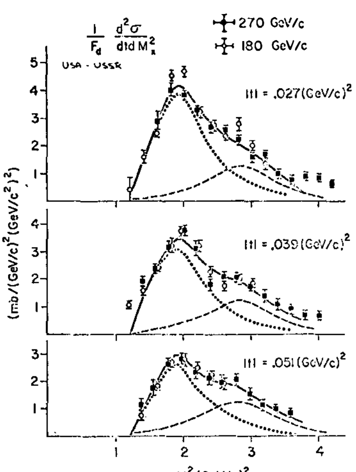

Fig. 6 - Resonant structures in the reaction p+d $\to$ d+x. The deuteron structure is taken into account by normalizing to the elastic form factor.

Data on the reaction

$$p + d \to d + x \qquad (6)$$

in which the coherent nature of the process on deuterium isolates a pure isoscalar exchange channel, giving a powerful selection criterion for diffractive reactions, show clear resonant contributions at 180 and 270 GeV/c[15] (Fig. 6). The low mass enhancement appears to have approximately the same cross section and t dependence at FNAL energies as the one measured in the 20 GeV range for the N*(1400).

Turning now to four-momentum and mass dependence of cross-sections the double differential cross sections $d^2\sigma/dM^2dt$ for $pp \rightarrow p+x$ can be very well represented by exponential fits, as expected given its dominant diffractive nature. An example is shown in Fig. 7.

The results are summarized in Fig. 8, where the exponential slope b(M) is shown as a function of the mass of the ex-

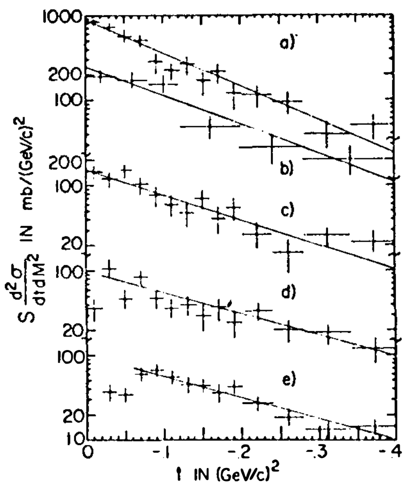

Fig. 7 - Invariant cross section versus t, for various missing mass intervals, for the reaction $p+p \rightarrow p+x$ at 205 GeV/c. (a) $M^2 < 5$ GeV^2, (b) $5 \leq M^2 < 10$ GeV^2, (c) $10 \leq M^2 < 25$ GeV^2, (d) $25 \leq M^2 < 50$ GeV^2, (e) $50 \leq M^2 < 100$ GeV^2.

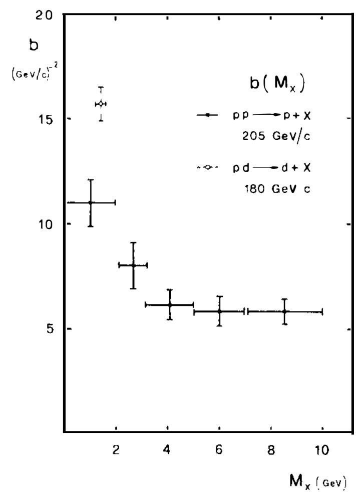

Fig. 8 - Exponential slope b as a function of missing mass at 205 GeV/c. Dashed point is from pd data at 180 GeV/c.

cited system. The strong slope-mass correlation, already present at lower energies, in again evident and shows a limiting value of about $6(GeV/c)^{-2}$.

The same general description applies for data from reaction (6) at higher energies.

3.4 Conclusions

The data shown in this section and the above considerations suggest the following conclusions on the general aspects of high energy proton excitation:

a - single-particle excitation, as already detected from the study of missing mass distributions in the 30 GeV region, is holding throughout the ISR energy range, as expected for a diffractive phenomenon

b - the diffractively excited states extend much beyond the known resonances, in effect up to excited hadronic states of 10 GeV and more

c - the cross section for such a single diffractive excitation mechanism is of the order of the elastic cross section

d - the final state multiplicities associated with these excited hadronic states can be relatively high and show a positive correlation with the mass of the dissociated final state. Furthermore the most prominent mass peaks are associated with the lowest multiplicities

e - in the low mass region ($M^2 < 4$ GeV^2) resonance excitation exists with energy dependence which is small or absent

f - the slope-mass correlation, known at low energies, is observed also at high energies with the same general features

g - inclusive double diffraction dissociation should be of the order of $.5 \div 1$ mb, or about 10% of the total inelastic diffraction cross section.

4. - THE EXCLUSIVE APPROACH

4.1 Open questions

The outstanding feature that the inelastic cross section, and its diffractive component in particular, are a monotonically rising function of energy leads immediately to enquire about the behaviour of the individual production cross sections. Decomposing the inclusive information into its exclusive contributions allows a direct investigation of how the overall phenomenon od inelastic diffraction is distributed among the increasing number of different channels.

The general behaviour of any exclusive channel cross section is known: following a rise after threshold to some peak value, whose height and position depend on the specific channel, there is a fall-off with some inverse power of the incident laboratory momentum, $\sigma \sim p_L^{-n}$.

The study of effective mass distributions, associated with full reconstruction of low-multiplicity events, has been employed to analize mainly the two and four-prongs events in greater detail. The present problems and the opportunities open to further investigation in the high energy behaviour of diffractive reactions can be summarized in the following points:

a - the invariant mass distribution of the produced secondaries is expected to reach with energy a limiting distribution. This phenomenon is the exclusive aspect of the impressive scaling observed at the ISR for single particle distributions in the fragmentation region.

b - In connection with point (a) a question can be raised concerning the resonance composition of the final states. Resonance excitation is known to contribute a considerable fraction of low-energy inelastic diffraction where N^* production is a clearly identifiable reaction having the specific signature of well defined spin-parity states. It is interesting to determine to what extent high energy inelastic diffraction can be considered as being kinematic in origin or dominated by resonance excitation.

c - The separation of the diffractive part in an exclusive reaction, certainly easier at high energies, can provide a better definition of Pomeron exchange. The comparison of several channels in a wide energy range can provide substantial information on (a) the s-behaviour of $\mathbb{P}$-exchange amplitudes, (b) the weight of different incoherent contributions to the total diffractive cross section at different energies.

d - The study of the function b(s,M), the slope parameter as a function of energy and produced mass, can give a deeper insight into the general mechanisms of diffraction. Elastic diffraction is essentially shadow scattering at these energies and it is important to check whether shrinking is a universal property of diffraction. The dependence of the slope on the produced mass is furthermore an important ingredient in s-channel impact-parameter descriptions of this class of processes and can represent a direct test of factorization if measured in double diffraction.

It is clear how these features and the detailed measurement of the related physical quantities are important for any prediction or comparison involving double diffraction dissociation processes. It is pherhaps worth to list what experimental information is needed for a deeper understanding of the diffraction picture. It can be summarized as follows:

- measurement of exclusive channel reactions in the widest possible energy range
- separation and identification of structures with high mass resolution
- measurement of the decay angular properties, which is also relevant to the general problem of helicity conservation in diffractive processes

- analysis of the properties of subsystems in the final state, particularly for high multiplicity reactions
- measurement of differential cross sections in a wide t-range allowing comparisons with structures, dips or breaks already observed in elastic scattering at the ISR and in low energy resonance production(16).

4.2 Experimental results: a few answers

Three experiments, the first in bubble chamber(17) at FNAL and two others performed with counter techniques at the ISR(18,19), have provided detailed information on the reactions

$$p+p \rightarrow p+(n\pi^+) \quad \text{at} \quad \sqrt{s} = 53 \text{ GeV}^{(18)} \qquad (7)$$

$$p+p \rightarrow p+(p\pi^+\pi^-) \quad \text{at} \quad \sqrt{s} = 20 \text{ GeV}^{(17)} \qquad (8)$$

and

$$\sqrt{s} = 45 \text{ GeV}^{(19)}$$

In the following their common features will be discussed with respect to the properties of the mass spectra, the production

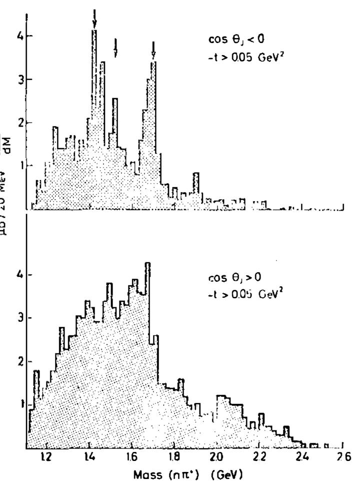

Fig. 9 - Effective mass distribution of the $(n\pi^+)$ system in $pp \rightarrow p(n\pi^+)$ at $\sqrt{s}$ = 53 GeV, backward and forward in the Jackson frame.

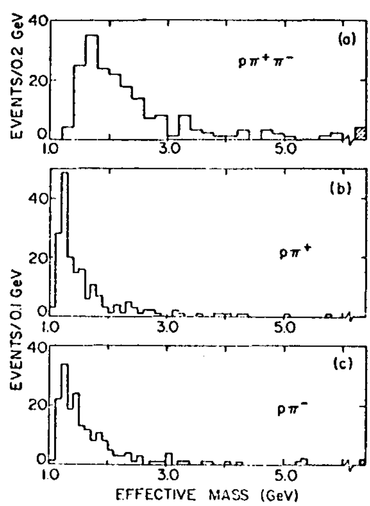

Fig. 10 - Effective mass distributions from the reaction $pp \rightarrow p(p\pi^+\pi^-)$ at 205 GeV/c.

cross sections and the characteristics of the differential cross sections, with reference to specific resonant states whenever possible.

Reaction (7), as measured at the ISR detecting all the final state particles, shows (Fig. 9) resonance excitation in the backward Jackson hemisphere with a clear N*(1688) and some excitation around 1.4 GeV and 1.51 GeV. Events in the two hemispheres of the Jackson frame show distinctly different distributions.

Bubble chamber results at 205 GeV/c on reaction (8) indicate the presence of an unresolved peak around 1.7 GeV; the analysis of the $(p\pi)$ subsystems shows excitation of the $\Delta^{++}(1236)$ with, if present, a much weaker Δ^{o} signal (Fig.10). The same feature for the same reaction at $\sqrt{s}$ = 45 GeV is advocated as evidence for I=0 exchange. In fact for a pure I = 1/2 $p\pi^{+}\pi^{-}$ state Clebsch-Gordan coefficients yield

$$\frac{Y\left[(\Delta^{++}{}_{3/2\ 3/2}\,\pi^{-})_{I=1/2}\longrightarrow p\,\pi^{+}\pi^{-}\right]}{Y\left[(\Delta^{o}{}_{3/2\ 3/2}\,\pi^{+})_{I=1/2}\longrightarrow p\,\pi^{+}\pi^{-}\right]}=\frac{9}{1} \qquad (9)$$

The mass-spectrum for this last experiment is shown in Fig. 11. Resonance excitation of masses around 1.5 GeV and 1.68 GeV seems to account for a large fraction of the observed events.

From the measured cross section of reaction (7), 270 ± 80 μb, it is possible to derive, using eq. (1), the total $(N\pi)$ cross section for the I=0 p-p channel. Since this reaction is known from isospin analysis to be denominated by I=0 exchange also at low energies it is then possible to determine the s-dependence of the isoscalar exchange cross section, as shown in Fig. 12.

The point from reaction (6), which is pure I=0 exchange too, does compare rather well with the fitted curve. It has to be remembered in fact that final states other than $(n\pi^{+}+p\pi^{o})$ contribute to this reaction through higher multiplicity states.

No such simple picture appears in the $p\pi^{+}\pi^{-}$ channel of reaction (8). The high energy points in the total cross section lie systematically above the power law extrapolating lower-energy data, suggesting either a break or a smaller exponent, closer to the value n = -.4, typical of the isoscalar exchange channel (Fig. 13a).

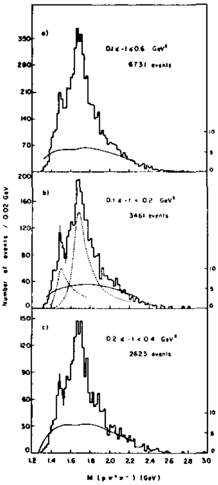

Fig. 11 - Effective mass distributions for the system ($p\pi^+\pi^-$) from the reaction $pp \longrightarrow p(p\pi^+\pi^-)$ at $\sqrt{s}$ = 45 GeV. Smooth curves indicate the acceptances of the apparatus. Dotted lines in (b) show the contributions of N*(1520) and N*(1688).

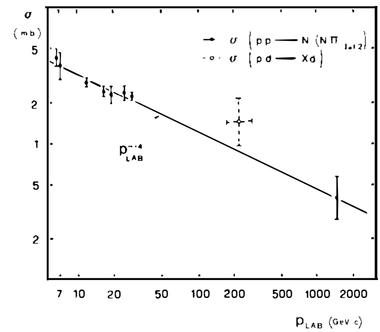

Fig. 12 - Cross section as a function of p_{LAB} for the reaction $pp \rightarrow N(N\pi)$ in pure I = 1/2 state. A point from reaction $pd \rightarrow d+x$ is shown (personal estimate from the data published in ref. 3 and 15).

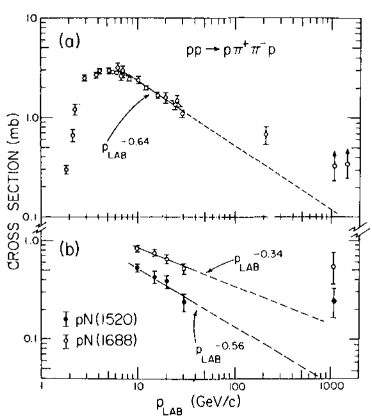

Fig. 13a,b - Cross sections for (a) $pp \rightarrow p(p\pi^+\pi^-)$ and (b) $pp \rightarrow pN^*(1520)$ and $pp \rightarrow pN^*(1688)$ as a function of p_{LAB}

Also the total cross sections for the excitation of the two isobars N*(1520) and N*(1688),

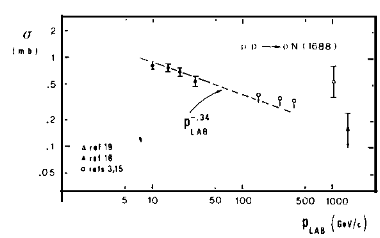

Fig. 13c - Cross section, as a function of p_{LAB}, for N*(1688) production. The upper limits are obtained by integration of published differential cross sections in the mass range 1.56 ÷ 1.8 GeV (see note 21).

scaled from the cross section of the $p\pi^+\pi^-$ channel using the known branching ratios, seem to deviate from the predicted behaviour in the direction of smaller, if not zero, exponents (Fig. 13b).

From the data[18] on reaction (7) one can estimate a cross section in the N*(1688) mass band of about $75 \pm 25\ \mu b$ from which, branching ratios and isospin factors taken into account, a total cross sections of $170 \pm 70\ \mu b$ for the excitation of that N* can be obtained[21a] at an equivalent $p_{LAB} = 1480$ GeV. Similarly we can estimate[21b] analogous values from the data on the reaction $pd \rightarrow xd$. The overall picture is shown in Fig. 13c. More data at other high energies are clearly needed.

The third piece of experimental information comes from the differential distributions in the four-momentum transfer. Figs. 14a,b show the differential cross sections for reactions (7) and (8) (the latter at 205 GeV/c) integrated over all masses.

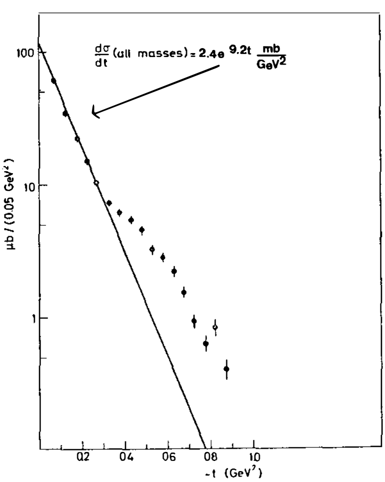

Fig. 14a - Differential cross section for the reaction $pp \rightarrow p(n\pi^+)$ at $\sqrt{s} = 53$ GeV integrated over the $(n\pi^+)$ invariant mass.

The processes are dominantly peripheral and exhibit very similar slopes, both slightly smaller than the elastic slope.

In Fig. 14a a structure appears around $t \sim .3\ (GeV/c)^2$; Fig. 15 indicates that this phenomenon is mainly associated with low-mass final states. The slope at ISR energies appear generally steeper than at PS energies (dotted lines in Fig. 15)[20]. A structure at small t appears also in the differential cross sections relative to reaction (8) at $\sqrt{s} = 45$ GeV (Fig. 16).

The exponential slope b as a function of mass is plotted in Fig. 17 for two different energies, 24 GeV/c and 1500 GeV/c.

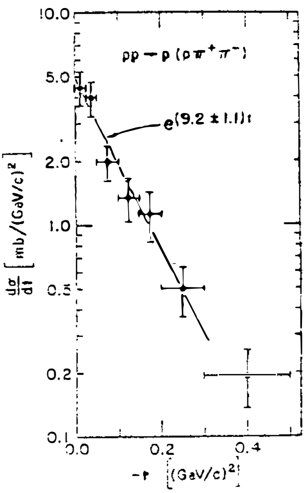

Fig. 14b - Differential cross section for the reaction $pp \rightarrow p(p\pi^+\pi^-)$ at 205 GeV/c integrated over the $p\pi^+\pi^-$ invariant mass up to M = 3 GeV.

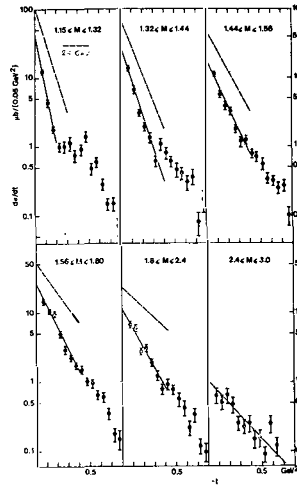

Fig. 15 - t-dependence of the cross section $d^2\sigma/dtdM^*$ in various mass regions for the reaction $pp \rightarrow p(n\pi^+)$ at $\sqrt{s}$ = 53 GeV. Broken lines are fits to data at 24 GeV/c (ref. 20).

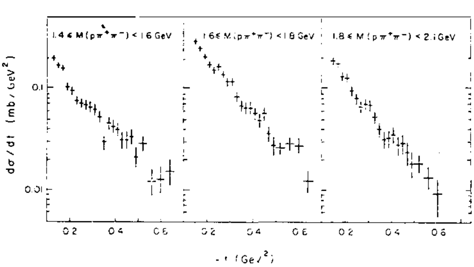

Fig. 16 - Differential cross section for the reaction $pp \rightarrow p(p\pi^+\pi^-)$ at $\sqrt{s}$ = 45 GeV for different mass intervals.

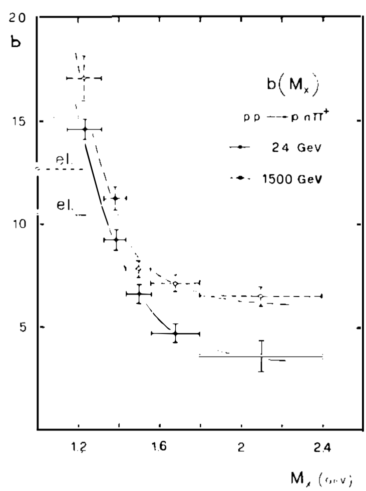

Fig. 17 - Slope b vs. mass at 24 and 1500 GeV/c for $pp \rightarrow p(n\pi^+)$. Elastic slopes at the same energies are also shown.

The shape seems invariant with energy whereas shrinkage, as observed in elastic scattering, appears as a general feature of inelastic diffraction, regardless of the produced mass.

Other results[19b] from reaction (8) confirm this trend.

4.3 Conclusions

The results discussed in this section represent the very first piece of detailed information available at high energies; preliminary and somewhat scattered as they are, they allow to draw some conclusions:

a - resonance excitation is present to a considerable extent. The competition with the non-resonant part of the cross section still appears open

b - a flattening, if note a rise, appears as the characteristic behaviour of many exclusive cross sections with increasing energy.

c - the slope-mass correlation in the momentum-transfer dependence is unchanged from the low-energy region apart from a sizeable shrinking

d - shrinking appears as a universal feature of diffraction, independent of the value of the produced mass and roughly equal to the corresponding shrinkage of the elastic peak.

e - structures appear in the low-mass regions in the range $.2 < t < .4$ $(GeV/c)^2$ of the differential cross sections.

5. - DOUBLE DIFFRACTIVE PROCESSES

This section will be somewhat different from the preceding ones since it is necessary to combine in it published and unpublished data. After discussing some relevant properties of factorization I shall briefly summarize the former and give a longer report on the latter on the basis of preliminary results.

5.1 Factorization

By factorization we mean a decomposition of the amplitude into vertex functions not dependent on s and on the other interacting particle and a propagator independent of the nature of the particles. At finite energies this simple picture is complicated by the presence, in the inelastic channels, of a number of effective masses, sub-energies and partial momentum transfers whose rôle in the factorized amplitude is not clear at all.

Various tests can be performed on single diffractive cross sections to check the validity of this hypotesis and the results obtained so far are strongly in favour of factorization which, even at low energies, seems to hold to within ± 20%. In general these tests on single diffraction look for the invariance of cross section ratios as a function of:

a - the nature of the incident particle

b - the energy

c - the four-momentum transfer

d - the mass of the excited system

or a combination of these.

For instance it is possible to check that (2) the excitation of a proton isobar can be independent of t, s, and the nature of the incident particle.

For example one can test whether the ratio

$$R = \frac{\sigma_D\left[pp \rightarrow p(p\pi^+\pi^-)\right]}{\sigma\left[pp \rightarrow pp\right]}$$

remains constant in s. Data are shown in Fig. 18.

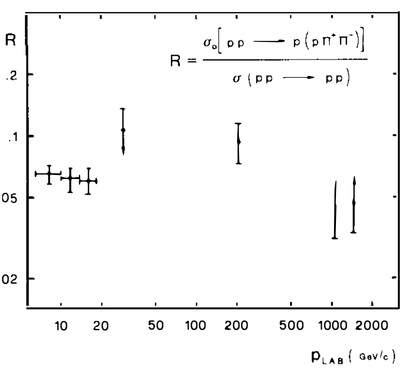

Fig. 18 - Ratio of the cross section for the reaction $pp \rightarrow p(p\pi^+\pi^-)$ to the cross section for elastic scattering as a function of inciden laboratory momentum.

The factorizability assumption for diffraction dissociation has serious consequences on the other hand when it is applied to double diffractive processes, namely to reactions where both initial particles become excited systems in the final state. Phenomenologically the asymptotic value of the single diffractive slope is approximately half the size of the slope obtained in elastic scatering (see Fig. 17). This would imply a value very close to zero for the slope of double diffractive processes.

A linear relationship among the slopes for different masses can be obtained as follows[23]:

$$\frac{d^3\sigma}{dt'dM_1^*dM_2^*} = \frac{d^2\sigma}{dt'dM_1^*}\,\frac{d^2\sigma}{dt'dM_2^*} \Big/ \left(\frac{d\sigma}{dt}\right)_{el}$$

or, diagrammatically

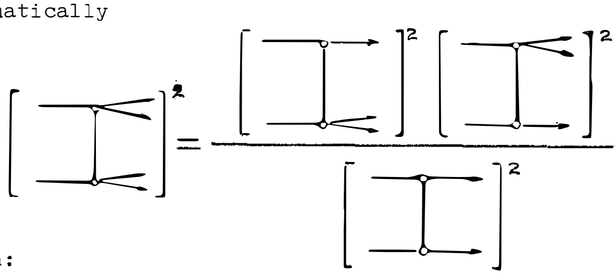

We have then:

$$b_{DD}(M_1^*, M_2^*) = b_D(M_1^*) + b_D(M_2^*) - b_{el}$$

In particular, for high effective masses $M^* \gg (m_p + m_\pi)$

$$\frac{d^2\sigma}{dt'dM^*} \sim e^{1/2\; b_{el} t'}$$

so that

$$\frac{d^3\sigma}{dt'dM_1^*dM_2^*} \sim \text{rougnly independent of } t'$$

Different models give various predictions; the main features expected for the slope-mass function are:

a - a very small asymptotic value for large produced masses since single dissociation has a less sharp t-dependence than elastic scattering

b - for a symmetric state in the two produced masses a cross-over of the two slope-mass functions (single and double) must appear around the value of the elastic slope

A detailed test of factorization as a function of s,t and M* is possible by comparing single and double diffractive processes at different energies.

5.2 Some experimental results

Low-energy experimental tests of factorization were first attempted looking for double diffractive events in π -p scattering reactions. Evidence for this type of events was found[24-27], through rather complex selections, in agreement with the behaviour predicted by factorization.

In the high energy region FNAL bubble chamber data at 300 GeV/c[28] support the factorization hypothesis in the semi-inclusive six-prong final state (neutrals included):

$$\sigma_{DD}(pp \rightarrow 6 \text{ prongs + neutrals}) = .12 \pm .05 \text{ mb}$$

$$\sigma_{D}(pp \rightarrow 4 \text{ prongs + neutrals}) = .82 \pm .08 \text{ mb}$$

The first value is consistent with the cross section (5) estimated in sec. 3.2 from inclusive data.

Evidence for double diffraction was also found[29] in the semi-inclusive reaction $pp \rightarrow p\pi^+\pi^- + x$ at the ISR at $\sqrt{s} = 45$ GeV where a quasi-elastic peak in the momentum spectrum of the $p\pi^+\pi^-$ system was seen excluding events in which x is just a single proton. The simultaneous detection of the single diffractive and elastic reactions allows a more detailed factorization test at different values of the four-momentum transfer. The cross section ratios again agree with the predictions.

First data on the double diffractive exclusive reaction

$$pp \rightarrow (p\pi^+\pi^-)(p\pi^+\pi^-) \qquad (10)$$

have been recently obtained by the Pavia-Princeton coll. at the ISR[30,31] at $\sqrt{s} = 23$, 31 and 53 GeV.

The differential distributions as a function of four-momentum transfer are displayed in Figs. 19 through 22. The slopes associated with the integral over all final-state masses are markedly smaller than those measured for single diffractive excitation and the distributions exhibit similar structures around $t \sim .3$ (GeV/c). These structures seem to get clearer with increasing energy.

The steeper points represent the same differential distribution with both masses selected in the N(1470) mass band. We see that the slope-mass correlation appears also in double dissociation with a conspicuous effect (roughly a fourfold increase in the exponential slope). As expected an intermediate value, $b \sim 5\ (\mathrm{GeV}/c)^{-2}$, is obtained by selecting one mass in the N(1470) band and integrating over the mass spectrum of the second $(p\pi^+\pi^-)$ system, as shown in Fig. 21 .

This type of analysis was performed for symmetrical final states as a function of the mass to compare the relative behaviour of the single and double diffraction slopes. The results at $\sqrt{s}$ = 53 GeV are shown in Fig. 22, where the dashed points are from reaction (7) at the same energy and the elastic slope is also indicated.

Although the two final states considered here are not directly related by factorization the comparison can be made if we accept the experimental evidence that the two processes share the same diffractive nature. The cross-over between the two slope-mass functions seems to be present at the value of the elastic slope and the general properties are those discussed in sec. 5.1.

5.4 Conclusions

Although the presently available data on double diffractive processes are much more limited and preliminary than those on single diffraction the comparison is stimulating and some trends can be identified:

a - factorization seems to hold as far as cross section ratios are concerned. Positive indications exist also as a function of four-momentum transfer

b - the general shape of the $(p\pi^+\pi^-)$ mass spectrum in double dissociation is very much similar to the corresponding distribution for single excitation into $p\pi^+\pi^-$ and changes very little with energy. Mass spectrum stability seems approximately valid and factorizable in the two vertices.[31]

c - resonance excitation exists also in double dissociation;[31]

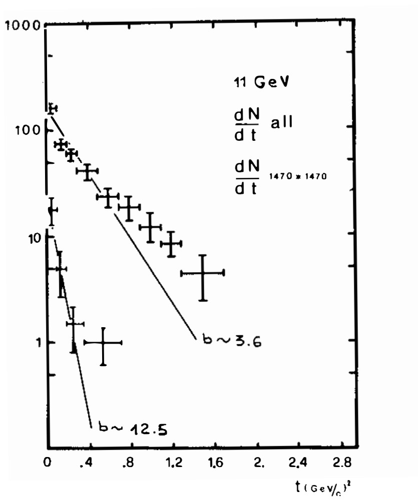

Fig. 19 - t-distributions for reaction (10) at $\sqrt{s}$ = 23 GeV. Data with a steeper slope refer to a mass selection of both $(p\pi^+\pi^-)$ systems in the N(1470) mass band.

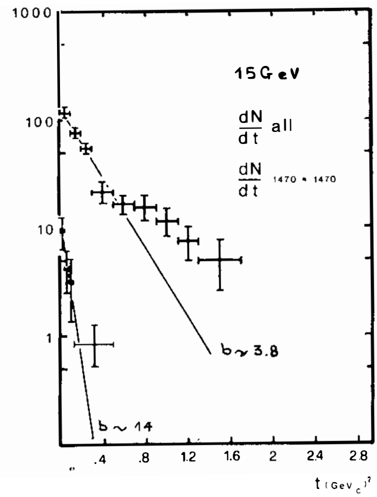

Fig. 20 - Same as in Fig. 19 but at $\sqrt{s}$ = 31 GeV.

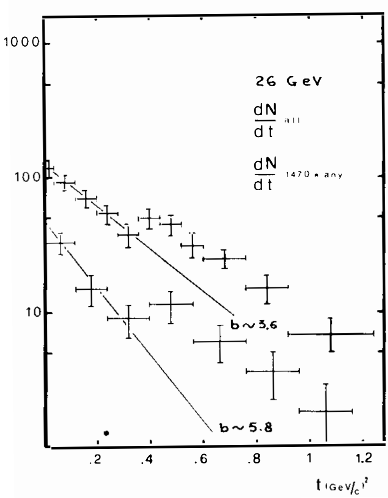

Fig. 21 - t-distributions for reaction (10) at $\sqrt{s}$ = 53 GeV. The curve with a steeper slope refers to events with one of the two masses in the N(1470) mass band, the second mass uncontrained.

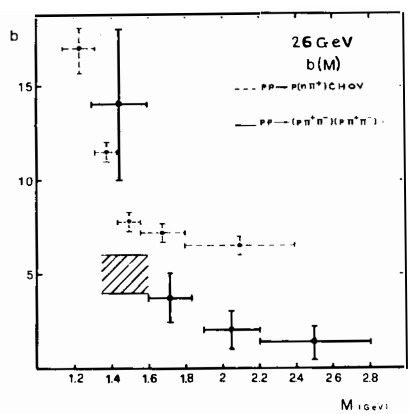

Fig. 22 - Exponential slopes as a function of excitation mass at $\sqrt{s}$ = 53 GeV for single and double dissociation. Data are from reaction (7) and reaction (10). The elastic slope is also shown. The dashed region represents the slope obtained in reaction (10) (double dissociation) constraining one of the two masses in the N(1470) band.

in particular double resonance excitation has been observed

d - a very small value for large produced masses is observed for the exponential slope in double dissociation

e - there is evidence in the behaviour of the slope-mass function for a direct relationship among the elastic, the single and the double diffractive slope.

The experimental results on high energy diffractive reactions in p-p collisions which were briefly summarized and discussed in this talk constitute just the preliminary survey of a wide new field of investigation. More detailed problems are now emerging which propose challenging experimental and theoretical questions on the nature of diffraction dissociation dynamics.

REFERENCES AND FOOTNOTES

1 - D.R.O. Morrison, Proc. of 5th Hawaii Topical Conf. (1973) and CERN/D. Ph. II/Phys. 73-46

2 - D.W.G.S. Leith, Proc. of 8th Rencontre de Moriond (1973) and SLAC-PUB 1263 (1973)

3a- A.N. Diddens, Proc. XVII Int. Conf. on High Energy Physics, London (1974) see also M. Derrick, ibid.

3b- F. Low, Proc. III Int. Coll. on Multiparticle Reactions, Zakopane (1973)

3c- J.E. Rushbrooke, ibid.

3d- H. Sata, K. Schilling, Proc. Coll. on Multiparticle Dynamics Helsinki (1971)

4 - U. Amaldi, Proceedings of the "Ettore Majorana" Int. School of Subnuclear Physics, Erice 1973 and references therein.

5 - D.R.O. Morrison, Proceedings of the 9th Rencontre de Moriond, and CERN/D. Ph. II/Phys. 74-8

6 - F.K. Loebinger, Proc. XVII Int. Conf. on High Energy Physics, London (1974)

7 - M.G. Albrow, A. Bagchus, D.P. Barber, A. Bogaerts, B. Bo-

snjakovic, J.R. Brooks, A.B. Clegg, F.C. Erné, C.N. Gee, D.H. Locke, F.K. Loebinger, P.G. Purphy, A. Rudge, J.C. Sens and F. Van der Veen, N.P. B 54, 6 (1973), N. P. B 51, 388 (1973), Phys. Lett. 42 B, 279 (1972)

8 - S.J. Barish, D.C. Colley, P.F. Schultz, J. Whitmore, P.R. L. 31, 1080 (1973)

9 - J. Whitmore, Phys. Reports 10, 273 (1974)

10 - K. Fialkowski, H.I. Miettinen, P.L. 43 B, 61 (1973)

11 - H. Harari, E. Rabinovici, P.L. 43 B, 49 (1973)

12 - L. Van Hove, P.L. 43 B, 65 (1973)

13 - K. Fialkowski, P.L. 41 B, 379 (1972)

14 - J. Van der Velde, Proc. XVI Int. Conf. on High Energy Physics, Chicago (1972)

15 - USA-USSR Collaboration Y. Akimova et al. see F.K. Loebinber, Proc. XVII Int. Conf. on High Energy Physics, London (1974)

16a- J. Allaby et al. Proc. XV Int. Conf. on High Energy Physics Kiev (1970) see also D.R.O. Morrison, CERN/D. Ph. II/Physics 71-10

16b- J.V. Allaby, A.N. Diddens, R.W. Dobinson, A. Klovning, J. Litt, L.S. Rochester, K. Schluppman, A.M. Wetherell, U. Amaldi, R. Biancastelli, C. Bosio, G. Matthiae, N. P. 52 B, 316 (1973)

16c- R.M. Edelstein, R.A. Carrigan, N.C. Hien, T.J. mc Mahon, I. Nadelhaft, E.W. Anderson, E.J. Bleser, G.B. Collins, T. Fujii, I. Menes, F. Turkot, P.R. D 5, 1073 (1972)

17 - M. Derrick, B. Musgrave, P. Schreiner, H. Yuta, Phys. Rev. D 9, 1215 (1974)

18 - W. Bartl, A. Brandt, C. Broll, G. Coignet, H. Dibon, J. Favier, G. Flugge, Ch. Gottfried, L. Massonet, E. Nagy, G. Neuhoger, F. Niebergall, M. Regler, K.R. Schubert, M. Vivargent, K. Winter, Proc. XVII Int. Conf. on High Energy Physics, London (1974)

19a- L. Baksay, A. Boehm, H. Foeth, A. Stande, W. Lockman, M. Meddinis, T. Meyer, J. Rander, P. Schlein, R. Webb, E. Ellis, B. Naroska, P. Strolin, Proc. XVII Int. Conf. on High Energy Physics, London (1974)

19b- R. Webb et al., (preprint to the published on Physics Lett.)

20 - K. Bockmann et al. Bonn-Hamburg-Munchen Collab., Preprint Bonn Univ. PIB 3-27 (1974)

21a- This is my personal estimate. A similar value can be found in ref. 3. The point is an upper limit since corresponds to the integral of the cross section in the (1.56 ÷ 1.8 GeV) mass bin.

21b- Three values, at 150, 260 and 385 GeV/c can be deduced (my personal estimate) from the integral over the same mass bin as in point (a) of the differential cross section $M_X^2 d^2\sigma/d(M_X^2)$ as given in ref. 3a. These values are therefore upper limits for the N(1680) whose signal is present as shown in Fig. 6.

22 - D.R.O. Morrison, Proc. XV Int. Conf. on High Energy Physics, Kiev (1970)

23 - S. Humble, N.P. 76 B, 137 (1974) and CERN Th. 1827 (1974)

24 - W. Kittel, S. Ratti, L. Van Hove, N.P. 30 B, 333 (1971)

25 - G. Rinaudo, A.E. Werbrouck, M. Rost, C. Kanazirsky, D.Z. Toet, R. Lestienne, N.C. 10 A, 1 (1972)

26 - D. Evans, K.P. Neat, G. Tomasini, G. Bassler, H. Nagel, P. Schilling, W.D. Schlatter, P. Borzatta, G. Cecchet, G. Costa, L. Liotta, S. Ratti, A. Daudin, M.L. Faccini, M. A. Jabiol, N.C. 13 A, 1102 (1973)

27 - H. Grassler, R. Honecker, P. Lauscher, G. Otter, H. Roloff, Ch. Spiering, K. Bockmann, G.J. Bossen, Ch. Kanazirsky, M. Rost, M.J. Counihan, J.D. Hansen, G.T. Jones, W. Kittel, D. Kuhn, D.R.O. Morrison, T. Hirose, E. Leitner, N.P. B 75, 1 (1974) and CERN/D. Ph. II/phys. 74-3

28 - A. Firestone, V. Davidson, F. Nagy, C. Peck, A. Sheng, F.T. Dao, R. Hanft, J. Lach, E. Malamud, F. Nezrik, A. Dzirba, R. Poster, W. Slater, FERMILAB-Pub. 74/101

29 - R. Webb, G. Thrilling, V. Telegdi, P. Strolin, A. Stande, B. Shen, P. Schlein, J. Rander, B. Naroska, F. Muller, T. Meyer, W. Marsh, W. Lockman, J. Layter, A. Kernan, H. Foeth, E. Ellis, A. Boham, L. Baksay (submitted to Phys. Lett.)

30 - Double isobar production at ISR, Proposal to study the reaction $pp \to (p\pi^+\pi^-)(p\pi^+\pi^-)$, Pavia-Princeton Collaboration, CERN/ISRC/72-23

31 - M. Cavalli Sforza, C. Conta, M. Fraternali, G. Goggi, F. Impellizzeri, G.C. Mantovani, F. Pastore, S. Ratti, B. Rossini, H. Sadrozinski, D. Scannicchio, Preliminary results on double diffraction dissociation and double isobar production in the reaction $pp \to (p\pi^+\pi^-)(p\pi^+\pi^-)$ studied with the SFM at the CERN ISR, This issue, p.

DIFFRACTIVE PRODUCTION OF THE $p\pi^+\pi^-$ SYSTEM AT THE ISR

P. Strolin, CERN

Abstract: The paper reports the results obtained in a series of experiments at the CERN ISR, where a multiparticle forward spectrometer equipped with multiwire proportional chambers has been used to study diffractive production of the $p\pi^+\pi^-$ system. Resonant structures in the invariant mass distribution of this system have been observed and cross-sections for nucleon resonance production at ISR energies have been measured.

Résumé: On présente les résultats d'une serie d'expériences effectuées aux ISR, dans lesquelles on a étudié la production diffractive du système $p\pi^+\pi^-$ en utilisant un spectromètre magnetique pour systèmes de plusieurs particules. La résolution en masse du spectromètre a permis l'observation de structures résonnantes dans la distribution de masse invariante de $p\pi^+\pi^-$ et la mesure des sections efficaces pour la production de resonances nucléoniques aux énergies ISR.

In the first generation of ISR experiments on proton fragmentation two complementary approaches have been taken. The Pisa-Stony Brook group has used a $\sim 4\pi$ scintillation counter system to study the pattern of the produced charged particles and its energy dependence (limiting fragmentation, diffractive component in the low multiplicities, correlation studies, etc.). The spectrometer approach of the CERN-Holland-Lancaster-Manchester group (and the Aachen-CERN-Harvard-Genova-Torino group, mainly active on elastic scattering) has produced single particle inclusive spectra and led to the discovery of diffractive production of large missing masses - much beyond the nucleon resonances observed at accelerator energies- recoiling against a quasi-elastic proton detected in the spectrometer. More recently the CHLM group(1) has supplemented their set-up by scintillation counter hodoscopes, and established that the particles associated with missing mass M (in GeV units) spread over a rapidity interval $\ln M^2$ in direct anology to the ln s spread in the general p-p collisions, where the available energy is $\sqrt{s}$.

We have now the first results(2,3,4,5) of experiments where multiparticle systems are fully analysed by magnetic spectrometers, having their angular aperture around the forward direction of one or both ISR beams. These experiments, where the mass of the system is directly measured with good resolution ($\sim$ 50 MeV, compared to a few GeV or more in missing mass measurements), are however limited to relatively low masses and multiplicities. When $\ln M^2 > \frac{1}{2} \ln s$, i.e. $M > 6 \div 7$ GeV at the ISR, proton fragments spill over to the opposite hemisphere. In practice available data are thus confined to $M < 3$ GeV, i.e. to the nucleon resonance region. The present paper reports the results obtained by the Aachen-UCLA-CERN(3) and Aachen-UCLA-Riverside-CERN(4) groups in studies of the reactions

$$p + p \rightarrow (p\pi^+\pi^-)_1 + X_2, \text{ and} \qquad (1)$$

$$p + p \rightarrow (p\pi^+\pi^-)_1 + p_2 \qquad (2)$$

where the system $p\pi^+\pi^-$ is detected by a multiparticle forward spectrometer in one of the arms (arm 1, as indicated by the subscript in the above eqs.) of the ISR intersection region 6.

The experimental set-up is shown in fig. 1. The spectrometer magnet (fig. 2) surrounds the ISR beam, which is shielded by an iron septum. The field integral ($\int B\,dl = 4.7 \times 2,5$ kGxm) is uniform within a few % across the magnet aperture, so that tracks are unambiguously and rapidly recognised and particle momenta are given essentially by the deflection. Furthermore the magnet does not distort the ISR beam and so the vacuum chamber is of minimal size and thickness, minimizing effects due to interactions in the chamber walls. The spectrometer is equipped with multiwire proportional chambers ($\sim$ 10,000 wires) and an eight-element atmospheric-pressure gas Cerenkov counter.

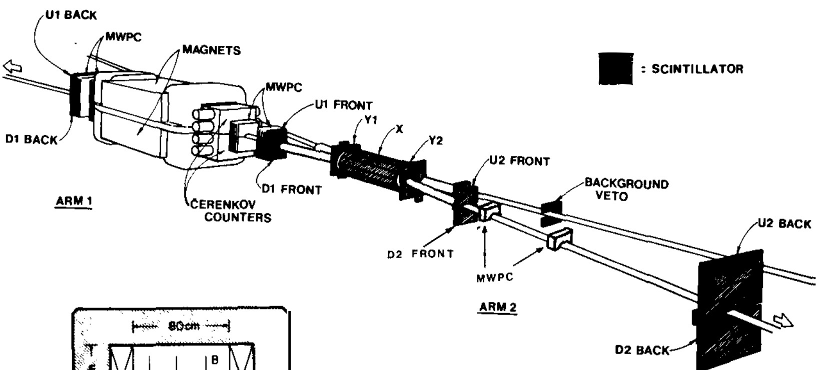

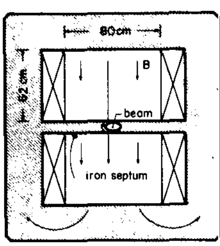

Fig.1 Experimental set-up.

Fig.2 Magnet aperture, viewed along beam 1.

The spectrometer covers the range 10 to 100 mrad with respect to the beam direction. For the three particle system $p\pi^+\pi^-$, and therefore for the inclusive reaction (1), the acceptance extends to $-t = 0$. In the study of the exclusive reaction (2), p_2 is detected by means of a telescope of small ($\sim$ 9x9 cm^2) MWPC in arm 2; for this reaction the minimum distance from the vacuum pipe at which these chambers could be made sensitive sets the limit $\theta \gg 15$ mrad, i.e. $-t > 0.12$ GeV^2 at $\sqrt{s} = 45$ GeV. Scintillation counters (~ 40 over a $\sim 4\pi$ solid angle) were used to trigger the read-out of the MWPC or to register the pattern of charged particles produced.

Fig. 3 shows the $p\pi^+\pi^-$ total momentum vector $\vec{p}_{tot}$ as measured by the spectrometer with an inclusive trigger - i.e. reaction (1). In analogy to inclusive proton spectra, a pronounced peak is seen at $x = 1$. Its width reflects the spectrometer resolution $\Delta p_{tot}/p_{tot} \simeq 7\%$ FWHM. It corresponds to events where the incident protons dissociates into a low mass system (fig. 4a) fully detected by the spectrometer: vetoing events with charged particles at large angles by means of the counter hodoscopes Y1($0.1 < \theta < 0.4$ rad) and/or X($0.4 < \theta < \pi -0.4$ rad) does not noticeably reduce the peak population (see fig. 3). From now on, any reference to reaction (1) implies only the events in this peak ($x > 0.9$).

For the two runs of figs. 3a and b, the beam momentum in the spectrometer arm was $p_{beam} = 26.6$ GeV/c, while the other beam had momentum 11.8 GeV/c

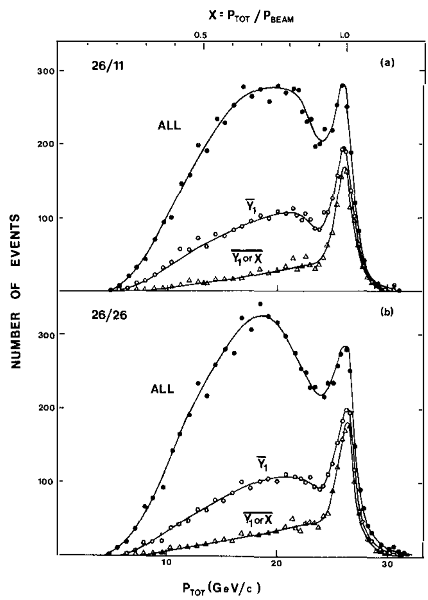

Fig.3 Inclusive $p\pi^+\pi^-$ spectrum.

($\sqrt{s}$ = 35 GeV) and 26.6 GeV/c ($\sqrt{s}$ = 53 GeV) respectively. In comparing these runs, at different s, the phase-space covered by the spectrometer is unchanged and no difference is observed in the production and decay of the multiparticle system (see fig. 4). Hence the effects of geometrical acceptance and all efficiencies cancel out in a first approximation. For the events in the peak one obtains:

$$\frac{\sigma(\sqrt{s} = 35)}{\sigma(\sqrt{s} = 53)} = 1.03 \pm 0.05 \qquad (3)$$

This result provides a test of limiting fragmentation(6), similar to the one by the Pisa-Stony Brook group(7) (comparing single-particle pseudo-rapidity distributions when the momentum of only one of the two beams is changed), but with magnetic analysis and applied to a specific reaction.

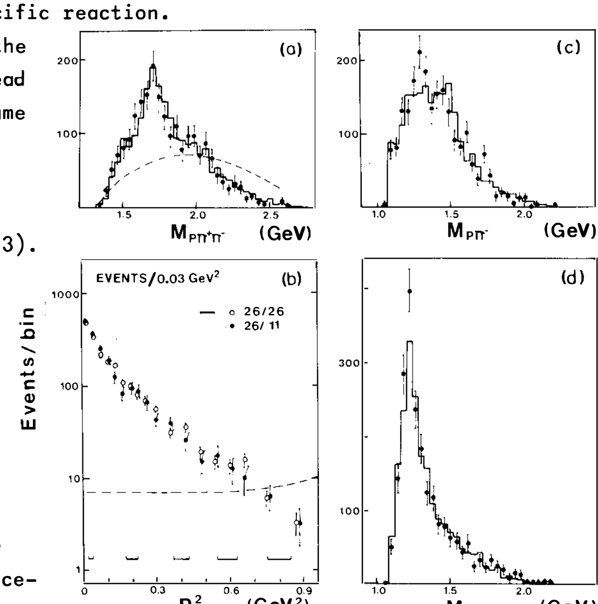

Fig. 4 Uncorrected distributions of (a) $p\pi^+\pi^-$ invariant mass (dashed curve shows the acceptance), (b) p_t^2, (c) $p\pi^-$ and (d) $p\pi^+$ invariant masses.

A comparison in the c.m. frame, instead of in the ISR frame as above, would give a result which negligibly differs from Eq.(3). The result then also implies s-indepenence of the invariant cross-section $E\, d^3\sigma/dp^3$, i.e. scaling(8).

A preliminary evaluation of the absolute acceptance-corrected cross-section gives (0.4 ± 0.1)mb (including a multiplication by a factor of two to allow for fragmentation of either proton) for $M(p\pi^+\pi^-) < 2.2$ GeV.

The $p\pi^+\pi^-$ mass spectrum (fig. 4a), dominated by a peak at ~ 1.7 GeV, will be examined in more detail when reporting the measurement on the exclusive reaction (2), the major contributor to reaction (1). A strong Δ^{++} (1236) signal is present in the $p\pi^+$ invariant mass spectrum (fig. 4d). Charge independence yields 9:1 for the ratio $(\Delta\pi)_{I=1/2} \rightarrow (p\pi^+)_{I=3/2}\pi^-$ to $\rightarrow (p\pi^-)_{I=3/2}\pi^+$. The relative suppression of a Δ^0 (1236) signal in the $p\pi^-$ invariant mass spectrum (fig. 4c) is compatible with a I = 1/2 dominance in the $p\pi^+\pi^-$ state. Evidence of isoscalar exchange is also provided by the observation[(2)] of reactions like (1) and (2) with the I = 1/2 system $\Lambda^0 K^+$ instead of $p\pi^+\pi^-$ (and cross-section of a few % of (1) and (2)).The sharp p_t dependence (fig. 4b) and the weak energy dependence (Eq.3) confirm the dominant diffractive production mechanism. Fig. 4b also shows no turn-off at small p_t^2.

Let us now examine X_2 as obtained with an inclusive trigger on $p\pi^+\pi^-$, and select events with momentum transfer small enough so that in the case of single dissociation (sd: $X_2 \equiv p_2$) the proton p_2 collinear to $\vec{p}_{tot}$ neither exits from the vacuum pipe nor interacts in it,and therefore no coincidence signals should be registered by the FRONT and BACK hodoscopes in arm 2. This is in fact the case for the majority of the events (NO HITS events, see fig. 5b). However HITS events also occur and in their p_{tot} distribution a peak is present at x = 1 (fig.5a). This peak, containing ~11% of all events with x > 0.9, provides evidence of double diffraction dissociation (dd). The clear

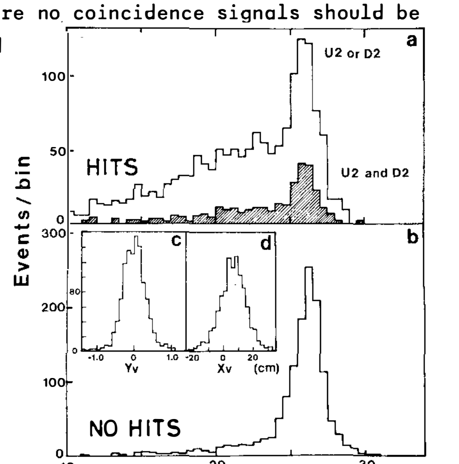

Fig.5 p_{tot} distribution with p_{X_2} inside the pipe. Projections of $p\pi^+\pi^-$ vertex (c,d) show absence of non beam-beam background identification of this process at the ISR is due to the large rapidity range which is available and which results in the separation of the two fragmentation regions. After corrections of losses, etc. the observed fraction of dd events is dd/(sd + dd) = (12 + 2.5)%. A test of Pomeron factorisation at the very small momentum transfers selected as described above ($< p_t^2 > = 0.03$ GeV/c^2), is obtained by comparing the above ratio to the ratio sd/(elastic + sd) $\simeq$ 13.5%, as evaluated from refs. (9) and (10) for the M and t ranges covered by our data.

For the study of reaction (2), the trigger required a particle through the MWPC telescope in arm 2 in coincidence with the inclusive trigger signal used for reaction (1), namely at least one particle in both the upper and lower half of the spectrometer and no signal in the barrel hodoscope X at large angles. Single diffractive events are positively identified by collinearity within a few mrad (see scatter plot in fig. 6) between $\vec{p}_{tot}$ and the track (p_2) detected in arm 2. The hatched p_{tot} distribution in fig. 6, obtained from a run at 22/22 GeV/c, shows that a background-free sample of single diffractive events is obtained. One also detects events where x ~ 1 and where in

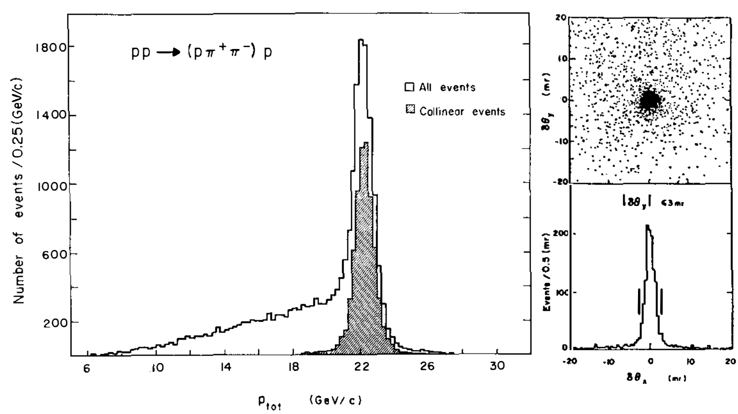

Fig.6 p_{tot} distribution with trigger for reaction (2) arm 2 there is a non-collinear track (i.e. $\neq p_2$), though having a common vertex with $(p\pi^+\pi^-)_1$. This gives further evidence of double diffraction dissociation. It also allows a test of factorisation which is exclusively based on data collected with the same apparatus, in identical experimental conditions, and implies a direct comparison of rates, rather than cross-sections. The experimental apparatus permits in fact the observation of reaction (1) with $X_2 \neq p_2$ i.e. dd, reaction (2), single dissociation in arm 2 $pp \rightarrow p_1X_2$ and elastic scattering $pp \rightarrow p_1p_2$. These reactions are related by the factorisation prediction :

$$\frac{d\sigma}{dt}(X_1X_2)\Big/\frac{d\sigma}{dt}(X_1p_2) = \frac{d\sigma}{dt}(p_1X_2)\Big/\frac{d\sigma}{dt}(p_1p_2) \qquad (4)$$

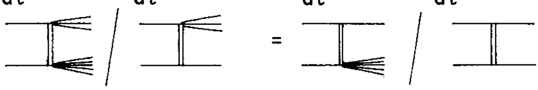

where the terms in parentheses are the various final states (all detected in the experiment) and $X_1 = (p\pi^+\pi^-)_I$. Because of the symmetrical fashion in which p_1, p_2, X_1 and X_2 enter into Eq. (4), effects of acceptance and of efficiencies cancel-out, and a relation similar to (4) holds for rates. We selected $M(p\pi^+\pi^-) < 1.85$ GeV, where the resonance centred at ~ 1.7 GeV dominates. As shown in Table 1 the result is consistent with factorisation over the full t-range covered by the arm 2 MWPC telescope and adds to our previous factorisation test at $t \sim 0$. Given that the exponential slope for single diffraction dissociation is in general smaller than the one for elastic scattering, this result implies that the slopes for single and double diffraction dissociation differ in the same fashion (see [5] also the preliminary results presented by Goggi at this meeting).

Table I. Factorisation test ($\sqrt{s} = 53$ GeV)

$-t$ range (GeV^2)	L.H.S./R.H.S. of Eq.4 (rates)
0.15 - 0.275	1.12 ± 0.14
0.275 - 0.40	1.15 ± 0.18
0.40 - 0.525	0.97 ± 0.15

For the study of reaction (2) we have used ~7000 events obtained in a run at 22/22 GeV/c colliding beam momenta ($\sqrt{s}$ = 45 GeV) where 2×10^6 triggers were recorded. As for reaction (1), the $M(p\pi^+\pi^-)$ distribution is dominated by a peak at ~1.7 GeV (fig. 7); a smaller structure is present at ~1.5 GeV. Similar features have been observed at incident laboratory momenta 10-30 GeV/c ; spin-parity analyses of diffractively produced $N\pi$ and $N\pi\pi$ systems(11) have led to their interpretation as being dominantly the nucleon resonant states N(1688) with $J^P=5/2^+$ and N(1520) with $J^P=3/2^-$ (among the states given by phase shift analyses in these mass ranges). Fits of the acceptance corrected $M(p\pi^+\pi^-)$ distribution with two Breit-Wigner amplitudes, added incoherently and superimposed to a fourth-order polynomial background (much reduced in comparison to low energies) have given for the central masses and widths of the peaks M = (1678±4) MeV, Γ= (148±16) MeV and M = (1500±8) MeV, Γ=(150±50)MeV respectively. This is consistent with their N(1688) and N(1520) interpretation. Dominance of $\Delta^{++}(1236)$ and relative suppression of a Δ^0 signal are in accordance with the I = 1/2 assignement. The geometrical acceptance of the apparatus has been calculated i) with a three-body phase-space description for the resonance decay and

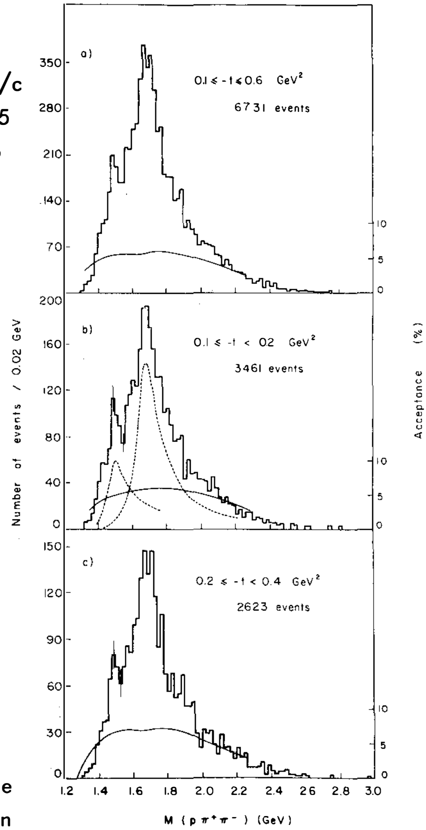

Fig.7 Experimental distributions of $M(p\pi^+\pi^-)$. Smooth curves represent the acceptance. Broken curves fitted resonances.

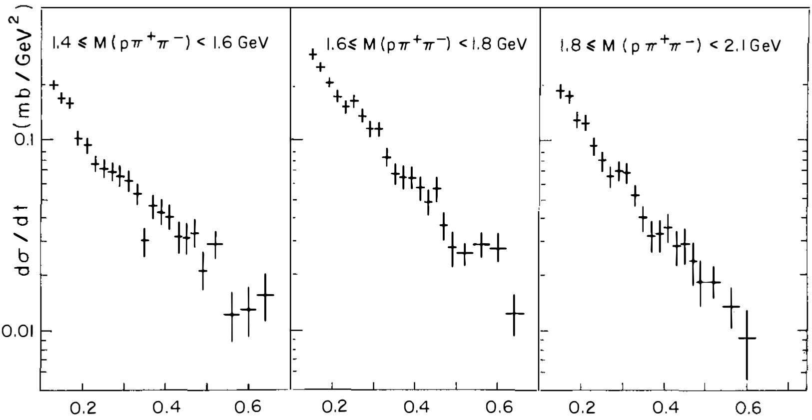

Fig.8 Differential cross-section $pp \Rightarrow (p\pi^+\pi^-)p$

also ii) for a decay through $\Delta^{++}(1236)$ with isotropic production and decay of the Δ^{++}; these different assumptions did not affect the results beyond quoted errors. We also note that a shorter run with a 26.6 GeV/c beam in the spectrometer arm (the acceptance is reduced by a factor ~2) and $\sqrt{s}$ = 53 GeV has provided acceptance-corrected mass distributions and cross-sections consistent with those obtained in the main run at 22/22 GeV/c. For a given $M(p\pi^+\pi^-)$ the acceptance changes by no more than 10% over the t-range of the experiment.

The acceptance-corrected differential cross-sections shown in fig. 8 suggest the presence of a structure at $-t \sim 0.2$ GeV^2. An analogous observation has been done (4) for the reaction $pp \rightarrow (n\pi^+)p$, as shown in fig. 9

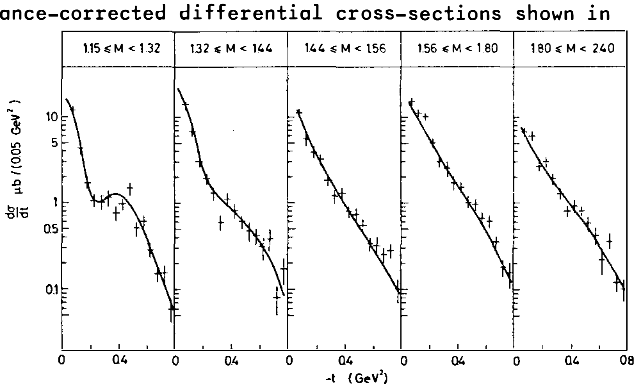

Fig.9 Differential cross-section $pp \Rightarrow (n\pi^+)p$ (refs. 4 and 12)

together with the fits by Humble[12], based on a peripheral impact parameter description for inelastic diffraction. According to this picture, the structure reflects the zero of the J_0 Bessel function which parametrizes the zero helicity flip amplitude, and for higher masses and maximum spins of the dissociated system gets washed out by the contributions from larger helicity flips. At approximately the t-value where indications of a structure exist for low masses, a change in slope is observed in fig. 4b. The fitted exponential slope in the $-t$ range 0.14-0.5 GeV^2 for the mass interval 1.6-1.8 GeV, i.e. essentially the N(1688), is $b = 6.3 \pm 0.4$ GeV^{-2}. At 24 GeV/c incident beam momentum the N(1688) slope is 5.1 ± 0.08 GeV^{-2} [13], implying a shrinking with increasing s which parallels the one for elastic scattering.

The total cross-section for $pp \to (p\pi^+\pi^-)p$ has been obtained by extrapolating to t=0 the measured $d\sigma/dt$ (a systematic error arising from the uncertainty in the forward slope has been allowed for in the error assignement). Introducing a factor of two to account for fragmentation of either proton, for $M(p\pi^+\pi^-) < 2.5$ GeV (from which the upwards arrows in fig.10) one obtains 0.33 ± 0.1 mb at $\sqrt{s} = 45$ GeV and 0.34 ± 0.1 mb at $\sqrt{s} = 53$ GeV. A comparison with cross-sections at accelerator energies indicates a decreasing s-dependence with increasing s. This is in accord with recent FNAL results [14] as well as with the invariance of the inclusive cross-section from $\sqrt{s} = 35$ to 53 GeV (Eq. 3). Fits to the $M(p\pi^+\pi^-)$ distribution give the fraction of the cross-section for reaction (2) which can be ascribed to the structures at 1.7 and 1.5 GeV: at $\sqrt{s} = 45$ GeV one obtains 0.19 ± 0.06 mb and 0.063 ± 0.02 mb respectively. Under the assumption that the observed structures are the

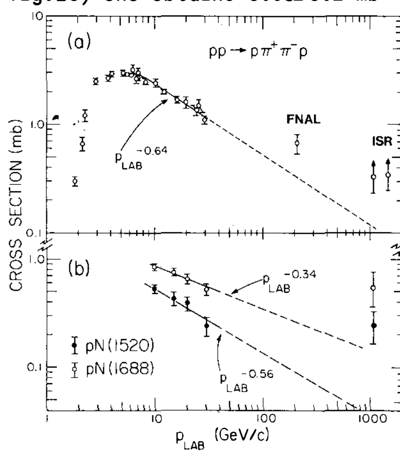

Fig.10 Total cross-sections for $pp = (p\pi^+\pi^-)p$, N(1520) p and N(1688) p

N(1688) and N(1520) and allowing for other decay modes of these resonances, for the reactions pp → N(1688)p and pp → N(1520)p one obtains 0.56±0.19 mb and 0.25±0.08 mb. As one can see from fig.10b, these cross-sections are practically unchanged from accelerator energies (the observed reduction in pp → $(p\pi^+\pi^-)$p is mainly due to the non-resonant background). Also in this respect there is a striking similarity with elastic scattering.

References

(1) M.G.Albrow et al.,Phys.Lett. 51B (1974) 424 and Nucl.Phys. (to be published)

(2) L.Baksay et al.,Measurements of pp → $(p\pi^+\pi^-)$ + X at the CERN ISR : scaling tests and evidence for double excitation, Contribution to the 17th Int.Conf. on High Energy Physics, London,June 1974.

L.Baksay et al.,Phys.Lett. 53B (1975) 484

L.Baksay et al.,Phys.Lett. 55B (1975) 491

(3) R.Webb et al.,Phys.Lett. 55B (1975) 331.

R.Webb et al.,Phys.Lett. 55B (1975) 336

(4) E.Nagy et al.,Experimental results on inelastic diffraction scattering in p-p collisions at the ISR,Contribution to the 17th Int.Conf. on High Energy Physics, London,June 1974.

(5) G.Goggi,Contribution to the X Rencontre de Moriond, 1975

(6) J.Benecke et al.,Phys.Rev. 188 (1969) 2159

(7) G.Bellettini et al.,Phys.Lett. 45B (1973) 69

(8) D.Amati et al.,Nuovo Cimento 26 (1962) 896, K.Wilson,Acta Physica Austriaca 17 (1963) 37 and R.P.Feynman,Phys.Rev.Lett. 23 (1969) 1415

(9) Y.Akimov et al.,p-d elastic scattering and diffraction dissociation from 50 to 400 GeV,Contribution to the 17th Int.Conf. on High Energy Phyisics, London,June 1974.

(10) U.Amaldi et al.,Phys.Lett. 44B (1973) 112

(11) see for example D.C.Colley et al.,Nucl.Phys. B55 (1973) 1 and Y.T.Oh et al.,Phys.Lett. 42B (1972) 497

(12) S.Humble,Nucl.Phys. B86 (1975) 285

(13) R.M.Edelstein et al.,Phys.Rev. D5 (1972) 1073

J.V.Allaby et al.,Nucl.Phys. B52 (1973) 316

(14) M.Derrick et al.,Phys.Rev. D9 (1974) 1215

COHERENT DIFFRACTION DISSOCIATION OF PROTONS ON DEUTERIUM AT HIGH ENERGIES*

STEPHEN L. OLSEN†
The University of Rochester
Rochester, New York 14627 (USA)

Abstract : We have measured p-d inelastic scattering at small momentum transfers by detecting the slow recoil deuterons from a deuterium gas jet target. We find that for low masses the cross section exhibits structure and is dominated by an enhancement at $M_x^2 \sim 1.9$ (GeV)^2. In the higher mass region, $M_x^2 \gtrsim 5.0$ (GeV)^2, we find the differential cross section $d^2\sigma/dtdM_x^2$ varies only slowly with energy and behaves to a good approximation as $1/M_x^2$.

Résumé : Nous avons observé la diffusion inélastique des protons sur une cible gaseuse de deuterium. Nous avons mesuré les impulsions des deuterons lents de recul. Pour des faibles masses, la section efficace a une structure et elle est dominée par un maximum vers $M_x^2 \sim 1.9$ (GeV)^2. Pour des masses plus grandes, $M_x^2 > 5.0$(GeV)^2, nous trouvons une section efficace differentielle $d^2\sigma/dtdM_x^2$ qui varie lentement avec l'energie incidente et qui, en bonne approximation, se comporte comme $1/M_x^2$.

†A. P. Sloan Fellow

*This experiment was done in collaboration with: Y. Akimov, R. Cool, L. Golovanov, K. Goulianos, D. Gross, A. Melissinos, E. Malamud, S. Mukhin, D. Nitz, H. Sticker, G. Takhtamyshev, V. Tsarev, R. Yamada and P.Zimmerman.

COHERENT DIFFRACTION DISSOCIATION OF PROTONS ON DEUTERIUM AT HIGH ENERGIES

In an experiment performed at the Fermi National Accelerator Laboratory, we studied the coherent inclusive reaction

$$p + d \rightarrow X + d$$

at small momentum transfer.[1,2] Here we report results for $m_p^2 < M_x^2 < 30$ $(\mathrm{GeV})^2$, at energies ranging from 50 to 400 GeV.

The target consisted of a deuterium gas jet placed in the internal beam of the accelerator. The recoil deuterons were detected in stacks of two silicon solid state detectors of thickness typically 200μm for the front and 1500μm for the rear detector. Only recoils stopping in the rear detector were accepted, and deuterons were unambiguously identified by the energy deposited in each detector. The detectors were placed on a moveable holder near 90° with respect to the beam direction, at a distance of 2.5m from the target with each stack subtending a solid angle of 16×10^{-6} steradians.

At a fixed recoil angle ω (measured from 90°) the mass M_x^2 is given by

$$M_x^2 = m_p^2 + 2P[\sin\omega \sqrt{|t|} - \frac{m_d + P}{2Pm_d} |t|]$$

where P is the incident momentum and $|t|$, the four-momentum transfer, is given by

$$|t| = 2m_d T$$

with T the kinetic energy of the recoil deuteron. The data were normalized by using a fixed detector stack which measured elastic scattering at $|t| = 0.043\ (\mathrm{GeV/c})^2$. The elastic p-d cross-section was taken to be

$$\left.\frac{d\sigma}{dt}\right|_{e\ell} = \frac{(\sigma_t(pd)^2}{16\pi} (1 + \rho^2)\ e^{-b|t| + ct^2}$$

with σ_t^{pd} the total pd cross-section and ρ the ratio of real to imaginary part of the forward elastic scattering amplitude. The parameters b and c were determined by simultaneous measurements which were made for elastic scattering.[3]

The resolution in M_x^2 is dominated by the uncertainty in the recoil angle, $\Delta\omega$. Detector size and the width of the jet limit $\Delta\omega$ to about ±3 mrad. It holds that

$$M_x^2 \simeq 2p\sqrt{|t|}\ \Delta\omega$$

For measurements in the low mass region (M_x^2 near m_p^2) at the higher incident energies we used a slit to limit the extent of the jet target (along the beam direction) seen by a particular detector. This reduced $\Delta\omega$ to ±1.2 mrad. Furthermore, slit scattering was monitored by running a jet at low energy (50 GeV) where essentially no inelastic protons are produced over the useful kinetic energy range covered by the detector. Since the elastic scattering is so dominant, the bulk of slit scattered deuterons originate from the elastic peak which is (practically) independent of the incident energy. Thus the 50 GeV slit data could be used to measure the background present at higher energies. Use of the slit is limited to $M_x^2 \lesssim 4\ \mathrm{GeV}^2$ because, to assure proper normalization, each detector must also monitor elastic scattering (i.e., be located at small angles).

The maximum M_x^2 reached is proportional to the incident energy. Since the Feynman scaling variable x, defined as $P_{||}/P_{max}$ of the deuteron in the c.m. system, is given by

$$1 - x \simeq \frac{M_x^2 - m_\rho^2}{2m_d{<}P_{lab}} \simeq \frac{\sqrt{|t|}}{m_d}\left(\sin\omega - \frac{\sqrt{|t|}}{2m_d}\right) ,$$

each detector samples the same x region independent of the incident energy. An ideal situation for testing scaling behaviour.

At the higher missing masses the counting rates are low and background from recoil deuterons which enter the detector stacks after rescattering from the walls of the scattering chamber becomes appreciable. We observed some recoils in the unphysical region $M_x^2 < m_p^2$ at a level of $\sim 3 \times 10^{-4}$ of the elastic counts at the same $|t|$ value. This was observed to be independent of angle over the range it could be observed. To correct for this we made a background subtraction which amounted to as much as a 15% correction to the results for the higher masses. The resulting cross section for $|t| = 0.035$ and $0.05\ (\text{GeV/c})^2$ and $P_{lab} = 275$ GeV is shown in Fig. 1. We note the existence of a prominent broad enhancement

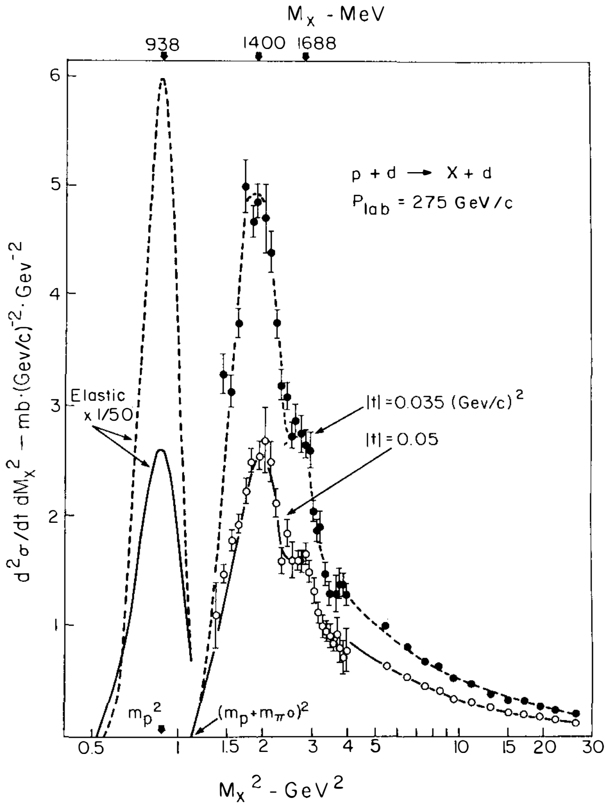

Fig. 1 - Differential cross sections vs. M_x^2 for $t=0.035$ and $0.05\ (\text{GeV/c})^2$ and $P_{lab} = 275$ GeV/c.

in the region $M_x^2 \simeq 1.9\ \text{GeV}^2$ and a small second peak or shoulder at $M_x^2 = 2.8\ \text{GeV}^2$ which is probably the $N^*(1688)$ nucleon resonant state. For the higher masses the cross section falls smoothly approximately as $1/M_x^2$.

We have fitted the differential cross-sections with the form

$$\frac{d^2\sigma}{dtdM_x^2} = A(s,M_x^2)e^{-b(s,M_x^2)(|t| - 0.05) + c(t^2 - 0.05^2)}$$

The value for c was taken from the deuteron coherence factor $F_d(t)$ defined as

$$F_d(t) \equiv \frac{\frac{d\sigma}{dt}(pd\to pd)}{\frac{d\sigma}{dt}(pp\to pp)} \simeq \frac{\sigma_T^2(pd)}{\sigma_T^2(pp)}\ e^{-b_o|t| + ct^2}$$

Here $b_o = 26\ (GeV/c)^{-2}$ and $c = 62.3\ (GeV/c)^{-4}$ are preliminary results from the analysis of the pd elastic scattering experiment[3]. If factorization is valid, the relation

$$\frac{d^2\sigma}{dtdM_x^2}(pd \to Xd) = \frac{d^2\sigma}{dtdM_x^2}(pp \to Xp)\ F_d(t)$$

should hold at small values of $|t|$. In this case the results of the fit for b can be related to the corresponding slope values for the pp reaction b_N by $b_N = b-b_o$. Our results indicate an abrupt variation over the low mass range and a more or less constant behaviour for $M_x^2 \gtrsim 5$ GeV. At $M_x^2 = 1.9\ GeV^2$, $b_N \simeq 24\ GeV^{-2}$, while for $M_x^2 = 2.8$, $b_N \simeq 12\ GeV^{-2}$ and for $M_x^2 \gtrsim 5\ GeV^2$, $b_N \simeq 7\ GeV^{-2}$. This change from roughly twice the value for the elastic pp slope parameter to half the elastic slope value has been observed in pp interactions at lower energies.[4] There was no evidence for any turnover in the cross section for values of $|t|$ down to $\sim .03\ (GeV/c)^2$. The factorization of the cross-section, at least for the lower masses, is demonstrated by comparing our results divided by the coherence factor with the results from a measurement of $pp \to Xp$.[5] This comparison is shown in Fig. 2. The data are consistent with the factorization hypothesis at least to the 10~20% level.

The energy variation of the low mass cross-section is shown in Fig. 3. Here the 20 GeV data from Edelstein et al., are included.

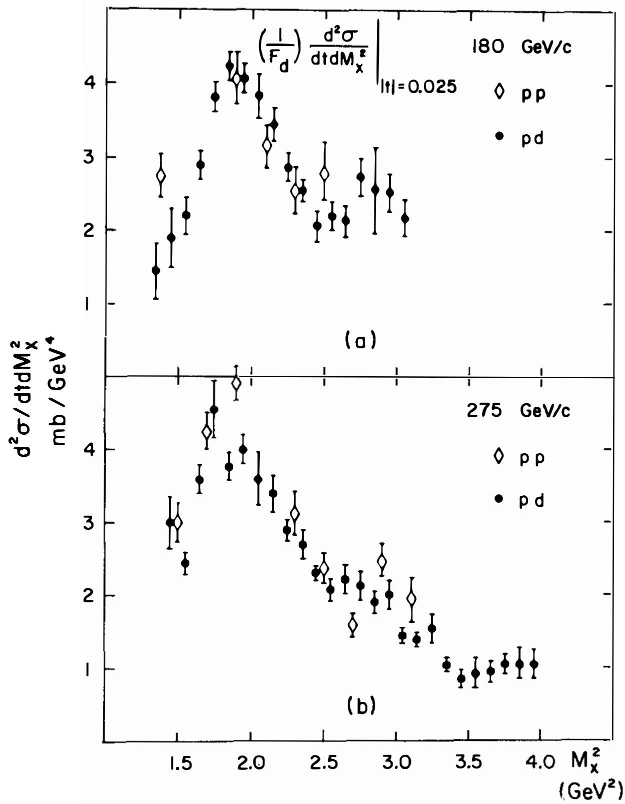

Fig. 2 - a) A comparison of $(1/F_d)(d^2\sigma/dtdM_x^2)\big|_{|t|=0.025}$ at 180 GeV 175 GeV pp data (ref. 5);

b) A similar comparison of our 275 GeV data with the 260 GeV data of ref. 5.

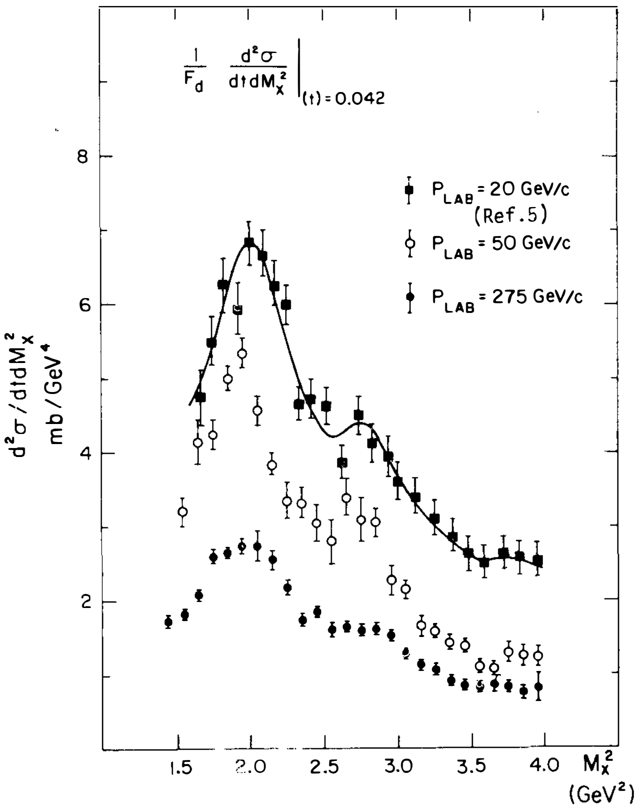

Fig. 3 - A comparison of our results for $(1/F_d)\left(\frac{d^2\sigma}{dtdM_x^2}\right|_{t=0.042}$ at 50 GeV and 275 GeV with the 20 GeV pp results reported in ref. 4.

The data are consistent with a constant cross section for the production of the M_x^2 = 1.9 and 2.8 GeV^2 states together with a smooth "non resonant" background which decreases with energy.

We have fit our data for $M_x^2 \gtrsim 5$ GeV^2 to the formula

$$\left.\frac{d^2\sigma}{dtdM_x^2}\right|_{|t|=0.05} = \frac{D}{(M_x^2)^\alpha}$$

This yielded the following results

P_{lab}	M_x^2 range GeV^2	$D(Mb/GeV^4)$	α	χ^2/d.f.
150	5.0 - 15.0	4.38 ± 0.33	1.068 ± .035	1.10
275	5.0 - 26.0	3.63 ± 0.17	1.028 ± .019	0.83
385	5.0 - 38.0	3.19 ± 0.15	1.004 ± 0.017	1.90

The values of α obtained from the fit are consistent with unity and a fit with α constrained to $\alpha = 1$ ($d^2\sigma/dtdM_x^2 \propto 1/M_x^2$) is statistically acceptable. These results are in general agreement with the fit of triple Regge formulae of Kaidalov et al[6].

This experiment was carried out as a joint effort between Soviet physicists from Dubna and American physicists from Fermilab, Rockefeller University and Rochester. Working in this international collaboration has been quite exciting both scientifically and socially. We were ably assisted by the Fermilab staff, in particular Drs. D. Jovanovic and P. Martsch of the Internal Target Lab, for which we are deeply grateful. Finally, we would like to thank Dr. R. R. Wilson of Fermilab and Dr. A. Baldin of the J.I.N.R. for their enthusiastic support and encouragement.

References

1. Y. Akimov et al., "Excitation of High Energy Protons into Low Mass States in p-d Interactions," Submitted to Phys. Rev. Lett.
2. Y. Akimov et al., "Diffraction Dissociation of High Energy Protons in p-d Interactions," submitted to Phys. Rev. Lett.
3. Y. Akimov et al., to be published.
4. R. M. Edelstein et al., Phys. Rev. D5, 1073 (1972).
5. V. Bartenev et al., Phys. Letters 51B, 299 (1974).
6. A. B. Kaidalov et al., Phys. Letters 45B, 493 (1973).

PRELIMINARY RESULTS ON DOUBLE DIFFRACTION DISSOCIATION AND DOUBLE ISOBAR PRODUCTION IN THE REACTION $pp \rightarrow (p\pi^+\pi^-)(p\pi^+\pi^-)$ STUDIED WITH THE S.F.M. AT THE CERN ISR

G. Goggi

Istituto di Fisica Nucleare, Università di Pavia, Italy
Istituto Nazionale di Fisica Nucleare, Sezione di Pavia, Italy

M. Cavalli Sforza, C. Conta, M. Fraternali, G. Goggi, F. Impellizzeri, G.C. Mantovani, F. Pastore, S. Ratti, B. Rossini, H. Sadrozinski, D. Scannicchio (Pavia-Princeton collaboration)

Abstract: Preliminary data are presented on the reaction $pp \rightarrow (p\pi^+\pi^-)(p\pi^+\pi^-)$ studied with the SFM at the CERN ISR, at three energies $\sqrt{s}$ = 23 GeV, 31 GeV, 53 GeV. Mass spectra of the systems $(p\pi^+\pi^-)$ show evidence for the double isobar production $pp \rightarrow N(1688)N(1688)$. Differential cross sections $d\sigma/dt$ are given. Comparison of slopes and mass distributions for double and single dissociation seems to support the hypothesis of factorization of diffractive cross sections.

Résumé : Nous présentons les données préliminaires sur la réaction pp $(p\pi^+\pi^-)(p\pi^+\pi^-)$ obtenues aux ISR à 3énergies $\sqrt{s}$ = 23 GeV, 31 GeV, 53 GeV. Le spectre de masse des systèmes $(p\pi^+\pi^-)$ montre l'évidence pour la production de 2 isobars $pp \rightarrow N(1688)N(1688)$. La comparaison des pentes et des distributions de masse pour les dissociations diffractives simples et doubles montre que l'hypothèse de la factorisation semble être vérifiée.

Single and double diffraction dissociation are processes responsible for a non negligible fraction of the total high energy collision cross sections. Their comparison may give relevant information on the mechanisms at work[1]. Factorization of production amplitudes and cross sections has been tested at low energies to be valid for several reactions (both diffraction-like or exchange-like) at a level of about 90%[2]. In the case of diffraction dissociation this may be connected with the rôle played by Pomeron exchange in diffractive phenomena.

We present preliminary data on the reaction

$$pp \rightarrow (p\pi^+\pi^-)(p\pi^+\pi^-) \qquad (1)$$

presently under investigation at the ISR at five different energies, using the Split Field Magnet Detector[3]. Statistics is available to date for $\sqrt{s}$ = 23, 31 and 53 GeV.

Events with low masses ($\lesssim$ 3 GeV) decaying symmetrically in the two opposite telescopes of the SFM were triggered, selected and geometrically reconstructed. The signature of the six prong events is characterized by a large rapidity gap between the two final ($p\pi^+\pi^-$) systems imposed by a veto on charged particles produced at (90 $\pm$ 45°).

The events have been fitted kinematically to reaction (1). Momentum balance with fitted and measured quantities clearly shows a strong correlation between rejected events and missing neutrals.

Fig. 1 shows the correlation between the value of the beam momentum reconstructed from the final particles in each telescope and the χ^2-value for the fit, as obtained at our highest energy.

We estimated that at this preliminary stage accepting events fitting reaction (1)

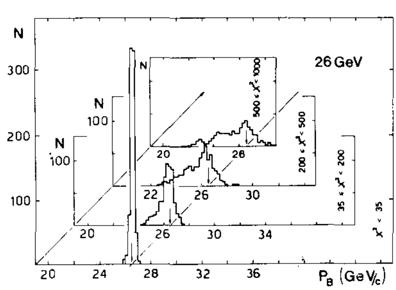

Fig. 1 - Reconstructed beam momentum for different χ^2 intervals at $\sqrt{s}$ = 53 GeV.

with $\chi^2 \leqslant 35$ is a safe criterion to select our statistical samples.

The χ^2-distributions (not shown) are such that a cut at $\chi^2 = 35$ reasonably reproduces a theoretical distribution for a 4-constraint fit superimposed to a flat background.

The numbers of events used in the present analysis are collected in Table I.

TABLE I

$\sqrt{s}$	N. of events $\chi^2 \leqslant 35$
23	537
31	498
53	403

The $(p\pi^+\pi^-)$ mass spectra for either of the two dissociated systems at the three energies are shown in Fig. 2. Structures around 1.4 and 1.7 GeV appear over a smooth distribution dominated by small-mass final states.

These data are not yet corrected for the acceptance of the apparatus and therefore some distortions in the spectra are to be expected. However the overall detection efficiency is a smooth function of $M(p\pi^+\pi^-)$ in the interval 1.5 GeV-2.5 GeV and falls off at threshold and for very large masses. In particular the structures in the region of N(1688) cannot be canceled out. The general shape of the distribution does not vary appreciably in the whole energy range investigated and compares very well with the corresponding spectra obtained in single $(p\pi^+\pi^-)$ excitation[4].

The produced $(p\pi^+\pi^-)$ systems are dominated by the presence of the $\Delta(1236)$ isobar. The $\Delta^{++}/\Delta^{\circ}$ ratio in the spectra of the $(p\pi)$ subsystems (shown in Fig. 3 only for $\sqrt{s}$ = 23 GeV) supports at all energies an isospin composition of the final state consistent with diffractively produced I = 1/2 systems $|1/2,1/2\rangle$ decaying into a $\Delta\pi$ pair in the ratio

$$R = \frac{|1/2,1/2\rangle \longrightarrow (\Delta^{++}\pi^-)}{|1/2,1/2\rangle \longrightarrow (\Delta^{\circ}\pi^+)} = \frac{9}{1} \qquad (2)$$

Particularly significant is the production of at least one N(1688) isobar (Fig. 2).

Selecting events with one of the two masses in the region of the

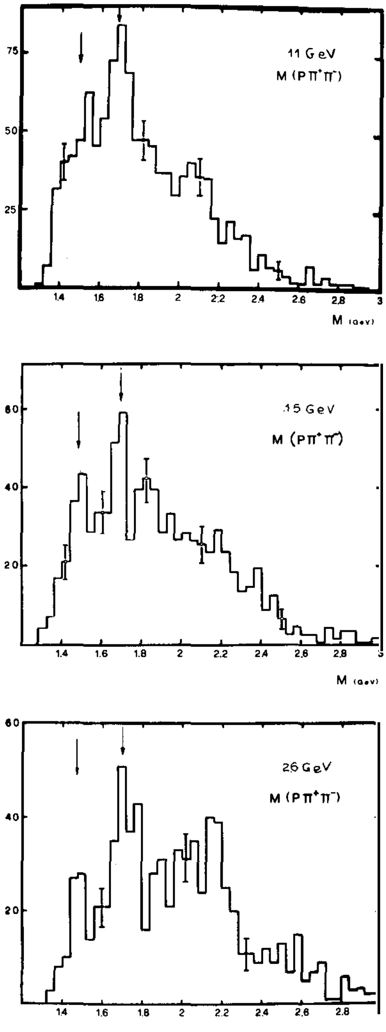

Fig. 2 - Mass spectra of the $p\pi^+\pi^-$ systems from reaction (1) at $\sqrt{s}$ = 23, 31 and 53 GeV; both values plotted for each event.

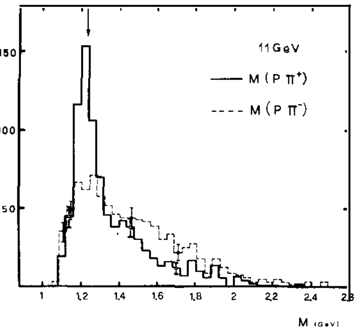

Fig. 3 - Mass distributions of the (p π) subsystems for reaction (1) at $\sqrt{s}$ = 23 GeV.

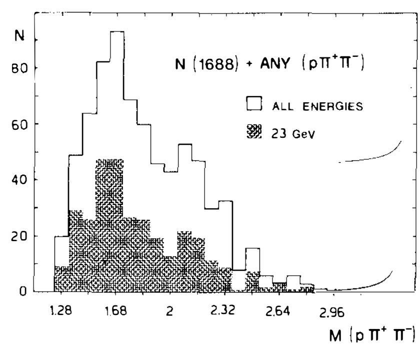

Fig. 4 - Mass distribution of one ($p\pi^+\pi^-$) system for reaction (1), the other mass constrained in the N(1688) band.

N(1688) at all energies produces a mass distribution of the companion ($p\pi^+\pi^-$) combination as shown in Fig. 4. The prominent structure in the same mass region, provides a supporting evidence for the double isobar production

$$pp \longrightarrow \underset{\hookrightarrow (p\pi^+\pi^-)}{N(1688)} + \underset{\hookrightarrow (p\pi^+\pi^-)}{N(1688)} \qquad (3)$$

The signal for this channel is particularly clear at $\sqrt{s}$ = 23 GeV (hatched histogram in Fig. 4); however it is present at all energies. Similar enhancements are present also with different mass cuts.

The four momentum transfer-square distributions are collected in Fig. 5, for all final state masses (Fig. 5a) and for a sample enriched in pp→N(1470)N(1470) (Fig. 5b). Due to a lack in statistics, at $\sqrt{s}$ = 53 GeV the latter distribution has been substituted by the useful sample (see later) enriched in $pp \rightarrow N(1470)X(p\pi^+\pi^-)$, where $X(p\pi^+\pi^-)$ stands for any mass of the final state (open circles in Fig. 5b).

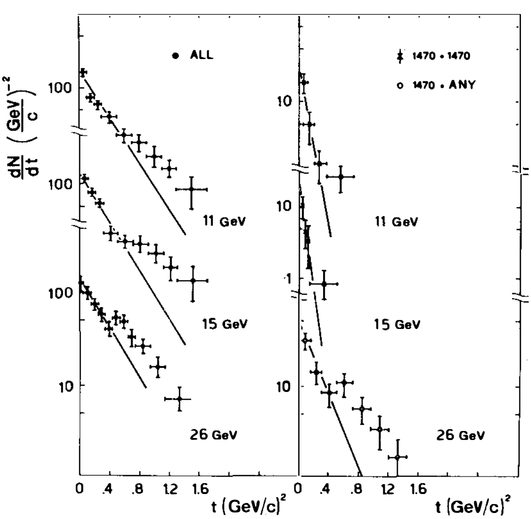

Fig. 5 - Differential distributions at three energies for all events and for selécted mass intervals. Typical slopes are b~4 (all), b~12 (2x1470), b~6 (1470·any)

The slopes of the distributions for all events are definitely smaller than those measured for single dissociation (1) but the distributions exhibit striking similarities with them; i.e. 1) there are structures in $d\sigma/dt$ at values around .3 ÷ .4 GeV/c; 2) such structures tend to become clearer with increasing energy.

The data of Fig. 5b show that there is a fourfold increase in the exponential slope for the events enriched in low $(p\pi^+\pi^-)$ masses in both telescopes of the SFM and, as easily expected, an intermediate value of the slope b ($b \sim 5$ $(GeV/c)^{-2}$) if an integration on all possible final masses in one telescope is performed.

In order to further investigate the slope-mass correlation and to compare the results with those obtained in the single diffractive channel[5]

$$pp \longrightarrow p(n\pi^+) \qquad (4)$$

at $\sqrt{s}$ = 53 GeV, we selected symmetrical masses in both telescopes and plotted in Fig. 6 the dependence of the slope b on the mass $M(p\pi^+\pi^-)$ for our sample at $\sqrt{s}$ = 53 GeV.

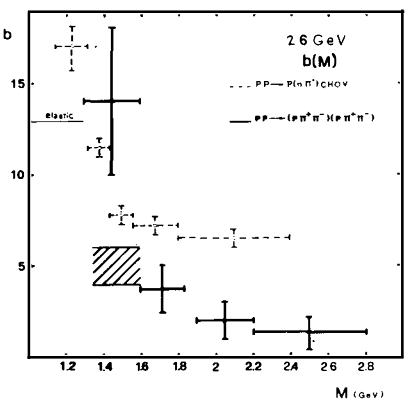

Fig. 6 - Exponential slopes as a function of excitation mass at $\sqrt{s}$ = 53 GeV for single and double dissociation.
The elastic slope is also shown.
The dashed region represents the slope obtained in reaction (1) (double dissociation) constraining one of the two masses in the N(1470) band.

In Fig. 6 the dashed points represent values from reaction (4). The value of b for elastic scattering is also indicated. On pure empirical grounds we observe that the behaviour of the slope-mass correlation is such that in double dissociation symmetric production of small masses results in a steeper slope than in single production of the same masses. The double production of symmetric large masses is on the contrary flatter in t than the corresponding single production.

We further observe that the two slope-mass functions cross-over at a value of b which is not different from that of the elastic slope.

It is very tempting to infer from these observations that reac tions (1) and (4) share a common diffractive nature and that the coincidence of the cross over point with the elastic slope may support the idea of factorization of the diffractive scattering amplitudes.

REFERENCES AND FOOTNOTES

1 - G. Goggi: Single and Double Diffraction Dissociation at FNAL and ISR Energies. This issue p.

2 - see a) Proceedings of the III International Colloquium on Multiparticle Reactions at Zakopane - Report Nr. 1421/VI/PH (1972) Warszawa

b) Proceed. of the IV International Symposium on Multiparticle Hadrodynamics at Pavia - Ed. by F. Duimio, A. Giovannini, S. Ratti (1973) Pavia

c) G. Tomasini, E. Bassler, M. Sahini, P.K. Schilling, P. Borzatta, G. Cecchet, L. Liotta, S. Ratti, A. Daudin, M.L. Faccini, M.A. Jabiol, Nuovo Cimento 7 A, 651, 821 (1972); 13 A, 1102 (1973)

3 - Double Isobar Production at ISR. Proposal to study the reaction $pp \to (p\pi^+\pi^-)(p\pi^+\pi^-)$; Pavia Princeton Collaboration CERN/ISRC/72-23

4 - see for instance Figs. 10 and 11 of reference 1

5 - W. Barth, A. Brandt, C. Broll, G. Coignet, H. Dibon, J. Favier, G. Flugge, Ch. Gottfried, L. Massonet, E. Nagy, G. Neuhofer, F. Niebergall, M. Regler, K.R. Schubert, M. Vivargent, K. Winter - Proceedings of the XVII International Conference on High Energy Physics, London (1974) s. also C. Broll, this issue p.

EXPERIMENTAL RESULTS ON LARGE ANGLE ELASTIC PP SCATTERING AT THE CERN ISR

CERN - HAMBURG - ORSAY - VIENNA COLLABORATION

Presented by E. NAGY

ABSTRACT

New experimental results are presented on proton-proton elastic scattering at centre-of-mass energies $\sqrt{s}$ = 23 GeV and $\sqrt{s}$ = 62 GeV. The data are obtained using the Split-Field-Magnet detector at the CERN Intersecting Storage Rings (ISR). The differential cross sections show an energy dependent behaviour: the pronounced diffraction minimum at $t \approx -1.3$ GeV^2 is moving inwards with increasing energy and the cross section at the second maximum is increasing with $\sqrt{s}$.

RESUME

Nous présentons de nouveaux résultats expérimentaux sur la diffusion élastique pp à grand angle pour des énergies au centre de masse de $\sqrt{s}$ = 23 GeV et $\sqrt{s}$ = 62 GeV. Les données ont été obtenues avec le détecteur SFM (Aimant à Champ Fractionné) des ISR (Anneaux de Collisions) au CERN. Le comportement de la section efficace différentielle est dépendant de l'énergie: le minimum diffractif observé à $t \approx -1.3$ GeV^2 se déplace vers l'intérieur quand l'énergie croît, et la section efficace du deuxième maximum augmente avec $\sqrt{s}$.

Since the first observation[1] of a pronounced minimum in the differential cross section of elastic proton-proton scattering at momentum transfers $t \approx -1.3$ GeV^2, it has been an open question whether this structure is depending on the reaction energy. New data have been obtained over the centre-of-mass energy range $\sqrt{s}$ = 23 GeV to 62 GeV using the Split-Field-Magnet Detector (SFM) at the CERN Intersecting Storage Rings (ISR). We are reporting here results[2] at the two extreme energies, corresponding to integrated luminosities of 1.1×10^7/mbarn at 23 GeV and 2.3×10^7/mbarn at 62 GeV, and discuss the observed s-dependence of the differential cross section.

The SFM Detector has been described before[3]: it contains two forward telescopes equipped with 28 multi-wire proportional chambers of 2 mm wire spacing, most of them 1 m high and 2 m wide. Each chamber has a vertical and a horizontal wire plane. The average magnetic field is 1.0 Tesla resulting in a momentum resolution for elastically scattered protons of $\Delta p/p = \pm 0.04$ to ± 0.09. The acceptance for elastic events increases from about 0.3 at the polar scattering angle Θ = 15 mrad to about 0.7 at 250 mrad. The data acquisition speed is about 100 events/sec.

The trigger is defined in two steps; a fast trigger using signals from the proportional chambers and a slow trigger using their memory levels[4]. The fast trigger, requiring at least one particle in each telescope, results in a rate corresponding to nearly the total pp cross section. The memory level trigger (decision time ≈ 2 μsec) requires rough collinearity of the two tracks and the absence of further tracks. It also determines the scattering angle Θ of the event and allows a Θ-dependent scaling-down; all events with large t and only a well defined fraction of events with low t are recorded onto magnetic tape. The memory level logics reduces the trigger rate by a factor 100 to 1000. The recorded events are passed through three analysis programs, performing track recognition, track fitting in the magnetic field and a kinematical fit. The results presented here are based on 380,000 (420) elastic events at 62 GeV and 63,000 (270) at 23 GeV (in brackets we give the number of events beyond the diffraction minimum).

In order to determine absolute differential cross sections, we have to apply t-dependent acceptance corrections and an overall normalization factor. The acceptance of the detector is calculated using Monte Carlo methods. This simulation takes into account the beam positions and their size, particle trajectories in the magnetic field, the detector geometry, absorption and scattering in the ISR beam tube and in the detector material, the trigger conditions, proportional chamber inefficiencies and losses in the reconstruction program and in the event selection. The quality of the simulation has been extensively checked by comparing distributions in the azimuthal scattering angle of real and Monte Carlo events at fixed t values. Great care is taken in calculating the length ℓ of traversed material. The largest uncertainty in acceptance is resulting in this part of the calculation, and therefore an estimated systematical uncertainty of ±0.2 of the average length $\langle \ell \rangle$ is taken into account in the evaluation of the cross section.

The absolute normalization is obtained by collecting monitor counts simultaneously with data taking. A scintillation counter monitor has been calibrated using the Van der Meer method[5]. The systematic accuracy of the monitor is estimated to be ±5% by comparing elastic scattering cross sections determined in different subsets of the data.

We present the evaluated cross sections in the t-region where the beam tube absorption uncertainties do not exceed ±15%, i.e. for $-t > 0.2$ GeV^2 at 62 GeV and for $-t > 0.02$ GeV^2 at 23 GeV. The results are shown in figure 1 and table 1. The error bars represent (added quadratically) the statistical errors of the data, the statistical errors of the acceptance calculation and the estimated systematical uncertainty of absorption in the beam tube[*)]. No background has been subtracted; a study of the collinearity-χ^2-distribution in several t-bins has shown that the background contamination is less than 5% for $|t| \leqslant 1.2$ GeV^2. In the region of larger t, the contamination is estimated to be less than 3.10^{-6} mbarn/GeV^2 at both energies.

*) The systematical errors are not independent in different t-bins.

TABLE 1

Differential cross section of pp elastic scattering data.

$\sqrt{s}$ = 62 GeV			
-t	Δt	dσ/dt	Error*
GeV^2		mbarn/GeV^2	
.210	.02	.9559E+01	.17E+01
.230	.02	.7550E+01	.13E+01
.250	.02	.5437E+01	.89E+00
.270	.02	.4165E+01	.66E+00
.290	.02	.3046E+01	.47E+00
.310	.02	.2452E+01	.37E+00
.330	.02	.2054E+01	.30E+00
.350	.02	.1729E+01	.25E+00
.370	.02	.1467E+01	.21E+00
.390	.02	.1196E+01	.17E+00
.410	.02	.1010E+01	.14E+00
.430	.02	.8296E+00	.12E+00
.450	.02	.6319E+00	.87E-01
.470	.02	.5331E+00	.73E-01
.490	.02	.4180E+00	.56E-01
.525	.05	.2721E+00	.36E-01
.575	.05	.1629E+00	.22E-01
.625	.05	.8607E-01	.12E-01
.675	.05	.5038E-01	.72E-02
.725	.05	.2324E-01	.35E-02
.775	.05	.1490E-01	.25E-02
.850	.10	.7742E-02	.12E-02
.950	.10	.2075E-02	.39E-03
1.050	.10	.5448E-03	.72E-04
1.150	.10	.9262E-04	.20E-04
1.250	.10	.2702E-04	.94E-05
1.350	.10	.5046E-04	.13E-04
1.450	.10	.3462E-04	.99E-05
1.550	.10	.6103E-04	.14E-04
1.650	.10	.6555E-04	.14E-04
1.750	.10	.7026E-04	.15E-04
1.850	.10	.9147E-04	.17E-04
1.950	.10	.6014E-04	.14E-04
2.100	.20	.5932E-04	.10E-04
2.300	.20	.3593E-04	.70E-05
2.500	.20	.2586E-04	.55E-05
2.700	.20	.1801E-04	.40E-05
2.900	.20	.7185E-05	.23E-05
3.100	.20	.9892E-05	.29E-05
3.300	.20	.3849E-05	.17E-05
3.500	.20	.3216E-05	.14E-05

* Errors include statistical and systematical errors added quadratically. An additional overall scale error of +/- 5% should be added to these figures at each energy.

Warning : The systematical errors may not be independent in different t-bins.

Table 1 (continued)

$\sqrt{s}$ = 23 GeV			
-t	Δt	dσ/dt	Error*
GeV^2		mbarn/GeV^2	
.030	.02	.5192E+02	.91E+01
.050	.02	.3962E+02	.55E+01
.070	.02	.3228E+02	.40E+01
.090	.02	.2586E+02	.30E+01
.110	.02	.1860E+02	.21E+01
.130	.02	.1393E+02	.15E+01
.150	.02	.1151E+02	.12E+01
.170	.02	.9079E+01	.90E+00
.190	.02	.8101E+01	.78E+00
.210	.02	.6066E+01	.64E+00
.230	.02	.4817E+01	.49E+00
.250	.02	.4272E+01	.41E+00
.270	.02	.3477E+01	.33E+00
.290	.02	.2708E+01	.25E+00
.310	.02	.2121E+01	.19E+00
.330	.02	.1766E+01	.16E+00
.350	.02	.1286E+01	.11E+00
.370	.02	.1214E+01	.11E+00
.390	.02	.9842E+00	.89E-01
.410	.02	.7037E+00	.60E-01
.430	.02	.6151E+00	.53E-01
.450	.02	.4416E+00	.39E-01
.470	.02	.3906E+00	.36E-01
.490	.02	.3812E+00	.32E-01
.525	.05	.2492E+00	.16E-01
.575	.05	.1473E+00	.95E-02
.625	.05	.9168E-01	.62E-02
.675	.05	.6374E-01	.45E-02
.725	.05	.4297E-01	.32E-02
.775	.05	.2395E-01	.18E-02
.825	.05	.1608E-01	.86E-03
.875	.05	.1021E-01	.59E-03
.925	.05	.6614E-02	.36E-03
.975	.05	.3865E-02	.22E-03
1.025	.05	.2515E-02	.16E-03
1.075	.05	.1504E-02	.10E-03
1.125	.05	.8880E-03	.71E-04
1.175	.05	.4664E-03	.46E-04
1.225	.05	.2356E-03	.30E-04
1.275	.05	.1075E-03	.20E-04
1.325	.05	.5429E-04	.14E-04
1.375	.05	.3037E-04	.10E-04
1.450	.10	.8165E-05	.37E-05
1.550	.10	.2067E-04	.58E-05
1.650	.10	.2635E-04	.65E-05
1.750	.10	.4384E-04	.84E-05
1.850	.10	.5492E-04	.98E-05
1.950	.10	.4582E-04	.92E-05
2.050	.10	.3373E-04	.79E-05
2.150	.10	.3660E-04	.82E-05
2.250	.10	.2973E-04	.74E-05
2.350	.10	.2810E-04	.72E-05
2.500	.20	.2279E-04	.46E-05
2.700	.20	.1425E-04	.35E-05
2.900	.20	.6718E-05	.24E-05
3.100	.20	.1098E-04	.33E-05
3.300	.20	.2853E-05	.17E-05
3.500	.20	.2727E-05	.16E-05

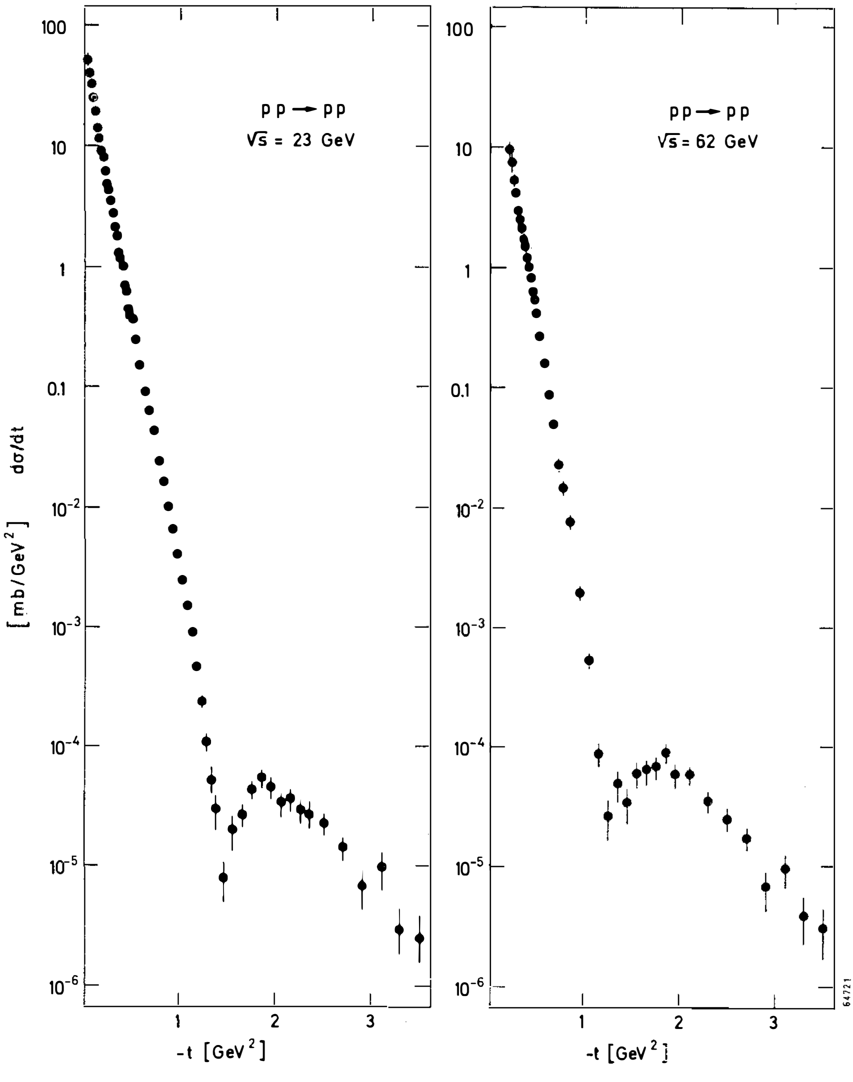

FIGURE 1

Differential cross sections of elastic proton-proton scattering at the two extreme ISR energies. The error bars represent statistical and estimated systematical errors for each t-bin. An additional overall scale uncertainty of ±5% is to be added separately for each energy.

A dominant property of the differential cross section is the narrow minimum near $t = -1.3$ GeV^2. This has already been observed at the three other ISR energies, 31, 45 and 53 GeV, by Böhm et al.[1)] without conclusions on its energy dependence. Our data show clearly that the position of the minimum changes to lower values of $|t|$ for increasing energy as expected from diffraction on an object of increasing radius. To determine the precise position of the minimum, we attempt to describe the data by a function[6)] of the form

$$\frac{d\sigma}{dt} = \left|\sqrt{A}\, e^{Bt/2} + \sqrt{C}\, e^{Dt/2 + i\phi}\right|^2 , \qquad [1]$$

folding it with the experimental resolution in t. The Monte Carlo simulation gives one-standard-deviation resolutions of $\Delta t = \pm 0.013$ GeV^2 at 23 GeV and ± 0.028 GeV^2 at 62 GeV in the vicinity of the minimum. Equation [1] gives an excellent description of the data in the t range between -0.6 and -3.6 GeV^2, the best fit values for the position of the minimum being:

$$t_{min} = -(1.44 \pm 0.02)\ \text{GeV}^2 \ \text{at}\ \sqrt{s} = 23\ \text{GeV}$$

$$t_{min} = -(1.26 \pm 0.03)\ \text{GeV}^2 \ \text{at}\ \sqrt{s} = 62\ \text{GeV}\ .$$

The errors include the one-standard-deviation of the fit and an estimated systematical uncertainty in the t scale of $\Delta t = 0.008(0.015)$ GeV^2 at 23(62) GeV.

We note the following further features of the data:

1. Between $t = -0.25$ GeV^2 and $t = -0.6$ GeV^2, $d\sigma/dt$ has an exponential shape compatible with energy-independence.
2. The slope between -0.6 GeV^2 and -1.1 GeV^2 increases with energy.
3. The differential cross section at the second maximum, as determined by averaging the experimental cross section in a t-range of ± 0.2 GeV^2 around the fitted maximum position, is rising with energy.
4. $d\sigma/dt$ for $-t > 2.0$ GeV^2 is again compatible with energy-independence.

	$b\,[GeV^{-2}]$ $t\varepsilon[-0.25,-0.6]$	$b\,[GeV^{-2}]$ $t\varepsilon[-0.6,-1.1]$	$t_{min}\,[GeV^2]$	$\frac{d\sigma}{dt}\left(2^{nd}_{max}\right)\left[\frac{mb}{GeV^2}\right]$	$\sigma_{tot}\,[mb]$ 7)
$\sqrt{s}$ = 62 GeV	10,3 ±0,3	11,8 ±0,3	1,26±0,03	$(7{,}2\pm1{,}0)10^{-5}$	44,1 ±0,9
$\sqrt{s}$ = 23 GeV	10,3 ±0,2	9,1 ±0,1	1,44±0,02	$(4{,}5\pm0{,}5)10^{-5}$	38,7 ±0,7
Ratio	1,00±0,04	1,29±0,04	$(1{,}14\pm0{,}02)^{-1}$	$(1{,}27\pm0{,}11)^{2}$	1,14±0,03
Scaling 8) Prediction	$\alpha\ R^2$	$\alpha\ R^2$	$\alpha\ R^{-2}$	$\alpha\ R^4$	$\alpha\ R^2$

TABLE 2

Observations 1. to 3. and the position of the minimum are summarized in table 2, where we also show values of the proton-proton total cross section[7]. The ratios of the observed quantities at $\sqrt{s}$ = 62 GeV and $\sqrt{s}$ = 23 GeV can be compared to the predictions derived from the hypothesis of geometrical scaling[8]. If the opacity of the colliding protons is a function of only one variable $\rho = \frac{r}{R(s)}$, where r is the impact parameter, the observed quantities should depend on the scaling parameter R(s) as given in line 4. Property 4. of the data has been predicted in a two-amplitude model of Phillips and Barger[6]; elastic scattering in the large t region is described by coherent superposition of two exponential amplitudes where the second one is energy-independent and the first one is shrinking with increasing energy. We have tested this hypothesis by fitting the two data sets in the range -0.6 to -3.6 GeV^2 with equation [1] and imposing equal values of the parameters C and D for both energies. The quality of the fit is good as can be seen in figure 2.

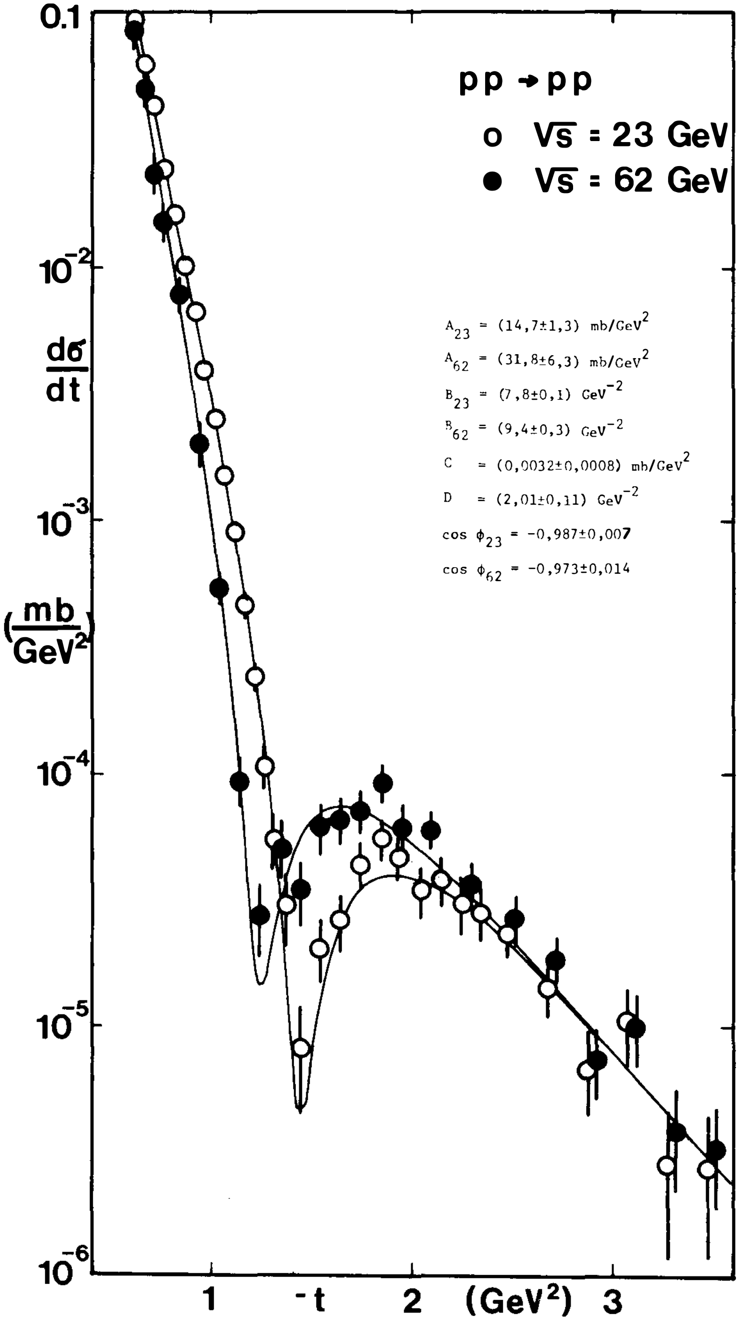

FIGURE 2

Differential cross sections for momentum transfer $-t > 0.6$ GeV^2. The t resolution in the vicinity of the minimum is ±0.013 GeV^2 at 23 GeV and ±0.028 GeV^2 at 63 GeV. The solid lines represent the best fit results of a two-amplitude model[6]*.*

REFERENCES

1. A. Böhm, M. Bozzo, R. Ellis, H. Foeth, M.I. Ferrero, G. Maderni, B. Naroska, C. Rubbia, G. Sette, A. Staude, P. Strolin and G. De Zorzi, Physics Letters 49B(1974)491.

2. Preliminary results of this experiment were presented at the XVII International Conference on High Energy Physics, London 1974.

3. R. Bouclier, G. Charpak, E. Chesi, L. Dumps, H.G. Fischer, H.J. Hilke, P.G. Innocenti, G. Maurin, A. Minten, L. Naumann, F. Piuz, J.C. Santiard and O. Ullaland, Nuclear Instruments and Methods 115(1974)235.

4. A. Brandt, H. Dibon, G. Flügge, F. Niebergall, K.R. Schubert, P.E. Schumacher and W. Wilmsen, A memory level decision for a 50.000 wire proportional chamber detector. To be published in Nuclear Instruments and Methods, April 1975.

5. S. Van der Meer, CERN Internal Report ISR-PO/68-31.

6. R.J.N. Phillips and V. Barger, Physics Letters 46B(1973)412.

7.a. U. Amaldi, R. Biancastelli, C. Bosio, G. Matthiae, J.V. Allaby, W. Bartel, G. Cocconi, A.N. Diddens, R.W. Dobinson and A.M. Wetherell, Physics Letters 44B(1973)112.

b. S.R. Amendolia, G. Bellettini, P.L. Braccini, C. Bradaschva, R. Castaldi, V. Cavasinni, C. Cerri, T. Del Prete, L. Foa, P. Giromini, P. Laurelli, A. Menzione, L. Ristori, G. Sanguinetti, M. Valdata, G. Finochchiaro, P. Grannis, D. Green, R. Mustard and R. Thun, Physics Letters 44B(1973)119.

c. K. Eggert, H. Frenzel, K. Giboni, W. Thomé, B. Betev, P. Darriulat, P. Dittmann, M. Holder, K.T. McDonald, T. Modis, H.G. Pugh, K. Tittel, V. Eckardt, H.J. Gebauer, R. Meinke, O.R. Sander and P. Seyboth, A measurement of the proton-proton cross section at the CERN ISR. Submitted to the Palermo Conference, June 1975.

8. J. Dias de Deus, Nuclear Physics B59(1973)231.
A.J. Buras and J. Dias de Deus, Nuclear Physics B71(1974)481.

ELASTIC SCATTERING IN THE REGGEON CALCULUS

AT ISR ENERGIES

A. CAPELLA, J. TRAN THANH VAN
Laboratoire de Physique Théorique et Particules Elémentaires, Orsay
J. KAPLAN
Laboratoire de Physique Théorique des Hautes Energies, Paris

Abstract : This talk contains two parts. The first part is a very brief review of some important aspects of the Reggeon Calculus. The second part deals with a perturbative approach relevant at present energies and its application to elastic scattering. The work described in this second part is the result of a collaboration between J. Kaplan, J. Tran Thanh Van and myself.

Résumé : Cet exposé contient deux parties. La première partie est un bref résumé de quelques aspects importants du Calcul de Reggeons. La deuxième partie traite d'une approche perturbative utilisable aux énergies actuelles et son application à la diffusion élastique. Le travail décrit dans cette deuxième partie est le résultat d'une collaboration entre J. Kaplan, J.Tran Thanh Van et moi-même.

The Reggeon Calculus is a t-channel dynamical theory of strong interactions - or at least of two body processes. The first contribution one considers is t-channel Pomeron exchange, i.e. a pole at $j = \alpha(t)$, with $\alpha(0) \approx 1$.[(*)] In order to implement t-channel unitarity, one considers, next, the contributions of graphs containing n Pomerons in the t-channel. In a field theoretical language these diagrams correspond to the emission of n Pomerons by the initial state of the t-channel and their subsequent absorption by the final state. Finally, one considers the graphs corresponding to the emission of n Pomerons which interact among them before being absorbed by the final state. (In the following, we shall restrict ourselves to 3-Pomeron interactions). The rules to compute these graphs are given by the Reggeon Calculus Technique due to Gribov[(1)] following a method originally introduced by Sudakov. It turns out that for a Pomeron of intercept exactly equal to one, the graphs without Pomeron interaction - called non-enhanced graphs - are asymptotically non-leading as compared to the pole. (This corresponds to the well known fact that an n Pomeron cut is depressed by a factor $(\ln s)^{-n+1}$). On the contrary, the graphs containing Pomeron interactions - called enhanced graphs - are dominant as compared to the pole. (This is only true in the case of a triple Pomeron coupling that does not vanish when all three Pomerons are massless. In what follows, we shall restrict ourselves to this case). The larger the number of 3-Pomeron interactions in an enhanced graph, the more important its asymptotic behaviour. Thus to get the asymptotic behaviour of a two body amplitude, one has to find the asymptotic behaviour of the sum of all the graphs containing triple Pomeron interactions.

It is possible to formulate the Reggeon Calculus as a non-relativistic theory for a quasi-particle (Pomeron), in 2 space dimensions and 1 time dimension, and obtain the asymptotic behaviour of the sum of all graphs using renormalization group techniques. Let me remind you very briefly how this is done. Let us consider the case of an input (bare) Pomeron with a linear trajectory

$$\alpha(q_T^2) = \alpha(0) - \alpha'(0)\, q_T^2 \quad ,$$

(*) To begin with the Pomeron is represented by a ladder diagram. However, in the Reggeon Calculus, one computes the asymptotic behaviour of any graph in terms of the asymptotic behaviour of the various ladders i.e one replaces each ladder by a Pomeron propagator.

where q_T is the tranverse momentum transfer (at high energies $t = -q_T^2$). Defining an "energy" E equal to 1 minus the angular momentum, $\alpha(q_T^2)$, one gets

(1) $E(q_T^2) = \alpha'(0)\, q_T^2 + 1 - \alpha(0)$,

which is analogous to the equation of a non-relativistic particle with mass $m = 1/2\, \alpha'(0)$ and energy gap $1 - \alpha(0)$. The important point is that one gets from the Gribov rules for the Reggeon diagrams that the energy E is conserved at the three Pomeron vertices (this is only true when 2 of the 3 Pomerons form a closed loop, i.e. when one considers a two body process).

The next step is to associate a quantized field $\psi(\vec{X},t)$ to the quasi-particle (Pomeron). Here t is the Fourier conjugate of the energy E- conserved at the vertices - and $\vec{X}$ are two space dimensions Fourier conjugate of $\vec{q}$ - which is obviously also conserved at the vertices. Finally, one writes a Lagrangian for the field $\psi(\vec{X},t)$. Its non-interacting part is determined by the fact that the equation of motion coïncide with eq.(1). For the interacting part, it is possible [(2),(3)] to write a cubic term in such a way that the Feynman rules associated to it - together with the commutation rules for the field - are identical to the Gribov's rules for the Reggeon graphs.

It can be seen from eq. (1) that if the Pomeron intercept is exactly equal to one, i.e. $\alpha(0) = 1$, one has $E(0) = 0$. Then, the conservation of E at the vertices implies that the singularities of the Reggeon graphs pile up at $E = 0$. One encounters an infrared problem which has been solved using group renormalization techniques. With these techniques one gets [(3), (4)] the following asymptotic behaviour of the total cross-section

(2) $\sigma_T(s) = C_1 (\ln s)^{\eta} + C_2 (\ln s)^{\eta - 1/2} + \ldots$

Here η is a critical exponent, independent of the quantities appearing in the lagrangian.

We shall not discuss the asymptotic solution (2) any further. Our aim is to argue that this solution is not valid at present energies and to develop a perturbative expansion relevant at those energies. The fact that one should not expect the solution (2) to be valid at ISR energies with only a few terms, can be made plausible by the following argument. Let us consider the Y-graph and the loop graphs (figs 1b and 1c). The latter behaves asymptotically as ln s and it is one of the graphs that build up the first term in eq. (2). The Y-graph has an asymptotic behaviour in ln ln s and contributes to the second term in eq. (2) - and not to the first term. However, at ISR energies the contribution of the Y-graph is one order of magnitude larger than that of the loop graph. Thus one does not expects C_2 in eq. (2) to be smaller than C_1 and in general a great deal of terms in eq. (2) will be needed at ISR energies.[7] The loop graph is proportional to the dimensionless quantity $(r^2/16\pi\,\alpha')\ln s$, where α' is the Pomeron slope and r the triple Pomeron coupling. With $\alpha' \sim 0.25\ \mathrm{GeV}^{-2}$ and the value of r obtained[5] from inclusive pp → pX data in the diffractive region, one gets for this quantity 0.01 ln s - which explains that even at the highest ISR energies (ln s ∼ 8) the loop graph contribution is very small. This provides the justification for a perturbative expansion, the graphs containing the second power of r being already very small, even at the highest ISR energies. In this perturbative approach the only diagrams that are important up to ISR energies are those shown in fig. 1. The diagram 1a - 1c can be computed when one knows the Pomeron trajectory, the particle-particle- Pomeron coupling and the triple Pomeron coupling (as indicated above the latter can be obtained from inclusive data). In order to compute the diagrams 1d without introducing extra parameters, one can use duality arguments for the Pomeron-particle amplitude, i.e., the energy integral of the imaginary part of these amplitudes is replaced, at low energies, by a sum of resonances and at high energies by (integrated) Pomeron exchange (for details see ref. 5). I am not going to discuss the phenomenological applications of this perturbative approach in any detail. I shall refer to the original publications [5]. Let me indicate here the main results and compare them to the asymptotic solution (2).

First of all it turns out that for a large range of values of the parameters, the contribution to, say, the total proton-proton cross-section of the sum of all the diagrams in fig. 1 (diffractive term) is not very far from a linear form in ln s(a + b ln s). Thus, if one has to explain the observed rise of σ_T^{pp} with such a diffractive term, its extrapolation to conventional accelarator energies will give a contribution much smaller than data (see fig. 2). Therefore, in order to describe the data at all energies one has to introduce secondary Regge trajectories with a large exchange degeneracy breaking. In this way, one obtains a good fit of the data on both σ_T and Re/Im for proton-proton scattering with only four parameters. The results are shown in figs 2 and 3 and details of the fit are given in the Figure Caption. Despite the large exchange degeneracy breaking exhibited in

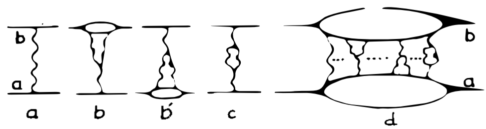

Fig. 1

The graphs in the Reggeon Calculus that are important up to ISR energies.

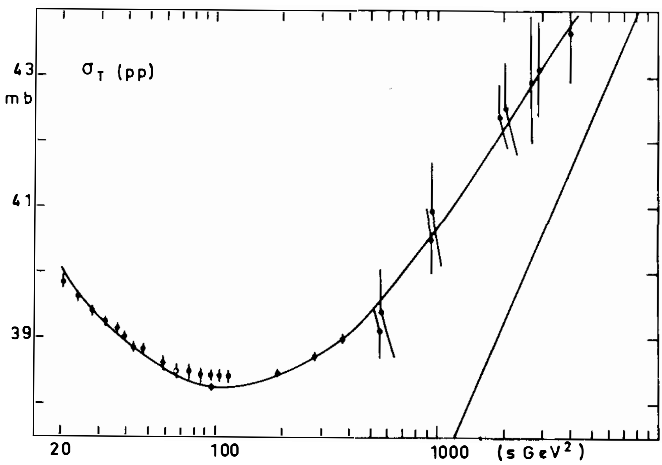

Fig. 2

Proton-Proton total cross-section. The curve is a fit containing four parameters : two for the diffractive term - the Pomeron intercept and the p-p-P coupling - and two for the f Regge trajectory - intercept and residue. (the contributions of the ω, ρ and A_2 Regge trajectories were obtained from difference of nucleon-nucleon total cross-sections). The(nearly) straight line is the contribution of the diffractive term with $\alpha_P(0) \sim 1.13$. The value of this diffractive term at 15 GeV/c is 27 mb. Note the large exchange degeneracy breaking.

fig.2, one gets the correct shrinking of the diffractive peak with a conventional value of the Pomeron slope ($\alpha' = 0.25$ GeV^{-2}). The intercept of the Pomeron turns out to be appreciably larger than one, $\alpha_p(0) \sim 1.13$. With this value of the Pomeron intercept it is possible to describe the data on total cross-sections for all elastic reactions. (see second ref. in (5)).

Finally, let me compare the above results with the asumptotic solution of references (3) and (4) (eq. (2)). The relevant question is the following : what is the position of the final J-phase singularity that corresponds to the intercept of the bare Pomeron we have found ($\alpha_p(0) \sim 1.13$). In the first references (3) and (5) and in (6) a formula was given that allows one to compute the renormalization of the Pomeron intercept due to the insertion of Pomeron loops in the Pomeron propagator, as a function of the triple Pomeron coupling r. In the Reggeon Calculus this renormalization is negative, i.e. tends to take the Pomeron intercept back to one. However, according to that formula, this renormalization effect is very small - of the order of 10^{-2} for the experimental value of r - and therefore the intercept of the bare Pomeron obtained above is practically unchanged and well above one. This is different from the case studied in references (3), (4) where one chooses to have the renormalized Pomeron exactly equal to one. Had we made the same choice we should have had a diffractive term that does not increase at all with s in the whole ISR energy region [(5)].

In our solution, due to a Pomeron intercept larger than one, the s-channel iterations (fig. 1d) - which were non leading in the asymptotic solution [(3),(4)] - become crucial at asymptotic energies in order to restore the Froissart bound. In fact, one expects at ultra high energies a behaviour in $(\ln s)^2$. At ISR energies, we have seen that a behaviour approximately linear in ln s is obtained instead.

In conclusion the perturbative approach we have advocated, appears to be a good candidate to describe physics up to ISR energies with a small number of parameters. However, the results we have obtained in the framework of this perturbative approach do not support the asymptotic solution of the Reggeon Calculus, with a Pomeron intercept chosen exactly equal to one.

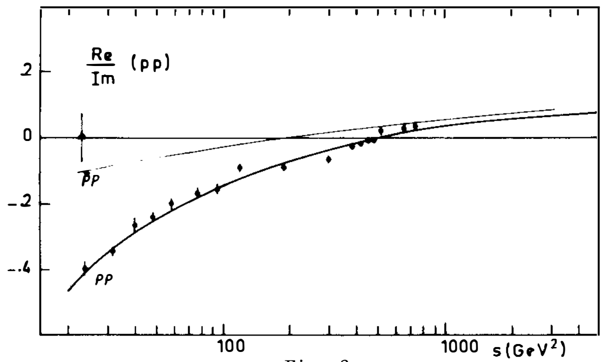

Fig. 3

Ratios of Real over Imaginary parts of proton-proton and proton-antiproton scattering. The curves are the result of a fit with the same four parameters of Fig. 2.

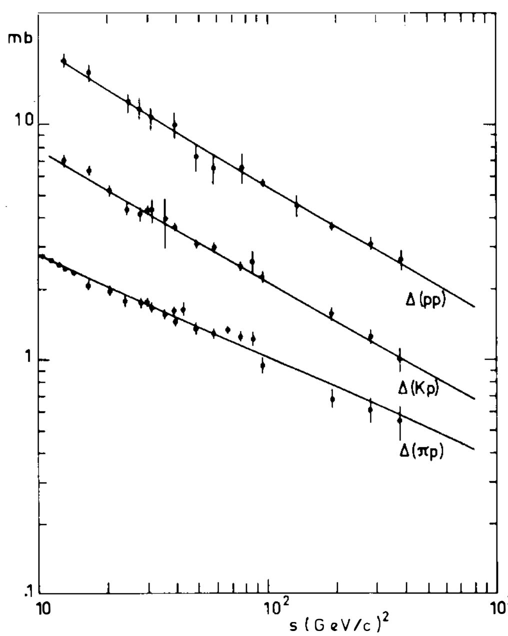

Fig. 4

Fit of differences of total cross-sections using universality. The best fit gives $\alpha_{\omega}(0) = 0.40$, $\alpha_{\rho}(0) = 0.57$. (For details see the second paper in ref. 5).

REFERENCES

1. V.N. Gribov, Zh Eksp. Teor. Fiz. 53 (1967) 654 ; Sov. Phys. Jetp 26 (1968) 414
2. V.N. Gribov and A.A. Migdal, Sov. Nucl. Phys. 8 (1969) 583 ; Yad. Fiz 8 (1968) 1002
3. A.A. Migdal, A.M. Polyakov, K.A. Ter Martirosyan, Phys. Lett. 48B (1973) 239 and ITEP report 1973 H.D.I. Abarbanel and J.B. Bronzan, Phys. Lett. 48B (1974) 345 ; Phys. Rev. D9 (1974) 2397.
4. J. Ellis and R. Savit. CERN preprint TH (1974) and contribution to this meeting.
   M. Baker, Phys. Lett. 51B, 158 (1974) and preprint ITEP (Moscou) 1974
   J.B. Bronzan and J. Dash, Phys. Letters 51B, 496 (1974)
5. A. Capella and J. Kaplan. Phys. Lett. 52B (1974) 448.
   A. Capella, J. Kaplan, J. Tran Thanh Van, Orsay preprint, to be published.
6. R.L. Sugar and A.R. White, N.A.L. preprint 74/59 THY (1974)
7. See also Amati's communication to this Rencontre.

HOW MUCH CAN WE TRUST THE REGGEON CALCULUS?

C.E. DeTar*)

CERN, Geneva, Switzerland

and

MIT, Cambridge, Mass., USA

Abstract: Some questions are raised regarding the generality of recent solutions of the reggeon calculus near J = 1 and their implications for the high-energy behaviour of the elastic scattering amplitude.

Résumé: Quelques questions se posent à propos de l'applicabilité générale des solutions récemment trouvées au calcul des reggeons autour de J = 1 et de leurs conséquences concernant la dépendance, aux hautes énergies, de l'amplitude de diffusion élastique.

---

*) A.P. Sloan Foundation Fellow

I would like to make a few short remarks in the hope of stimulating the discussion of an important and as yet incompletely answered question, namely: To what extent can the reggeon calculus be thought of as a theory complete enough to tell us something fundamental about hadron scattering at high energies?[1] What I have in mind specifically is the question, To what extent is s-channel unitarity incorporated in the calculus? (s is the asymptotic variable).

To draw attention to the elements of the problem, I refer to Fig. 1, which in my view shows the relationship between the various developments of the calculus. The basic motivation of the reggeon calculus was a set of J-plane discontinuity formulas which follow from the assumption of the existence of a factorizable Regge pole and from t-channel unitarity, projected and continued into complex t-channel angular momentum J [2]. The formulas resemble rather closely the unitarity equations one would write in a non-relativistic theory with energy $E = 1 - J$ and two-vector momentum k_T, the transverse momentum transfer. Hence they could as well be called J-plane unitarity equations. The Regge poles in these equations are supposed to be physical (fully renormalized) singularities. These equations are, of course, very difficult to solve directly. However, just as ordinary Feynman perturbation theory can be thought of as a clever way of constructing solutions to ordinary unitarity, one can imagine seeking a corresponding "solution" to the J-plane unitarity equations. Such a solution is the reggeon field theory, a non-relativistic Lagrangian field theory[3]. The perturbative solution to the theory has a graphical representation called the reggeon calculus and can be shown to satisfy the J-plane discontinuity formulas order-by-order in the perturbation theory, where the Regge poles in this case are the bare (unrenormalized) singularities. Of course, as with ordinary field theory, one is mainly interested in the properties of the solutions to the reggeon field theory. Recently, powerful field theoretic techniques (renormalization group) have been applied in an attempt to find one extremely interesting property of the full solution, namely, the nature of the J-plane singularity at $J = 1$ and the corresponding ultra-high-energy behaviour of the elastic scattering amplitude[4]. The result is that the elastic scattering amplitude has the ultimate asymptotic behaviour

$$A(s,t) \sim i\ s(\log s)^{\eta}\ F\left[t(\log s)^{\nu}\right] , \qquad (1)$$

where μ and ν are determined.

As I see it, there are two basic theoretical problems connected with the reggeon field theory. The first is the usual problem of which

Lagrangian to choose. There are many alternatives which lead to solutions of the J-plane discontinuity formulas. My friends who work with the reggeon field theory tell me that this does not lead to a great deal of arbitrariness in the values of μ and ν, because these quantities are mysteriously independent of the fine details of the Lagrangian[5]. However, certainly the rate of approach to the asymptotic behaviour (1) is affected by the choice of Lagrangian, and so, therefore, is the energy beyond which the solution can be compared with experiment. The second problem is whether the reggeon field theory incorporates s-channel unitarity. Since the J-plane discontinuity formulas arise from t-channel unitarity, one might well ask whether some essential information is being omitted from an approach devoted strictly to the J-plane. Some well-known s-channel constraints are easily translated into the J-plane language. The Froissart bound, derived from elastic s-channel unitarity, forbids singularities to the right of J = 1, or so strong as to cause the elastic amplitude to grow faster than s $(\log s)^2$. Thus it is possible *a posteriori* to limit the choice of Lagrangians in the reggeon field theory (or the nature of solutions sought) so that the results are not in plain contradiction to s-channel unitarity; but, since bounds like Froissart's need not express the full content of s-channel unitarity (who can say that inelastic unitarity might not give a more stringent bound?), one can never be completely sure that a given restriction on the Lagrangian is adequate.

To put the s-channel problem in a more vivid light, it is interesting to consider yet another route to the reggeon calculus. This route starts with ordinary perturbation theory (Fig. 1). Historically, this approach predates the reggeon field theory[6]. It is well known that in some field theories, e.g. $\lambda\phi^3$, sums of ladder graphs lead to Regge poles. Thus one might imagine a scheme in which graphs in a given field theory are summed in a particular order so that ladders are summed first. This would then lead, if done properly[1], to a perturbation theory in which the basic propagators were Regge poles and the basic amplitudes, multi-reggeon scattering amplitudes. It is thought that doing a J-plane projection of these amplitudes then leads to the diagrams in the reggeon calculus. Although no one has ever done it, one could well imagine a similar exercise starting with the dual resonance model, focusing on the Pomeron singularity. The vertices in the reggeon calculus obtained in this way are more complicated than those usually chosen for the reggeon field theory -- they have structure. [The general form of such an expansion has been used as a basis for phenomenological applications[7].]

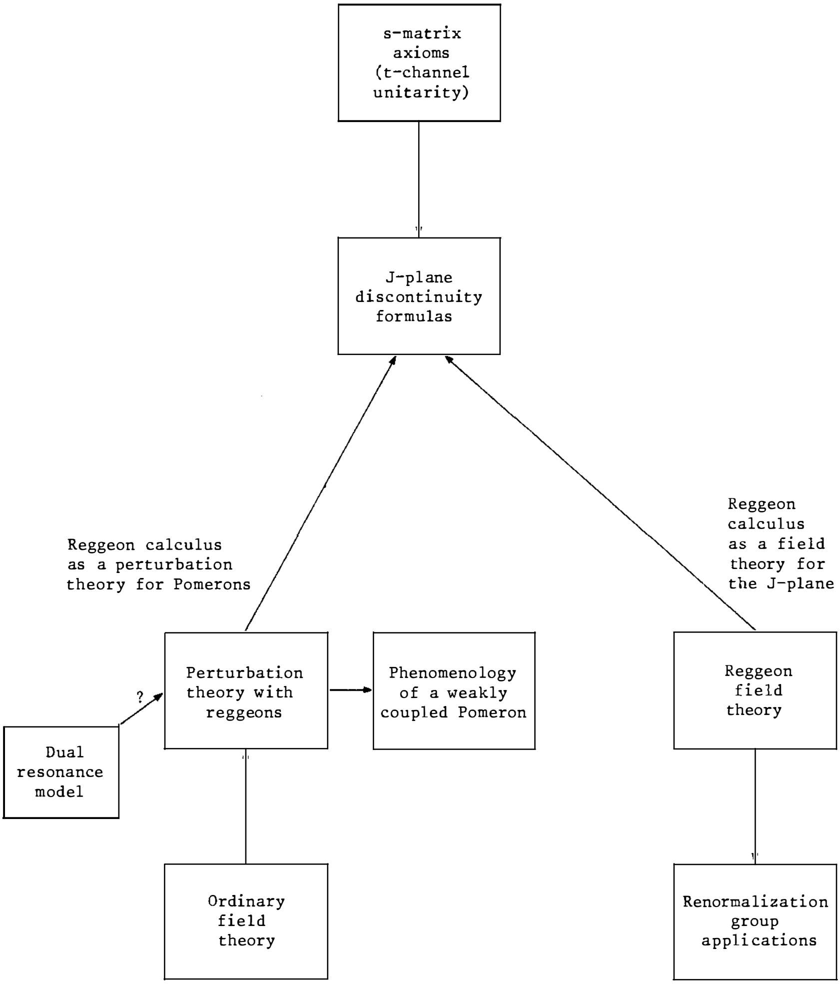

Fig. 1 Development of the reggeon calculus

What is interesting about this particular approach is that it starts with a model which, at least in a perturbative sense, satisfies both s- and t-channel unitarity. Consequently, one might expect to use it to learn more about the relationship between s-channel constraints and the reggeon calculus. For example, let us consider elastic s-channel unitarity. A particularly interesting case is the model of Cheng and Wu which involves a bare Pomeron with an intercept above J = 1 [8]. Such a singularity is in conflict with elastic unitarity. But consistency is restored if the Pomeron is iterated in the s-channel sense (Fig. 2). For simplicity, let us consider a bare pole with zero slope, located at $J = 1 + \varepsilon$. The "cuts" formed

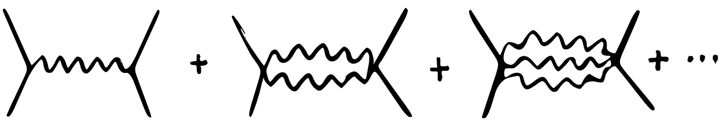

Fig. 2 s-channel iteration of a single reggeon

from the bare pole are actually poles in the zero slope limit, the n-Pomeron "cut" being located at $J = 1 + n\varepsilon$. The series in the s-plane for the imaginary part of the elastic amplitude can be represented schematically as follows:

$$\mathrm{Im}\,A(s) = \beta^2 s^{1+\varepsilon} - \frac{\beta^4 s^{1+2\varepsilon}}{2!} + \frac{\beta^6 s^{1+3\varepsilon}}{3!} - \ldots , \tag{2}$$

which can be summed exactly to yield

$$\mathrm{Im}\,A(s) = s(1 - e^{-\beta^2 s^{\varepsilon}}) , \tag{3}$$

which is somewhat like the exponentiation obtained by Cheng and Wu. Although individual terms in the series rise faster than s^1, evidently the total does not. This exercise in algebra thus imitates the mechanism by which the eikonal series leads to an amplitude obeying the Froissart bound. Now let us do the same summation in the reggeon calculus. Projecting the series term by term one obtains

$$A(J) = \frac{\beta^2}{J - 1 - \varepsilon} - \frac{\beta^4}{2!}\,\frac{1}{J - 1 - 2\varepsilon} + \frac{\beta^6}{3!}\,\frac{1}{J - 1 - 3\varepsilon} - \ldots , \tag{4}$$

whereas for the sum (3), the J projection is simply

$$A(J) = \frac{1}{J - 1} + f(J) , \tag{5}$$

where f is entire in J. The sum of the projected terms (4) is nicely convergent, but it is not at all like the projection of the sum of the terms (5). In other words, summing the infinite series does not commute with the

J-plane projection. "Exponentiation" does not translate into the J-plane language. The mathematical reason is fairly obvious -- in order to do the J-plane projection correctly, one must project at a value of J to the right of all singularities, which is clearly impossible term by term in the series since there are singularities arbitrarily far to the right. (There is no problem in converting to the J-plane when $\varepsilon < 0$.) Also the field theory in the J-plane does not make much sense, because the bare singularity with intercept above one corresponds in the field theory to a particle with negative rest energy, i.e. a sort of tachyon.

Thus we conclude from this elementary example that requiring that a theory makes sense in the J-plane may be so restrictive as to eliminate from consideration a number of interesting models, such as that of Cheng and Wu. At the same time, we conclude that the full content of s-channel unitarity is probably not capable of a direct translation into the J-plane language.

So what can we do with the reggeon calculus? One possibility is to find a way around the exponentiation problem. Cardy has a model with a bare intercept above J = 1, and shows that with a clever choice of the n-reggeon-to-m-reggeon coupling it is possible first to exponentiate and then to project into the J-plane and obtain a factorizable singularity at J = 1 in terms of which the reggeon field theory is then developed[8]. The key problem is to obtain a factorizable singularity, since without factorization the reggeon diagrams do not make sense. However, Cardy's trick works only for an unusual n-to-m-reggeon coupling. In general one would not expect exponentiation to yield a factorizable singularity at J = 1 [10].

Another possibility is to view the reggeon calculus only as a perturbation theory for a limited range in log s. However, one would then be abandoning the hope of learning something about very high energy behaviour.

A third possibility would be to restrict one's attention to Lagrangians which make sense in the J-plane. However, one cannot then claim that the results are generally valid.

Acknowledgements

I am indebted to Francis Low for discussions of the J-plane transformation of the Cheng and Wu series. I would also like to express my appreciation for the hospitality of J. Tran Thanh Van during the "rencontre".

REFERENCES

1) C.E. DeTar, Phys. Rev. D (to be published).

2) V.N. Gribov, I. Ya. Pomeranchuk and K.A. Ter-Martirosyan, Yadernaya Fiz. 2, 361 (1965) [Soviet J. Nuclear Phys. 2, 258 (1965)];
Phys. Rev. 139, B184 (1965).
A.R. White, Nuclear Phys. B50, 93, 130 (1972); Phys. Rev. D 10, 1236 (1974).

3) V.N. Gribov and A.A. Migdal, Yadernaya Fiz. 8, 1002, 1213 (1968) [Soviet J. Nuclear Phys. 8, 583, 703 (1969)].

4) A.A. Migdal, A.M. Polyakov and K.A. Ter-Martirosyan, Phys. Letters 48B, 239 (1974), Moscow preprint ITEP-102 (1973).
H.D.I. Abarbanel and J.B. Bronzan, Phys. Rev. D 9, 2397 (1974); Phys. Letters 48B, 345 (1974).
H.D.I. Abarbanel, Phys. Letters 51B, 295 (1974).

5) R. Savit, this conference.
R.C. Brower, J. Ellis, R. Savit and W.J. Zakrzewski, Ref. TH.1973-CERN (1975).
J. Ellis and R. Savit, Ref. TH.1974-CERN (1975).

6) V.N. Gribov, Zh. Eksper. Teor. Fiz. 53, 654 (1967) [Soviet Phys. JETP 26, 414 (1968)].

7) See A. Capella, this conference (following paper).

8) H. Cheng and T.T. Wu, Phys. Rev. Letters 24, 1456 (1970).

9) J.L. Cardy, Nuclear Phys. B75, 413 (1974).

10) Bronzan uses a more general approach and obtains factorization only to leading order in log s: J.B. Bronzan, Phys. Rev. D 10, 746 (1974).

HIGH-ENERGY SCATTERING AS A CRITICAL PHENOMENON

R. SAVIT

CERN - Geneva

Abstract : Asymptotic (large s, small t) scattering can be studied as a critical phenomenon, akin to the infra-red behaviour of massless field theories, or the study of phase transitions in statistical mechanics. The Reggeon calculus provides a framework for the discussion. The important concept of universality is described, and it is suggested that the asymptotic behaviour of scattering amplitudes may be independent of the details of the physics. Lattice and field theoretic methods for the calculation of critical exponents are explained and results are presented. Finally, phenomenological implications for present energies are outlined.

Résumé : La diffusion asymptotique (grand s, petit t) peut être étudiée comme un phénomène critique, apparenté au comportement infrarouge des théories de champ à masse nulle, ou à l'étude des transitions de phase en mécanique statistique. Le calcul des Reggeons fournit un cadre à cette discussion. Le concept important d'universalité est décrit, et on suggère que le comportement asymptotique des amplitudes de diffusion peut être indépendant des détails de la physique. Des méthodes théoriques des réseaux et de la théorie des champs pour le calcul des exposants critiques sont expliquées et des résultats sont présentés. Finalement, les implications phénoménologiques pour les énergies actuelles sont décrites.

1. INTRODUCTION

Why should the theory of critical phenomena, phase transitions, long-range order and stuff like that have anything at all to do with high-energy scattering? In order to understand where such ideas might be applicable, let us start at a very intuitive, almost kinematical level.

Many of the notions developed for high-energy physics during the past several years have reflected our bias that when you hit something hard, it usually gets a big kick sideways, while a glancing blow generally does not impart much transverse momentum. Certainly in two dimensions it is true: events with large transverse momenta are sensitive to small impact parameters -- or, more precisely, to structure over small transverse distances -- while near forward events are insensitive to this structure, and tell us something about larger impact parameters. In the longitudinal direction we can make a similar argument. When we perform a Fourier transform we always have factors like

$$\exp i\{p_\mu x^\mu\} = \exp i\{Et - p_\parallel x_\parallel - \vec{p}_\perp \cdot \vec{x}_\perp\} = \\ = \exp i\{\tfrac{1}{2}(E + p_\parallel)(t - x_\parallel) + \tfrac{1}{2}(E - p_\parallel)(t + x_\parallel) - \vec{p}_\perp \cdot \vec{x}_\perp\} \ . \quad (1)$$

Assuming that the integrand is not too pathological, the major contribution when integrating over d^4x, will come when the object in brackets is not too large. When the energy (or s) and $p_\perp$ are both large, then $|E + p_\parallel|$ and $|E - p_\parallel|$ are both large which means that $|t - x_\parallel|$ and $|t + x_\parallel|$ are both small, so that $|t|$ and $|x_\parallel|$ are both small. Thus all the components of x^μ are small. On the other hand, when s is large but $p_\perp$ is small, similar reasoning shows that all components of x^μ are large. (For small s we have a mixed case -- one of $|x_\parallel|$ or $|t|$ is small, while the other is large.) Consequently, high-energy, small $p_\perp$ scattering appears to have the characteristics of an infrared problem in that this kinematic régime is sensitive only to the large wavelength structure in coordinate space. As we move out of this régime -- either to larger $p_\perp$ or to smaller s, we become more sensitive to the short distance structure -- that is, to the details of the physics.

This argument suggests that, if we are interested in large s, small t physics, it might be useful to borrow techniques from other areas of physics which have dealt with infrared problems. Two such areas are field theory -- especially field theories with massless particles, and statistical mechanics -- especially the study of phase transitions. Both these disciplines study critical phenomena, or the appearance of long-range ordering in a system, which is the infrared problem.

To apply the techniques of these fields to high-energy scattering, we need to find a convenient language in which to talk about our problem -- a language into which we can clearly translate field theory or statistical mechanics. Let me briefly describe two such languages, both of which are based on the reggeon calculus[1)]. I want to emphasize that while these languages seem to be rather specific models, the answers to the questions which we shall ask of them are expected to be pretty much model independent -- universal, in the statistical mechanics parlance. Indeed, we should expect that other languages will also manifest critical behaviour. At the end of the talk, I will give an example by showing qualitatively how we may expect to see a phase transition exhibited in the language of the Feynman fluid analogy.

The techniques of field theory can be used if we talk about high s small t scattering in terms of the Reggeon field theory[1)]. This theory, in its usual form[2,3)], looks like a non-relativistic field theory in two-space and one-time dimension with a particle, the pomeron, represented by a complex field, ψ. Its propagator is of the form

$$\frac{i}{E - \alpha' k^2 - \Delta + i\varepsilon} \tag{2}$$

$E = 1 - j = 1 -$ [angular momentum in the t-channel] and $k^2 = -t =$ (transverse momentum)^2. The coordinate space variables are $\underset{\sim}{b}$ = impact parameter (space), and $\tau = i \ln s$ (time). The propagator blows up when we are on the pomeron trajectory, thus, $\Delta = 1 - \alpha_p(0)$ plays the role of a $(\text{mass})^2$ [sort of a relativistic $(\text{mass})^2$ -- the non-relativistic mass is $1/2\alpha'$.] The theory has a three-point coupling,

$$i\, g\, \psi^+ \psi (\psi + \psi^+) =$$ 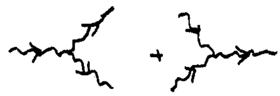

Fig. 1

with a purely imaginary coupling constant. The phase of the coupling constant is dictated by the fact that the pomeron has positive signature and an intercept near one. This field theory has the virtue that it explicitly satisfies the discontinuity equations of t-channel unitarity[4].

To calculate the behaviour of, for example, the elastic-scattering amplitude, we must, in general include contributions not only from the single pomeron exchange [Fig. 2a], but also from other diagrams, such as those shown in Figs. 2b, c, and d.

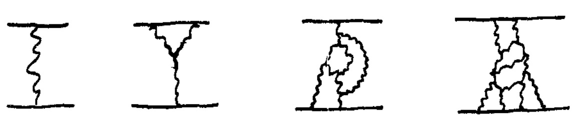

(a) (b) (c) (d)

Fig. 2

If the pomeron intercept is at one*), so $\Delta = 0$ (massless pomeron), then all these graphs are *a priori* equally important, since they all contribute to an angular momentum plane singularity which is at one for $t = 0$. This is how the infrared behaviour of large s, small t scattering manifests itself in the reggeon field theory. Recall, for comparison, that in QED an electron undergoing a mild acceleration can emit any number of zero mass photons which can propagate over large distances. The amplitudes for all these emissions have singularities in momentum space at $k^2 = 0$. In the same way a particle scattering near $t = 0$ can emit any number of zero mass pomerons

*) Actually, we want the renormalized pomeron intercept to be at one. The distinction is not important for this intuitive discussion.

with singularities which pile up at the "momentum" space origin $E = k^2 = 0$ of the reggeon field theory. The massless pomerons also propagate over large distance, i.e. relatively large $\underset{\sim}{b}$ and large ln s. In Section 2 I will briefly describe the technique, the renormalization group (and the ε-expansion) which is used to obtain information about these problems.

Let us now turn to the second language, which can be used to translate statistical mechanics. This language is a lattice version of the reggeon calculus -- in particular, a latticization of the reggeon field theory[5]. To construct this language, you write down your original field theory, and make space and time take on discrete values. Derivatives of fields that appear in the Lagrangian then become differences of field values at nearby points in space and time. For example, a derivative like $\partial_\mu \phi \partial^\mu \phi$, which appears in ordinary ϕ^4 theory becomes, on a lattice $\sim \phi_i \phi_{i+1}$ + local terms, where the fields ϕ_i are the field values at the i^{th} lattice site. Now in the usual field theory, ϕ can take on values in the range $(-\infty, \infty)$. But this is sometimes an inconvenient measure for lattice calculations, so one often changes the measure, for example letting $-1 \leq \phi_i \leq 1$, or even just letting $\phi_i = \pm 1$. With this last choice, Euclidean ϕ^4 theory when placed on a lattice looks just like the standard Ising model with nearest neighbour interactions[6].

Now why do we want to bother to put the theory on a lattice? There are really two reasons[7]:

i) The nature of critical behaviour in the field theory, i.e. the infrared behaviour, may show up on the lattice as a phase transition, and the nature of this critical phenomenon is often more transparent on the lattice than the associated critical phenomenon in the field theory.

ii) There are techniques which are applicable to lattice theories, but which cannot be used in the continuum limit for the calculation of certain quantities, the critical exponents of the theory. So, if we can argue that the lattice theory and the continuum theory are in some sense the same (which really is not at all obvious given how we have chopped up the system to put it on a lattice), then we can use statistical mechanics techniques to learn about, in our case, the reggeon calculus, or more generally large s small t scattering.

In the next section I will talk about critical behaviour in field theory, in particular, in the reggeon field theory. Included is a description of the renormalization group and the ε-expansion. In Section 3 I will discuss critical behaviour in statistical systems. The focus of most of this section will be a lattice formulation of the reggeon calculus, and a discussion of phase transitions and the high temperature expansion. At the end of Section 3 I will qualitatively describe how another statistical formulation of high energy scattering, the Feynman fluid, may be related to the reggeon calculus. Finally, the standard conclusion and comments section is the fourth one.

2. CRITICAL BEHAVIOUR IN REGGEON FIELD THEORY

There are two important properties of critical phenomena which I want to emphasize in this and the next sections: scaling laws and universality. The importance of these ideas will become clear as we go along.

In field theory, an approach which we can use to help understand the infrared problem is the renormalization group[6]. The idea is really quite simple: when you do field theory you have to do renormalization. The renormalized theory contains a normalization point, some value of the momenta at which certain Green's functions are defined. The unrenormalized theory contains no information about the renormalization procedure, so

$$\left.\frac{d}{dE_N}\right|_{\mathrm{BARE}} \Gamma_u = 0 , \tag{3}$$

where E_N labels the normalization point, Γ_u is any unrenormalized Green's function, and the differentiation is carried out holding the bare parameters (coupling constants) fixed. This is the renormalization group equation.

Now we can write Γ_u in terms of the renormalized Green's function Γ_R and the renormalized coupling constants. Doing that and using the chain rule of differentiation, we can write (3) as a differential equation for Γ_R. This equation can be solved and gives us a general form for Γ_R [8]. For the Reggeon field theory, the renormalization group tells us that the leading behaviour of the Green's functions in the infrared limit $[E_i, \vec{k}_i \to 0]$ is

$$\Gamma_R^{(n,m)}(E_i, \vec{k}_i, g^*, \alpha') \sim (E)^{1+\left(\frac{n+m}{2}\right)\eta(g^*)+\frac{d}{4}(2-n-m)\nu(g^*)}$$
$$\times F_{n,m}\left(\frac{E_i}{E},\ (E)^{-\nu(g^*)}\ \frac{\vec{k}_i \cdot \vec{k}_j}{E_N}\ \alpha', g^*\right) + \ldots \qquad (4)$$

$E \to 0$ such that the E_i/E stay finite, g^* is some value of the renormalized triple pomeron coupling called the fixed point value, and $\eta(g^*)$ and $\nu(g^*)$ are indices of the theory called the critical exponents. d is the number of space dimensions (for the reggeon field theory, physical d is 2), and n and m refer to the number of external legs of the connected, one-pomeron irreducible, renormalized Green's function.

$\Gamma_R^{(n,m)}$ = n 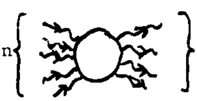 m

The scaling form of the Green's functions (4) is an important property of the solutions of the renormalization group equation in the infrared limit, and as we shall see has its counterpart in the theory of phase transitions in statistical mechanics.

Now it is a fact that the infrared behaviour of these Green's functions can be exactly determined when $d = 4$. For $d = 4$, $g^* \to 0$: $\eta(g^*) \to 0$, and $\nu(g^*) \to 1$. Away from $d = 4$, $g^* \propto \varepsilon^{1/2}$, where $\varepsilon = 4 - d$. Likewise the deviations of η and ν from their canonical values of 0 and 1 can be expressed as a power series in ε. So the hope is that if ε is in some sense small, we may be able to get reliable estimates of η and ν by computing only one or two orders in the ε-expansion. There are only two hitches: i) $\varepsilon = 2$ for $d = 2$, which is the point of physical interest, and 2 is generally not a good expansion parameter; ii) in any event, the ε-expansion probably does not converge and may be only an asymptotic expansion. Therefore, we must truncate the series someplace, but *a priori* we do not know where. Nevertheless, we can keep our fingers crossed and calculate η and ν to some order in ε. This has been done to order ε^2 [8,9] and the results are shown in the second and third columns of Table 1.

Table 1

Exponent	High-temperature expansion preferred range	$O(\varepsilon)$	$O(\varepsilon^2)$
η	$\frac{1}{2} \sim 1$	0.17	0.38
ν	$1\frac{1}{2} \sim 2$	1.08	1.18

Now remember that in the reggeon field theory E is $1 - j$. So if we Mellin transform (4) with respect to E we can deduce the contributions of the Γ_R to the asymptotic elastic cross-section. As long as $\eta < (2/d)\nu$ [10] the Green's function $\Gamma_R^{(1,1)}$, the renormalized pomeron propagator, dominates the large s, small t amplitude, and gives

$$A(s,t) \sim i\ s(\ln s)^{\eta} f\left[t(\ln s)^{\nu}\right] . \qquad (5)$$

Besides the general scaling form of the solutions (4) and (5) in the infrared limit, there is another important property of these functions. That property goes under the name universality[6,11] and states that, within certain limits, the critical exponents of the theory (in our case η and ν)

are independent of the detailed nature of the theory. Put another way, any theory with the same symmetry properties constructed in the same number of dimensions has the same infrared behaviour, in that the critical exponents are the same. There is no general proof of this property, but studies of various theories indicate that it is generally true. For instance, if we add to the reggeon field theory Lagrangian a bare quartic coupling or to the bare trajectory a term $\propto k^4$, η and ν are unaffected[2] (at least to each order in ε). The reggeon field theory has often been criticized as being rather arbitrary -- certainly Gribov's original derivation based on considerations of an underlying ϕ^3 theory seems, superficially, to be model dependent. But if we believe universality (as we probably should) then at least the asymptotic behaviour of the theory is quite general. In fact, as we shall discuss below, universality is more general than just relating the infrared behaviour of different (in our case, reggeon) field theories, and may well apply even at the level of the underlying particle dynamics. Actually, this makes sense: the infrared behaviour deals with the long wavelength structure of the theory, and so, as we argued in the Introduction, should be independent of the details of the physics -- only when we go to larger t or smaller s do we become sensitive to such structure. Of course, the claim here is a very big one: namely, *the asymptotic behaviour of the scattering amplitude is almost completely independent of the details of the physics.*

With the exciting possibility of really determining, in a model independent way, the asymptotic behaviour of large s, small t cross-sections, it is clearly worthwhile to seek other methods of calculating η and ν and learning more about this critical phenomenon[5,7]. With that in mind we turn to the following.

3. CRITICAL BEHAVIOUR IN STATISTICAL SYSTEMS

As we mentioned, universality is really more general than just relating different field theories. For example, it also relates lattice theories to field theories. If I can find (or construct) a lattice theory with the same symmetry properties and infrared structure as a given field theory, then I should be able to use lattice methods to calculate the critical exponents. Again, this universality is physically reasonable. If I consider just the long wavelength kinematic régime, that is, wavelengths large compared with the lattice spacing, it should not matter that there is a lattice at all -- all the bumps get smoothed out. In addition (although this is a little less obvious), the exact measure of the fields should not matter for determining the nature of the phase transition and the values of the critical exponents.

In lattice theories, the objects of physical interest are the averages of operators or spins (fields) on the lattice in the limit that the number of lattice sites goes to infinity (thermodynamic limit):

$$\langle\theta\rangle = \frac{\sum_{\text{states}} \theta e^{-\beta H}}{\sum_{\text{states}} e^{-\beta H}} = \frac{\sum_{\text{states}} \theta e^{A/T}}{\sum_{\text{states}} e^{A/T}}, \tag{6}$$

where A is the action, and we have explicitly included a scale factor 1/T. The last form demonstrates the connection with field theories. An N-point Green's function in field theory is related to the thermodynamic average of an N-spin operator. For example, the analogue of the configuration space propagator may be taken to be $\langle\phi_i\phi_j\rangle - \langle\phi_i\rangle\langle\phi_j\rangle$ where i and j refer to the lattice sites.

Now, in a lattice theory there is a temperature parameter as well as some coupling constants. Some of these couplings are related to the kinetic energy terms of the continuum field theory, as we explained in the Introduction, while others are related to the interaction terms of the field theory. Phase transitions of the system occur when long-range order sets in. This happens when the values of the coupling constants and temperature are related in a certain way which defines a critical surface in the parameter space. There is an assumption in statistical physics called the Kadanoff scaling hypothesis[12], which asserts that near the critical surface, the thermodynamic averages are generalized homogeneous functions of $\delta = T - T_c$, and $\xi_i = G_i - G_{ic}$, where the G_i are all the coupling constants, and the subscript c refers to their critical values. So, for example, in a system with two independent coupling constants in addition to the temperature, the thermodynamic averages near the critical surface have the form

$$\langle \theta(\delta,\xi_i) \rangle \sim \delta^{-p} f(\xi_1/\delta^q, \xi_2/\delta^r) \ . \tag{7}$$

The Kadanoff scaling hypothesis also assumes that in the infrared region, i.e. when the differences in space and time between the lattice points $\to \infty$, the correlation functions, for example the propagator, are generalized homogeneous functions. For instance, if we set all the $\xi_i = 0$ then we can write for the two-spin correlation function in the reggeon calculus

$$\Gamma(\delta,r,t) = \langle \phi_i \phi_j \rangle - \langle \phi_i \rangle \langle \phi_j \rangle \sim \delta^A f\left(\frac{|r|}{\delta^B}, \frac{t}{\delta^C}\right) = r^{A/B} f'\left(\frac{|r|}{\delta^B}, \frac{t}{\delta^C}\right) = $$
$$= t^{A/C} f''\left(\frac{|r|}{\delta^B}, \frac{t}{\delta^C}\right) . \tag{8}$$

Consequently, we see that the behaviour of the propagator as $\delta \to 0$ is related to its behaviour as r or $t \to \infty$. (Remember that the reggeon calculus looks non-relativistic, so space and time are on a different footing.)

In the field theory, the onset of critical behaviour is related to the fact that the renormalized pomeron intercept is at one -- otherwise we do not get the build-up of cuts in the j-plane, which we associate with the analogue of a massless particle, i.e. with long-range forces. In the lattice language we know we must have δ small to be near the critical surface. Now, if all the $\xi_i = 0$, only the size of δ tells us how far away we are from the phase transition. In the field theory, on the other hand, if $g = g^*$, the fixed point value, then only $1 - \alpha_p(0)$ is a measure of how far away we are from critical behaviour. Hence, we can write

$$1 - \alpha_p(0) \sim \delta^\lambda \propto (T - T_c)^\lambda \tag{9}$$

Now look again at (8). In the reggeon calculus $t \sim \ln s$, so the contribution of the two-spin correlation function to the total cross-section is just given by the Fourier transform of (8) with respect to $\underset{\sim}{r}$ for $|\underset{\sim}{k}| = 0$, evaluated when $\alpha_p(0) = 1$, that is when $\delta = 0$. This is just

$$G(\delta = 0, |k| = 0, t) \sim t^{(A+dB)/C} \sim (\ln s)^{(A+dB)/C} . \tag{10}$$

So $\eta = (A+dB)/C$ (Physical $d = 2$). Similarly, the slope parameter ν is easily shown to be $\nu = 2B/C$.

The exponents, A, B and C are related to the behaviour of various combinations of the correlation functions (and other thermodynamic averages) as $\delta \to 0$. If we can determine these behaviours, then we can deduce the values of η and ν. This is a job for the high-temperature expansion[7,13].

Very roughly, the high-temperature expansion consists in expanding the right-hand side of (6) in a power series in $1/T$, and trying to identify the first few terms of the expansion as terms contributing to a divergence for $T \simeq T_c$ like δ^{-p}. If we write

$$\langle \theta \rangle = \sum_\ell a_\ell \frac{1}{T^\ell} \propto \delta^{-p} , \tag{11}$$

then, expanding δ^{-p} in powers of T^{-1}, we can write

$$R_\ell \equiv \frac{a_\ell}{a_{\ell-1}} = T_c\left(1 + \frac{p-1}{\ell}\right) \tag{12}$$

and R_ℓ plotted as a function of $1/\ell$ should be a straight line whose intercept is T_c and from whose slope we can extract exponent, p. Non-leading terms on the right-hand side of (11) will, in general, cause deviations of R_ℓ from a straight line, especially for small ℓ, but the hope is that they will not be too big, and will not persist for too many orders in ℓ. Notice that the high temperature expansion is an expansion in *all* the couplings of the action, including the kinetic energy terms. That is what makes it difficult to do in the continuum.

Using a variation of this technique we determined η and ν (as well as some other exponents) by calculating terms to $O(1/T^3)$ [7]. This is a relatively low order as far as these expansions are concerned, so we were only able to get fairly crude estimates of the exponents. These are shown in Table 1. It is really quite remarkable that these numbers come out to be so reasonable (a fact which one appreciates intensely after going through the calculation). I want to remind you that neither the ε-expansion nor the high temperature expansion is a rigorous method so *a priori* our numbers could have come out to be anywhere between $-\infty$ and $+\infty$ (and almost did)[14].

So now we have a reasonably good indication that the reggeon calculus may have a sensible infrared behaviour. But the argument is quite loose. On the lattice we assumed the existence of a phase transition with valid scaling laws, but we really do not know if one exists. Furthermore, we assumed the applicability of universality in a rather broad sense. To get some idea about whether these assumptions are reasonable or not, we solved exactly a one-dimensional model with many of the properties of the reggeon calculus[7]. The model looks like an Ising model in an imaginary magnetic field. The phase of the magnetic field reflects the imaginary triple pomeron coupling of the reggeon calculus. That is,

$$ig\psi^+\psi(\psi^+ + \psi) \underset{\psi=\vec{\phi}+i\chi}{} ig\phi(\phi^2 + \chi^2) \underset{\phi,\vec{\chi}=\pm 1}{} \propto ig\phi \tag{13}$$

Surprisingly, this one-dimensional system has a phase transition at a non-zero T_c. The transition is in some ways like a first-order transition, but nevertheless appears to obey universality and scaling laws. All these results I find very encouraging.

I promised to try to say something about the relation of all this stuff to the Feynman fluid picture[15]. I think it it worth qualitatively describing the nature of what I believe is the connection. I will not be very precise because a *full* description of the Feynman fluid implies a more detailed knowledge of the dynamics (since it requires a knowledge of the equation of state) than we have assumed so far. Nevertheless, this system should show evidence of a phase transition. Generally, this comes about as follows.

We argued before that $1 - \alpha_p(0)$ was proportional to some power of $T - T_c$. Now suppose $\alpha_p(0) < 1$ $(T > T_c)$. The Reggeon calculus diagram which gives the leading contribution to the elastic cross-section is shown in Fig. 3.

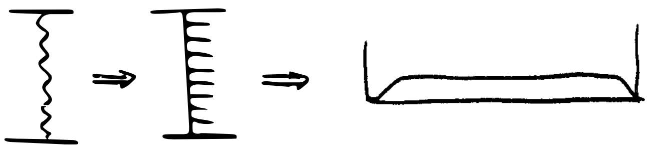

Fig. 3

All other iterations of the singularity give contributions which are lower in the j-plane*). In the usual way we imagine that this reggeon is built up by some multiperipheral mechanism, and gives a uniform distribution of hadrons in the Feynman cylinder (except near the ends). Next, suppose $\alpha_p(0) > 1$ $(T < T_c)$. (It really may not be possible to define such a theory, but for the moment let us imagine that we can. If we cannot, it does not matter -- it just means that the critical temperature must be approached from above.) In this phase the biggest contribution to the cross-section from n pomerons comes when they are all lined up in parallel:

*) This is not quite true. Other diagrams may contain poles at the same place as the diagram of Fig. 3, but the cuts will be lower.

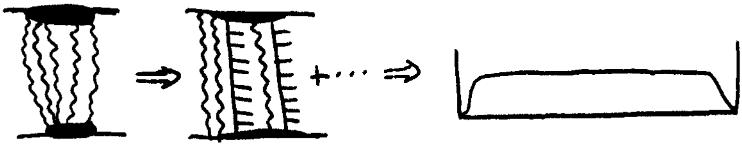

Fig. 4

Now depending on what you think the correct cutting rules are, you get different kinds of intermediate state contributions, one of which is shown in Fig. 4. In any event, we again expect a uniform distribution of hadrons, with, in general, a different (probably greater) density than in the case $\alpha_p(0) < 1$.

Imagine now starting in the phase of Fig. 3 and letting $\alpha_p(0) \to 1$. As we approach 1, graphs of the form shown in Fig. 5 become just as important as the graph of Fig. 3

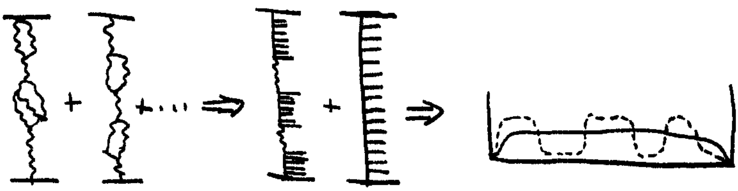

Fig. 5

and we see the appearance of droplets, high mass clusters of hadrons coming from intermediate states like (a) mixed in with a uniform distribution of hadrons from intermediated states like (b) -- just like steam condensing into water, as we lower the temperature. This should have the effect of causing large fluctuations in, for instance, the density distribution, as schematically indicated in Fig. 5. Thus, even in the language of the Feynman gas we expect to see evidence of a phase transition if $\alpha_p(0) = 1$. That is, at the critical point we should see something like the two phases of Fig. 3 and Fig. 4 existing simultaneously. Of course, the more room there is in the cylinder and the more particles there are the more clearly we will see the effect, so again the phase transition shows up most dramatically at asymptopia.

Now this argument is only heuristic. I have assumed a very simple structure for the pomeron, simple cutting rules, etc. In fact reggeon field theory aficionodos will recoil in horror, since I have not distinguished between bare and renormalized pomerons. Nevertheless, something like this should happen: new intermediate states which correspond to another phase of the system should be present if $\alpha_P(0)$, the renormalized pomeron intercept is one, but not if $\alpha_P(0) < 1$. If this is right, there may be important phenomenological implications. The effects of pomeron renormalization should begin when loops in pomeron propagators start to contribute. This should occur at about 6 units of rapidity. But, by the argument we have just given, this is also the region where we should begin to see the onset of a phase transition (i.e. enough energy to produce events with high mass clusters reasonably well separated, cf. Fig. 5). The highest ISR energy provides 10 units of rapidity; thus we have 4 units in which to look for the effects of phase transitions -- as for example, the beginning of divergences of certain thermodynamic quantities[16]. This is clearly a delicate job, phenomenologically, but with care we may be able to see something like the beginning of an approach to a phase transition.

4. CONCLUSIONS AND COMMENTS

Let me list them:

i) From the study of solvable (one-dimensional) lattice systems, as well as estimates of the critical exponents using the high temperature expansion and the ε-expansion, we conclude that the reggeon calculus probably has a sensible infrared behaviour.

ii) Studies both on lattices and in the field theory indicate that universality is applicable to the reggeon calculus. It may even be applicable at the level of the underlying particle dynamics (this seems reasonable), so the asymptotic behaviour deduced from the reggeon calculus may be correct, and independent of the details of the physics.

iii) If (ii) is true then we can save a lot of money. We have one (or several) lattice formulations of the reggeon calculus. Now all we have to do is find a material that can be described by this lattice (at least in the sense of universality) and measure its thermodynamic properties near its phase transition. From these measurements we can determine η and ν, and hence the asymptotic behaviour of scattering amplitudes.

iv) Even without explicitly measuring the leading divergences near the phase transition (either with super high energy accelerators, or, more elegantly, with heat baths and thermometers), we can hope to begin to see the approach to a phase transition by a careful analysis of the data. If we are approaching a critical point, then certain measurable quantities, for example, the correlation length should start showing signs of a divergence.

v) I am very excited about all this. There is a lot to do, and I think we can learn a lot about this kind of physics by studying it as a critical phenomenon. It is true that asymptotic scattering is complicated -- but in a very simple way.

Acknowledgements

I am grateful to many people for interesting and stimulating discussions, especially D. Amati, J. Ellis, and J. Zinn-Justin. I also want to thank J. Cardy and R. Sugar for keeping us informed about their work. Finally, J. Tran Than Van and F. Schrempp deserve a round of applause for organizing such a pleasant and rewarding conference.

REFERENCES AND FOOTNOTES

1) V.N. Gribov, Zh. Eksp. Teor. Fiz., 53, 654 (1967) [Soviet Phys. JETP 26, 414 (1968)].
V.N. Gribov and A.A. Migdal, Zh. Eksp. Teor. Fiz., 55, 1498 (1968) [Soviet Phys. JETP 28, 784 (1969)]; Yad.Fiz., 8, 1002 (1968) [Sov. J. Nucl. Phys. 8, 583 (1969)]; Yad. Fiz. 8, 1213 (1968) [Sov. J. Nucl. Phys. 8, 703 (1969)].
V.N. Gribov, E.M. Levin and A.A. Migdal, Yad. Fiz. 12, 173 (1970) [Sov. J. Nucl. Phys. 12, 93 (1971)] and Zh. Eksp. Teor. Fiz. 59, 2140 (1970) [Soviet Phys. JETP 32, 1158 (1971)].

2) It is possible to change the theory by including other kinds of couplings, or extra terms in the trajectory. As we shall discuss, these modifications generally do not change the critical behaviour of the system. See for example, G. Callucci and R. Jengo, Nuclear Phys. B84, 413 (1975).

3) When we speak of the reggeon calculus in this paper, we refer only to the pomeron subspace of the theory. For a discussion of the pomeron boson sector of the reggeon field theory, see H.D.I. Abarbanel and R.L. Sugar, Phys. Rev. D 10, 721 (1974). The fermion-pomeron sector is discussed by J. Bartels and R. Savit, FNAL-Pub-74/60-THY (to appear in Phys. Letters B) and FNAL-Pub-74/61-THY (to be published in Phys. Rev. D.)

4) A.R. White, Nuclear Phys. B50, 130 (1972).

5) R. Brower, J. Ellis, R. Savit and W. Zakrzewski, CERN preprint TH-1973 (1975), Nuclear Physics B, to be published. G. Parisi [Frascati preprint (1975)] has recently proposed a somewhat similar reggeon lattice theory. In addition, a rather different lattice theory has been investigated by J. Cardy and R. Sugar, Santa Barbara preprint (1975).

6) See, for example, K. Wilson and J. Kogut, Phys. Reports 12 C, 75 (1974), and references therein. See also E. Brézin, J.-C. Le Guillou and J. Zinn-Justin, "Field Theoretical Approach to Critical Phenomena", to be published in Vol. VI of "Phase Transitions and Critical Phenomena" (Eds. C. Domb and M.S. Green) (Academic Press, N.Y.).

7) J. Ellis and R. Savit, CERN preprint TH-1974 (1975), Nuclear Phys. B, to be published.

8) A.A. Migdal, A.M. Polyakov and K.A. Ter-Martirosyan, Phys. Letters 48B, 239 (1974) and ITEP (Moscow) preprint 102 (1974); H.D.I. Abarbanel and J.B. Bronzan, Phys. Letters 48B, 345 (1974), and Phys. Rev. D 9, 2397 (1974).

9) First-order terms were calculated in Ref. 8. Terms of order ε^2 have been calculated by M. Baker, Phys. Letters 51B, 158 (1974) and Nuclear Phys. 80B, 62 (1974); and J.B. Bronzan and J.W. Dash, Phys. Letters 51B, 496 (1974), and Phys. Rev. D10, 4208 (1974).

10) Notice that $\eta \leq (2/d)\nu$ is an inequality imposed by the simple s-channel unitarity constraint $\sigma_{el} \leq \sigma_T$. On the other hand, this is also the inequality which is required in order that the statistical formulation of the reggeon calculus (see Section 3) exhibit a phase transition of which is of second, or higher order. (J. Ellis and R. Savit, in preparation). All this raises the possibility that the reggeon calculus may satisfy s-channel unitarity, at least as far as the critical exponents are concerned. Cardy and Sugar, in their lattice formulation, have also reported progress in determining the conditions under which the reggeon calculus satisfies the Froissart bound. J. Cardy and R. Sugar, Op. cit.

11) See for example, L.P. Kadanoff, Proceedings of the International School of Physics "Enrico Fermi", (Ed. M. Green) (Academic Press, New York, 1971), and Ref. 7. Universality in the context of the reggeon field theory has also been discussed by A.R. White in a talk at the 1974 SLAC Topical Conference on Strong Interactions, FNAL preprint FERMILAB-Conf-74/77-THY (1974).

12) L.P. Kadanoff, Phys. 2, 263 (1966); L.P. Kadanoff et al., Rev. Mod. Phys. 39, 395 (1967).

13) For a more complete discussion of the high temperature expansion, see H.E. Stanley, Introduction to Phase Transitions and Critical Phenomena (Oxford University Press, London, 1971).

14) We have reason to believe that a slightly different version of the theory used in Ref. 7 will give very accurate values of η and ν at very low orders in the high temperature expansion. This work is nearing completion and will be reported elsewhere.

15) For a discussion of the Feynman fluid analogy, see for example, J.D. Bjorken in Particles and Fields - 1971, Ed. A.C. Melissinos and P.F. Slattery (American Institute of Physics, New York, 1971); M. Bander, Phys. Rev. D 6, 164 (1972); R. Arnold, Phys. Rev. D 5, 1724 (1972).

16) There is, for example, some evidence that the correlation length grows with energy. See A.J. Buras and J. Dias de Deus, Nuclear Phys. B78, 445 (1974).

SELF-CONSISTENT DIFFRACTION IN THE MULTIPERIPHERAL MODEL

James S. Ball*)

CERN, Geneva, Switzerland

Abstract: Self-consistency requirements in the Multiperipheral (MP) model are reviewed. With a simple assumption regarding the vanishing of the triple-Pomeron vertex, a non-linear integral equation is obtained for the asymptotic scattering amplitude. A previously obtained exact solution to this equation is given and a comparison of this model with the ISR elastic scattering data is made. A satisfactory fit to that data is obtained, but the values of the parameters indicate that, within this model, ISR energies are far from being asymptotic.

Résumé : Les exigences de consistance dans le modèle multipériphérique (MP) sont passées en revue. Avec une hypothèse simple concernant l'annulation du vertex 3-Pomeron, une équation intégrale non-linéaire est obtenue pour l'amplitude de diffusion asymptotique. Une équation exacte obtenue précédemment pour cette équation est donnée et une comparaison de ce modèle avec les données de la diffusion élastique aus ISR est faite. Un ajustement aux données satisfaisant est obtenu, mais les valeurs des paramètres indiquent que, dans le cadre de ce modèle, les énergies des ISR sont loin d'être asymptotiques.

*) On leave from the University of Utah, Salt Lake City, Utah, USA.

1. INTRODUCTION

This paper will discuss the model of ultra-high-energy scattering and particle production developed by F. Zachariasen and myself[1]. This model has the following virtues: i) it is derived simply from the conventional multiperipheral (MP) model when one insists on self-consistency at infinite energies; ii) it produces both diffractive and multiperipheral terms in the scattering amplitude and in production cross-sections; iii) the total cross-section rises like ln s.

This paper will begin by reviewing the conventional MP model, pointing out its inconsistencies in the case that the total cross-section is constant or growing. A simple example of a self-consistent Pomeron is given for the case that the Pomeron is a fixed pole. The next section of the paper will describe our self-consistent MP model, together with generalizations that retain the asymptotic self-consistency. The final section contains the results of fitting the ISR elastic scattering data, and a discussion of the relevance of the model to present energies is given.

2. THE CONVENTIONAL MULTIPERIPHERAL MODEL

The MP model is basically a model for particle production and is a straightforward generalization of the one-pion exchange model.

The amplitude for two pions to N pairs of pions T_N is given by

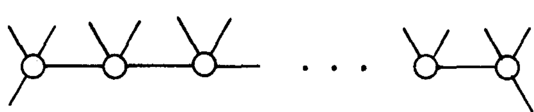

when all of the momentum transfers along the chain are small. The lines represent pions and the circles are pion-pion elastic scattering amplitudes. Since amplitudes generally fall off rapidly with increasing momentum transfer, it is reasonable to assume that this form dominates in the regions of phase space in which the amplitude is large. If one then adds the assumption that the region of phase space where one ordering is large does not overlap the region where another ordering is large, the scattering amplitude satisfies a Bethe-Salpeter type equation.

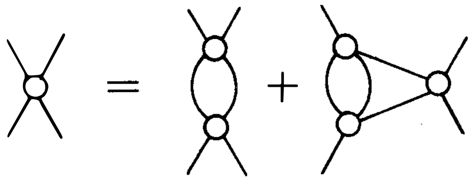

This equation is partially diagonalized in the J-plane, and is usually assumed to be completely diagonal, i.e. an algebraic equation. Assuming that the high-energy scattering amplitude is imaginary, one obtains:

$$A(J,t) = A_0(J,t) + KA_0(J,t)\ A(J,t) \ , \tag{1}$$

where the J-plane representation is the Laplace transform with respect to ln s of the amplitudes, i.e.

$$A(J,t) = \int_0^\infty e^{-(J-1)\ \ln s}\ A(s,t)\ d(\ln s) \ . \tag{2}$$

Here A is the imaginary part of the scattering amplitude, A_0 is the imaginary part produced by the two-body intermediate state in the s-channel, and K is related to the pion propagators and is not singular in the J-plane near the Pomeron singularity:

$$A_0(s,t) = \frac{1}{s}\int dt_1 \int dt_2\ \frac{A(s,t_1)A(s,t_2)}{\sqrt{-\lambda(t,t_1,t_2)}} \tag{3}$$

$$\lambda(t,t_1,t_2) = t^2 + t_1^2 + t_2^2 - 2tt_1 - 2tt_2 - 2t_1t_2 \ .$$

The usual MP lore then is that the most important part of A_0 is that part due to low-energy resonances, which are dual to normal Regge poles. Therefore the singularities of A_0 in the J-plane should look like a cut due to two rho's, and since this cut begins at $2\alpha_P(0) - 1$ its behaviour near J = 1 can be approximated by a pole at $J = \alpha_0$:

$$KA_0(J,t) = \frac{\beta K}{J - \alpha_0} .$$

Then A has a pole at $J = \alpha_0 + \beta K$.

If $\alpha_0 + \beta K = 1$ at $t = 0$ the total cross-section is constant and the multiplicity $\langle n \rangle = \beta K \ln s$. The t-dependence produces a diffraction peak with shrinkage $\sim \ln s$. The topological cross-sections are obtained by expanding the denominator of Eq. (1) giving a Poisson distribution in N:

$$\sigma_N = \beta s^{\alpha_0 - 1} \frac{(K\beta \ln s)^N}{N!}$$

$$\sigma_t = \beta .$$

The ln s growth of the multiplicity and the near constancy of the cross-section at relatively low energies is then the result of the low subenergy portion of the kernel, i.e. resonance contributions to A_0.

At high energies the internal inconsistency of the foregoing model becomes apparent. If $A(J,t)$ is singular at $J = 1$ and $t = 0$, then $A_0(J,t)$ is also singular at that point. Thus the large subenergy portion of the kernel cannot be neglected even though the size of this term may be numerically small when J is not near the Pomeron singularity.

A simple model which is self-consistent can be obtained if one assumes that a fixed Pomeron pole is produced by the MP model at $J = 1 - \varepsilon = \alpha_P$, then

$$A = \frac{A_0}{1 - KA_0} \simeq \frac{\beta(t)}{J - 1 + \varepsilon}$$

where

$$KA_0 = 1 \quad \text{at} \quad J = \alpha_P .$$

If we again assume that K is independent of J for J near α_P, we obtain the following equation for β:

$$\beta(t) = - \frac{A_0^2(\alpha_P, t)}{\frac{d}{dJ} A_0(J,t) \Big|_{J=\alpha_P}} .$$

If we now substitute the pole form for A into Eq. (2) we obtain

$$\beta(t) = \int \frac{dt_1 dt_2\ \beta(t_1)\ \beta(t_2)}{\sqrt{-\lambda(t,t_1,t_2)}}$$

which has a solution of the form $RJ_1(R\sqrt{-t})/\sqrt{-t}$ independent of the pole position. In the limit $\varepsilon \to 0$ the coupling K must vanish, which in this simplified model plays the role of the triple Pomeron coupling. A more sophisticated model of this type may be applicable in the energy range above that of the simple MP Pomeron discussed earlier and below asymptotic energies where the self-consistent Pomeron of the next section applies, particularly when one notes that the experimental Pomeron slope is unusually small.

3. SELF-CONSISTENT MP MODEL

To produce a Pomeron singularity that is internally self-consistent in the MP model, we begin by separating the amplitudes involved in Eq. (1) according to their behaviour at J = 1 and t = 0; singular amplitudes are denoted by a subscript P and regular by R. We then keep only those terms in Eq. (1) that are singular:

$$A_P = A_{0P} + K_R A_{0R} A_P + K_P A_{0P} A_P \ , \tag{4}$$

where A_{0P} is given in terms of A_P through Eq. (3).

We know before proceeding further that the equivalent of the triple Pomeron vertex in this model must vanish when the t's associated with each Pomeron are zero, in order to satisfy the Froissart bound. Furthermore, it appears that this condition must be put in, as the MP model seems to have no mechanism for producing this behaviour.

The term $K_P A_{0P} A_P$ in Eq. (4) couples three Pomeron amplitudes together. If one assumes that this coupling is linear in the three t's, one discovers that the leading power of ln s from this term is proportional to $tA_{0P}A_P$ provided the diffraction peak shrinks.

The other assumption which we make is that the low subenergy terms would produce a Pomeron pole with intercept $\alpha_P = 1$. Equation (4) then becomes

$$A_P = \frac{\beta A_{0P}}{J - 1 - \gamma t A_{0P}} \tag{5}$$

where β and γ are constants. An exact solution to Eqs. (5) and (3) is

$$A_P(s,t) = 2\sigma_D \frac{J_1(x)}{x} \ln s$$

and

$$A_{0P}(s,t) = \frac{\sigma_D}{\beta} \frac{J_1(x)}{x}$$

where $x = R_0 \ln s \sqrt{-t}$.

The general properties of this model are

$\sigma_T \sim \ln s$ shrinkage $\sim \ln^2 s$

$\langle n \rangle \sim \ln s$

σ_{el} = constant.

Since the basic treatment of the triple Pomeron coupling was based on keeping only leading powers of ln s, we will list other modifications to the amplitudes which will not affect the self-consistency to leading powers of ln s:

i) The fixed pole produced by the low subenergy kernel can be a moving pole with intercept at one.

ii) Terms proportional to $J_0(x)$ and $J_1(x)/(x)$ can be added to A_P. These result from keeping a constant and a term linear in J - 1 in the numerator of Eq. (5).

iii) All terms can be multiplied by exponential t-behaviour, as the diffraction peak will shrink inside any fixed t-dependence.

4. COMPARISON WITH ISR DATA

The parametrization used to fit the elastic scattering data is given below:

$$A(s,t)/s = \sigma_D \exp\left\{\left[b + \alpha' \ln (s/s_0)\right]t\right\} \ln (s/s_0) \frac{2J_1(x)}{x} +$$

$$+ \sigma_M \exp\left\{\left[b' + \alpha' \ln (s/s_0)\right]t\right\} J_0(x) ,$$

where $x = \left[R_0 \ln (s/s_0) + R_1\right] \sqrt{-t}$.

The real part of the amplitude was parametrized as follows:

$$\mathrm{Re}\, T(s,t) = \mathrm{Re}\, T(s,0)\, e^{b''t} ,$$

where Re T(s,0) was calculated from our amplitude using a once subtracted dispersion relation to produce a zero at $s \cong 470$, as is observed at NAL[2]. Some of the results of the fit are shown in Figs. 1 and 2. The values of the parameters are as follows:

$$\sigma_D = 3.71 \qquad \sigma_n = 74.5 \qquad s_0 = 0.57$$
$$R_0 = 0.144 \qquad R_1 = 2.03 \qquad \alpha' = 0.0$$
$$b = 1.73 \qquad b' = 4.5 \qquad b'' = 3.24 .$$

With these parameters a χ^2 of 1060 was obtained for approximately 600 data points[3].

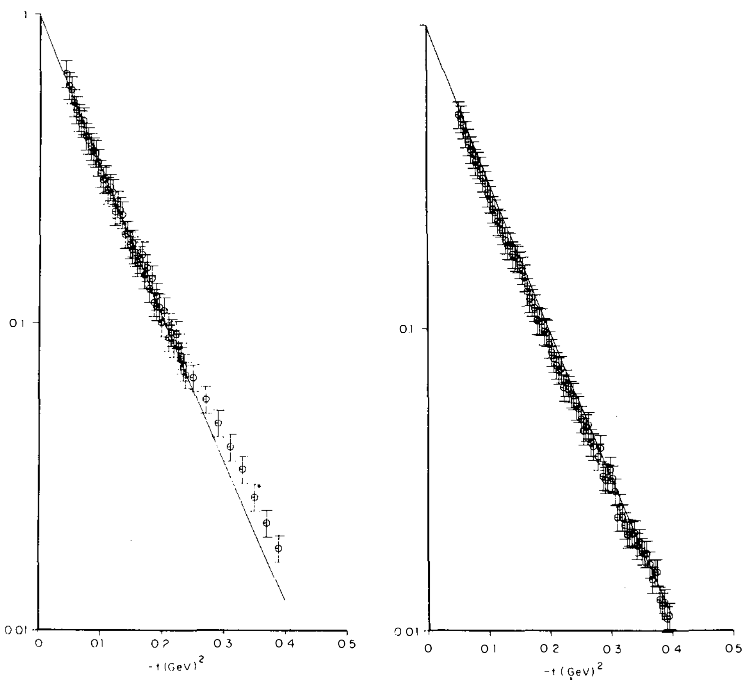

Fig. 1 Fit to $d\sigma/dt$ for t small at s = 560 and s = 2840 (GeV)^2.

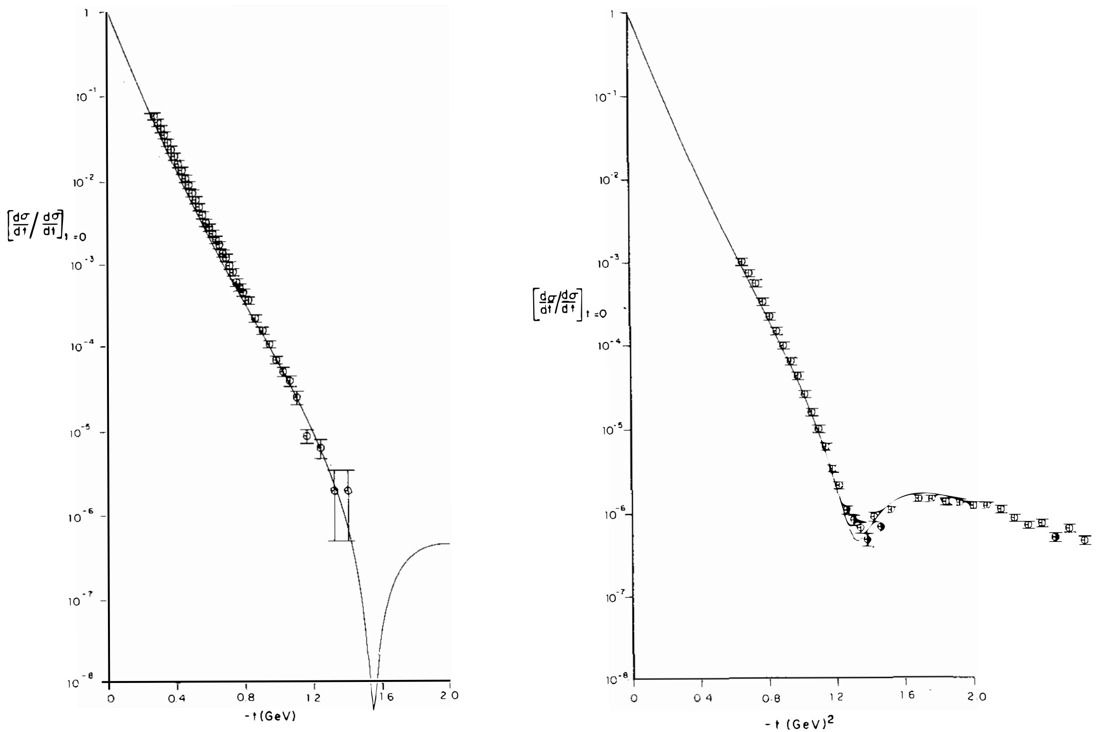

Fig. 2 Fit to dσ/dt for t large at the same two energies. The data is from Ref. 3.

Some comments on these fits are in order. First, we note that superficially the fits are quite satisfactory. The dip is primarily associated with the first zero of $J_1(x)$.

The remarkably small ratio of R_0/R_1 should be noted. This is clearly forced by the small amount of shrinkage observed in the data. In particular the quantity $R_0 \ln s$ is essentially the expansion parameter, which should be large in the region of consistency. We see that even at the highest ISR energy $R_0 \ln s$ is still less than R_1, which means that while a form that is asymptotically self-consistent produces a reasonable fit to the data, the requirements of asymptotic self-consistency provide little constraints on the amplitudes at existing energies.

If we could produce a successful marriage between the asymptotic form which has $x \simeq R_0 \ln s \sqrt{-t}$ and the fixed-pole Pomeron of Section 2 which has $x = R_1 \sqrt{t}$, we might be able to justify the Bessel function forms as being significant at ISR energies. The consistency would then become a comparison of x^2/t with the various b's, i.e. 7-9 compared to 2-4.

Finally, if we could actually calculate the triple Pomeron coupling, the expansion in powers of ln s could be avoided and we would expect self-consistency requirements to produce important constraints on the amplitudes at ISR energies.

REFERENCES

1) J.S. Ball and F. Zachariasen, Phys. Letters 40B, 411 (1972); Nuclear Phys. B72, 149 (1974); Nuclear Phys. B78, 77 (1974); Nuclear Phys. B85, 317 (1975).

2) V. Bartenev et al., Phys. Rev. Letters 31, 1367 (1973).

3) A. Bohn et al., Phys. Letters 49B, 491 (1974). The actual data used in the fitting procedure has had the relative normalization of the small-t and large-t experiments adjusted to produce smooth t-dependence. At this time we are fitting the experimental data points directly.

COMMENTS ON THE SYSTEMATICS OF POMERON EXCHANGE REACTIONS

Uri MAOR†
Service de Physique Théorique
Centre d'Etudes Nucléaires de Saclay
BP n°2 - 91190 Gif-sur-Yvette
France

Abstract

Some of the experimental properties of high energy elastic p-p scattering are reassessed in search for possible systematics. The different b-space profiles obtained for elastic and inelastic diffraction are understood once s-channel unitarity corrections are implemented.

Résumé

Un certain nombre de caractéristiques expérimentales de la diffusion élastique p-p à haute énergie sont passées en revue afin d'en extraire une systématique éventuelle. L'introduction de corrections d'unitarité dans le canal direct permet de comprendre les différentes fonctions de profil dans l'espace des b pour la diffraction élastique et inélastique.

1. Introduction

This contribution contains some comments on the systematics of pomeron exchange in elastic scattering and inelastic diffraction. Limitations of time and space do not provide for a more comprehensive exposition. In sections 2 and 3 we discuss some of the experimental properties of high energy elastic p-p scattering and attempt to reassess the validity of general schemes such as geometrical scaling and the Chou-Yang eikonal model. Section 4 relates to the analysis of inelastic diffraction and its consistency with our knowledge on elastic scattering.

2. Geometrical Scaling

The hypothesis(1) of geometrical scaling (GS) has attracted recently a considerable amount of attention(2), mostly because of its simplicity and strong empirical support(3). GS as such is not compatible with most of our theoretical prejudices, notably the exchange of t-channel poles. It is, therefore, very intriguing to check whether its experimental support is really compelling enough so as to present a systematics that must be incorporated into any theoretical understanding of elastic scattering.

The important observable consequences of GS are :

$$\begin{aligned} \frac{d\sigma}{dt} &= R^4 f(R^2 t) & \sigma_{in} &\sim R^2 \\ \sigma_T &\sim R^2 & B &\sim R^2 \\ \sigma_{el} &\sim R^2 & t_o &\sim R^{-2} \end{aligned} \qquad (1)$$

where R(s) is a radial scale energy dependent parameter. B is the logarithmic slope, and t_o is the position of a dip or a maximum. There is no dispute that GS provides a gross description compatible with high energy p-p scattering(2-4). In the following we shall examine some experimental details in order to point out problematic aspects of this hypothesis.

1) The following table summarizes ISR values for σ_T and forward slope values. Whereas the slopes in the very extreme forward direction (B_o and B_1) are compatible with GS, the slope parameter B_2 is not. The differential cross-section at $.15 \leqslant t \leqslant .4$ GeV^2 does not exhibit any shrinkage over ISR range and if we are to trust the experimental findings(6), we have a severe

$\sqrt{s}$	σ_T (5)	$B_o(t\to 0)$ (5)	$B_1(t<.15)$ (6)	$B_2(.15\leq t\leq .4)$ (6)
23.5	39.1±.4	11.8	11.57±.30	10.42±.17
30.6	40.5±.5	12.3	11.87±.28	10.91±.22
44.9	42.5±.5	12.8	12.87±.20	10.83±.20
52.8	43.2±.6	13.1	12.40±.30	10.80±.20

discrepancy with GS. The problem is not removed by Kroll's modification[4] as the values of the real part of the amplitude in this t range are too small to affect the results. Compatability of slope parameters with GS is conveniently examined through the relation[3]

$$\alpha_{eff}(s,t) - 1 = (1 + \frac{Bt}{2}) \frac{d \log R^2}{d \log s} . \tag{2}$$

We refer the reader to Martin's contribution to this meeting[7] who finds similar incompatibilities.

2) GS is supposed to be an asymptotic property, but its onset is not too clear. For example, Kroll[4] has demonstrated that GS assumed for $\tau_{in}(b,s)$ has a different low energy continuation than GS assumed for $\mathrm{Im}\, F(b,s)$. In any approach GS implies the same energy dependence for B and σ_T over ISR range. Indeed, GS high energy parametrizations[2,3] have been employing an overall log s growth which is dictated by the energy dependence of the forward slopes. We claim that such parametrization provides only marginal σ_T fits, or alternatively implies a complete breakdown of exchange degeneracy (ExD) at lower energies. We have compared[8] two optional parametrizations for a combined p-p and $\bar{p}$-p total cross section fit above P_L = 10 GeV .

$$\sigma_T = A + B \log s + C s^{-1/2} \tag{3}$$

$$\sigma_T = A + B \log^2 s + C s^{-1/2} \tag{4}$$

Both fits were constrained to have $C < 35$ mb GeV for σ_T(p-p) which amounts to a small ExD breaking effect. Our results are summarized in the following table. We have used 55 p-p data points and 24 $\bar{p}$-p data points. Very recent data[9] is not included in this compilation but does not seem to change our conclusion.

Parametrization	A	B	C(p p)	C($\bar{p}$-p)	χ^2
(3)	30.23	1.21	26.86	79.50	229
(4)	31.86	0.156	31.65	85.56	117

A considerable improvement of fit (3) can be achieved[10] if ExD is abandoned altogether, even as a crude approximation. It is an open question if such a sacrifice is really justified.

3) We turn our attention now to detailed model calculations of p-p elastic scattering and their compatibility with GS. We have observed over the past few years an impressive accumulation of elastic p-p scattering data which includes low and medium energy polarization and spin state measurements[11]. These measurements which span over a very wide energy range ($10 < s < 3600$ GeV^2) do not enable, as yet, for a complete amplitude analysis but do enforce very severe limitations on the freedom that we have in choosing p-p parametrizations. In the present context we are interested in the behaviour of the non-flip amplitude which can be deduced from the combined high and low energy systematics[12]. The pomeron contribution has been conveniently decomposed into a Bessel expansion

$$\mathrm{Im}\,\Phi_{NF} = -s\left[A_o\, e^{-a_o P_T^2} J_o(R_o\sqrt{-t}) + A_1\, e^{-a_1 P_T^2} \frac{J_1(R_1\sqrt{-t})}{R_1\sqrt{-t}} + A_2\, e^{-a_2 P_T^2} J_2(R_2\sqrt{-t})\right] . \tag{5}$$

The relevant result is that the three radius parameters <u>are not consistent with GS</u>, namely :

$$R_o \sim \log s \quad ; \quad R_1 \sim \text{const.} \quad ; \quad R_2 \sim \sqrt{\log s} \quad . \tag{6}$$

Kane[20] has treated the same problem with a different theoretical input. His results differ from ours in details but offer also very little comfort for GS. These results are admitedly model dependent, but the failure to formulate a p-p parametrization compatible with GS with proper low energy behaviour is a severe deficiency.

To summarize : it seems that GS provides only a very crude description of high energy p-p scattering. In our opinion problems relating to medium t range ($.15 \leqslant t \leqslant .4$ GeV^2) and low energy continuation must be clarified if GS is to be implemented as a proper systematics.

3. <u>The Chou-Yang Eikonal Model</u>

The Chou-Yang eikonal model[13] is based on two intuitively appealing assumptions :

1) The opacity $\Omega(b,s)$, in an eikonal model, approaches a limiting distribution which is propostional to the matter density distribution of the colliding particles

$$\Omega(b,s) \rightarrow \Omega(b) = K\,\rho(b) \tag{7}$$

K is the absorption coefficient.

2) The matter distribution $\rho(b)$ equals the charge distribution, i.e. :

$$\rho(b) = \int G_E^2(t)\; J_o(b\sqrt{-t})\sqrt{-t}\;\; d\sqrt{-t} \quad . \tag{8}$$

The model has been applied mostly in p-p analysis and accounts in a natural way for the forward concaveness observed in $d\sigma/dt$ and the ISR dip at $t \simeq 1.4\ \mathrm{GeV}^2$. The following is a summary of the main outstanding problems in the application of the model to p-p scattering[8].

1) Total cross sections keep growing through the ISR range. For some time it was hoped that the p-p system has reached a limiting distribution and that K is energy dependent so that

$$\Omega(b,s) \rightarrow K(s)\,\rho(b) \quad . \tag{9}$$

It was, however, shown[14] that such a possibility is highly unlikely because it would imply a very rapid growth of the second $d\sigma/dt$ maximum, contrary to the ISR data. Also, if (9) holds we expect the Ω increment over ISR to be central (and proportional to $\rho(b)$) whereas it is actually peripheral. It is very interesting to examine the ISR data and check for the possibility that <u>we have not reached a limiting distribution as yet</u>. Such an option corresponds to σ_T approaching a finite limiting asymptotic value at super high s .

2) Numerical analysis depends crucially on a good knowledge of the E.M. isoscalar form factor employed in (8). Theoretically, it is not clear at all whether one should use G^2 , as most recent papers do, or F_1^2 as originally suggested. In the present study we have examined both form factors. Experimental knowledge of the neutron form factor is considerably inferior to

our knowledge of the proton form factor. Our comparison is based on Fried and Gaisser parametrization[15] which provides the best analytical reproduction of the proton form factor data[16].

3) A proper Chou-Yang analysis must take into account the real part of the amplitude. In our study we have used the Kroll's tables[4], from which we have obtained the imaginary part of the p-p opacity denoted by $\Omega_K(b,s)$.

Fig.1 presents the ratios of Ω_K relative to KG^2 and KF_1^2 as a function of the impact parameter b at the two extreme ISR energies. Since the small b opacities are energy independent (they saturate at about 95% of the unitarity limit), the values of K were readily obtained at $b = 0$. Some immediate conclusions can be drawn from this comparison.

a) $\Omega_K(b)$ is smaller than $KG^2(b)$ and may be approaching it as a limiting distribution. This is, however, an unlikely arrangement. If the ISR rate of convergence continues, the high energy limit will be reached at excessively high energies. Moreover,,such a situation requires the second $d\sigma/dt$ maximum to increase by orders of magnitude while approaching its limiting value. This phenomenon is not at all indicated by the ISR data. It is a good opportunity to stress the necessity of simultaneous b and t space studies if one is to avoid systematic distortions.

b) In our opinion, F_1^2 is a more appealing choice. Fig.1 suggests an intriguing possibility. The proton density matter distribution equals the charge distribution plus a second component which is E.M. neutral. This second component is peripheral and can be parametrized as a gaussian. Referring to the previous section the second component does not geometrically scale !

4. Inelastic Diffraction

Inelastic diffraction, unlike elastic scattering, is peripheral in b-space[17]. In this section we show[18] that this is a direct consequence of the implementation of s-channel unitarity corrections.

We consider a single excitation diffractive reaction which we examine in a Deck like model (Fig.2). The elastic amplitude, after being corrected for initial and final state rescatterings, is approximated by $A\, e^{Bt}$ (which is $\frac{A}{2B}\exp(-b^2/4B)$ in b-space). Standard calculations replace the pomeron exchange sector of Fig.2 by the experimental cross section. That is, the input pomeron used in inelastic calculations includes elastic corrections relating to the rescattering of the incoming particle on the exchanged (virtual) π or R of Fig.2 . To this we must add the genuine initial and final state corrections relevant to Fig.2 . For actual calculations we follow Caneschi and Schwimmer[19] and evaluate the influence of initial state absorption in the triple Regge limit (Fig.3). The differential cross section in b-space is given by

$$\frac{d\sigma}{dx}(b,b') = \int e^{-(b-\tilde{b})^2/4B} \; e^{-(b'-\tilde{b}')^2/4B} \; \delta^2(\tilde{b}-b-\tilde{b}'+b') \; d(b-\tilde{b})^2 \; d(b'-\tilde{b}')^2 \tag{10}$$

Initial state absorption is introduced by multiplying the integrand of (10) by absorptive damping factors. Let us assume complete absorption for b , b' smaller than b_o (black disc absorption). After integration we obtain a peripheral gaussian profile $\exp(-(b-b_o)^2/4B)$ which is different from the central $\exp(-b^2/4B)$ input.

Our result is further clarified in an exclusive eikonal model calculation. For a two-body problem we have

$$f(b) = \frac{1}{2i} \left(e^{-\Omega(b)} - 1\right) \tag{11}$$

When extending (11) to a N multichannel problem, the scalar Ω is replaced by a NxN matrix denoted by χ . Let us discuss a two channel system with elastic and one inelastic diffraction mode. We have then

$$\chi(b) = \Omega(b) \left(I + \varepsilon(b)\sigma_x\right) \tag{12}$$

To first order in ε we get

$$2i \; f(b) = I(e^{-\Omega(b)} - 1) + \sigma_x \; \varepsilon(b) \, \Omega(b) \; e^{-\Omega(b)} \tag{13}$$

Namely, the output profile breaks into a diagonal term which is central and a non diagonal diffractive term which is peripheral. As can be clearly seen, the peripherality of the diffractive amplitude comes out as a direct consequence of the central character of the elastic profile. As can be seen directly from Eq.(13) the non vanishing of the diffractive channel forces the elastic amplitude to saturate below the unitarity limit. As is well known, this phenomenon is actually observed.

References

1) J. Dias de Deus, Nucl. Phys. B59 (1973) 231.
2) V. Barger, Proceedings of the 18th Int. Conf. on High Energy Physics, London, (1974).
3) V. Barger, J. Luthe and R.J.N. Phillips, Wisconsin preprint (1975).
4) P. Kroll, contribution to this meeting ; W. Grein, R. Guigass and P. Kroll, to be published in Nucl. Phys. B.
5) U. Amaldi et al., Phys. Lett. 44B (1973) 112.
6) G. Barbielini et al., Phys. Lett. 39B (1972) 663.
7) A. Martin, contribution to this meeting.
8) U. Maor, E. Leader, P.G. Williams and J. Kasman, to be published.
9) A.S. Carroll et al., FNAL Preprint (1975).
10) A. Capella and J. Tran Thanh Van, private communication.
11) A. Yokosawa, contribution to this meeting.
12) E. Gotsman and U. Maor, to be published in Nuovo Cimento Letters.
13) T.T. Chou and C.N. Yang, Proc. Conf. on High Energy Physics and Nuclear Structure, Rehovot (1967).
14) F. Hayot and U.P. Sukhatme, Phys. Rev. D10 (1974) 2183.
15) H.M. Fried and T.K. Gaisser, Phys. Rev. 179 (1969) 1941 .
16) P.N. Kirk et al., Phys. Rev. 8D (1973) 63.
17) N. Sakai and J.N.J. White, Nucl. Phys. B59 (1973) 511 ; S. Humble, Nucl. Phys. B76 (1974) 137 ; Nucl. Phys. B86 (1975) 285.
18) G. Cohen-Tannoudji and U. Maor, Saclay preprint (1975).
19) L. Caneschi and A. Schwimmer, Nucl. Phys. B44 (1972) 31 ; Nucl. Phys. B48 (1972) 519.
20) G.L. Kane, private communication.

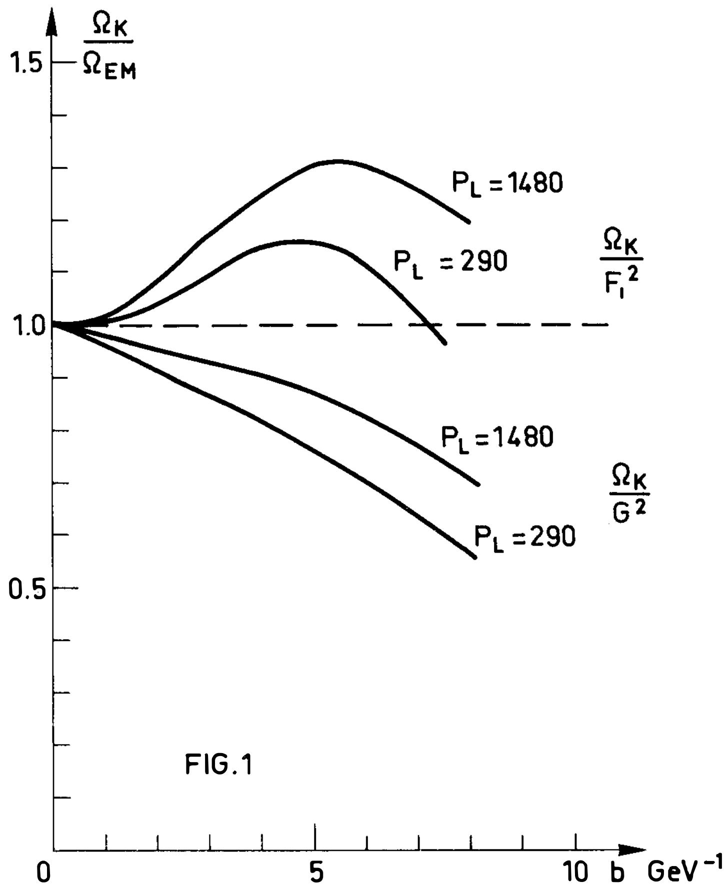

FIG.1

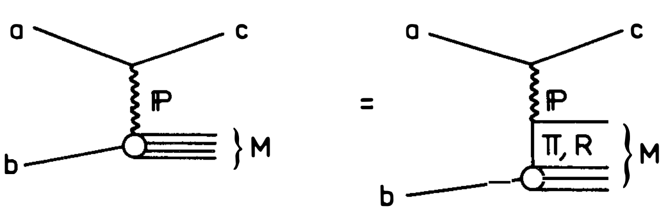

FIG.2

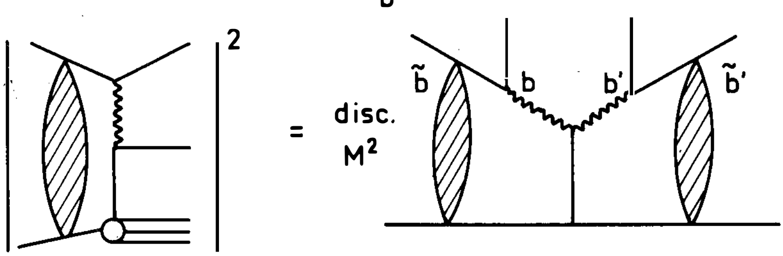

FIG. 3

GEOMETRICAL SCALING IN PROTON-PROTON SCATTERING

P. Kroll

Institut für Theoretische Kernphysik
University of Karlsruhe

Abstract: The influence of the real part of the elastic amplitude on geometrical scaling will be discussed. It will be shown that the inelastic overlap function scales above 50 GeV and not the elastic amplitude. Consequences of this result for elastic scattering will be discussed.

Résumé : Nous discutons de l'influence de la partie réelle de l'amplitude de diffusion élastique sur l'invariance d'échelle géométrique. Nous montrons que la fonction de recouvrement inélastique vérifie l'invariance d'échelle pour des énergies supérieures à 50 GeV contrairement à l'amplitude élastique. Les conséquences de ce résultat sur l'amplitude élastique seront discutées.

1. INTRODUCTION

Some time ago Dias de Deus[1] has suggested a scaling law for the inelastic overlap functions of hadronic scattering reactions at high energies

$$\tau_{in}(b,p) = \tau_{in}(b/R) \tag{1}$$

where $R = R(p)$ is the interaction radius of the hadrons involved and p is the momentum of the incoming particle in the stationary target system. This geometrical scaling (GS) behaviour - originally proposed in order to explain KNO scaling[2] in geometrical models for particle production - has also very interesting consequences for elastic scattering. Neglecting the real part (- and of course spin effects -), it follows from unitarity that the imaginary part of the impact parameter transformed amplitude scales too

$$\mathrm{Im}\,\tilde{F}\,(b,p) = \mathrm{Im}\,\tilde{F}\,(b/R) \tag{2}$$

and hence

$$\mathrm{Im}\,F\,(t,p) = pR^2 g(R^2 t) \tag{3}$$

A lot of relations for observables follow immediatly from eq. (3)

$$\text{i) } \sigma_{tot},\ \sigma_{el},\ \sigma_{in},\ B = \frac{d\sigma}{dt}\,\ell n\,\frac{d\sigma}{dt} \sim R^2 \tag{4}$$

ii) $\frac{d\sigma}{dt}(t,p)/\frac{d\sigma}{dt}(t = 0,p)$ considered as a function of $R^2 t$ is independent of the energy

iii) for the position t_o of a dip or a maximum of the differential cross section one has $R^2\ t_o$ = const. and so on.

These relations have been studied in great detail in pp scattering at ISR energies and it has been found out that GS works quite successfully in this case (compare Bargers[3] talk at the London conference) even if some problems remain[4].

In the following the influence of the real part on GS will be discussed. From an analysis of pp scattering which will be described in the next section, it turns out that the inelastic overlap function exhibits GS above 50 GeV whereas the scaling behaviour of Im F is disturbed by the real part. Consequences of this result for elastic scattering, that is modifications of the relations (4) due to the real part will be discussed in the final section.

2. IMPACT PARAMETER ANALYSIS OF PROTON-PROTON SCATTERING INCLUDING THE REAL PART

In many investigations[5] the overlap function for pp scattering have been studied at ISR energies, neglecting generally the spin and the real part. For lower energies, it is not a priori, clear that these assumptions are correct. The next step towards a complete analysis is the inclusion of the real part. One may hope that this is the more important correction because as can be seen from the polarization data, spin effects are very small in pp scattering and decrease very fast with energy at least for small $|t|$ $(P \sim 1/p)$. Such an analysis has been done by the authors of ref. 6. The real part has been calculated for $p > 10$ GeV and $0 < |t| < 3\text{GeV}^2$ using a dispersion relation between the modulus and the phase of the crossing symmetric part of the amplitude and assuming Regge behaviour for the crossing odd part. Since the real part is only a correction in the impact parameter analysis this procedure should provide a sufficient approximation for it.

Using these results, the impact parameter transformed amplitude, defined by

$$\tilde{F}(p,b) = \frac{2}{p} \int_0^\infty \sqrt{-t}\, d\sqrt{-t}\; J_o(b\sqrt{-t})\; F(p,t) \tag{5}$$

has been evaluated and then the inelastic overlap function via the unitarity relation

$$\tau_{in} = \mathrm{Im}\, \tilde{F} - \frac{1}{4} |\tilde{F}|^2 \tag{6}$$

As expected from the behaviour of $\frac{d\sigma}{dt}$, i.e. the approximate exponential diffraction peak, τ_{in} behaves roughly as a Gaussian. The main deviations from it are observed in the tail at large b and around b=0 where τ_{in} flattens out. These facts are well known[5].

The interesting point here is the energy dependence of the overlap function which is displayed in fig. 1. τ_{in} and Im $\tilde{F}$ at $b = 0$ have been plotted as a function of the energy and furthermore the difference between τ_{in} at a given momentum and of that at the highest one ($p_m = 1480$ GeV)

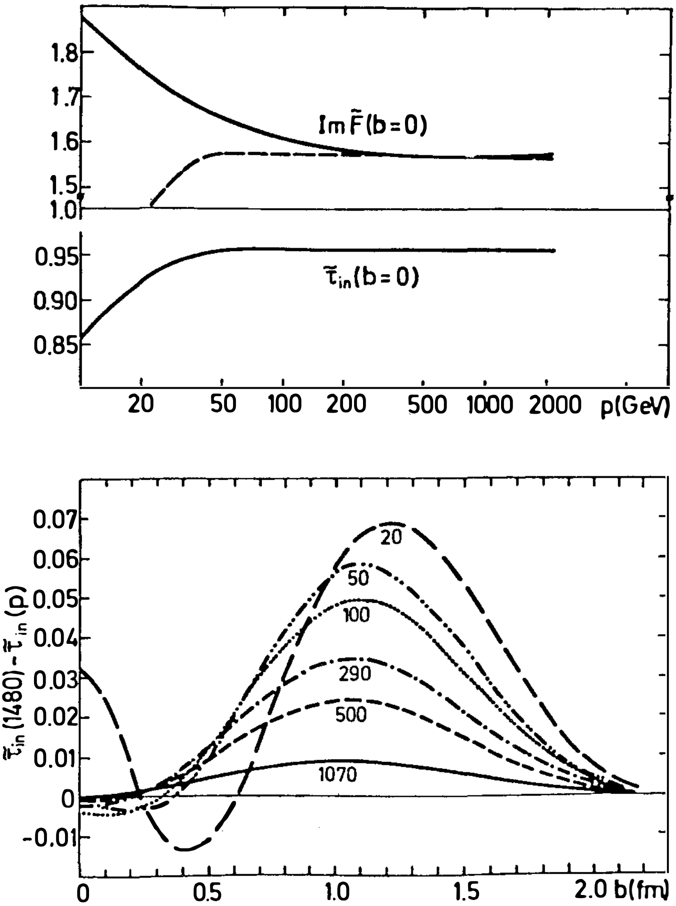

Fig. 1: a) Im $\tilde{F}$ and τ_{in} at b = 0 as a function of p (solid lines). The dashed line represents a result for Im $\tilde{F}$ belonging to the same τ_{in} but without taking into account the real part. The statistical errors of the overlap functions are of the order of 0.005.

b) The energy dependence of the inelastic overlap function (cf. eq. (7)). Typical statistical errors are of the order of 0.007.

$$\Delta(p,p_m) = \tau_{in}(p_m,b) - \tau_{in}(p,b) \tag{7}$$

The remarkable fact is that τ_{in} – and not Im $\tilde{F}$ – at b = 0 is constant within the errors (± 0.005) and it clearly increases peripherally. Im $\tilde{F}(b = 0)$ is approximately constant only in the ISR region.

The difference between both functions is due to the real part whose principal behaviour is sketched in fig. 2 below.

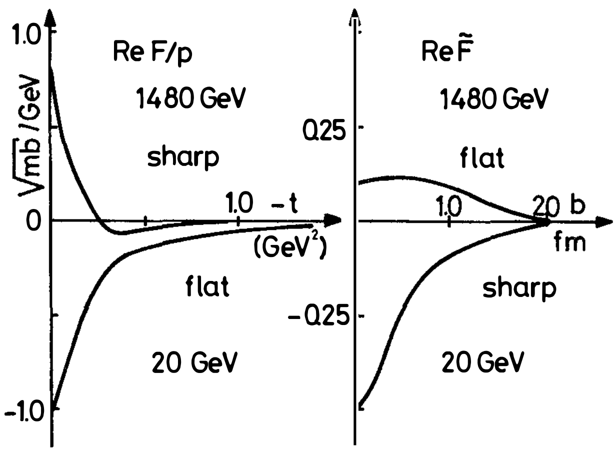

Fig. 2: The structure of the real part in the t and b space.

Although the real part is small it is not negligible in the unitarity relation for small b. Then,solving eq. (6) for Im $\tilde{F}$

$$\text{Im}\,\tilde{F} = 2\left\{1 - \sqrt{1 - \tau_{in} - \frac{1}{4}(\text{Re}\,\tilde{F})^2}\right\} \tag{8}$$

one sees that Re $\tilde{F}$ has only to compete with $1 - \tau_{in}$ which is small for $b \simeq 0$ too. For larger b Re $\tilde{F}$ is completly negligible so that τ_{in} and Im $\tilde{F}$ behave similarly.

From fig. 1 one reads off that τ_{in} (and not Im $\tilde{F}$) scales geometrically in the very large energy interval from 50 to 1500 GeV. From GS of τ_{in} follows only

$$\sigma_{in} \sim R^2$$

whereas all other relations represented in eq. (4) are disturbed by the real part. From the behaviour of σ_{in} one finds for the radius (compare Fig. 3)

$$R = r_o + r_1 \ln p/p_1 \tag{9}$$

with $r_o = 0.904$ fm, $r_1 = 0.016$ fm and $p_1 = 1$ GeV. Of course, a fit with $R^2 = c_o + c_1 \ln p/p_1$ is also possible.

It should be mentioned that if R is growing as $\ln p$ for $p \to \infty$, GS holds asymptotically as shown by Auberson, Kinoshita and Martin[7]. In this case the amplitude is dominantly imaginary

$$\frac{\mathrm{Re}\ F}{\mathrm{Im}\ F} \to \pi/\ln p$$

and behaves as

$$\mathrm{Im}\ F \to \frac{a}{4} R^2 \frac{2J_1(R\sqrt{-t})}{R\sqrt{-t}}$$

corresponding to a grey disk for $\mathrm{Im}\ \tilde{F}$ as well as for τ_{in}

$$\tau_{in} \to a(1 - \frac{1}{4} a)\ \Theta(R - b)$$

However, at present energies τ_{in} is very far from being a grey disk.

3. IMPLICATIONS FOR ELASTIC SCATTERING

In this section disturbances of the relations eq. (4) which follow from perfect GS, i.e. GS of the full elastic amplitude (- or GS of Im F if Re F is negligible -) will be discussed. In doing that we start from a scaling τ_{in} and the old unchanged real part. Using the overlap function at 1480 GeV, the elastic amplitude at a given energy is calculated from eqs. (9), (8) and the inverse of eq. (5).

i) the total cross section

As is wellknown σ_{tot} behaves not similar to σ_{in}. Re $\tilde{F}$ distorts via unitarity Im F. Expanding eq. (8) with respect to $\sqrt{1 - \tau_{in}}$ one finds

$$\mathrm{Im}\ \tilde{F} \simeq 2 \left\{ 1 - \sqrt{1 - \tau_{in}} \right\} + \frac{1}{4} \frac{\mathrm{Re}\ F^2}{\sqrt{1-\tau_{in}}}$$

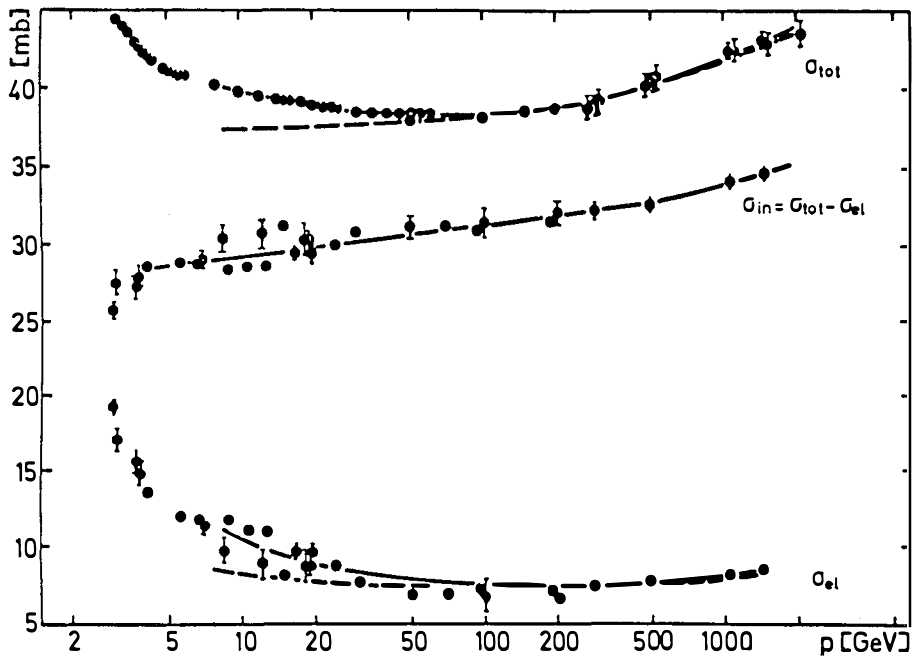

Fig. 3: The momentum dependence of the total, elastic and inelastic pp cross sections. For references to the data compare ref. 6. The solid lines represent the corresponding quantities of the analysis of ref. 6. The dashed lines are the results for σ_{tot} and σ_{el} of calculation without the real part, starting from the same inelastic overlap function.

The first term on the right hand side scales if τ_{in} does

$$\text{Im}\,\tilde{F} = \text{Im}\,\tilde{F}_{GS} + \frac{1}{4}\frac{\text{Re}\,\tilde{F}^2}{\sqrt{1-\tau_{in}}}$$

Hence

$$\text{Im}\,F = \text{Im}\,F_{GS}\left\{ 1 + \frac{p}{8\text{Im}\,F_{GS}}\int bdb\, J_o(b\sqrt{-t})\,\frac{\text{Re}\,\tilde{F}^2}{\sqrt{1-\tau_{in}}}\right\} \qquad (1o)$$

At $t = 0$ the real part gives a positive correction to $\text{Im}\,F_{GS}$ - stronger at small energies, weaker at higher energies - which makes σ_{tot} flatter (and produces actually a minimum) than σ_{in}. (Compare fig. 3).

ii) The slope parameter

In a very good approximation one has

$$B = 2\,\frac{1}{\text{Im}\,F}\,\frac{d}{dt}\,\text{Im}\,F\Big/_{t\,=\,0}$$

From eq. (1o) it follows

$$B = 2\,\frac{1}{\text{Im}\,F}\,\frac{d}{dt}\,\text{Im}\,F_{GS} + \frac{p}{16\text{Im}\,F}\int b^3db\,\frac{\text{Re}\,\tilde{F}^2}{\sqrt{1-_{in}}}$$

The first term on the right hand side dominates (checked numerically), therefore

$$B = \frac{\text{Im}\,F_{GS}}{\text{Im}\,F}\,B_{GS} \simeq B_{GS}\left\{ 1 - \frac{p}{8\text{Im}\,F_{GS}}\int bdb\,\frac{\text{Re}\,\tilde{F}^2}{\sqrt{1-\tau_{in}}}\right\} \qquad (11)$$

i.e. the slope is changed by the same term as σ_{tot} but in the opposite direction. The slope becomes steeper than σ_{in}.

From eq. (11) one sees furthermore, that

$$\frac{\sigma_{tot}}{\sigma_{in}}\,B \sim B_{GS} \sim R^2 \qquad (12)$$

This relation is tested in Fig. 4a). It can be seen that it works very well.

Notice the fact that neither σ_{in} nor σ_{tot} B/σ_{in} change their behaviour around 50 GeV. This may be a hint that GS sets in at much lower energies and only the incomplete analysis described

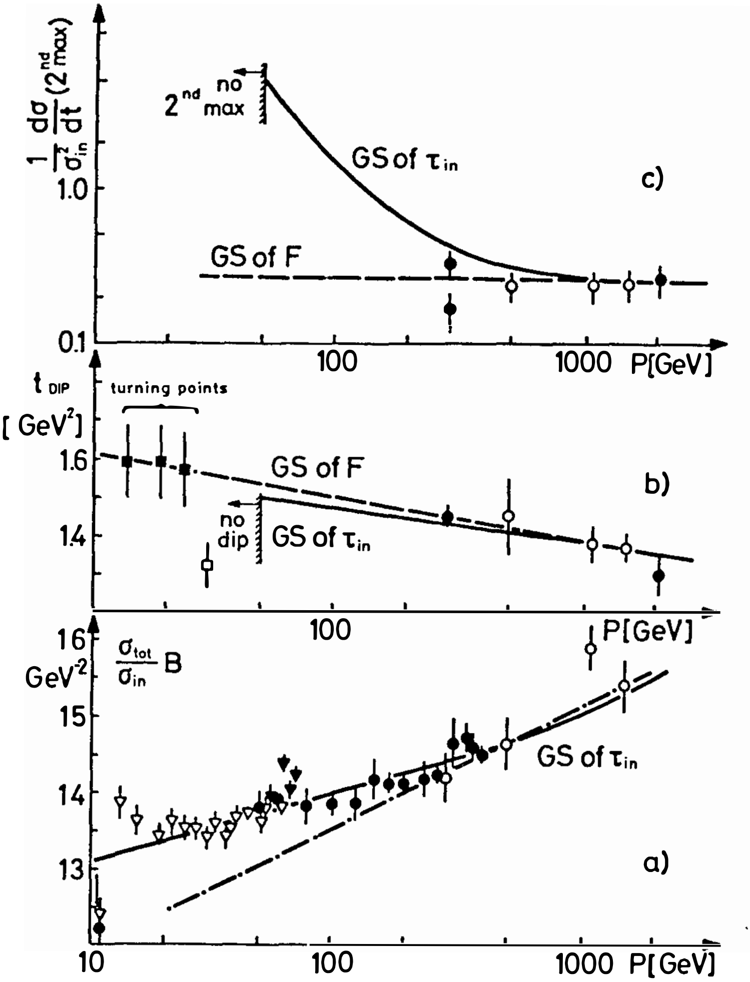

Fig. 4: Predictions of GS

a) $\sigma_{tot}\, B/\sigma_{in}$ compared with the energy dependence of σ_{in} (solid line). The dashed-dotted line represents the energy dependence of the slope itself.

b) the position of the dip of $d\sigma/dt$

c) the height of the secondary maximum

References to the data are given in ref. 6).

in the preceding section produces the deviations from GS below 50 GeV. The next two phenomena are much more complicated because the real part enters now twice, directly in the elastic amplitude and indirectly in the unitarity relation. Therefore it is only possible to give numerical results.

iii) the dip position of $\frac{d\sigma}{dt}$
The data together with the predictions from perfect GS and from GS of τ_{in} are displayed in Fig. 4b. Agreement with the data is observed. There is only a little difference between the prediction of both types of GS. However, below 50 GeV perfect GS predicts still a dip contrary to GS of τ_{in}.

iv) the height of the secondary maximum of $\frac{d\sigma}{dt}$ (Fig. 4c)
Below ISR energies the height of the 2^{nd} maximum should increase with decreasing energy, whereas perfect GS predicts a constant value of $\frac{1}{\sigma_{in}^2}\frac{d\sigma}{dt}$ (2^{nd} max). The increase is not only the direct effect of the real part (compare eq. (1o)), because it contributes only 40% at 50 GeV to $\frac{d\sigma}{dt}$ and 20% at 1500 GeV.

Of course, not only these two phenomena can be calculated from GS but the whole differential cross sections. (Compare fig. 7 of ref. 6). Forthcoming data from FNAL especially such for $|t| > 1$ GeV^2 will enable us to do a crucial test of GS. Preliminary data for $|t| < 1$ GeV^2 are in agreement with GS of τ_{in} [8].

4. SUMMARY

From an analysis of elastic pp scattering one finds that the inelastic overlap function shows GS within the experimental errors above 50 GeV but not the elastic amplitude. In order to obtain that result it is necessary to take into account the real part of the amplitude.

The main consequences of GS of τ_{in} are:

i) Referred to Im F **at** 1480 GeV Im F at a given p < 1480 GeV is larger than GS of Im F would predict

ii) σ_{tot} shows a minimum around 150 GeV

iii) the slope is rising faster than σ_{in}, so that $\sigma_{tot}\ B/\sigma_{in}^2$ is constant.

iv) $\frac{1}{\sigma_{in}^2} d\sigma/dt$ at the secondary maximum is decreasing with increasing energy.

However, at ISR energies, both types of GS that is GS of τ_{in} and GS of Im F, agree within the errors.

REFERENCES

1. J. Dias de Deus, Nucl.Phys. B59 (1973) 231
   see also
   A. J. Buras and J. Dias de Deus, Nucl.Phys. B71 (1974) 481
2. Z. Koba, H.B. Nielsen and P. Olesen, Nucl.Phys. B40 (1972) 317
3. V. Barger, Proceedings of the 18th Int.Conf. on High Energy Physics, London (1974)
4. A. Martin, preprint Durham (1975)
5. U. Amaldi, Proceedings of the 2nd Int.Conf. on Elementary Particles, Aix-en-Provence (1973)
6. W. Grein, R. Guigas and P. Kroll, to be published in Nucl.Phys. B
   P. Kroll, Nucl.Phys. B82 (1974) 510
7. G. Auberson, T. Kinoshita and A. Martin, Phys.Rev. D3 (1971) 3185
8. J. Cutts, private communication

DOES THE POMERON OBEY GEOMETRICAL SCALING ?

Alexander MARTIN

Centre de Physique Théorique
C.N.R.S., Marseille

Abstract : Tests of the validity of the Geometrical Scaling Hypothesis are reviewed.

Résumé : Nous proposons une vérification expérimentale de la validité de l'hypothèse de géométrie d'échelle.

The hypothesis of Geometrical Scaling has had some success in correlating the qualitative features observed in the elastic scattering of protons at ISR energies, namely the shinking of the diffraction peak and the shift forward of the dip are linearly related to the rise in total cross section[1]. In the following I will review briefly the physical ideas behind the hypothesis and then assess its validity in a quantitative confrontation with the data.

The conjecture is most plausibly stated in terms of the impact-para meter decomposition of the scattering amplitude $f(s,t)$ namely that only the length scale changes with energy, the functional dependence remaining unchanged :

$$h = h\left(b / R(s) \right) \tag{1}$$

In this form the hypothesis is very hard to test since there is a lot of manipulation involved in extracting the impact-parameter profile from the data, so it is very fortunate that one can give an equivalent statement in terms of s and t :

$$f(s,t) = f_o(s)\, g\,(f_o t) \tag{2}$$

where $f_o(s) = f(s,o)$ and $g(o) = 1$.

It is usual to neglect the real part[*], and using the optical theorem to write :

$$f(s,t) = \sigma_T \; F(\sigma_T\, t) \tag{3}$$

We illustrate schematically what happens as we go from energy s_1 to energy s_2 with $S_2 > S_1$ and $\sigma_T(S_2) > \sigma_T(S_1)$. We see that the diffraction pattern shrinks as a consequence of the rescaling of the momentum transfer.

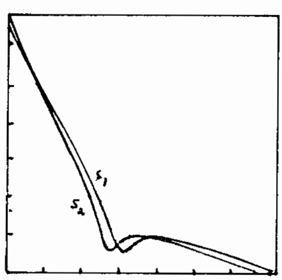

Fig. 1

(*) Despite some claims to the contrary[2] it can be shown that the inclusion of the real part makes no detectable difference in any of the checks mentioned below.

The immediate consequences of 3 are

(i) $B(s,0) \propto \sigma_T$,

(ii) $t_{min} \propto \frac{1}{\sigma_T}$,

(iii) $\left.\frac{d\sigma}{dt}\right]_{2nd\ max} \propto \sigma_T^2$, and

(iv) $\frac{1}{\sigma_T^2} \frac{d\sigma}{dt}$ points lie on a universal curve vs. $\sigma_T t$

These predictions have been checked extensively by Barger and his collaborators and found to be in agreement with experiment [3,4]. Preliminary results on points (ii) and (iii) have been presented by Nagy [5] and, though the experiment, when it is completely analyzed, should be able to test prediction (iii) , at present this is not the case. The experimental quantities necessary for the verification of points (i) - (iii) are either ill-defined or not well known, and do not provide serious tests for the hypothesis. As for point (iv) which considers the data at all t , it is not apparent that it excludes a systematic deviation from Geometrical Scaling. We shall see by the following that such a violation is indeed seen, and that it is not small compared with the observed change with energy.
It is apparent that the full weight of the exceedingly accurate data available has not been utilized in these checks. Such an objective is realized when one looks at the difference with energy of the differential cross section at fixed t , for G-S relates it, in a very direct way, to the difference in t at fixed s . It can be shown that Eq.2 is equivalent to the following derivative-relation [4,6] :

(4) $$\alpha_{eff}(s,t) - 1 = \epsilon\,[\,1 + B(s,t)\,t\,] \qquad (4)$$

where $\alpha_{eff} - 1 \equiv \frac{\partial}{\partial \ln s} \ln f(s,t)$,

$B = \frac{\partial}{\partial t} \ln f(s,t)$, and $\epsilon = \alpha_{eff}(s,0) - 1$.

The left-hand side of this relation is the well-known effective Regge-trajectory, and is relatively well determined by the data [6]. We will treat the right-hand side as the prediction of Geometrical Scaling for this quantity. The comparison is shown in Fig. 2 , where the solid curve represents the G-S prediction ,

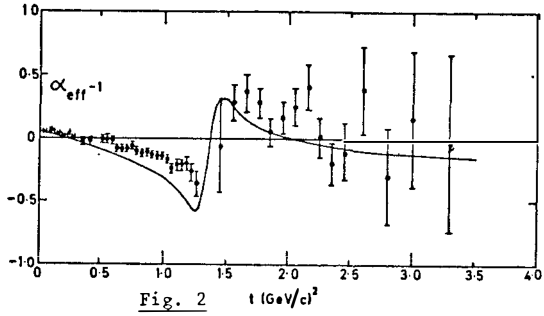

Fig. 2

It is apparent from this graph that G-S predicts roughly 50 % more energy dependence than is seen. We first discuss the uncertainties involved in the analysis before taking up the subject of the implications for G-S :

1) The errors on the experimental α_{eff} are compounded of statistical errors and normalization errors, taken all to be 5 % . This generally overestimates the normalization uncertainties but it should be kept in mind that a renormalization would shift whole blocks of points up or down.

2) $B(s_o, t)$ was taken from a smoothing function which fits the ISR data with a χ^2 per point of 1.5, with no apparent systematic departure. It is good to better than 10 % at any point in $0 < |t| < 1\,(GeV/c)^2$, and furthermore such systematic deviations as would be needed to explain the discrepancy are excluded by the cumulative effect they would have on $d\sigma/dt$.

3) ϵ is a critical parameter since it sets the scale for the G-S prediction and it should be determined by the rise of the total cross-section at ISR in the form $\sigma_T \propto s^{\epsilon}$

However, we know that the amplitude is the sum of a Pomeron and a secondary Regge-pole exchange, and one wants to extract the asymptotic scaling properties. Therefore we should make allowance for the fact that in general $\alpha_{eff}^{exp} \neq \alpha_{eff}^{pom}$ although, for a normally shrinking Reggeon, the contribution is so steep in t , that, at ISR energies, it is negligible in all but the very forward direction. A fit of the form $\sigma_T = As^{\epsilon} + Bs^{-\frac{1}{2}}$ then yields values which depend on the estimate of the Reggeon contribution. Our result $\epsilon = .07$ [7] comes from a fit of this form down to $s = 15\,GeV^2$.

In models where the Pomeron component $\propto \ln s$ the Reggeon contribution would be much bigger and ϵ correspondingly higher. The rock-bottom value of ϵ is given by a fit to σ_T at ISR with B = 0 , resulting in ϵ = .059 ± .004. Now Barger, Luthe and Phillips have claimed confirmation of G-S using a value of ϵ =.045. Fig. 3 is a comparison of their σ_T fit with the data. For clarity we show only a statistical average of the data at each ISR energy.

In conclusion, we have shown that G-S , though extremely precise in its predictions, is not easy to test. The indications are that there is a large violation at $t \simeq .1 (\mathrm{GeV}/c)^2$ which should be confirmed by more accurate measurements of σ_T combined with normalized $d\sigma/dt$ measurements. With respect to the validity of the hypothesis several alternatives may be envisaged :

1) It is not true and should be discarded.

2) It is possible that the energy is not high enough and one is seeing interference with non-asymptotic terms. The logarithmic trajectory proposed by Coon and Tran Than Van may be what is necessary.

3) Higher derivatives may be important. This would call for a more elaborate treatment, i.e. fitting with polynomials, or to a restriction to smaller intervals in S . It is certain that the results would be less conclusive.

4) Perhaps G-S should not be taken more seriously than any other model which purports to describe elastic scattering at high energy.

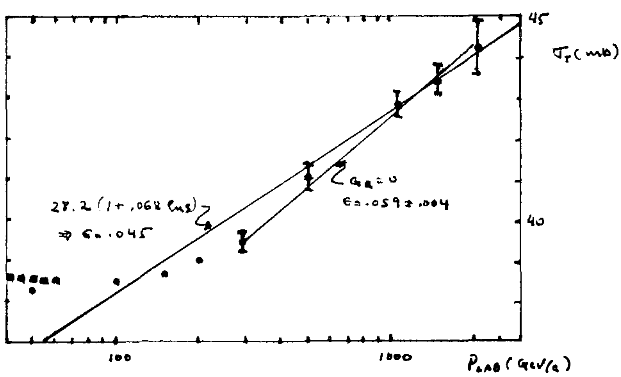

- REFERENCES -

(1) A.J. BURAS and J. DIAS de DEUS
Nucl. Phys. 71 B , 481 (1974)

(2) J. DIAS de DEUS
Rutherford preprint

(3) V. BARGER
Rapporteur's talk at the XVIIth International Conference on High Energy Physics (London 1974)

(4) V. BARGER, J. LUTHE, and R.J.N. PHILLIPS
University of Wisconsin preprint

(5) E. NAGY
Preliminary results of the CERN-Hamburg-Orsay-Vienna collaboration presented at this conference.

(6) A. MARTIN
Durham University Report and Nucl. Phys. 77 B , 226 (1974)

(7) P.D.B. COLLINS, F.D. GAULT, and A. MARTIN
Nucl. Phys. B 83 , 241 (1974)

EFFECTS OF THE INCLUSIVE DIPOLE POMERON
TO EXCLUSIVE PROCESSES*

N.G. Antoniou
Nuclear Research Centre "Demokritos"
Aghia Paraskevi Attikis, Greece

Abstract

The consequences of the inclusive dipole Pomeron for the exclusive processes are investigated. The factorization of the dipole in the Mueller diagrams is consistent with positivity if we impose that the self coupling of the double pole is zero ($g_{dd}=0$). In the weak coupling g_{sd} approximation, keeping only first order terms in the generating function we obtain a two component mechanism for the exclusive production. The simple pole component of the inclusive Pomeron leads to the Poisson distribution and the double pole component to the diffractive component. A meson trajectory appears in the multi-peripheral chain with intercept α_R depending on the coupling g_{ss} whereas the exclusive Pomeron has the same dipole structure at j=1.

*This work was done in collaboration with C.B. Kouris, E.K. Manesis and G.M. Papaioannou, and it is published in Physics Letters 55B, 77 (1975).

p-p SCATTERING-AMPLITUDE MEASUREMENTS WITH POLARIZED BEAMS AND POLARIZED TARGETS AT 2 to 6 GeV/c

A. Yokosawa
Argonne National Laboratory
Argonne, Illinois 60439
(U.S.A.)

There are two groups doing p-p elastic scattering with polarized beams at the ZGS; one of them, ANL(HEP)-Northwestern Collaboration, is interested in the complete determination of p-p amplitudes at relatively small $|t|$ and the other, ANL(ARF)-Michigan-St. Louis Collaboration, is trying to determine only the magnitude of amplitudes at relatively large $|t|$.

In this talk, I concentrate on "first-stage" scattering-amplitude measurements from 2 to 6 GeV/c involving a relatively simple experimental setup, covering a small $|t|$ region where one can accomplish a high-precision measurement.

The elastic p-p scattering amplitude consists of the scalar amplitudes $a(k,\theta)$, $c(k,\theta)$, $m(k,\theta)$, $g(k,\theta)$, and $h(k,\theta)$, in the M matrix:[1]

$$\begin{aligned} M = a(k,\theta) &+ i\,c(k,\theta)(\sigma_1\cdot N+\sigma_2\cdot N) \\ &+ m(k,\theta)(\sigma_1\cdot N\sigma_2\cdot N) \\ &+ g(k,\theta)(\sigma_1\cdot P\sigma_2\cdot P+\sigma_1\cdot K\sigma_2\cdot K) \\ &+ h(k,\theta)(\sigma_1\cdot P\sigma_2\cdot P - \sigma_1 K\sigma_2\cdot K), \end{aligned}$$

where σ_1 and σ_2 are the Pauli matrices of the incident and target protons; N, P, and K are unit vectors along $k_i \times k_f$, $k_f + k_i$, and $k_f - k_i$; and k_i and k_f are initial and final center-of-mass momenta as shown in Fig. 1.

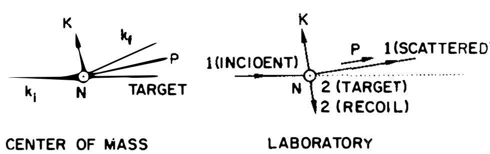

FIG. I UNIT VECTORS N, P AND K

We note here that, in the nonrelativistic case, vectors P and K defined in the center-of-mass system coincide with the directions of scattered and recoil particles, respectively. However, this is not exactly true for the relativistic case, especially at large $|t|$ region.

Although the use of vectors K and P seems unnecessary for the relativistic case, we find them convenient in order to follow traditional p-p scattering parameters.[1, 2, 3]

Recently Halzen and Thomas[4] worked out experimental observables in the relativistic case and these observables are expressed in terms of exchange amplitude. Their vectors are chosen on a practical basis in the laboratory system and are directly responded to the experimental setup. Therefore, we use their notation and at the same time refer to the traditional one.

If all the measurements are to be made on the horizontal scattering plane, the spin directions, N, L, and S, of polarized beam, polarized target, and recoil particles are defined as shown in Fig. 2.

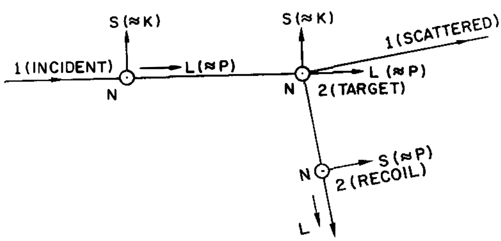

N: NORMAL TO THE SCATTERING PLANE
L: LONGITUDINAL DIRECTION
S = N x L IN THE SCATTERING PLANE

FIG. 2 UNIT VECTORS N, L AND S

We define the polarized target with N direction as "N type," and the one with S and L directions as "H type."

Measurements made so far include differential cross section, $I_o = /a/^2 + 2/c/^2 + /m/^2 + 2/g/^2 + /h/^2$, and polarization parameter, $I_oP = 2\,\mathrm{Im}\,(a+m)c^*$. We need at least seven more measurements to determine five amplitudes and their relative phases.

Possible experiments obtaining spin direction of particles 1 and 2 by means of polarized beam, polarized target, or spin analysis of final state are listed following (*indicates that spin direction is known; 0 means that spin direction is not known):

(1) Beam	+	(2) Target	→	(1) Scattered	+	(2) Recoil	Parameters
*		*		0		0	C_{jk}, Correlation Tensor
*		0		0		*	K_{jk}, Polarization Transfer Tensor
0		*		0		*	D_{jk}, Depolarization Tensor
*		*		0		*	H_{ijk}, Higher-rank Spin Tensor

Single-scattering experiments include C_{jk} measurements and double-scattering experiments include K_{jk}, D_{jk}, and H_{ijk} measurements. We list these parameters in terms of the amplitudes in the M matrix.

Single Scattering

C_{jk} Measurement

Polarized Target	Observables (1,2;1,2)		Historical Notation	Coefficients of the M Matrix[1]
N type	(N,N;0,0)	$\approx$	I_oC_{NN}	$2\left[\mathrm{Re}(am^*) + /c/^2-/g/^2+/h/^2\right]$
H type	(S,S;0,0)	$\approx$	I_oC_{KK}	$2\ \mathrm{Re}\left[(a-m)g^* - (a+m)h^*\right]$
H type	(S,L;0,0)	$\approx$	I_oC_{KP}	$-4\ \mathrm{Re}\ c\ h^*$
	(S,L;0,0)	=	(L,S;0,0)	
H type	(L,L;0,0)	$\approx$	I_oC_{PP}	$2\ \mathrm{Re}\left[(a-m)g^*+(a+m)h^*\right]$

Double Scattering

1) K_{jk} Measurement

(N,0;0,N)	$\approx$	I_oK_{NN}	$2\left[\mathrm{Re}\ a^*m + /c/^2+/g/^2-/h/^2\right]$
(S,0;0,L)	$\approx$	I_oK_{KK}	$2\ \mathrm{Re}\left[(a+m)g^* - (a-m)h^*\right]$
(S,0;0,S)	$\approx$	I_oK_{KP}	$-4\ \mathrm{Re}\ c\ g^*$
(L,0;0,S)	$\approx$	I_oK_{PP}	$2\ \mathrm{Re}\left[(a+m)g^* + (a-m)h^*\right]$

2) D_{jk} Measurement

N type	(0,N;0,N)	$\simeq$	$I_o D_{NN}$	$/a/^2+2/c/^2+/m/^2-2/g/^2-2/h/^2$
H type	(0,S;0,L)	$\simeq$	$I_o D_{KK}$	$/a/^2-/m/^2+4$ Re gh^*
H type	(0,S;0,S)	$\simeq$	$I_o D_{KP}$	$2\ \mathrm{Re}\left[(a-m)c^*\right]$
H type	(0,L;0,S)	$\simeq$	$I_o D_{PP}$	$/a/^2-/m/^2-4\mathrm{Re}\ gh^*$

We note that D_{NN}, D_{KP}, and D_{PP} are commonly called the "D parameter," "R parameter," and "A parameter," respectively.

3) H_{ijk} Measurement

In this type of measurement, we can determine three parameters simultaneously for one measurement. Since changing the configuration of the polarized target is harder than changing the direction of the polarized beam, we list various experimental observables with respect to different spin directions of the polarized proton target.

Polarized Target	Experimental Observables		Historical Notation	Coefficients of the M Matrix	Simultaneous Observables
N type	(S,N;0,S)	$\approx$	$I_o H_{KNP}$	$2\mathrm{Im}\left[(a-m)g^*(a+m)h^*\right]$	(0,N;0,N),(S,0;0,S)
	(L,N;0,S)	$\approx$	$I_o H_{PNP}$	$-4\ \mathrm{Im}\ ch^*$	(0,N;0,N),(L,0;0,S)
H type (Transverse)					
	(N,S;0,S)	$\approx$	$I_o H_{NKP}$	$2\mathrm{Im}\left[-am^* + 2\ gh^*\right]$	(0,S;0,S),(N,0;0,N)
	(S,S;0,N)	$\approx$	$I_o H_{KKN}$	$-4\ \mathrm{Im}\ cg^*$	(S,S;0,0),(0,S;0,S),(S,0;0,S)
	(S,S;0,N)	=	(L,L;0,N)		
	(L,S;0,N)	$\approx$	$I_o H_{PKN}$	$2\mathrm{Im}\left[(a+m)g^*+(a+m)h^*\right]$	(L,S;0,0),(0,S;0,S),(L,0;0,S)
H type (Longitudinal)					
	(N,L;0,S)	$\approx$	$I_o H_{NPP}$	$2\ \mathrm{Im}\left[(a-m)c^*\right]$	(0,L;0,S),(N,0;0,N)
	(S,L;0,N)	$\approx$	$I_o H_{KPN}$	$2\mathrm{Im}\left[-(a-m)g^*-(a+m)h^*\right]$	(S,L;0,0),(0,L:0,S),(S,0;0,S)
	(L,L;0,N)	$\approx$	$I_o H_{PPN}$	$-4\ \mathrm{Im}\ cg^*$	(0,L;0,S),(L,0;0,S)
	(L,L;0,N)	=	(S,S;0,N)		

By considering experimental simplicity and feasibility, we emphasize only measurements that do not require longitudinal spin analysis of recoil particles. The use of a longitudinally polarized beam produced by a vertical bending magnet is not quite suitable to measurements requiring a polarized-proton target.

C_{NN} measurements have been recently completed by ANL-Northwestern collaborators[5] at 2, 3, 4, and 6 GeV/c. The results at 6 GeV/c is shown

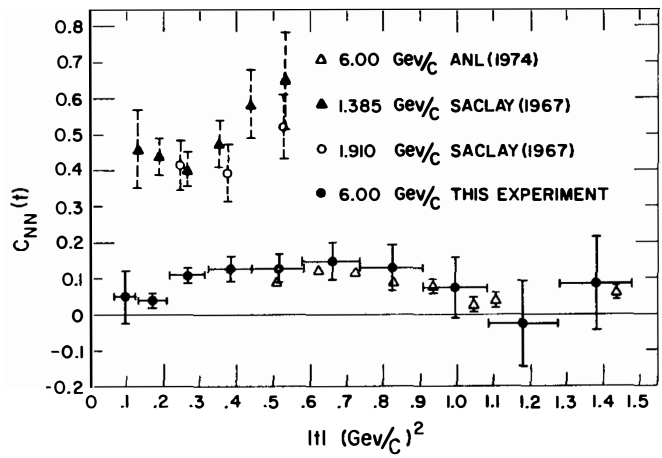

in Fig. 3 together with earlier data by ANL-Michigan-St. Louis Collaboration.[6] Comparing with the data at 1.4 and 1.9 GeV/c[7] we see a strong energy dependence. We expect to make measurements of other parameters in the near future.

References

1. We follow the notation used by M. J. Moravcsik, The Two-Nucleon Interaction, Clarendon Press, Oxford (1963).
2. L. Wolfenstein and J. Ashkin, Phys. Rev. 85, 947 (1952).
3. L. Wolfenstein, Phys. Rev. 96, 1654 (1954).
4. F. Halzen and G. H. Thomas, Phys. Rev. D10, 344 (1974).
5. G. Hicks, et al, ANL-HEP-75-01.
6. R. C. Fernow et al, Phys. Rev. Lett. 52B, 243 (1974).
7. G. Cozzika et al., Phys. Rev. 164, 1672 (1967); Y. Ducros, Rev. Mod. Phys. 39, 531 (1967).

THE STRUCTURE OF AMPLITUDES OF TWO-BODY REACTIONS

A.P. Contogouris *

Laboratoire de Physique Théorique et Particules Elémentaires, Orsay

Abstract : A method combining fixed-t dispersion relations with an (incomplete) set of experimental data and leading to amplitude analyses is presented and applied to certain two-body nondiffractive reactions. Characteristic regularities of the resulting amplitudes are pointed out. A comparison to F E S R leads to an understanding of the t-structure of the real parts.

Résumé : A partir des relations de dispersion à t fixé et un ensemble (incomplet) des données expérimentales on introduit une méthode d'analyse en amplitudes ; cette méthode est ensuite appliquée à un nombre de réactions à deux corps non diffractives. Quelques régularités caractéristiques des amplitudes trouvées sont signalées. La comparaison avec les règles de somme à énergie finie apporte une compréhension de la structure en t des parties réelles des amplitudes.

* On sabbatical leave from McGill University, Montreal, Canada.

1.As an example of the application of our method we consider $\pi^- p \to \pi^0 n$ [1], which will also offer an important test. At high s and fixed t the nonflip (M_0) and flip (M_1) s-channel helicity amplitudes (SHA) are given in terms of the well-known invariants $A^{(-)}$, $B^{(-)}$ by

$$M_0(\nu,t) = 2M \{A^{(-)}(\nu,t) + \nu B^{(-)}(\nu,t)\} \tag{1}$$
$$M_1(\nu,t) = (-t)^{\frac{1}{2}} A^{(-)}(\nu,t)$$

where $\nu = (s-u)/4M$, M = nucleon mass. Then at fixed t :

$$\mathrm{Re}M_n(\nu,t) = \frac{2\nu}{\pi} \int_{\nu_t}^{\infty} \mathrm{Im}M_n(\nu',t) \frac{d\nu'}{\nu'^2 - \nu^2} \quad ; \tag{2}$$

n = 0,1 and the integral includes possible Born term contributions. For $\nu > N$, N to be specified below, we write

$$\mathrm{Im}M_n(\nu,t) = b_n(t)\nu^{\alpha_n(t)} \tag{3}$$

where $\alpha_n(t)$ = effective Regge exponents. Then we split the integral (2) in two parts : A low-energy one, $\nu_t \leq \nu \leq N$, where $\mathrm{Im}M_n$ can be calculated in terms of phase-shifts ; and a high energy one, $N \leq \nu < \infty$, where the expression (3) is a reasonable approximation. Thus N is determined by the limiting energy of the phase-shift analysis. Hence at each t, both $\mathrm{Im}M_n$ and $\mathrm{Re}M_n$ are determined via two real parameters, $b_0(t)$ and $b_1(t)$. These can be calculated from the experimental differential cross-section and polarization P at a given energy. Having specified $b_n(t)$ from the data at one energy, we can predict SHA, $d\sigma/dt$ and P at other high energies.

Due to large differences between polarization data calculations are presented with two different polarization inputs[2] (in Figs. 1, 2, 4 : full lines CERN P, broken lines Argonne P). The simplest choice for the effective Regge trajectories is the ρ trajectory :

$$\alpha_n(t) = \alpha(t) = 0.45 + 0.9\ t \tag{4}$$

The resulting SHA at 6 GeV are shown in Figs. 1 and 2, where comparison is also made with a number of amplitude analyses.[3] Their essential features can be summarized as follows :

(i) $\mathrm{Im}M_1$ has a t-structure of the form $\sim J_1(R\sqrt{-t})$ with $R \approx 1$ f, in agreement with the dual absorption model (DAM). $\mathrm{Re}M_1$ shows a "double-zero" structure at $t \simeq -0.5\ \mathrm{GeV}^2$. On the whole $M_1(\nu,t)$ appears to be dominated by a single Regge pole exchange, so

$$\mathrm{Re}M_1(\nu,t) \simeq \mathrm{Im}M_1(\nu,t)\tan\frac{\pi\alpha(t)}{2} \tag{5}$$

(ii) $\mathrm{Im}M_0$ has a t-structure more of less like $\sim J_0(R\sqrt{-t})$. $\mathrm{Re}M_0$ has a turning point at $t \approx -0.6$ and bears no simple relation to $\mathrm{Im}M_0$.

§2. We now turn to the reactions $K^-p \to \bar{K}^0 n$ and $K^+n \to K^0 p$ [4] These are described in terms of the SHA $M_n^{(\pm)}(\nu,t)$, $n = 0,1$, where $(\pm)$ corresponds to t-channel tensor/vector exchange (ρ/A_2). Data exist on $d\sigma/dt$ for both reactions, but on polarization only for $K^-p \to \bar{K}^0 n$. Thus to proceed with our method we have to make some assumption. We assume that for $\nu > N$:

$$\mathrm{Im}M_1^{(-)}(\nu,t) = \mathrm{Im}M_1^{(+)}(\nu,t), \tag{6}$$

namely that exchange degeneracy holds between the imaginary parts of the vector and tensor flip amplitudes. We use again (4) as effective trajectory, and in fact for both vector and tensor exchange.

The resulting amplitudes at 8 GeV are shown in Fig. 3. Clearly the vector exchange SHA, $M_1^{(-)}$ and $M_0^{(-)}$, are very much the same as before. On the tensor exchange SHA we notice :
(i) $M_1^{(+)}(\nu,t)$ also appears to be dominated by a single Regge pole (here $\mathrm{Re}M_1^{(+)} \approx -\cot\frac{\pi\alpha}{2}\,\mathrm{Im}M_1^{(+)}$).
(ii) $\mathrm{Im}M_0^{(+)}$ somewhat deviates from the DAM form of $J_0(R\sqrt{-t})$, since it has a second zero at $t \simeq -0.4$. This has also been noticed in other analyses involving tensor exchange[5][1]. $\mathrm{Re}M_0^{(+)}$

has no simple relation to $\mathrm{Im}M_0^{(+)}$ and, as in other analyses involving tensor exchange[4], it appears to change sign somewhere at $|t| < 0.5$ GeV^2.

Concerning tensor exchange we note that similar results have been obtained by Girardi et al[6], who follow a completely different approach (e.g. the EXD relation (6), used as an assumption in our analysis, is an outcome in Ref. 6).

§3. We now turn to the comparison of our results with finite energy sum rules (FESR) and to an understanding of the structure of real parts. Fig. 4 presents FESR for $\pi^- p \to \pi^0 n$ corresponding to the lowest two moments (k = 0 and k = 1, moment = 2 k + 1). The essential point to be made is in connection with the lowest moment FESR : for the flip amplitude they are very well satisfied up to $t \simeq -0.6$, for both of our solutions ; but for the nonflip, they are not well satisfied. The higher moment FESR are, on the whole, better satisfied. We would like now to show that these results for FESR together with the fact that $\mathrm{Im}M_n(\nu,t)$ have the structure of $J_n(R\sqrt{-t})$ lead to an understanding of the t-structure of $\mathrm{Re}M_n(\nu,t)$.

We begin with $\mathrm{Re}M_1(\nu,t)$ and shall show how the double-zero structure arises. We re-write Eq. (2) in the form

$$\mathrm{Re}M_1(\nu,t) = \frac{2\nu}{\pi}\int_{\nu_t}^{N} \mathrm{Im}M_1(\nu',t)\frac{d\nu'}{\nu'^2-\nu^2} + \frac{2\nu}{\pi}\, b_1(t)\times \tag{7}$$

$$\times\left\{ ⨍_0^{\infty} \frac{\nu'^{\alpha}d\nu'}{\nu'^2-\nu^2} - \int_0^{N}\frac{\nu'^{\alpha}d\nu'}{\nu'^2-\nu^2}\right\}$$

Using a well-known Hilbert transform for the integral $⨍_0^{\infty}\dots$ and expanding the rest in powers of $1/\nu^2$ we finally obtain

$$\mathrm{Re}M_1(\nu,t) = \mathrm{Im}M_1(\nu,t)\tan\frac{\pi\alpha}{2} + \frac{2}{\pi\nu}\, D_1^{(1)}(t) + \mathcal{O}\left(\frac{1}{\nu^3}\right) \tag{8}$$

where

$$(9) \qquad D_1^{(1)}(t) = b_1(t)\,\frac{N^{\alpha+1}}{\alpha+1} - \int_{\nu_t}^{N} \mathrm{Im}M_1(\nu,t)\,d\nu$$

Notice that $D_1^{(1)}(t) = 0$ is just the lowest moment FESR for the amplitude n = 1. Now, both $\mathrm{Im}M_1$ and $\tan\frac{\pi\alpha}{2}$ have simple zeros at $t \simeq -0.5$ so that the first term in the r.h. side of (8) has a double zero. Since the flip FESR is well satisfied and $D_1^{(1)}$ is further multiplied by $\frac{2}{\pi\nu}$ ($\approx \frac{1}{9}$ at 6 GeV), the remaining terms in (8) are negligible. Thus Eq. (5) is approximately satisfied.

Next we turn to $\mathrm{Re}M_o(\nu,t)$. Similar procedure gives

$$(10) \qquad \mathrm{Re}M_o(\nu,t) = \mathrm{Im}M_o(\nu,t)\tan\frac{\pi\alpha}{2} + \frac{2}{\pi\nu}\,D_o^{(1)}(t) + O\left(\frac{1}{\nu^3}\right)$$

where $D_o^{(1)}$ is given by (8) with n = 0 replacing n = 1. Here $\mathrm{Im}M_o \sim J_o(R\sqrt{-t})$ and Fig.5 (a) - (c) indicates how the structure of $\mathrm{Re}M_o$ arises : since the lowest moment nonflip FESR is not well satisfied the term $D_o^{(1)}(t)$ provides a non-negligible correction. The precise final form of $\mathrm{Re}M_o$ (full or broken line of Fig. 1(c) depends on the details, but some sort of turning point near t = -.5 will arise.

Similar remarks on $\mathrm{Re}M_n$ can be made on the basis of the FESR for $K^-p \rightarrow \bar{K}^o n$ and $K^+n \rightarrow K^o p$.(4)

§4. Recently a set of derivative relations for SHA has been conjectured.(7) These can be written

$$(11) \qquad M_{n+1}(s,t) \sim (\sqrt{-t})^n \,\frac{d}{d\sqrt{-t}}\left(\frac{1}{(\sqrt{-t})^n}\,M_n(s,t)\right)$$

The relations (11) should be considered as approximate ; nevertheless it is of interest to see how they are satisfied by the SHA of our amplitude analyses.

First, concerning $\mathrm{Im}M_n(\nu,t)$, notice that Eqs. (11) are identical to the well-known relations of Bessel functions :

$$J_{\nu+1}(x) = -x^{\nu} \frac{d}{dx} \left(\frac{1}{x^{\nu}} J_{\nu}(x) \right)$$

Since our $\mathrm{Im}M_n$ have essentially the Bessel function structure, they approximately satisfy (11).

Next, concerning real parts, for n = 0 Eq. (11) implies

$$(12) \qquad \mathrm{Re}M_1(s,t) \sim \sqrt{-t} \frac{d}{dt} \mathrm{Re}M_0(s,t)$$

Starting with the form of $\mathrm{Re}M_0$ discussed in paragraph 4, we indicate in Figs. 5 (c) - (e) how we end up with a "double-zero" structure for $\mathrm{Re}M_1$ which is in approximate agreement with our solution (Fig.2). It is not difficult to see that our SHA for the two KN charge-exchange reactions (Fig.3) approximately satisfy the derivative relations.

§5. We consider the application of our method to $\gamma p \to \pi^0 p$[8]. In general this reaction involves 4 SHA, one nonflip, two flip and one double-flip. Experimental data exist on $d\sigma/dt$, photon asymmetry $A = (\sigma_{\perp} - \sigma_{/\!/})/(\sigma_{\perp} + \sigma_{/\!/})$, polarized target assymmetry T and recoil proton polarization P. Present data are consistent with $T \approx P$ and this allows to take the two flip amplitudes as identical.[9] Thus we analyze $\gamma p \to \pi^0 p$ by means of 3 amplitudes $M_n(\nu,t)$, n = 0,1,2.

Our SHA at 4 GeV are shown in Fig. 6 and have the following basic features :

(i) All $\mathrm{Im}M_n(\nu,t)$, including n = 2, have the DAM zero structure

(ii) $\mathrm{Re}M_0(\nu,t)$ is much the same as for $\pi^- p \to \pi^0 n$.

(iii) $\mathrm{Re}M_1(\nu,t)$ has two zeros but rather far apart ; roughly speaking, it has a shifted "double-zero" structure.

Before considering the comparison of our solution with FESR, which will also offer an understanding of (iii), we shall briefly discuss the application of the derivative relations (11) to our $\gamma p \to \pi^{o} p$ solution. Fig. 7[9] presents the modulus $|M_1|$ and the phase φ_1 of the flip amplitude generated from our double-flip amplitude M_2 (Fig.6) and the relations (11), and also compares it to $|M_1|$ and φ_1 obtained directly from our solution (Fig.6). The agreement is remarkable.

§6. We now turn to a comparison of our solution with FESR. Fig. 8 presents the results for the lowest moment (k = 0) and for two higher moments (k = 2 and 3; again, moment = 2k + 1). Clearly the lowest moment FESR are very poorly satisfied. However, as we increase the moment, the agreement markedly improves.

The reason is that the Δ (1236) resonance, which gives a strong contribution to pion photoproduction, introduces into the FESR integrands terms with a zero structure that much deviates from that of $J_n(R\sqrt{-t})$. The same is true for the nucleon (Born) terms. On the other hand, higher mass resonances do lead to terms with Bessel function zeros. As the moment increases, the Born and Δ(1236) terms are suppressed relative to high mass resonance terms, and the agreement with the imaginary parts of our solution improves.

To understand the structure of $\mathrm{Re}M_1$ (point (iii) of § 5) we only need to write the corresponding dispersion relation in a form similar to Eq. (8). The fact that the FESR for n = 1, k = 0, is poorly satisfied implies a significant correction ($\sim D_1^{(1)}(t)$), which shifts the "double-zero" of $\mathrm{Im}M_1 \tan\frac{\pi\alpha}{2}$ towards negative values.

An important conclusion of the above FESR comparison is that FESR, in particular of the lowest moment, do not always reflect correctly the t-structure of the imaginary parts of the high energy amplitudes. In $\gamma p \to \pi^{o} p$, if we were to rely on the k = 0 FESR we would obtain imaginary parts of SHA much deviating from DAM. In contrast the imaginary parts of our high energy solution (Fig.6) do exhibit the DAM structure.[10]

REFERENCES AND FOOTNOTES

1. E.N. Argyres, A.P. Contogouris, S. Ray and M. Svec, Ann. Phys. (N.Y) 85, 283 (1974).

2. (a) CERN polarization : O. Guisan, Proceedings of the 1971 Rencontre de Moriond, ed. by J. Tran Thanh Van ; P. Bonamy et al, Nucl. Phys. B52, 392 (1973)

   (b) Argonne polarization : D. Hill et al, Phys. Rev. Lett. 30, 239 (1973)

3. (a) F. Halzen and C. Michael, Phys. Lett. B 36, 367 (1971)

   (b) R.L. Kelly, Phys. Lett. B 39, 635 (1971)

   (c) P. Johnson et al., Phys. Rev. Lett. 30, 242 (1973)

4. E.N. Argyres, A.P. Contogouris and J.P. Holden, Phys. Rev. D10, 2095 (1974)

5. V. Barger, Rapporteur's Talk at the XVII International Conference on H.E. Physics, London, 1974.

6. G. Girardi et al, Saclay preprints DPh - T/74 - 10 and DPh - T/74 - 63.

7. B. and F. Schrempp, Proceedings of the 1975 Rencontre de Moriond (this volume) ; J. Ader, R. Peschanski, R. Lacaze, G. Cohen-Tannoudji and C. Gilain, CERN preprint TH 1903 (1974)

8. E. Argyres, A.P. Contogouris, J.P. Holden and M. Svec, Phys. Rev. D8, 2068 (1973)

9. We are much indebted to Fridger and Barbara Schrempp for providing us with Fig. 7 before the appearance of their work (preprint CERN-TH-2015)

10. Unfortunately a number of papers submitted to the XVII International Conference on H.E. Physics, London 1974 (see Proceedins) try to determine the t-structure of SHA from FESR, with various confusing results.

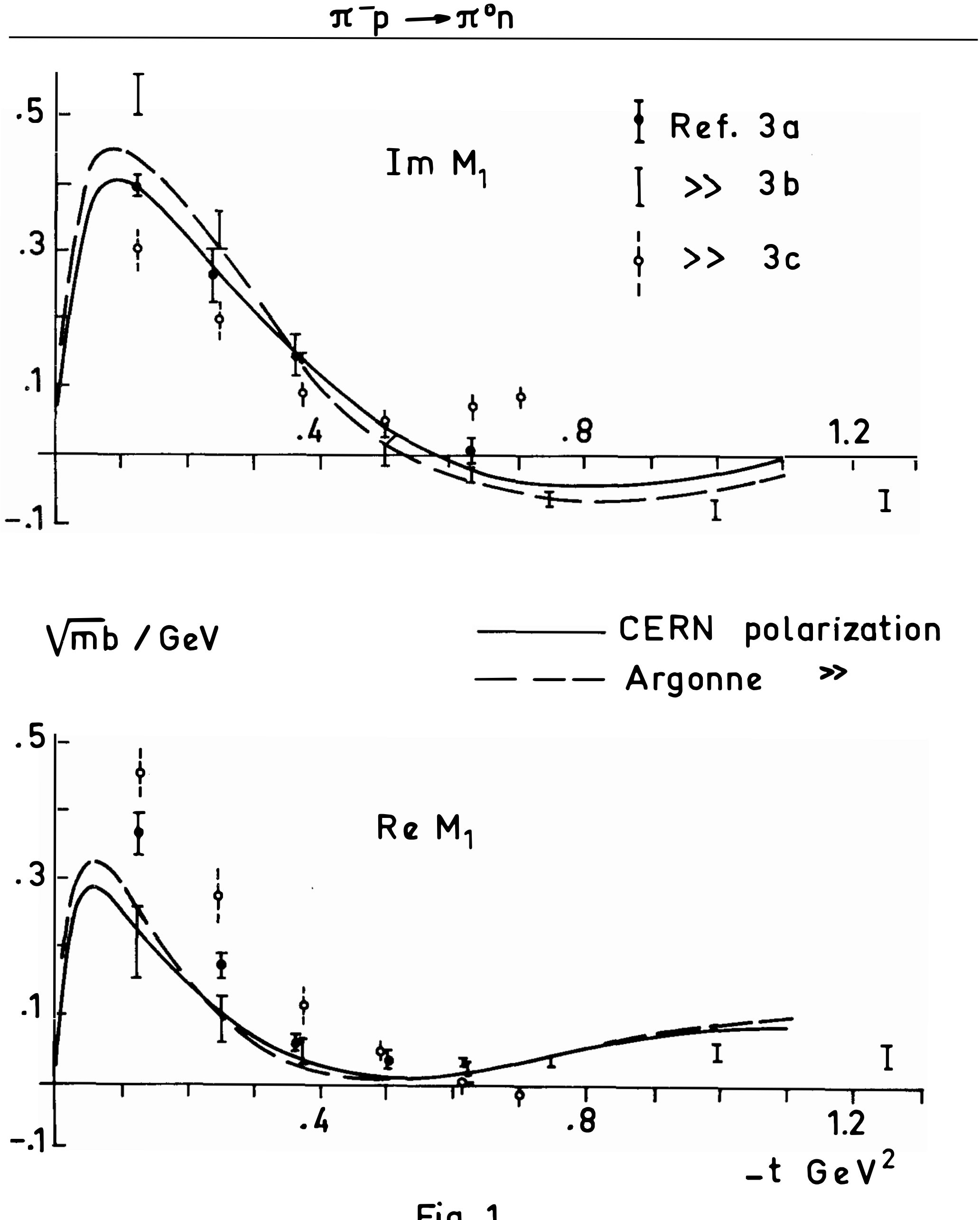

$\pi^- p \to \pi^0 n$
Im M_1
Ref. 3a
» 3b
» 3c
.5
.3
.1
-.1
.4
.8
1.2
$\sqrt{mb}$ / GeV
CERN polarization
Argonne »
Re M_1
.5
.3
.1
-.1
.4
.8
1.2
$-t$ GeV^2

Fig. 1

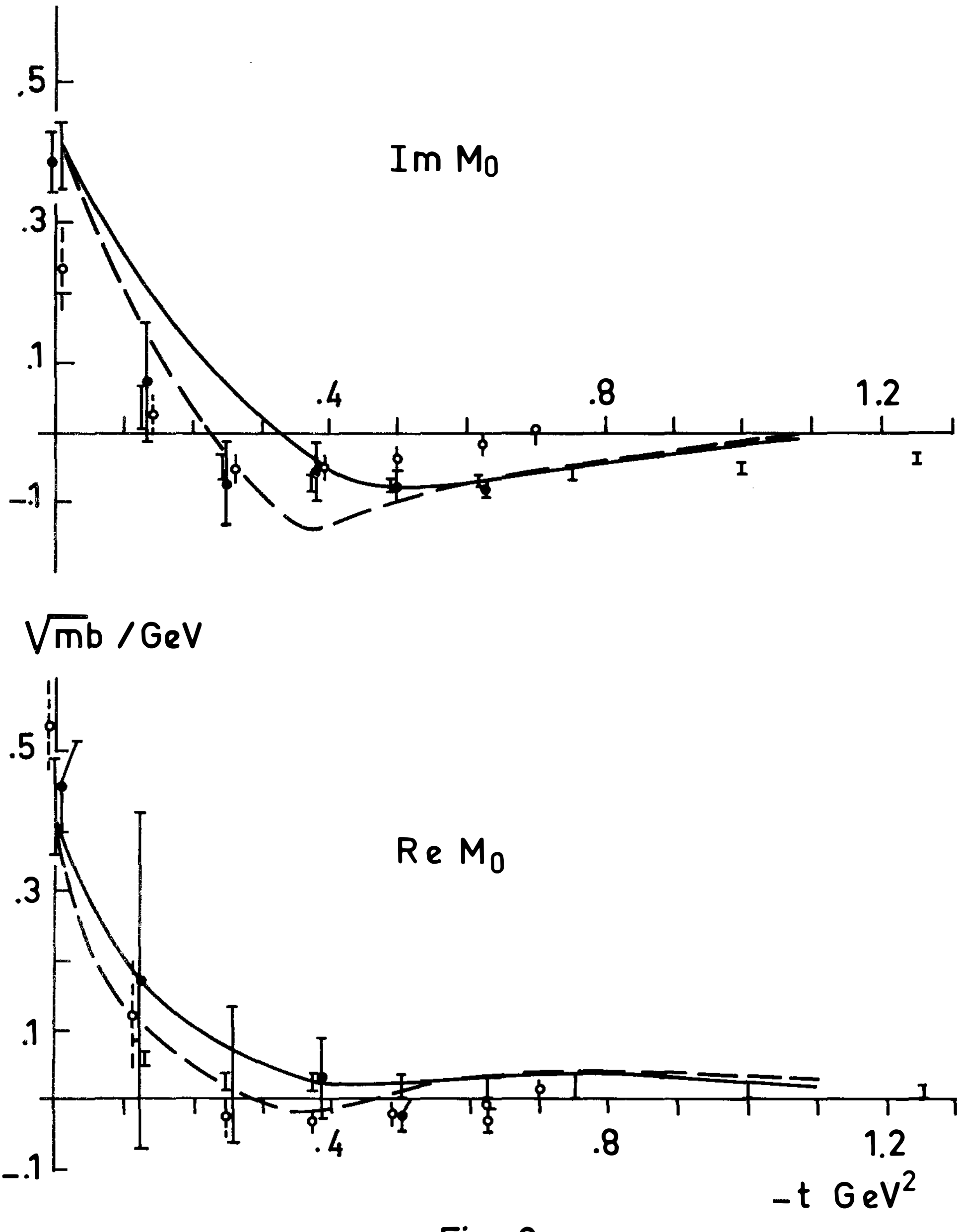

Fig. 2

$k^- p \rightarrow \bar{k}^o n \quad \& \quad k^+ n \rightarrow k^o p$

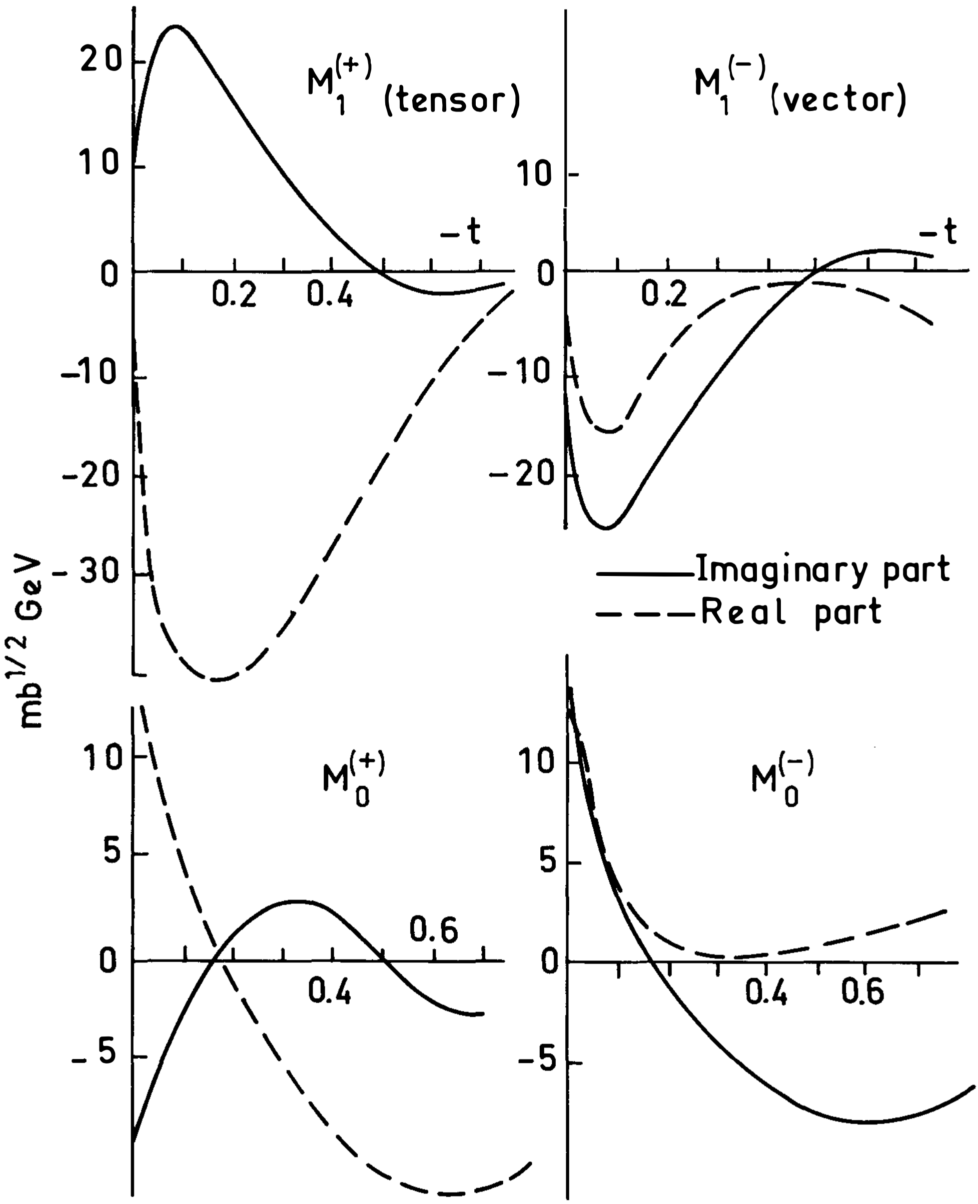

Fig.3

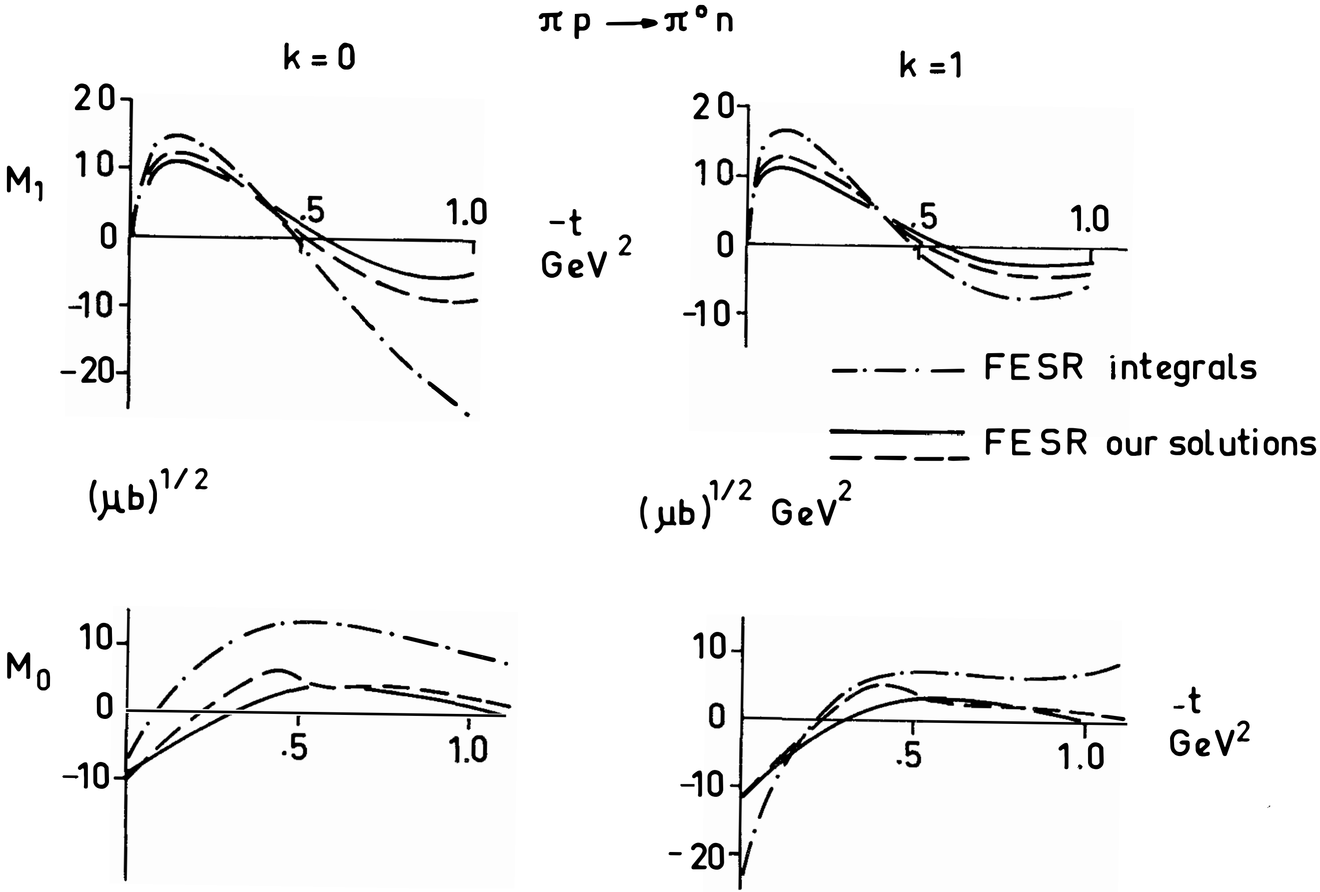
π p → π° n
k = 0
k = 1
M1
M0
(μb)^1/2
(μb)^1/2 GeV^2
−t GeV^2
FESR integrals
FESR our solutions

Fig. 4

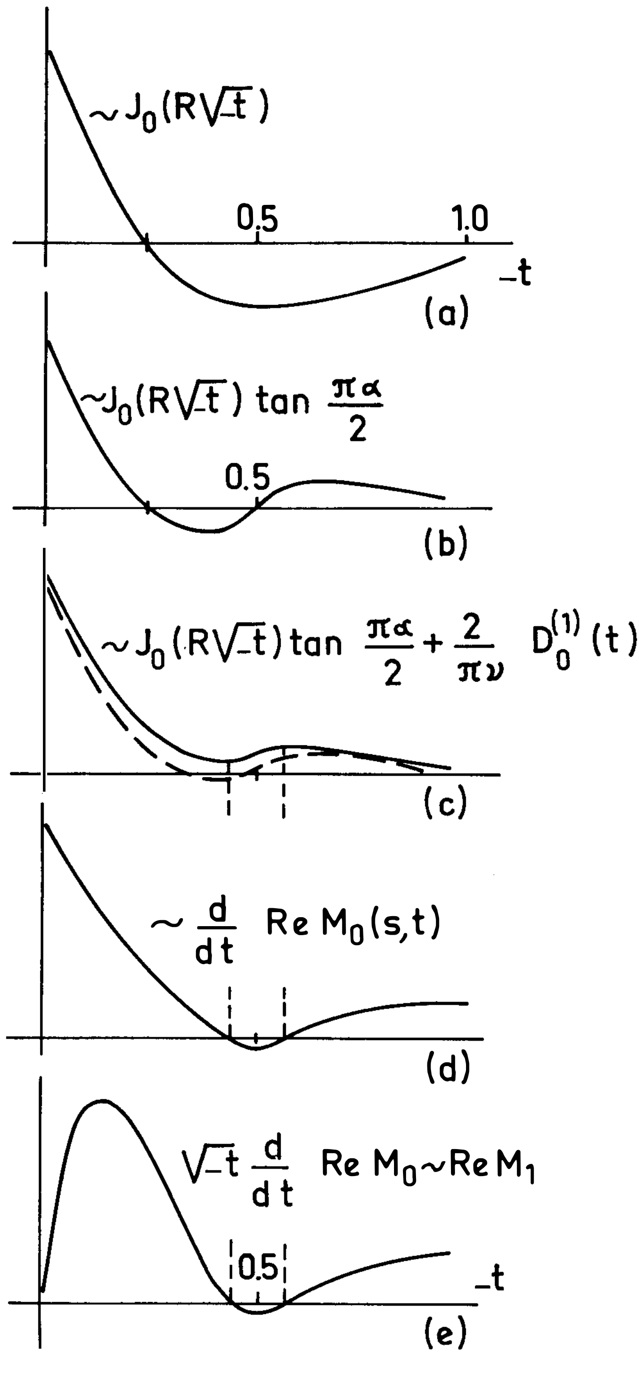

$\sim J_0(R\sqrt{-t})$
0.5
1.0
$-t$
(a)
$\sim J_0(R\sqrt{-t})\tan\frac{\pi\alpha}{2}$
0.5
(b)
$\sim J_0(R\sqrt{-t})\tan\frac{\pi\alpha}{2}+\frac{2}{\pi\nu}\,D_0^{(1)}(t)$
(c)
$\sim\frac{d}{dt}\,\mathrm{Re}\,M_0(s,t)$
(d)
$\sqrt{-t}\,\frac{d}{dt}\,\mathrm{Re}\,M_0\sim\mathrm{Re}\,M_1$
0.5
$-t$
(e)

Fig. 5

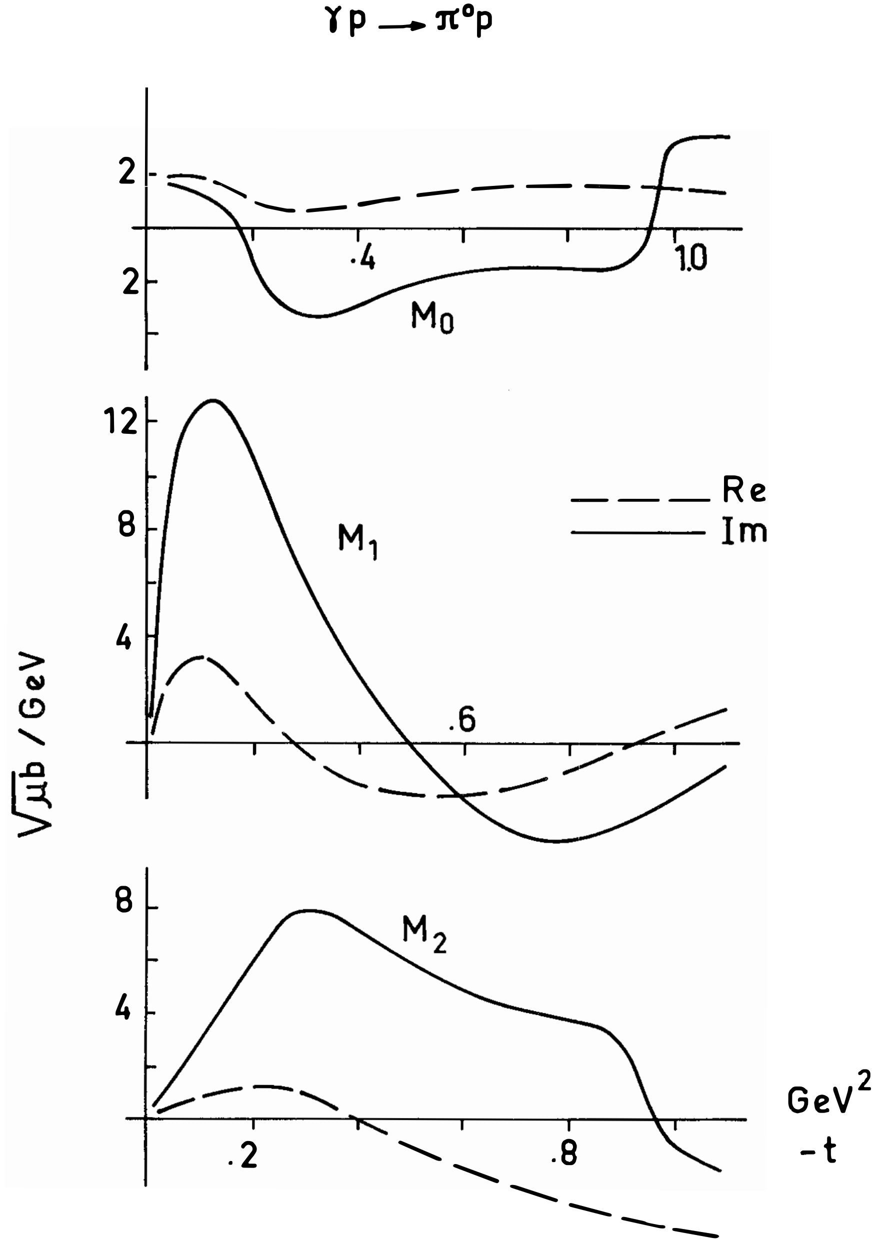

Fig. 6

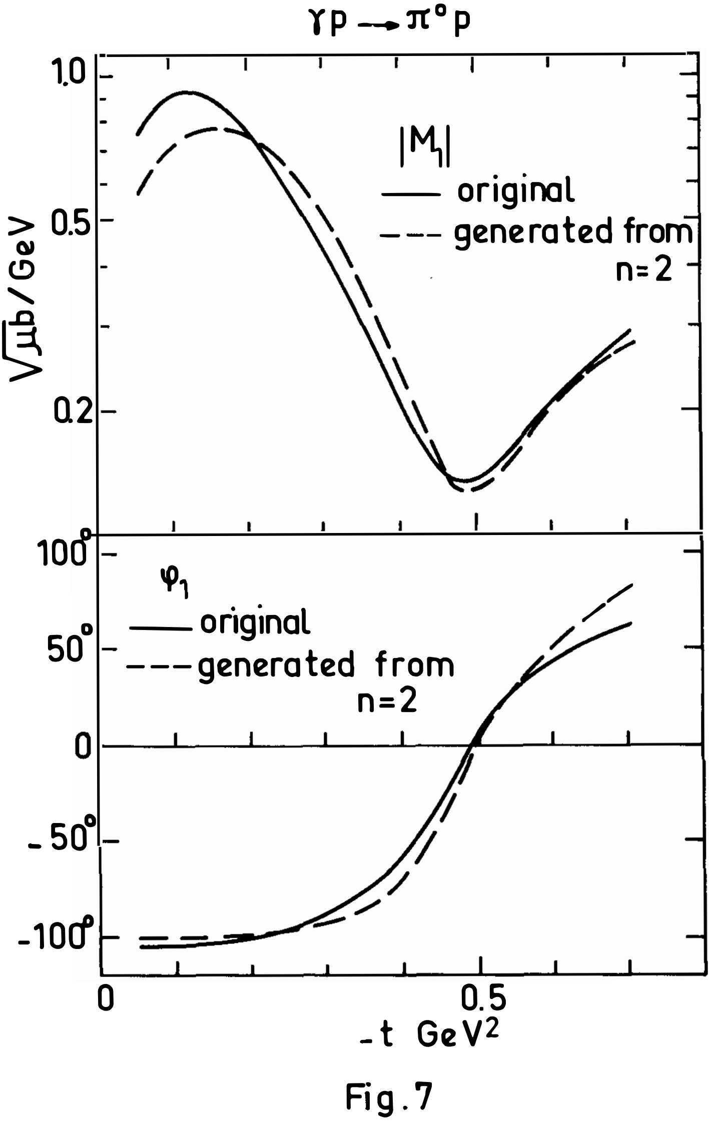

γp → π°p
|M1|
original
generated from n=2
√μb / GeV
1.0
0.5
0.2
φ1
original
generated from n=2
100°
50°
0
-50°
-100°
0
0.5
-t GeV²

Fig. 7

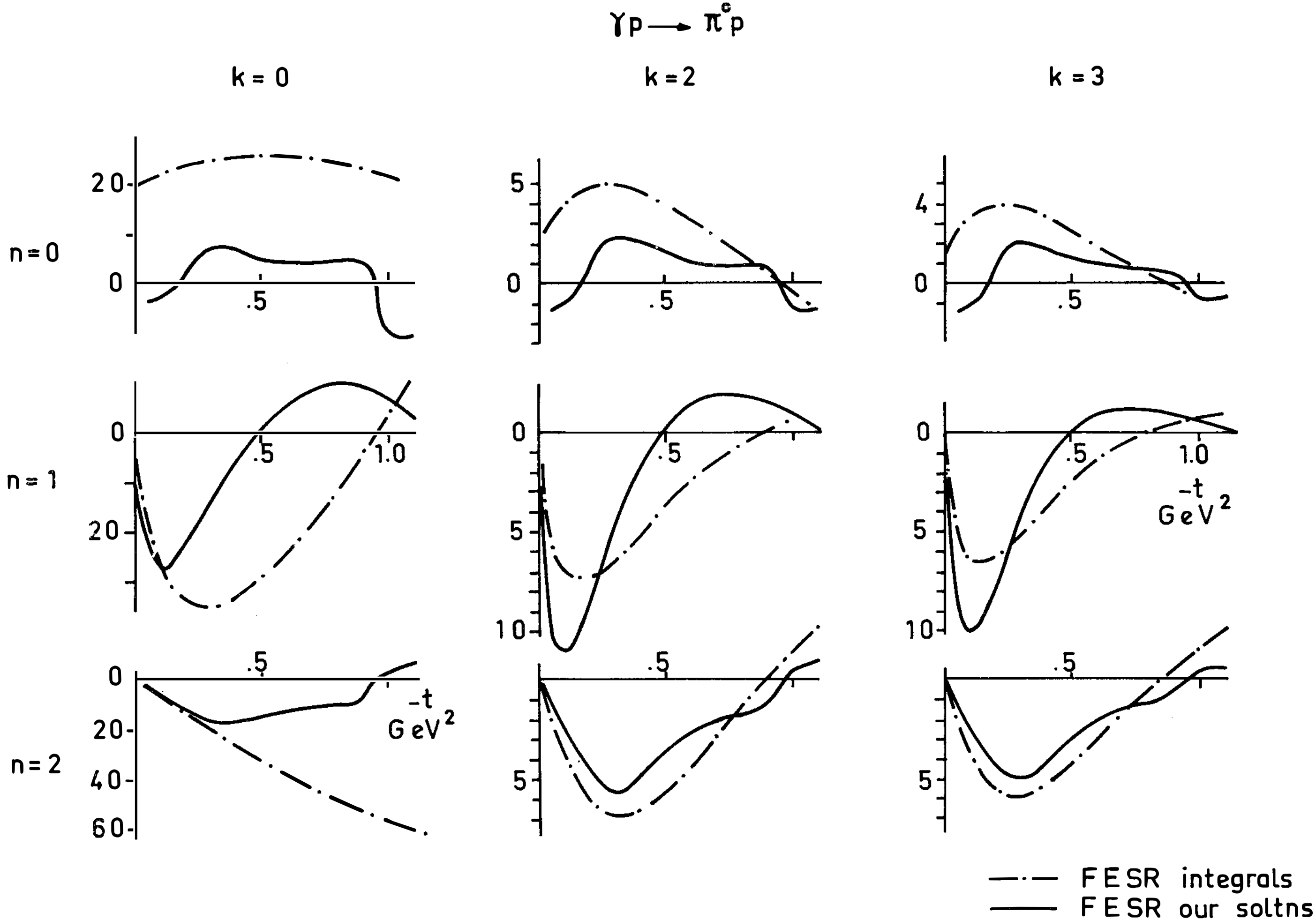
γp ⟶ π°p
k = 0
k = 2
k = 3
n = 0
n = 1
n = 2
20
0
.5
5
4
1.0
10
40
60
−t
GeV²
FESR integrals
FESR our soltns

Fig. 8

TOWARDS A SOLUTION FOR THE HELICITY DEPENDENCE OF SCATTERING AMPLITUDES

B.SCHREMPP and F.SCHREMPP
CERN, Geneva

Abstract: Derivative rules, relating all s channel helicity amplitudes of a two-body reaction to a single one, are discussed and tested.

Résumé: Nous discutons et vérifions la loi de dérivation, permettant d'obtenir à partir d'une seule amplitude toutes les autres amplitudes d'hélicité de la voie s d'une réaction à deux corps.

Since a long time it has been a major problem in two body physics to find a convincing systematics for the helicity dependence of the amplitudes. We shall discuss in this contribution an interesting and powerful hypothesis for the helicity dependence

$$F_{\lambda_c\lambda_d,\lambda_a\lambda_b}(s,t) = C_{\lambda_c\lambda_d,\lambda_a\lambda_b}(s) \sqrt{-t}^{\,\Delta\lambda} \left(\frac{1}{\sqrt{-t}} \frac{\partial}{\partial\sqrt{-t}} \right)^{\Delta\lambda} F_{\Delta\lambda=0}(s,t) \quad (1)$$

$$(\Delta\lambda = |\lambda_c-\lambda_d-\lambda_a+\lambda_b|)$$

which relates all s channel helicity amplitudes - via derivative relations - to a single one.

An analogous relation appeared already a long time ago in nuclear physics [1]. More recently it has been proposed for high energy physics [2)-7)].

A physical motivation [8] is given by the dual peripheral model [3),4)]. This is an s channel approach for nondiffractive reactions at high energies. It describes the amplitudes in terms of one single s channel Regge pole $\alpha(s)$ (interpolating the peripheral resonances with spins $J+1/2 \simeq R\cdot k_{cms}$, $R \simeq 1$ fermi) dominating the right hand cut amplitude $G(s,t)$ and its analytic continuation $\alpha(u)$ building up correspondingly the left hand cut amplitude $\tilde{G}(u,t)$ $\left[F(s,t) = G(s,t) + \tilde{G}(u,t)\right]$.

The assumption of one single s channel Regge pole is equivalent to the requirement of the simultaneous validity of the following two "downward" and "upward" derivative relations (plus a boundary condition for $-t \to \infty$)

$$G_{\lambda_i}(s,t) = A_{\lambda_i}(s) \sqrt{-t}^{\,\Delta\lambda} \left(\frac{1}{\sqrt{-t}} \frac{\partial}{\partial\sqrt{-t}} \right)^{\Delta\lambda} G_{\Delta\lambda=0}(s,t) \quad (2)$$

$$G_{\Delta\lambda=0}(s,t) = B_{\lambda_i}(s) \left(\frac{1}{\sqrt{-t}} \frac{\partial}{\partial\sqrt{-t}} \right)^{\Delta\lambda} \left(\sqrt{-t}^{\,\Delta\lambda} G_{\lambda_i}(s,t) \right) \quad (3)$$

(A_{λ_i} and B_{λ_i} being related).

Each single one is free of the deficiency of the dual perpheral model, the singularity at $t = 0$. The first one - which is identical to eq. (1) - is the more attractive one of the two, since it allows for the naively expected "threshold behaviour" $b^{\Delta\lambda}$ for $b \to 0$ in the impact parameter amplitudes. So far for the physical motivation.

It is clearly interesting to study the derivative relations (1) detached from the dual peripheral model. Let us nevertheless use the model once more to get an idea about their domain of validity; one expects [8]

i) the kinematical restriction: s large, $0 \leqslant -t \ll s$ (and for $t \leftrightarrow u$: s large, $0 \leqslant -u \ll s$)

ii) validity only for amplitudes with definite "t channel exchange", characterized by t channel signature and (effective) trajectory intercept (and nothing more)

and one obtains in addition that for these amplitudes the helicity weights

$$C_{\lambda_i}(s) \quad \text{are energy independent and real.} \tag{4}$$

Refs. 3)-7) contain tests of the derivative relations in conjunction with additional theoretical assumptions; these tests are qualitatively very encouraging, however, partly failing on the quantitative level. It seems that these deficiencies are due to the additional model assumptions: in Ref. 8) we performed model independent tests for the reactions $\pi^- p \to \pi^0 n$, $\gamma p \to \pi^0 p$, $\overset{(-)}{K}N$ CEX and πN diffraction scattering; in all cases a very good success of the derivative relations was found. Also the prediction (4) appeared to be confirmed by the data. Figs. 1 and 2 show representative examples for such tests. The test methods have been described in great detail in Ref. 8).

As an <u>outlook</u> for the future let us discuss two lines which one might pursue

i) it appears that the derivative relations (1) - once they are established - may be very <u>powerful for amplitude analyses</u> with incomplete experimental information. For a $0\,\frac{1}{2} \to 0\,\frac{1}{2}$ process e.g. the measurements of $d\sigma/dt$ and P are sufficient input into an <u>eigenvalue problem</u> for the function $y = |F_{\Delta\lambda=0}(s,t)|^2$ given by the <u>nonlinear</u> differential equation (C real)

$$\frac{C^2}{4}\, y'^2 + y^2 - \frac{d\sigma}{dt}\, y + \left(\frac{P}{2}\frac{d\sigma}{dt}\right)^2 = 0 \qquad \left(y' = \frac{\partial}{\partial\sqrt{-t}}\, y \right) \tag{5}$$

in conjunction with the boundary condition

$$0 \leqslant \frac{1}{2}\frac{d\sigma}{dt}\left(1 - \sqrt{1-P^2}\right) \leqslant y \leqslant \frac{1}{2}\frac{d\sigma}{dt}\left(1 + \sqrt{1-P^2}\right) \tag{6}$$

and a solution for the nonflip phase

$$\delta_{\Delta\lambda=0}(t) = \delta_{\Delta\lambda=0}(0) + \int_0^{\sqrt{-t}} d\tau\, \frac{P}{2}\frac{d\sigma}{dt} \Big/ y(\tau). \tag{7}$$

In all practical applications up to now (like e.g. in $\pi^- p \to \pi^0 n$) this eigenvalue problem seems to have a <u>unique</u> solution.

ii) A speculation about a more general origin of the derivative relations (1): they might be due to an <u>asymptotic symmetry</u> ($s \to \infty$, t fixed). As is well known the symmetry under the rotation group manifests itself in the independence of the partial wave amplitudes $f_J(s)$ on M, the third component of J, in the Legendre expansion. Correspondingly the independence of the coefficients f_k on $\Delta\lambda$ in the Laguerre expansion

$$F_{\lambda_i}(s,t) = D_{\lambda_i}(s) \sum_k f_k \left[- \frac{\partial}{\partial\sqrt{-t}} A(t) \right]^{\Delta\lambda} e^{-A(t)} \; L_k^{\Delta\lambda}(A(t)) \qquad (8)$$

- which automatically fulfils the derivative relations (1) - may be an indication for the presence of an (asymptotic) symmetry.

References

1) see e.g. L.S. Rodberg, Nuclear Physics 15, 72 (1959);
2) H. Högaasen, Physica Norvegica 5, 219 (1971);
3) B. Schrempp and F. Schrempp, Nuclear Physics B54, 525 (1973), ibid. B60, 110 (1973); Proceedings of the IV GIFT Seminar in Theoretical Physics, University of Barcelona/Spain, April 1973, p. 328 and CERN preprint TH-1736 (1973);
4) B. Schrempp and F. Schrempp, Nuclear Physics B77, 453 (1974); Proceedings of the IX Rencontre de Moriond, Méribel, March 1974, Vol. I, p. 113;
5) F. Halzen, University of Wisconsin Report COO-881-409 (1974);
6) J.P. de Brion and R. Peschanski, Nuclear Physics B81, 484 (1974); J.P. Ader, R. Peschanski, R. Lacaze, G. Cohen-Tannoudji and G. Gilain, CERN preprint TH-1903 (1974);
7) V. Barger and R.J.N. Phillips, University of Wisconsin report COO-881-418 (Nov. 1974);
8) B. Schrempp and F. Schrempp, CERN preprint TH-2015 (1975);
9) H. Hecht, H.P. Jakob and P. Kroll, Nuclear Physics B71, 1 (1974);
10) V. Barger and R.J.N. Phillips, Phys. Rev. 187, 2210 (1969).

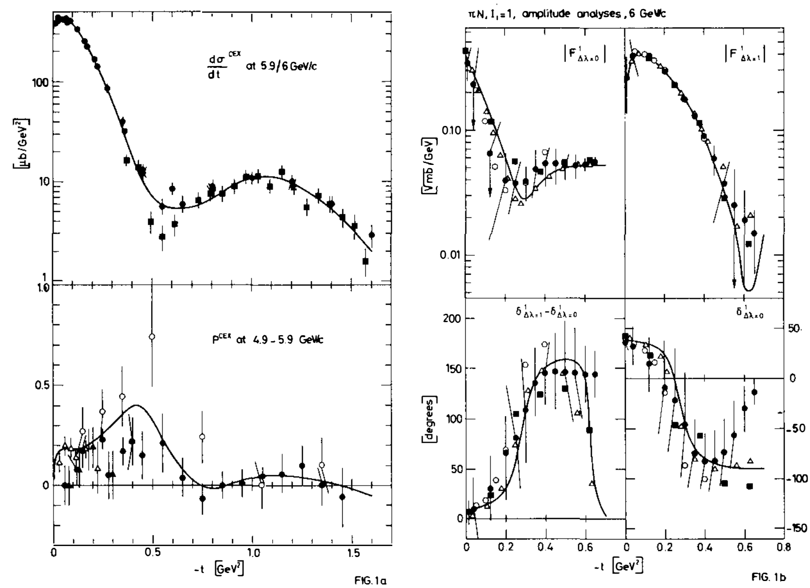

Figure 1:

shows a model independent test of the derivative relation $F_1=C(\partial/\partial\sqrt{-t})F_0$ for the s channel helicity amplitudes $F_{\Delta\lambda=0,1}$ in $\pi^- p \rightarrow \pi^0 n$ at 6 GeV/c. The curves are the result of a fit of the amplitudes - being parametrized as a sum (8) of properly weighted Laguerre polynomials such as to automatically fulfil the derivative relation - to the complete experimental information available; a) contains dσ/dt and P, b) contains all available amplitude analyses. The fit yields $1/|C| = 2.4$ GeV^{-1} and $\pi-\phi_C = -8.6^{\circ}$ with $C = |C|e^{i\phi_C}$. For data Refs. see Ref.8.

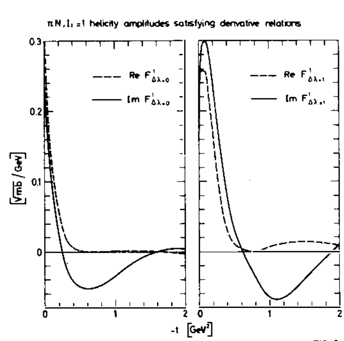

Figure 2:

shows the πN, $I_t=1$ helicity amplitudes $F^1_{\Delta\lambda=0,1}$ as they result from the fit shown in Fig.1. They fulfil the derivative relation $F_1=C(\partial/\partial\sqrt{-t})F_0$ exactly.

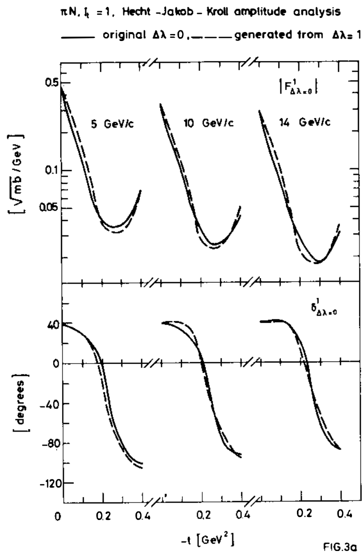

FIG.3a

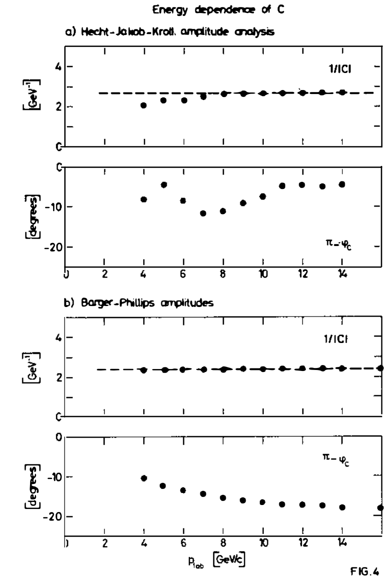

FIG.4

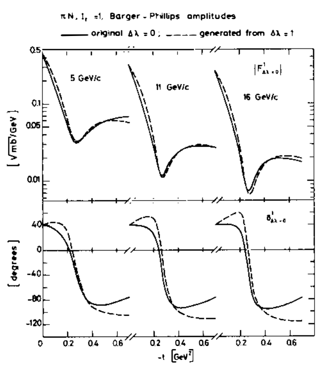

FIG.3b

Figure 3:

shows a model independent test of the derivative relation $F_1=C(\partial/\partial\sqrt{-t})F_0$ in $\pi^- p \to \pi^0 n$ at various energies. The full curves represent the left hand sides (l.h.s.) of the integrated form

$$|F_0(t)| = |F_0(0)| \exp\left[\frac{1}{|C|}\int_0^{-t} d\tau \frac{|F_1|}{|F_0|}\cos(\delta_1-\delta_0-\phi_C)\right]$$

$$\delta_0(t) = \delta_0(0) + \frac{1}{|C|}\int_0^{-t} d\tau \frac{|F_1|}{|F_0|}\sin(\delta_1-\delta_0-\phi_C)$$

of the derivative relation; the broken lines are the results of a fit of the r.h.s. to the l.h.s. with the two free parameters $|C|$ and ϕ_C. a) shows the results with the Hecht-Jakob-Kroll amplitude analysis [9] at the representative energies 5,10 and 14 GeV/c, b) those with the Barger and Phillips amplitudes [10] at 5,11 and 16 GeV/c.

Figure 4:

The energy dependence of the function C(s) in $\pi^- p \to \pi^0 n$ as obtained model independently point by point by means of the procedure described in the caption of Fig.3. $1/|C|$ seems to reach soon a constant value and $\pi-\phi_C$ remains small.

GEOMETRICAL VERSUS CONSTITUENT INTERPRETATION OF LARGE ANGLE EXCLUSIVE SCATTERING

B.SCHREMPP and F.SCHREMPP
CERN, Geneva

Abstract: It is pointed out that the large angle pp $\to$ pp data suggest an exponential behaviour in p_T modulated by a regular oscillation in p_T more naturally than a power law s^{-N}. It is argued that these effects are due to a manifestation of the same geometrical length scale $R \simeq 1$ fermi which is known to control small angle scattering.

Résumé: Nous montrons que les résultats à grand angle de pp $\to$ pp suggèrent un comportement exponentiel en p_T, modulé par une oscillation régulière en p_T plutôt qu'une loi de puissance en s^{-N}. Nous soulignons aussi la possibilité que ces effets soient dûs à la manifestation de l'échelle géometrique $R \simeq 1$ fermi, connue pour contrôler la diffusion à petit angle.

It is the purpose of this contribution to point out that the large angle data of pp → pp give support [1] to a geometrical interpretation rather than to a constituent picture.

The characteristics of these two pictures are as follows:

i) geometry [2]: the hadron behaves like an extended object with a roughly universal interaction radius $R \simeq 1$ fermi. This is the length scale, which is known to manifestly control the features of the data at small angles (t fixed, $s \to \infty$). Representative models are all t channel Regge models, where the scale is set by the universal slope $\alpha' \simeq (R/2\pi)^2 \simeq 1\ \mathrm{GeV}^{-2}$ of the Regge trajectories, or the "dual peripheral model" [3], which has the advantage of holding out to rather large values of $-t$.

The dual peripheral model is an s channel Regge approach for non-diffractive two-body reactions in the limit t fixed, $s \to \infty$. It starts off from one nonlinear, complex s channel Regge trajectory which interpolates the peripheral s channel resonances with spins $J + 1/2 \simeq k_{cms} \cdot R$, $R \simeq 1$ fermi. In a dual way it generates t channel Regge behaviour involving a $\sqrt{-t}$ type t channel Regge trajectory. Typically for fixed s it predicts a behaviour [3] like (see Fig. 2)

$$d\sigma/dt \propto \frac{1}{\sqrt{-t}} e^{-R\cdot A\cdot\sqrt{-t}} \left(1 + C\cdot\cos(R \sqrt{-t} + \Phi)\right) , \quad R \simeq 1 \text{ fermi}, \qquad (1)$$
$$(t \neq 0)$$

$$| C | \leq 1, \quad A = \frac{2}{\pi} \log (s/s_o), \quad C \text{ weakly dependent on } \log (s/s_o),$$

where the length scale R controls manifestly the exponential fall off in $\sqrt{-t}$ as well as the period of the oscillation in $\sqrt{-t}$ ($\sqrt{-t} \to \sqrt{-u}$ for u fixed $s \to \infty$).

ii) constituents: As is well known, scaling in deep inelastic ep scattering suggests a constituent interpretation of the hadron. Analogously, one might expect [4] to find indications for constituents in exclusive large angle scattering data (Θ fixed, $s \to \infty$). This implies in particular the loss of the geometrical scale $R \simeq 1$ fermi ($\alpha' \to 0$) for sufficiently high transverse momenta. Representative for such a constituent approach is the quark counting rule [5] for a process $A + B \to C + D$

$$d\sigma/dt \underset{\Theta\ \text{fixed}}{\overset{s\to\infty}{\sim}} s^{-(n_A + n_B + n_C + n_D) + 2} f(\Theta) \qquad (2)$$

(n_I = number of valence quarks in particle I).

Let us confront the two forementioned pictures with the large angle $pp \to pp$ data, which are by far the best data available in the "deep" region.

a) Comparison with the constituent picture: Fig. 1 shows [1)] the large angle $pp \to pp$ data in a plot log $d\sigma/dt$ versus log s. For $p_{lab} \gtrsim 6$ GeV/c they are consistent with the predicted power law s^{-10}, even though the data at the highest energies seem to prefer a higher power (s^{-12} ?). (For further tests of the power law s^{-N} see Refs. 6).

b) Comparison with the geometrical picture: here we ask the question: is there a scale of the order of 1 fermi appearing in the large angle $pp \to pp$ data? The presence of coherent effects in the deep region has been pointed out already [7),8)]. However, our conclusions in detail are different from the observations made in Ref. 7).
The cleanest signals for the presence of a dimensional scale are of course exponentials and regular oscillations -typical features of the geometrical region. The main task is to find the appropriate variable in which to look for such exponentials and oscillations in the large angle data. As a guideline, let us use the dual peripheral model [3)], which originally has been formulated for t (u) fixed, $s \to \infty$. Even though it is an s channel approach, it cannot straightforwardly be extrapolated to large angles. The reason is that it does not properly take care of t-u crossing symmetry requirements, which become crucial near $\Theta = 90^o$, i.e. near $t = u$. In view of the result (1) it is, however, very suggestive to simply try instead of $\sqrt{-t}$ (or $\sqrt{-u}$) the t-u crossing symmetric variable $p_T = k_{cms} \cdot \sin \Theta_{cms}$ with the additional property

$$p_T \underset{-t\ \text{small}}{\simeq} \sqrt{-t} \quad \text{and} \quad p_T \underset{-u\ \text{small}}{\simeq} \sqrt{-u} \quad . \tag{3}$$

Thus, in analogy to eq. (1), at fixed Θ_{cms} we might look for a behaviour of the following type [1)]

$$d\sigma/dt \propto e^{-R\cdot g\cdot p_T} \left(1 + C\cdot\cos\left(R\cdot p_T + \Phi\right)\right) \tag{4}$$

with $g = g(\Theta)$ and $C = C(\Theta)$ dimensionless; i.e. an exponential fall off in p_T, possibly modulated by an oscillation which is regular in p_T with a period $2\pi/R$ given in terms of the hadronic scale $R \simeq 1$ fermi.

Fig. 3 shows [1)] the same large angle $pp \to pp$ data as in Fig. 1 at fixed angles $\Theta = 90^o, 68^o, 55^o$, but this time with log $d\sigma/dt$ plotted versus p_T

(similar to the Orear plot). We realize first of all: there does not seem to be any indication of a change in the characteristics of the p_T behaviour for fixed Θ_{cms} almost from threshold up to 25 GeV/c - in contrast to the power law behaviour, which agrees with the data only for $p_{lab} \gtrsim 6$ GeV/c (cf. Fig. 1). Secondly, the data seem to oscillate regularly around a straight line corresponding to an exponential of the type $e^{-R \cdot g(\Theta) \cdot p_T}$ (in case of the 55^o data, the oscillation vanishes in the statistical fluctuations of the data). In order to be able to study these oscillations more closely, we divided the data for $d\sigma/dt$ by the appropriate exponential. The results for 90^o and 68^o are shown [1] in Figs. 4a and b: a clear indication of a strikingly regular oscillation in p_T; the curves correspond to an eyeball fit to $1 + C \cos(R \cdot p_T + \Phi)$ with a period of $2\pi/R \simeq 1.7$ GeV/c, i.e. with $R \simeq 0.73$ fermi. A comparison of Fig. 4a with Fig. 4b shows that the zero positions of the oscillation remain fixed in p_T, independent of Φ. Thus altogether $d\sigma/dt(pp \to pp)$ seems to behave for large fixed angles as suggested in eq. (4).

Our analysis leads us to the following conclusion. The exponential, and in particular, the oscillations are a strong indication for the presence of a length scale. Moreover, this scale looks very much like the well-known hadronic radius $R \simeq 1$ fermi.

The interpretation of a parton optimist might be: at highest available transverse momenta we see the transition region where the resolution is just good enough to make out the constituents within the extended proton (remember the compatibility of the data with a power law s^{-10} for $p_{lab} \gtrsim 6$ GeV/c). The pure parton behaviour, i.e., the loss of the length scale characterizing the size of the proton, will show up at higher transverse momenta $p_T > 3.5$ GeV/c. The oscillations will then die away.

A parton pessimist might conclude: there is no convincing evidence for partons in the large angle $pp \to pp$ data. Instead, a geometrical picture, in terms of an exponential in p_T modulated by a regular oscillation, describes the data uniformly almost from threshold up to $p_{lab} \simeq 25$ GeV/c.

References

1) B. Schrempp and F. Schrempp, Phys. Letters 55B, 303 (1975);

2) See, for example, B. Schrempp and F. Schrempp, Proceedings of the IV GIFT Seminar in Theoretical Physics, University of Barcelona, April 1973, p.328; and CERN Preprint TH.1736 (1973);

3) B. Schrempp and F. Schrempp, Nuclear Phys. B54, 525 (1973); Nuclear Phys. B60, 110 (1973); Nuclear Phys. B77, 453 (1974); Proceedings of the IX Rencontre de Moriond, Méribel, March 1974, Vol. I, p. 113;

4) R. Blankenbecler, S.J. Brodsky and J.F. Gunion, Phys. Letters 39B, 649 (1972); Phys. Rev. D6, 2652 (1972); Phys. Letters 42B, 461 (1973); Phys. Rev. D8, 287 (1973);

R. Blankenbecler, S.J. Brodsky, J.F. Gunion and R. Savit, Phys. Rev. D8, 4117 (1973);

P.V. Landshoff and J.C. Polkinghorne, Phys. Rev. D8, 927 (1973);

P.V. Landshoff, Report at the 17 th Int. Conf. on High Energy Physics, London 1974;

G. Preparata, Phys. Rev. D7, 2973 (1973); Erice Lectures, July 1974 and references cited therein;

5) V. Matveev, R. Muradyan and A. Tavkhelidze, Lett. Nuovo Cimento 7, 719 (1973),

S.J. Brodsky and G.R. Farrar, Phys. Rev. Letters 31, 1153 (1973); SLAC Preprint SLAC-PUB-1473 (1974);

6) See, for example, S.J. Brodsky, in AIP Conference Proceedings No. 15 (1973) (ed. C. Quigg), p. 275;

P.V. Landshoff and J.C. Polkinghorne, Phys. Letters 44B, 293 (1973);

7) A.W. Hendry, Phys. Rev. D10, 2300 (1974),

8) For a review see D. Sivers, SLAC Preprint SLAC-PUB-1457 (T/E) (1974), submitted to Annals of Physics;

9) $pp \rightarrow pp$ data:

B.A. Ryan et al., Phys. Rev. D3, 1 (1971),

D.T. Williams et al., Nuovo Cimento 8A, 447 (1972);

R.C. Kammerud et al., Phys. Rev. D4, 1309 (1971);

C.W. Akerlof et al., Phys. Rev. 159, 1138 (1967);

J.V. Allaby et al., Phys. Letters 25B, 156 (1967);

E.J. Sacharidis, Rutherford Lab. Report RHEL/R 186 (1969) (unpublished) (Summary of final results of CERN experiments by Allaby et al.);

G. Cocconi et al., Phys. Rev. 138B, 165 (1965).

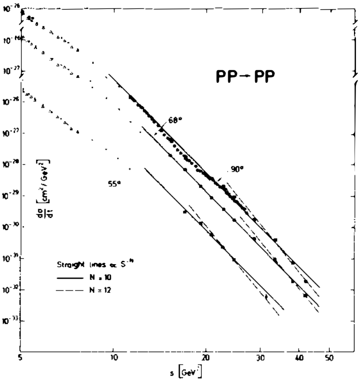

Fig. 1. Data for log $d\sigma/dt(pp \to pp)$ versus log$s$ at the fixed angles $\theta_{cms} = 90°$, 68° and 55°. The solid lines correspond to a power law behaviour like s^{-10}, the broken lines to one like s^{-12}. Data from ref. [9].

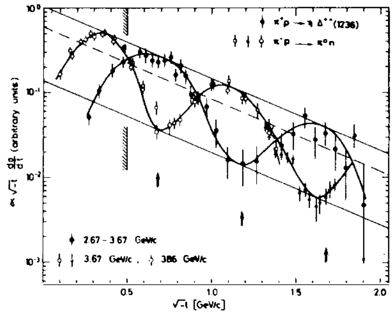

Fig. 2. Data for two representative reactions plotted in the form log$[\sqrt{-t}(d\sigma/dt)]$ versus $\sqrt{-t}$. This is to illustrate the agreement with a characteristic prediction of the dual peripheral model: an exponential drop-off in $\sqrt{-t}$ modulated by an oscillation which is regular in $\sqrt{-t}$. Figure from ref. [3].

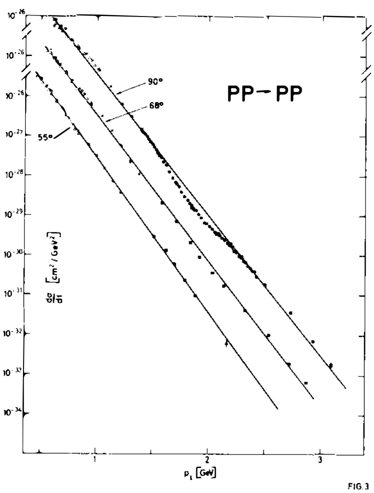

Fig. 3. Data for log $d\sigma/dt(pp \to pp)$ versus $p_\perp$ at the fixed angles $\theta_{cms} = 90°$, 68° and 55°. The straight lines correspond to an exponential behaviour like $\exp(-8.13p_\perp)$, $\exp(-8.42p_\perp)$ and $\exp(-8.95p_\perp)$ respectively. Data from ref. [9].

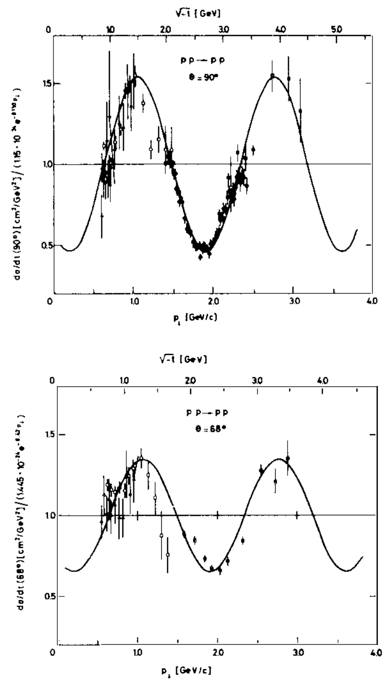

Fig. 4. a) Data for $d\sigma/dt(pp\to pp)_{90°}$ divided by the exponential of fig. 3: $d\sigma/dt(pp\to pp)_{90°}$ [cm²/GeV²]/(1.15 × 10^{-24} $\exp(-8.13p_\perp)$) versus $p_\perp$. The solid line $[1 - 0.54\cos(3.7p_\perp - 0.774)]$ is an eyeball fit indicating a regular oscillation of the data. Data from ref. [9]. b) The same as in a), but for 68°. Data points: $d\sigma/dt(pp\to pp)_{68°}$ [cm²/GeV²]/(1.445 × 10^{-24} $\exp(-8.42p_\perp)$), curve: $[1 - 0.35\cos(3.7p_\perp - 0.774)]$, i.e., the same oscillation as in a), only with a smaller amplitude. Data from ref. [9]).

INCLUSIVE CROSS SECTIONS FOR $p + n \to p + X$ BETWEEN 50 AND 400 GeV

F. SANNES
Department of Physics
Rutgers, The State University
New Brunswick, New Jersey 08903

Abstract : We have measured inclusive cross sections for the reaction $p + d \to p + X$ in the region $0.15 < |t| < 0.39$ GeV^2, $100 < s < 750$ GeV^2 and $0.80 < x < 0.92$ using the acceleration ramp and deuterium gas jet target at Fermilab. These measurements are combined with our earlier measurements of $p + p \to p + X$ to obtain inclusive cross sections for $p + n \to p + X$.

Résumé : Nous avons mesuré la section efficace de la réaction inclusive $p + d \to p + X$ dans la région cinématique $0.15 < |t| < 0.39$ GeV^2, $100 < s < 750$ GeV^2, $0.80 < x < 0.92$, utilisant la cible de gaz deutérium pendant le cycle d'accélération à Fermilab. Ces mesures, combinées avec nos mesures antérieures de $p + p \to p + X$, déterminent les sections efficaces inclusives de $p + n \to p + X$.

INCLUSIVE CROSS SECTIONS FOR $pn \to pX$ BETWEEN 50 AND 400 GeV

In a recent experiment we have measured the inclusive cross sections for the reactions

$$p + p \to p + X \quad (1 + 2 \to 3 + X) \qquad (1)$$

$$p + d \to p + X \quad (1 + 2 \to 3 + X) \qquad (2)$$

using the hydrogen and deuterium gas jet targets in the Fermilab main ring. The results of the $pp \to pX$ measurements were reported earlier.[1] In this letter we present cross sections for the reaction $pd \to pX$ and combine the two sets of measurements to obtain invariant cross sections for the reaction

$$p + n \to p + X \quad (1 + 2 \to 3 + X) \qquad (3)$$

Since we wish to compare pd data to pp data, it is convenient to use the nucleon rather than the deuteron mass in defining the kinematic variables of Reaction (2), i.e. we assume independent nucleon-nucleon interactions, the second nucleon in the deuteron being a spectator. In order to take into account the smearing of the kinematic variables due to Fermi motion we use the average values defined by

$$\langle s \rangle = s + E_1 \langle p_F^2 \rangle / m_2 \qquad (4)$$

$$\langle t \rangle = t - E_3 \langle p_F^2 \rangle / m_2 \qquad (5)$$

$$\langle x \rangle = x - \langle p_F^2 \rangle / 2m_2^2 \qquad (6)$$

where m_2 is the nucleon mass, $x \equiv 1 - M_X^2/s$ and s, t and M_X^2 are the squares of the total center of mass energy, the four momentum transfer and the mass of X respectively for a target nucleon at rest and $\langle p_F^2 \rangle = 0.012$ GeV^2 is the mean square of the nucleon momentum in the deuteron due to Fermi motion. For the kinematic region of this experiment we have $\langle s \rangle / s \simeq 1.006$, $\langle t \rangle \simeq -t \simeq -0.013$ GeV^2 and $\langle x \rangle - x \simeq -0.007$.

The recoil particles were detected and identified as protons in a spectrometer consisting of a series of scintillation counters as described in Ref. 1. In addition, we detected elastically scattered deuterons in a small solid state detector at 85.5° from the beam direction. The beam-target luminosity was determined as in Ref. 1 using the pd elastic differential cross sections of Akimov et al.[2] and the total pd cross sections of Carroll et al.[3]

The $pd \to pX$ data are shown in Fig. 1. Only statistical errors to which we have added quadratically systematic errors of $\pm$ 3 % are displayed. The uncertainty in the overall normalization is ± 15 % as for our earlier measurements[1] of $pp \to pX$. However, since both reactions were studied with the same apparatus, the only difference being the gas used in the jet target, we estimate the relative error between the pp and pd data to be only ± 4 % due solely to uncertainties in the pp and pd elastic cross sections.

The cross sections for $pd \to pX$ look very similar to those for $pp \to pX$.[1] They show a weak s dependence and an exponential t dependence of $\sim e^{6t}$. There is a minimum in the x distribution at $x = 0.87$ and the absolute value of the $pd \to pX$ cross section is about twice that of $pp \to pX$. However, it should not be assumed from this similarity that the cross sections for $pn \to pX$ are the same as for $pp \to pX$. The measured shapes of the pd inclusive spectra in our kinematic region (x near 1, low $|t|$) are determined to a large extent by the Fermi motion of the target nucleons as well as the rescattering of the recoil particle off the spectator nucleon in the deuteron.

To extract the $pn \to pX$ spectra we assume the impulse approximation. In this approximation the proton and neutron in the deuteron are considered as independent particles in close proximity. The closeness of the nucleons give rise to a shadowing of one by the other, effectively lowering the luminosity of both relative to an equal number of free particles. We assume the decrease in luminosity for inclusive reactions is the same as that for total cross sections, i.e., $\sigma_{pd} = \sigma_{pp} + \sigma_{pn} - \delta$ where $\delta = \sigma_{pn}\sigma_{pp}/4\pi < r^2 >$ with $< r^2 > = 31$ mb. This is the cross section deficit of Glauber theory[4] and amounts to a decrease of ~ 5 % in the effective pd cross section over our energy range.

The effect of the deuteron potential in the impulse approximation is to give the nucleons a center of mass momentum or Fermi motion. As a result of this our spectrometer will detect recoil protons originating from elastic scattering off the moving target proton. To estimate this effect we use the Hulthen wave function[5] and measured pp elastic scattering cross sections[6] in a Monte Carlo program to simulate the pp elastic spectra as seen by our spectrometer. These spectra are approximately gaussian centered around $x = 1 - M_p^2/s$. The same Monte Carlo program is used to smear the inelastic $pp \to pX$ spectra for which we use a composite input of all available data[7,8,9] in addition to our published measurements.[1]

For both the pp elastic and inelastic cross sections mentioned above we use the forms for "free" protons but modified by the deuteron form factor[4] $S(t)$ in order to exclude interactions which result in a deuteron in the final state which is not detected, i.e., for the pp differential cross sections we use $d\sigma/dt_{free}\left[1 - S^2(t)\right]$.

An additional feature of the Monte Carlo program is the inclusion of an estimate of the rescattering of the recoil protons by the spectator neutron which has the effect of spreading the x distributions for those protons which interact. For this we assume that the neutron on average sits at an rms radius of $\sqrt{31\ mb}$ and that the reaction is the same as for free np scattering. The probability for an interaction was taken to be simply $\sigma_{pn}/4\pi\langle r^2\rangle$ and the scattering angle was weighted by low energy np differential cross section measurements.[10]

Summarizing, our final $pn \to pX$ cross section were obtained in the following manner : 1) Our $pd \to pX$ cross sections were multiplied by 1.05 to correct for the shadowing effect. 2) From the resulting cross sections we subtracted the $pp \to pp$ elastic and $pp \to pX$ inclusive cross sections both of which were Fermi smeared, corrected for coherent pd scattering (by including the deuteron form factor) and corrected for rescattering off the spectator neutron. A typical spectrum and the distributions from which it was derived is shown in Fig. 2.

The final $pn \to pX$ spectra are plotted in Fig. 3. They contain the effects of Fermi motion and rescattering which have not been unfolded. The normalization errors have been calculated by taking into account the fact that the absolute uncertainties in the $pp \to pX$ and $pd \to pX$ data are correlated due to the use of the same apparatus for both measurements. This leads to overall normalization uncertainties for the $pn \to pX$ data of $\pm$ 5.6, $\pm$ 4.0, $\pm$ 2.9 and $\pm$ 1.8 mb/GeV^2 at $\langle -t \rangle$ = 0.17, 0.21, 0.26 and 0.34 GeV^2 respectively.

As can be seen from Fig. 3 the invariant cross section for $pn \to pX$ falls as x tends to 1 in contrast to that for $pp \to pX$ which rises above x = 0.88. Also, at fixed x and t the $pn \to pX$ data show no significant energy dependence although a 20 % drop between the two extreme energies is possible within errors.

The study of the charge exchange reaction $pn \to pX$ (or equivalently $pp \to nX$)[11] near x = 1 provides valuable information on the nondiffractive component of the reaction $pp \to pX$. The most popular phenomenological framework for discussing both reactions in our kinematic region has been the triple Regge (TR) formalism[11] which leads to a prediction for the invariant cross section for particle 3 in Reactions (1) and (3) of

$$\frac{sd^2\sigma}{dt\, dM_X^2} = \frac{s_o}{s} \sum_{ijk} G_{ijk}(t)\left(\frac{s}{M_X^2}\right)^{\alpha_i(t)+\alpha_j(t)}\left(\frac{M_X^2}{s_o}\right)^{\alpha_k(0)} \qquad (7)$$

where $s_o = 1$ GeV^2 and the G_{ijk} are the TR couplings.[12]

It was first suggested by Bishari[13] that pion exchange might be dominant mechanism for the charge exchange Reaction (3). By extrapolating to the pion pole, Field and Fox[11] estimate the contribution of the $\pi\pi P$ and $\pi\pi R$ terms to the process $pn \to pX$. They obtain

$$G_{\pi\pi k}(t) = \frac{1}{4\pi}\,\frac{g^2_{\pi np}}{4\pi}\,\sigma_t^{\,k}(\pi p)\,\frac{(-t)\;e^{b(t-\mu^2)}}{(t-\mu^2)^2} \qquad (8)$$

for the TR couplings where k represents pomeron or reggeon exchange and $\mu^2 = m_\pi^2$. The total πp cross section is taken to be $\sigma_t(\pi p) = \sigma_t^P(\pi p)/\sqrt{s}$ with $\sigma_t^P(\pi p) = 21$ mb and $\sigma_t^R(\pi p) = 20$ mb and the on mass shell coupling $g^2_{\pi np}/4 = 2\, g^2_{\pi pp}/4\pi$ is 30. For simplicity we neglect any off shell corrections by putting $b = 0$ in Eq.(8) and in the TR formula (7) we use $\alpha_\pi(t) = 0.0 + t$, $\alpha_P(0) = 1$ and $\alpha_R(0) = 0.5$. Furthermore, in order to compare with the data, we modify the theoretical prediction by a Monte Carlo program to account for Fermi motion and rescattering. The results, which are shown in Fig. 3 for $<s> = 506$ GeV^2 and $<t> = -0.17$ and -0.34 GeV^2, are in reasonable agreement with the data strongly supporting the hypothesis that pion exchange plays an important role in the charge exchange reaction $pn \to pX$. The $\pi\pi P$ and $\pi\pi R$ terms should therefore be included in any analysis of the reaction $pp \to pX$ which otherwise will overestimate the other TR contributions, mainly the RRP term.

Finally, at high energy and large M_X^2 the cross sections for the reaction $pn \to pX$ are expected to be similar to those for $pp \to nX$, assuming the dominant mechanism to be pion exchange, since $\sigma_+(\pi^+ p) \simeq \sigma_t(\pi^- p)$. We therefore find it difficult to reconcile the difference between the cross sections reported in this letter and those of a recent ISR experiment[14] for the reaction $pp \to nX$ which are a factor three or more lower in the kinematic region where the two experiments overlap.

We wish to thank the members of the Fermilab Internal Target Laboratory and the Accelerator Section for their help and cooperation.

REFERENCES

★ Research supported by the U.S. National Science Foundation and the Science Research Council, U.K. Development and operation of hydrogen jet target supported by the State Committee for Utilization of Atomic Energy of the U.S.S.R., Moscow.

1. K. Abe et al., Phys. Rev. Lett. 31, 1527 (1973)
2. Y. Akimov et al., Proceedings of the XVII International Conference on High Energy Physics, London 1974.
3. A.S. Carroll et al., Fermilab Preprint No NAL-PUB-74/75-Exp., 1974.
4. V. Franco and R.J. Glauber, Phys. Rev. 142, 1195 (1966)
5. L. Hulthen and M. Sugawara, Handbuch der Physik 39, 1 (1957).
6. G. Giacomelli, Proceedings of the XVI International Conference on High Energy Physics, Batavia, 1972, p. 219.
7. M.G. Albrow et al., II International Conference on Elementary Particles, Aix-en-Provence, 1973.
8. J.W. Chapman et al., University of Rochester Preprint No. UR-458, 1973.
9. S.J. Barish et al., Argonne National Laboratory Preprint No. ANL/HEP 7338, 1973.
10. Hadley et al., Phys. Rev. 75, 351 (1949)
11. R.D. Field and G.C. Fox, California Institute of Technology, Preprint No. CALT-68-434, 1974.
12. K. Abe et al. Phys. Rev. Lett. 31, 1530 (1973).
13. M. Bishari, Phys. Lett. 38B, 510 (1972).
14. J. Engler et al., Nucl. Physics B84, 70 (1975).

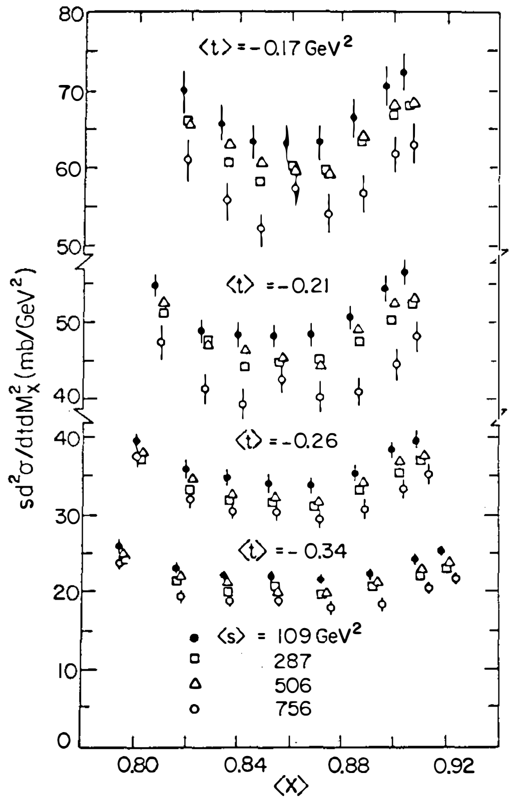

Fig. 1 Inclusive cross sections for the reaction pd → pX. The variables <s>, <t> and <x> are defined as if the target consisted of protons and neutrons with Fermi motion rather than deuterons (see text and Eqs. (4), (5) and (6)).

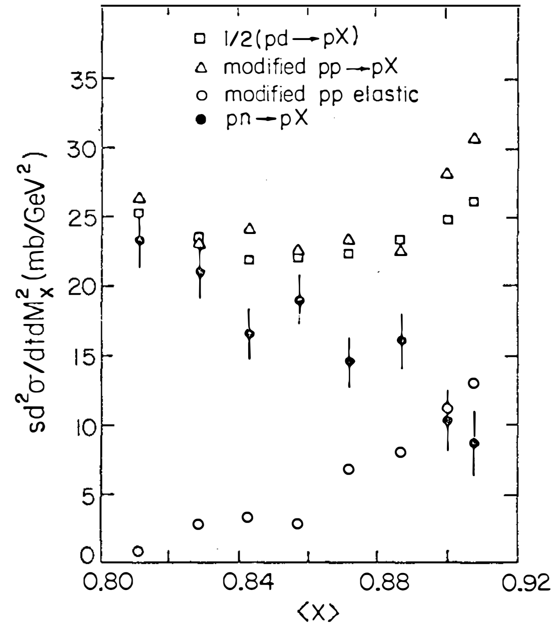

Fig. 2 Sample extraction of pn → pX cross sections from pd → pX, pp → pX and pp → pp cross sections at <s> = 287 GeV^2 and <t> = -0.21 GeV^2.

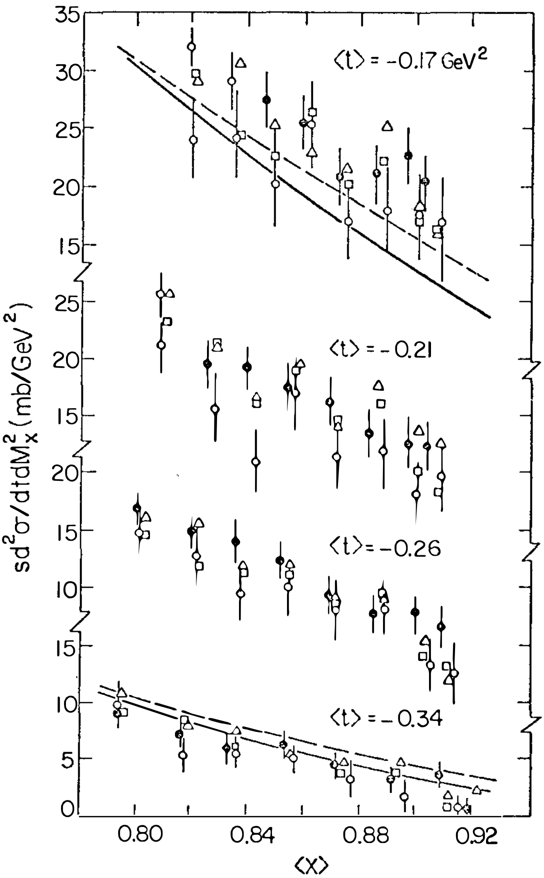

Fig. 3 Inclusive cross sections for the reaction $pn \to pX$. The symbols representing $\langle s \rangle = 109$, 287, 506 and 756 GeV^2 are as defined in Fig. 1. The solid curves are the sum of the $\pi\pi P$ and $\pi\pi R$ contributions to the TR formula (7) with couplings given by Eq. (8). These theoretical curves have been modified, resulting in the dashed curves, to account for Fermi motion and rescattering effects which have not been unfolded from the data.

RESULTS ON INCLUSIVE CHARGED PARTICLE PRODUCTION IN THE CENTRAL REGION AT THE CERN ISR

G. Jarlskog
CERN, Geneva, Switzerland
and
Lund University, Lund, Sweden
[British-Scandinavian Collaboration*)]

Abstract: An over-all description is given of data on inclusive production of $\pi^{\pm}$, $K^{\pm}$, p, and $\bar{p}$ collected at the CERN Intersecting Storage Rings (ISR). The kinematical range covered is $23 < \sqrt{s} < 63$ GeV, $0.1 < p_T < 5.0$ GeV/c, and $30° < \Theta_{cm} < 90°$. The larger p_T data are compared with the prediction of the constituent interchange model, and a qualitative agreement is found.

Résumé: Nous donnons une description générale des résultats inclusifs obtenus pour la production de $\pi^{\pm}$, $K^{\pm}$, p et $\bar{p}$ aux ISR du CERN. Ces données couvrent le domaine $23 < \sqrt{s} < 63$ GeV, $0.1 < p_T < 5.0$ GeV/c, et $30° < \Theta_{cm} < 90°$. Les résultats à grande impulsion transversale sont comparés aux prédictions du modèle d'échange de constituants. Un accord qualitatif est obtenu.

*) The other members of this Collaboration are:

B. Alper, H. Böggild, P. Booth, L.J. Carroll, G. von Dardel, G. Damgaard, B. Duff, J.N. Jackson, L. Jönsson, A. Klovning, L. Leistam, E. Lillethun, M. Prentice and J.M. Weiss.

INTRODUCTION

The data presented here on inclusive charged hadron production were collected during 1972 and 1973 by the so-called wide-angle spectrometer experiment at the CERN ISR. Preliminary results for the low transverse momentum range[1,2], $p_T < 1$ GeV/c, and final results on the high transverse momentum range[3], $1.0 < p_T < 5.0$ GeV/c, have already been published. The aim of this talk is to point out some important features in our data, and in particular to discuss recent results of over-all fits to the data.

EXPERIMENTAL ARRANGEMENT

The high p_T configuration of the spectrometer is shown in Fig. 1. It consisted of a 1 m bending magnet, wire spark chambers with magnetostrictive read-out, counter hodoscopes, and two high-pressure gas Čerenkov counters providing unique particle identification above 1.6 GeV/c. In the range 1.0 to 1.6 GeV/c the first Čerenkov counter could be used to distinguish between pions and kaons and time-of-flight measurements to separate kaons and protons. The solid angle of the spectrometer was about 12 msr. In the low p_T configuration the spectrometer had no Čerenkov counters. The particle identification was achieved by time-of-flight measurements, and an additional 0.5 m bending magnet was used in the position of Čerenkov 1 of Fig. 1 in order to get the option of a shorter spectrometer for the very low momentum region.

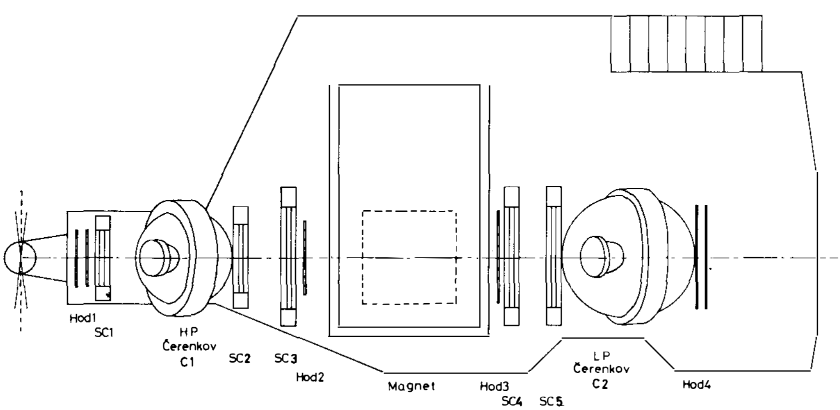

Fig. 1 Layout of the spectrometer for the high p_T model of data-taking.

ERRORS

The details of the data reduction have been described elsewhere[1-3]. Only the major uncertainties in the data will be stated here. The accuracy in normalization depends on how well the luminosity of the ISR can be determined. Our monitor was calibrated by the method of van der Meer[4]. Although this was done as frequently as possible, sometimes only a few measurements could be done for a given monitor (this was modified several times during the course of the experiment), which makes it difficult to assign an error to the measurement. For the high momentum data the calibration procedure is estimated to be: 6% for $\sqrt{s}$ = 44.6 and 52.8 GeV, 10% for 30.6 and 63.0 GeV, and 15% for 23.4 GeV. (The latter value is somewhat uncertain.) The corresponding errors associated with the low momentum data are: 3-6% for $23 < \sqrt{s} < 53$ GeV and 6-10% for $\sqrt{s} = 63$ GeV.

In the lowest range of the high p_T experiment, i.e. $1.0 < p_T < 1.4$ GeV/c, the nuclear absorption in the freon and in the steel walls of Čerenkov counter 1 was fairly large, and we estimate, for the case of antiprotons, that there might be a systematic uncertainty in our corrections of up to 30%. This uncertainty has not been applied to the data points. It should be stressed that such an error is s-independent.

The contribution from $K_S^0 \to \pi\pi$ to the pion spectra has not yet been corrected for. The uncertainty due to all other systematic errors is estimated to be of the same order as or smaller than the statistical uncertainty in the data.

In the following fits the estimated systematic errors (7%) have been applied to the data points, and the over-all normalization uncertainty for a given energy is taken into account.

DISCUSSION OF RESULTS

Figure 2 gives an example of the data obtained, namely at $\sqrt{s}$ = 52.8 GeV and $\Theta_{cm} = 89°$. Although the experimental conditions for the low and high momentum configurations were quite different, the consistency between the measurements in an overlap region is good. In order to arrive at a more convenient form of presenting all the data, the data points were shifted to fit a grid with steps of 0.2 in the rapidity y, and with steps of 0.1 GeV/c in the transverse momentum p_T, as can be seen from Fig. 3 for π^+. For each particle type, a "universal" fit in s, y, and p_T was attempted using the following two-component expression:

$$E \frac{d^3\sigma}{dp^3} = A_1\ e^{-A_2 p_T}\ e^{-A_3 y^2} + A_4\ (p_T^2 + A_5^2)^{-N}\ (1 - 2\ p_T/\sqrt{s})^P \ ,$$

where the first term is similar to the predictions of hydrodynamical models, which are known to describe the low p_T data adequately, and the second term gives the power dependence in p_T, observed at larger p_T, in a form similar to parton model predictions.

For π^+ such a fit gives the values: $A_1 = 210$, $A_2 = 7.6$, $A_3 = 0.2$, $A_4 = 10.7$, $A_5 = 1.03$, $N = 4.0$, and $P = 10.9$, with $\chi^2/N = 1977/1324$. Figure 4 shows the 90° spectra of π^+ at all five ISR energies. The fit given above is indicated on the $\sqrt{s} = 44.6$ GeV data points. For all particles except protons there is a clear s-dependence already at low p_T. For pions this amounts to an increase with s in $d\sigma/dy$ of about 25% over the ISR energies. For protons, which are shown in Fig. 5, there is no such marked s-dependence in the

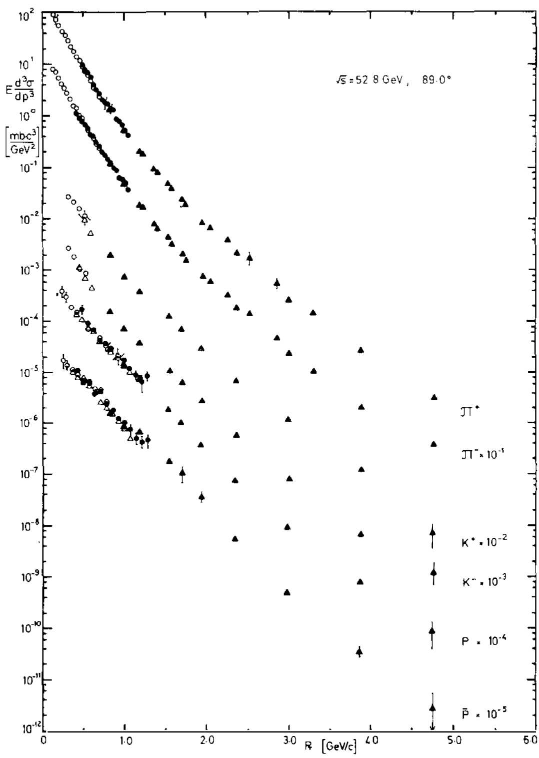

Fig. 2 The invariant differential cross-section for the production of pions, kaons, protons and antiprotons at $\sqrt{s} = 53$ GeV and $\Theta_{cm} = 89°$. The symbols correspond to different triggering modes or configurations of the experiment. Error bars indicate statistical errors only.

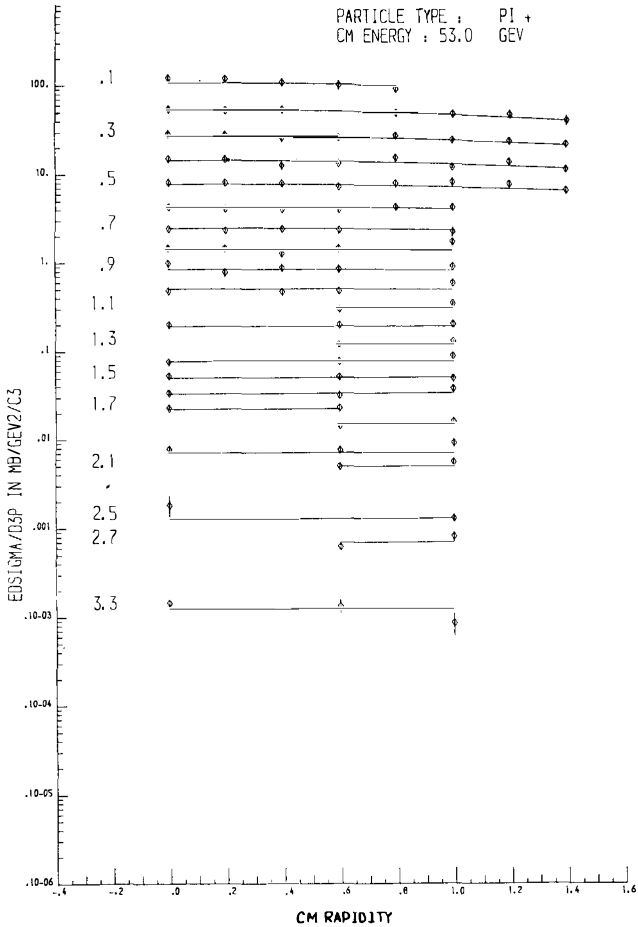

Fig. 3 The rapidity dependence of the invariant differential cross-section for π^+ at $\sqrt{s}$ = 53 GeV and at fixed transverse momenta between 0.1 and 3.3 GeV/c.

low p_T region, indicating that a big fraction of the low-momentum protons are diffractively produced. The fit to the proton data shown in Fig. 5 is given by A_1 = 5.3, A_2 = 3.79, A_3 = -0.20, A_4 = 15.7, A_5 = 1.20, N = 7.5, P = 0.0, with χ^2/N = 1024/666. The relative composition of produced particles exhibits a strong dependence on both p_T and s. Figure 6 shows the p_T dependence of the common charged hadrons as a fraction of p_T for $\sqrt{s}$ = 53 GeV.

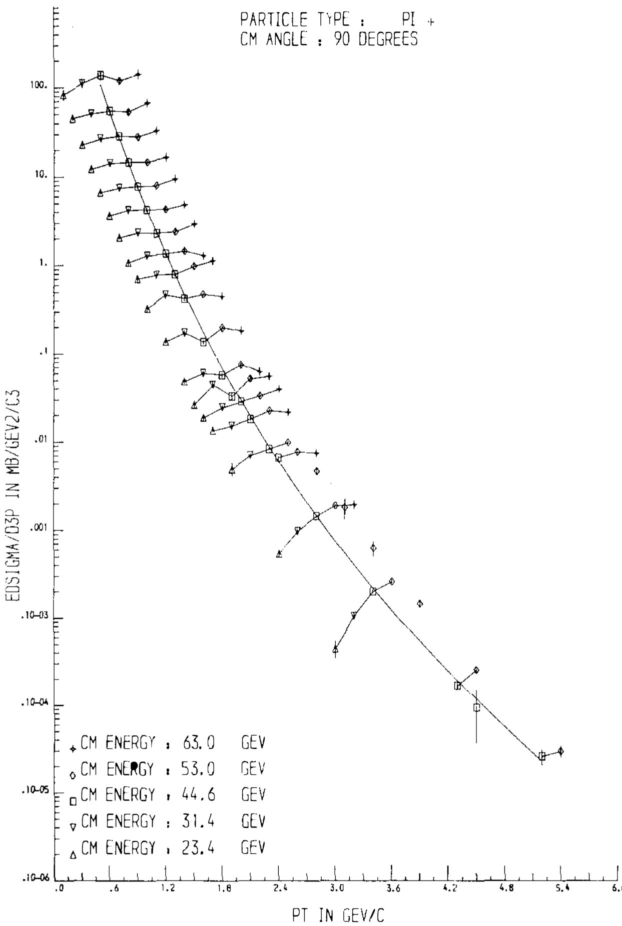

Fig. 4 The invariant differential cross-section for π^+ at $\Theta_{cm} = 89^\circ$ for five different ISR energies. The horizontal scale in p_T, referring to $\sqrt{s}$ = 23.4 GeV, has been shifted one division between energies in order to display the energy dependence. The solid line shown on the $\sqrt{s}$ = 44.6 GeV data gives a comparison with the over-all fit to the π^+ data for all s and Θ_{cm}.

At low p_T almost 90% of the secondaries are pions with a π^+/π^- ratio about 1.04. All the heavier particles become, however, more abundent as p_T increases up to about 1.5 GeV/c, where some stability seems to be reached with

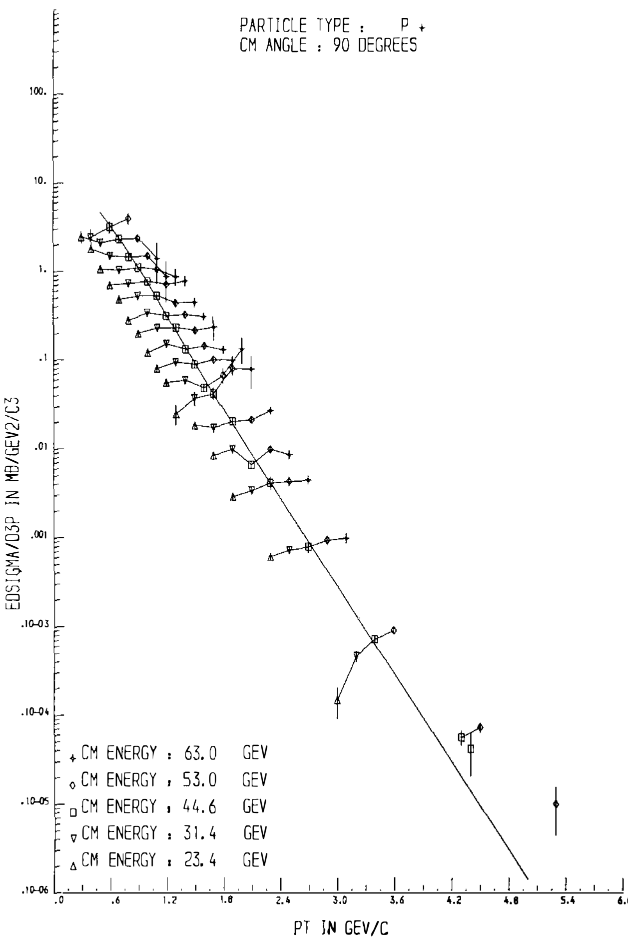

Fig. 5 As Fig. 4 for protons.

pions accounting for only 60% of the secondaries with a π^+/π^- ratio of about 1.15. The fraction of antiprotons, which increases very fast below 1 GeV/c seems to decrease above 2 GeV/c. The behaviour of the fractional yields of protons and antiprotons is different both as a function of p_T and of s as shown in Fig. 7, where the $\bar{p}/p$ ratio increases with s and indicates a broad peak in the region of 1.5 GeV/c.

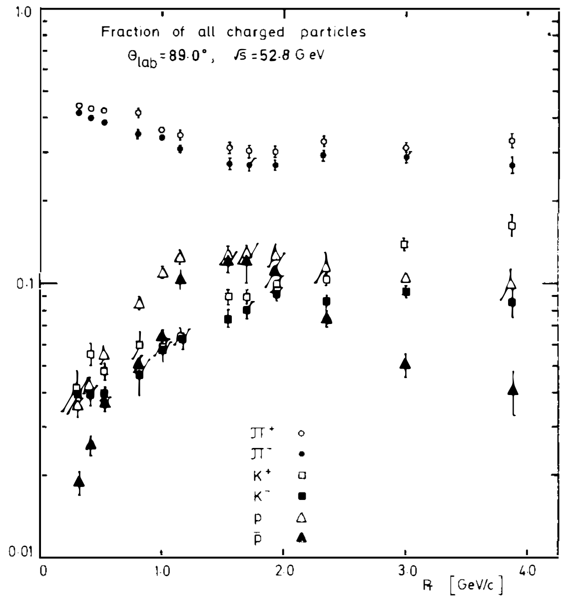

Fig. 6 The p_T dependence of the charged particle composition at $\sqrt{s}$ = 53 GeV for Θ_{cm} = 89°.

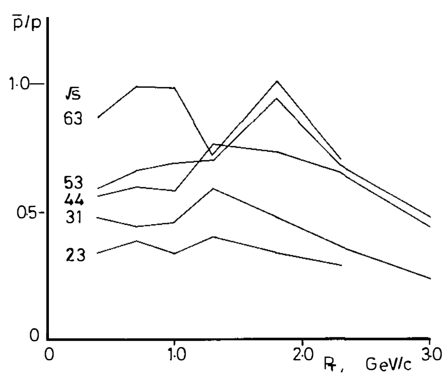

Fig. 7 A crude indication of the variation of the $\bar{p}/p$ ratio as a function of p_T and s.

A COMPARISON OF DATA WITH PREDICTIONS OF THE CONSTITUENT INTERCHANGE MODEL (CIM)

In last year's Rencontre de Moriond on high-energy hadronic interactions[5)] Blankenbecler described the CIM of Blankenbecler, Brodsky and Gunion[6)]. The predictions of this model have since become more specific[7,8)] and the qualitative features of these can be compared with our data. Although Blankenbecler et al. are ambitiously trying to describe processes within the whole Peyrou plot, we restrict our comparison to the large p_T region where parton models probably should be relevant. A basic assumption of the CIM is that hadrons can be represented by the naive quark model without gluons. An inclusive process, as shown in Fig. 8, can be described by adding up all contributing so-called hadron irreducible subprocesses. The leading behaviour is in general given by the subprocess, $a + b \rightarrow C + d^*$, Fig. 8, containing the smallest number of quarks (although direct quark-quark scattering is not allowed). The differential cross-section of the subprocess is given by

$$E \frac{d^3\sigma}{dp^3} = (p_T^2 + M^2)^{-N} (1 - |p|/p_{max})^P I ,$$

where I is assumed to be constant or a slowly varying function and M is a "mass" parameter. The second parenthesis contains the inelasticity ε, to a

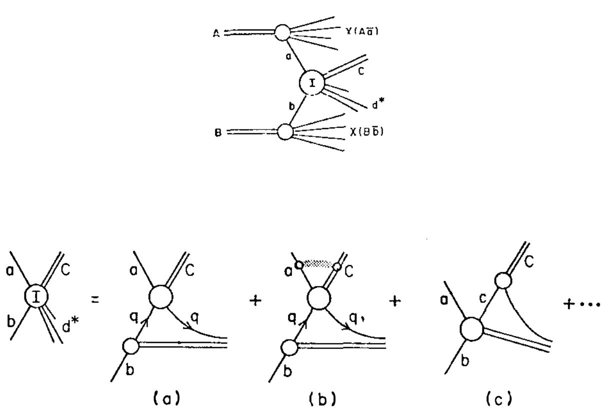

Fig. 8 The general decomposition of inclusive processes in the constituent interchange model. The process $A + B \rightarrow C + x$ is written as a sum of hadron-irreducible processes $a + b \rightarrow C + d^*$ (Ref. 7).

power P, which can be predicted as well as the power of p_T by using a simple dimensional counting rule[9]. The prescription for this game is that

$$N = n_a + n_b + n_C + n_{d^*} - 2 ,$$

where n_i is the number of quarks in particle i.

The power P is given by

$$P = n - 3 - N ,$$

where n is the number of quarks in the corresponding exclusive limit channel.

Consider as an example $p + p \to \pi + X$, where one of the dominant subprocesses are $q + \pi \to q + \pi$ with the exclusive limit channel $p + p \to \pi + \pi + + p + p$. We get $N = 4$, $n = 16$, and $P = 9$. A detailed discussion of this procedure is given in Ref. 7.

One typically finds for the processes $p + p \to \pi^{\pm}, K^{+} + X$:

$$E \frac{d^3\sigma}{dp^3} = (p_T^2 + M^2)^{-4} \, (h_1 \, \varepsilon^9 + h_2 \, \varepsilon^{11}) + (p_T^2 + M^2)^{-6} \, h_3 \, \varepsilon^5 + \; \ldots ,$$

where the constants h_1, h_2, and h_3 refer to different properties of the recoiling system. No estimate is given for the relative amplitudes of h_i, which makes it difficult to know which term is dominating. The lowest power of p_T is in general expected to dominate, but if ε is small a lower power of ε may be preferred. This is in qualitative agreement with the observation of the need for larger values of N than 4 to fit pion data at large x_T $(= 2p_T/\sqrt{s})$ at FNAL[10].

We have attempted to fit the high p_T data (p_T > 1 GeV/c) of all five energies and angles simultaneously to the CIM using the form

$$E \frac{d^3\sigma}{dp^3} = A_4 (p_T^2 + A_5^2)^{-N} \, (1 - 2 \, p_T/\sqrt{s})^P$$

assuming the existence of only one leading subprocess. This form differs from the CIM in that we are using p_T rather than $|\bar{p}|$ in the second parenthesis in order to get a good fit over the complete angular interval of the data ($40^\circ < \Theta_{cm} < 90^\circ$). With all four parameters free, one gets the results of Table 1.

Table 1

	π^+	π^-	K^+	K^-	p	$\bar{p}$
A_4	6.9 ± 0.3	7.4 ± 0.3	9.9 ± 3.4	10.4 ± 1.6	52 ± 8	9.0 ± 1.5
A_5	0.86 ± 0.01	0.89 ± 0.01	1.30 ± 0.06	1.33 ± 0.03	1.35 ± 0.03	1.08 ± 0.03
N	3.85 ± 0.02	3.89 ± 0.01	4.36 ± 0.15	4.38 ± 0.03	5.19 ± 0.04	4.6 ± 0.1
P	11.0 ± 0.2	11.9 ± 0.2	9.0 ± 1.0	12.2 ± 0.3	7.3 ± 0.3	14.0 ± 0.6
χ^2/N	532/202	604/203	245/111	198/111	233/114	287/114

All the fits were done using the CERN program chain MINUIT. Notice that the parameters are strongly correlated. The errors correspond to a change in χ^2 of 1. In Table 2 the model predictions are given and compared with the

Table 2

	Model		Exper.		Exper.		
	N	P	N	P	N	P	χ^2/N
π^+	4	9-11	3.9	11.0	4	9.7	537/202
π^-	4	9-11	3.9	11.9	4	11.0	606/203
K^+	4	9-11	4.4	9.0	4	10.4	251/111
K^-	4	11-13	4.4	12.2	4	13.6	202/111
p	6	5	5.2	7.3	6	5.7	251/114
$\bar{p}$	6	15	4.6	14.0	6	11.5	318/114

results of these fits. If one fixes the parameter N to the value 4 for $\pi^\pm$ and $K^\pm$ and to 6 for p and $\bar{p}$, which is very close to the free choice, the χ^2/N does not become significantly worse. In Figs. 9a-f the data is shown with these fits. One may notice a systematic deviation in the normalization of the $\sqrt{s}$ = 23 GeV data and also some indication of a rise in the data above the fits in the region of smaller p_T for all energies. The relatively high values quoted for χ^2/N are not alarming considering these effects and the varying experimental conditions during the two years of data collection. One finds that the experimentally determined parameter P is within the range of the predictions for all particles.

A fit has also been made using the total energy E of the particle instead of p_T, i.e. the term $(1-2E/\sqrt{s})^P$. This is closer to the Blankenbecler expression $(1-2|p|/\sqrt{s})^P$, but gives normally much worse fits. The values for

χ^2/N are the following: π^+ 1119/202, π^- 1058/203, K^+ 438/11, K^- 258/11, p 300/114, and $\bar{p}$ 156/114. Only the fit to the antiproton data is better; the parameters are in this case: $A_4 = 35.6 \pm 1.5$, $A_5 = 1.20 \pm 0.01$, $N = 5.10 \pm 0.02$, $P = 12.7 \pm 0.3$.

Considering that the predictions of the CIM for the leading behaviour of the invariant cross-section preceded the availability of high p_T data on $K^{\pm}$, p, and $\bar{p}$, the qualitative agreement with our experiment is remarkable. It would be very interesting to learn about what quantitative predictions can be made on the basis of this model.

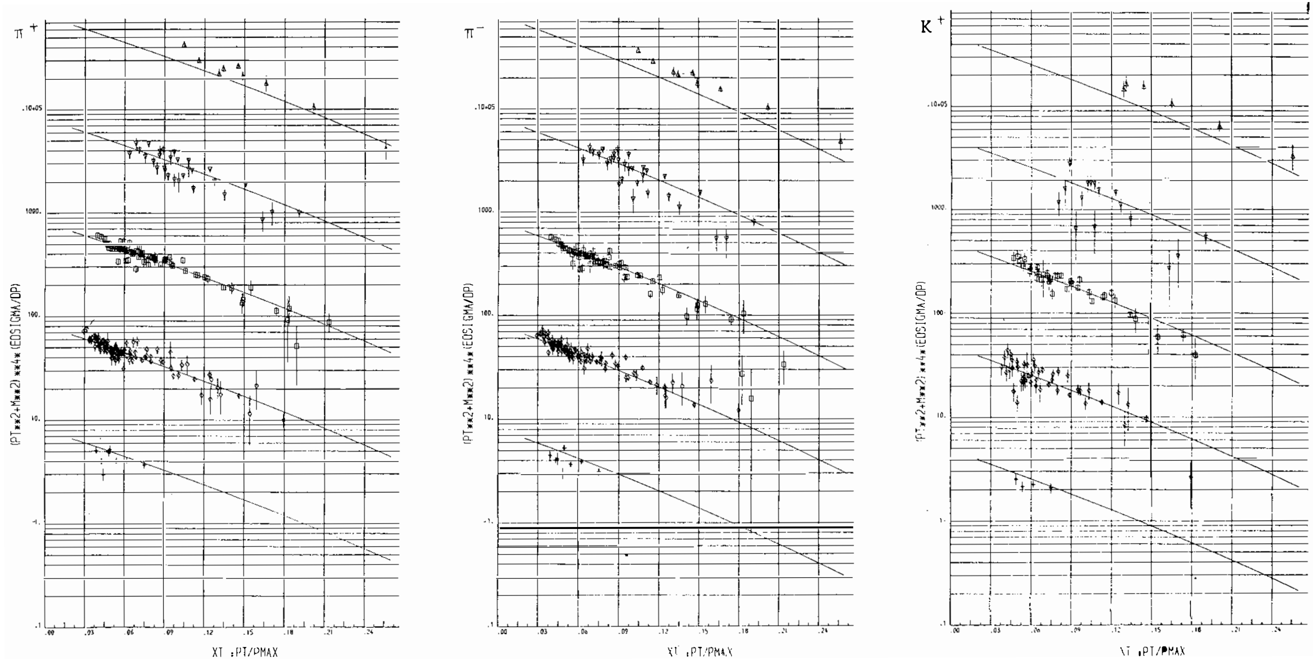

Fig. 9 a–c The large p_T data for $\pi^{\pm}$ and K^{+} for $\sqrt{s}$ = 23, 31, 45, 53, and 63 GeV displayed to illustrate the possible agreement with CIM predictions. The data points are displaced vertically by one decade between energies. The fits are given in Table 2. Error bars indicate statistical errors only.

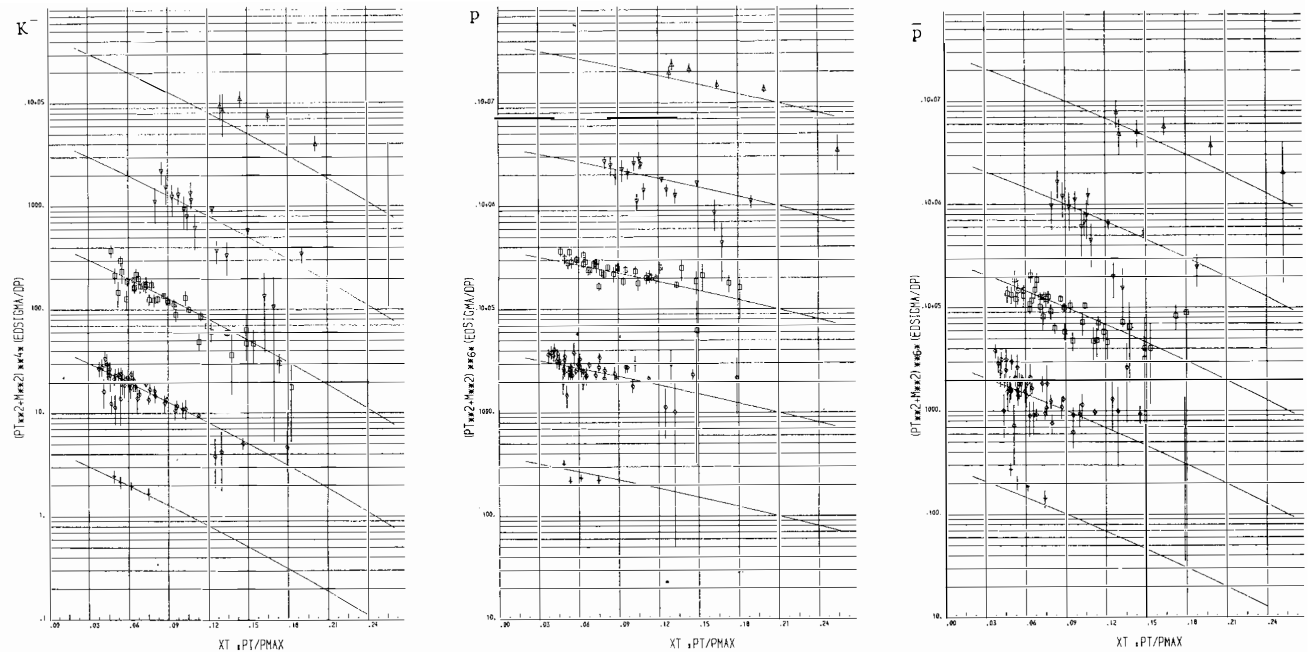

Fig. 9 As Fig. 9 a-c for K^-, p, and $\bar{p}$.
d-f

REFERENCES

1) B. Alper et al., Phys. Letters 47B, 75 (1973).

2) B. Alper et al., Phys. Letters 47B, 275 (1973).

3) B. Alper et al., Nuclear Phys. B87, 19 (1975).

4) S. Van der Meer, CERN-PO/68-31.

5) R. Blankenbecler, Proc. Conf. on High-Energy Hadronic Interactions, Rencontre de Moriond, 1974 (ed. J. Tran Thanh Van, Orsay, France).

6) J.F. Gunion, S.J. Brodsky and R. Blankenbecler, Phys. Rev. D6, 2652 (1972).

7) R. Blankenbecler and S.J. Brodsky, SLAC-PUB-1430 (1974).

8) R. Blankenbecler, SLAC-PUB-1438 (1974).

9) S.J. Brodsky and G.R. Farrar, Phys. Rev. Letters 31, 1153 (1973).

10) J.W. Cronin, H.J. Frisch, M.J. Shocher, J.P. Boymond, P.A. Piroué and R.L. Sumner, Phys. Rev. Letters 31, 1426 (1973).

MEASUREMENTS ON TWO-PARTICLE CORRELATIONS AT THE CERN ISR

R. Castaldi*)
CERN, Geneva, Switzerland

Abstract : Correlations between charged particles and a photon emitted at intermediate and large angles are presented as a function of the transverse momentum of the photon. The correlation function between charged secondaries and a particle (π^-, K^-, $\bar{p}$, or n) produced in the fragmentation region is also investigated.

Résumé : On présente les corrélations entre un photon émis à grands et moyens angles et les particules chargées associées, pour plusieurs valeurs de l'impulsion transversale du photon. On étudie aussi la fonction de corrélation entre une particule (π^-, K^-, $\bar{p}$, ou n) produite dans la région de fragmentation et les particules chargées associées.

*) On leave from Istituto Nazionale di Fisica Nucleare, Sezione di Pisa, Italy.

INTRODUCTION

Since the very high energy machines at CERN and FNAL started operating, great interest has been focused on the study of particle correlations in many-body reactions. In fact, only at the ISR and at FNAL does the available phase space become sufficiently large that the "true" dynamical correlations can be disentangled from those imposed by energy-momentum conservation.

During the last few years the Pisa-Stony Brook (PSB) Collaboration has collected at the ISR a large amount of data, in several different experimental conditions, with the aim of obtaining an extended insight into the dynamics of particle correlations. The results[1)] of fully inclusive measurements have shown the existence of strong positive short-range correlations between charged particles in the central region. In addition, evidence for long-range correlations has also been found in the data; this effect was interpreted as an indication of the existence of an important diffractive-like component in the inelastic cross-section.

In these early measurements, neither the charge sign nor the nature of any of the detected particles was identified. The next natural step in the two-particle correlation study is to measure the correlation function between a momentum-analysed particle (identified by a suitable detector) and the associated charged secondaries.

I shall report on three experiments recently performed along this line by the PSB Collaboration[2)] alone and together with the CERN-Roma[3)] and DESY-Karlsruhe[4)] Collaborations.

EXPERIMENTAL PROCEDURE

The schematic layout of the three experiments is shown in Fig. 1. The basic experimental apparatus was the same 4π-detector already used to measure the proton-proton total cross-section. This apparatus, which has been described in detail elsewhere[5)], consisted of large arrays of scintillation counters which divided the solid angle around the interaction region into 45 independent θ-bins, for the measurement of the polar angle of the emitted

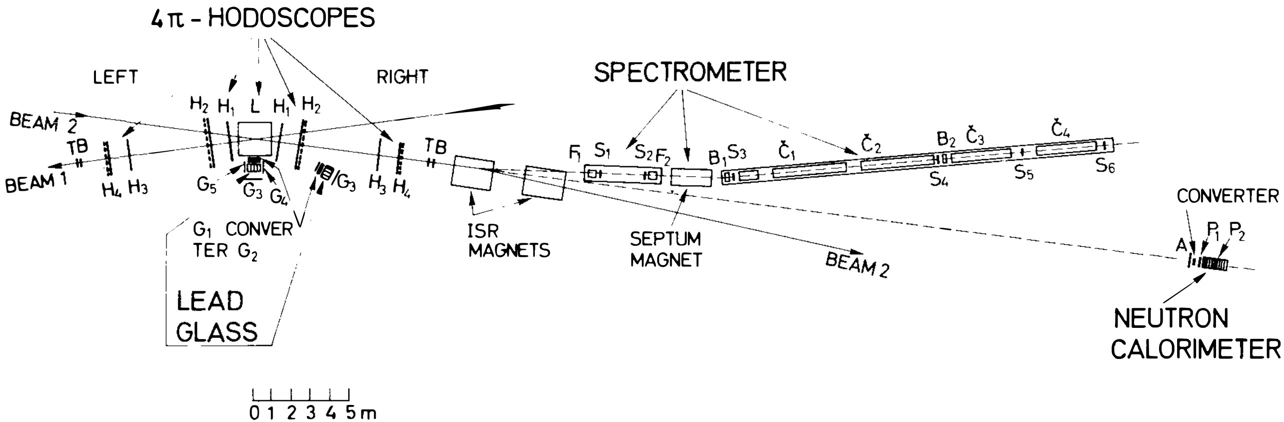

4π - HODOSCOPES
LEFT
RIGHT
SPECTROMETER
BEAM 2
BEAM 1
TB
H₂ H₁ L H₁ H₂
H₄ H₃
G₅
G₃ G₄
G₃
H₃ H₄
TB
F₁ S₁ S₂ F₂
B₁ S₃
Č₁
Č₂
B₂ Č₃
Č₄
S₄
S₅
S₆
G₁ CONVERTER G₂
LEAD GLASS
ISR MAGNETS
SEPTUM MAGNET
BEAM 2
CONVERTER
A P₁ P₂
NEUTRON CALORIMETER
0 1 2 3 4 5m

particles, and four ϕ-bins for the measurement of the associated azimuthal angles. In addition, in the region around $\theta = 90^\circ$, a special hodoscope allowed the measurement of the azimuthal angle in 20 independent bins. The main features of the system consisted in the large coverage of the solid angle ($\sim 3.2\pi$ sr) and in the very high efficiency of the trigger ($\sim$ 97% of all inelastic events were detected).

In the present specific study of correlations, this apparatus was implemented by the addition of particular detectors to provide different trigger signatures.

In the first experiment[6], the PSB Collaboration has studied the charged particle production associated with one photon emitted with a c.m. polar angle $\theta = 90^\circ$ and $\theta = 17.5^\circ$. The photon was detected and its energy measured by an array of lead-glass Čerenkov counters.

In the second experiment[7] (CERN-Roma-PSB Collaboration), π^-, K^-, or $\bar{p}$ emitted at $\theta = 0$ were detected and their momentum measured by a small-aperture magnetic spectrometer[8], while the emission angles of the accompanying charged particles were measured by the 4π-hodoscopes.

In the third experiment[9] (CERN-Roma-DESY-Karlsruhe-PSB Collaboration), the charged particle angular distribution was measured in events containing a forward emitted neutron. The neutron was detected and its energy measured by a total absorption calorimeter[10].

DEFINITION OF THE EXPERIMENTAL QUANTITIES

Let us define the single-particle and the two-particle density distributions ρ_1 and ρ_2 in terms of the rapidity y *)

$$\rho_1(y) = \frac{1}{\sigma_{inel}} \frac{d\sigma}{dy} \tag{1}$$

$$\rho_2(y_1,y_2) = \frac{1}{\sigma_{inel}} \frac{d^2\sigma}{dy_1 dy_2} \; . \tag{2}$$

*) The longitudinal variable y is defined as $y = \frac{1}{2} \ln \left[(E+p_L)/(E-p_L)\right]$, where E and p_L are respectively the energy and the longitudinal momentum of the detected particle.

ρ_2 gives the probability of a coincidence of two particles at y_1 and y_2. Correlations between two particles can be expressed in terms of the correlation function

$$R(y_1,y_2) = \frac{\rho_2(y_1,y_2)}{\rho_1(y_1)\ \rho_1(y_2)} - 1 \ . \tag{3}$$

If the two particles at y_1 and y_2 were emitted independently, $R(y_1,y_2)$ would be zero.

For relativistic particles in the angular range covered by the PSB hodoscope system, the rapidity y is well approximated by the polar angle variable $\eta = -\ln\tan\theta/2$. Since the 4π-detector measures only angles but no momenta, the variable η will be used instead of y for the particles detected by this apparatus. For a fixed value $y = y_1$ of the momentum-analysed particle, the correlation function (3) simply becomes:

$$R(y_1,\eta) = \left[\frac{1}{N_c}\,\Delta N_c(\eta)\right] \Big/ \left[\frac{1}{N_0}\,\Delta N_0(\eta)\right] - 1 \ . \tag{4}$$

In Eq. (4) N_0 is the counting rate of inelastic pp collisions and $(1/N_0)\ \Delta N_0(\eta)$ is the single-charged particle density distribution measured by the 4π-detector when the inclusive inelastic trigger is required; N_c and $(1/N_c)\ \Delta N_c(\eta)$ are the corresponding quantities for the sample of events with the selected signature. The quantity $R(y_1,\eta)$ defined by Eq. (4) is therefore the ratio of counting rates measured by the same apparatus for two different trigger conditions; to a first approximation one can then neglect corrections due to spurious secondary effects such as photon conversion, δ-ray production, hadron showers in the beam pipes, and to the finite angular resolutions of the counters.

CORRELATIONS BETWEEN CHARGED PARTICLES AND A PHOTON

The photon identification was provided by a 6-counter hodoscope G_1 followed by a 12 × 12 counter hodoscope G_2 with a 1 cm thick lead plate in between. The photon energy was measured by a matrix of 4 × 4 lead-glass Čerenkov counters. In Fig. 1 the photon detector is shown positioned at the two settings at which data were taken. Each of the 16 lead-glass blocks was calibrated in an electron test beam and the stability was continually monitored during the experiment. The resulting uncertainty of the energy calibration during the data taking was ±5%, and the FWHM energy resolution measured in the test beam was $\Delta E/E = 0.14\ (\mathrm{GeV})^{\frac{1}{2}}/\sqrt{E}$. Beam-beam events were identified by requiring the appropriate time of flight between the signals contributing to the trigger. In the 90° measurement the background rejection was improved by requiring no signal in the counters G_4 or G_5 placed on the sides of the lead-glass. The level of residual background contamination was less than 2% and the bias introduced in the results was negligible.

Figure 2 shows the behaviour of $R(\eta) + 1$ for different values of the transverse momentum of the detected photon at a c.m. energy $\sqrt{s} = 53$ GeV. Open points are 90° data, while full points are 17.5° data: the corresponding rapidity values of the photon are $y_\gamma \simeq 0$ and $y_\gamma \simeq 1.9$. The correlation functions have been measured separately in the two hemispheres, toward and away from the detected photon.

The low $p_\perp$ data show the usual short-range correlation effect already found in other γ-charge[11)] and charge-charge[1,12)] correlation measurements. As the transverse momentum of the observed photon increases, the two-body correlation function in the "away" hemisphere shows a rapid increase over a very wide η region. On the other hand, little $p_\perp$ dependence is found in the "toward" hemisphere.

A better understanding of the $p_\perp$ dependence of the correlation function is achieved using a different presentation. As a matter of fact, when the η distribution associated with a high $p_\perp$ photon is divided by the inclusive η distribution, the short-range correlation effect due to the presence of the photon itself makes less evident the manner in which the correlation function changes with increasing $p_\perp$. On the other hand, if the η distribution for a high $p_\perp$ photon is normalized to the distribution associated with a low $p_\perp$ photon, the resulting function illustrates the $p_\perp$ dependence of the correlation in a more suitable way. In Fig. 3 the distributions are shown normalized to the data of the low $p_\perp$ bin $0 \leq p_\perp \leq 0.5$ GeV/c.

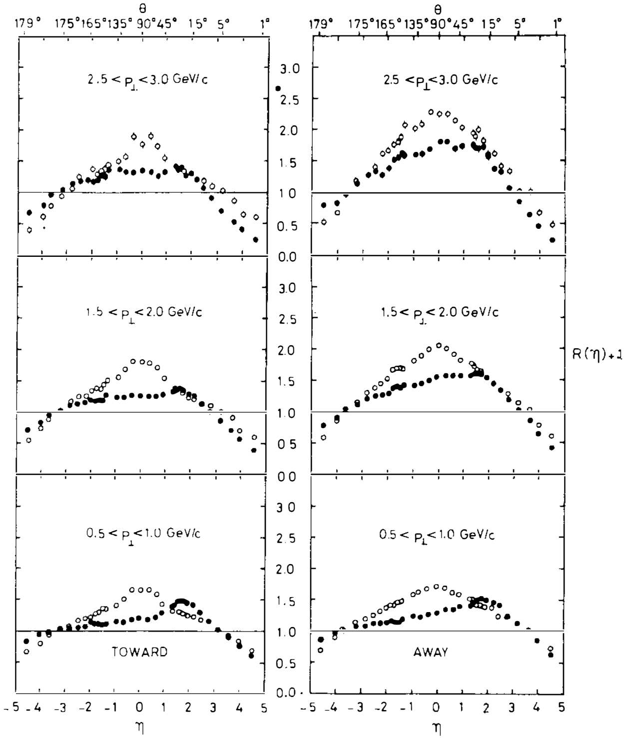

Fig. 2: Correlation functions R(η) + 1 at $\sqrt{s}$ = 53 GeV in the two azimuthal hemispheres toward and away from the detected photon. Open points are 90° data and full points are 17.5° data.

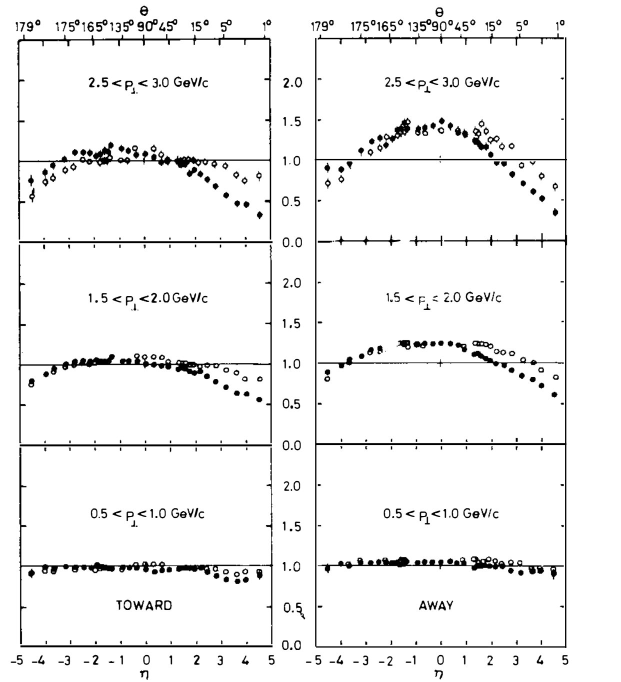

Fig. 3: Normalized η distributions at $\sqrt{s}$ = 53 GeV in the two azimuthal hemispheres toward and away from the detected photon. Data are normalized to the values for 0 ≤ ≤ $p_\perp$ ≤ 0.5 GeV/c. Open points are 90° data and full points are 17.5° data.

For a 90° photon, the "away" correlation increases with $p_\perp$ over a broad angular region around $\eta = 0$, while the "toward" correlation remains almost constant. At small angles, on the contrary, the data show a depression of the correlation with increasing $p_\perp$ in both azimuthal hemispheres.

For the 17.5° photon data, the behaviour of the "away" correlation is qualitatively the same, except for a more pronounced decrease at forward angles in the polar hemisphere of the detected photon. This negative correlation may have a kinematical origin when the photon takes away a large fraction of the available energy. In addition, a small increase of the correlation is seen around the central region in the "toward" hemisphere.

The growth with $p_\perp$ of the "away" correlation, which is evident both in the 90° and in the 17.5° data over a broad angular region, is a very interesting phenomenon which sheds some light on the dynamics of the large transverse momentum balance.

In order to understand this point better, it is convenient to study the azimuthal distribution of the associated particles. For 90° photons the partial multiplicities, normalized to the low $p_\perp$ data, in the interval $-0.7 < \eta < 0.7$, are shown in Fig. 4 as a function of the c.m. azimuthal angle ϕ for different values of $p_\perp$. The origin of the ϕ angle scale has been chosen in the direction of the photon detector. The associated charged multiplicity shows a definite growth with $p_\perp$ in a broad azimuthal region centred at $\phi = 180°$.

Figure 5 shows the $p_\perp$ dependence of the charged particle azimuthal distribution for the 17.5° photon data. The partial multiplicities, normalized to the low $p_\perp$ values, are shown as a function of ϕ in three different η regions. The average η value of the detected photon is $\eta_\gamma \simeq 1.9$ and therefore the following η intervals, $-1.9 \leq \eta \leq -1.3$, $-0.7 \leq \eta \leq 0.7$, $1.3 \leq \eta \leq 1.9$, have been chosen to display the effects associated with the transverse momentum balance. For all the three η regions the azimuthal distribution shows an important increase with $p_\perp$ of the charged multiplicities in the

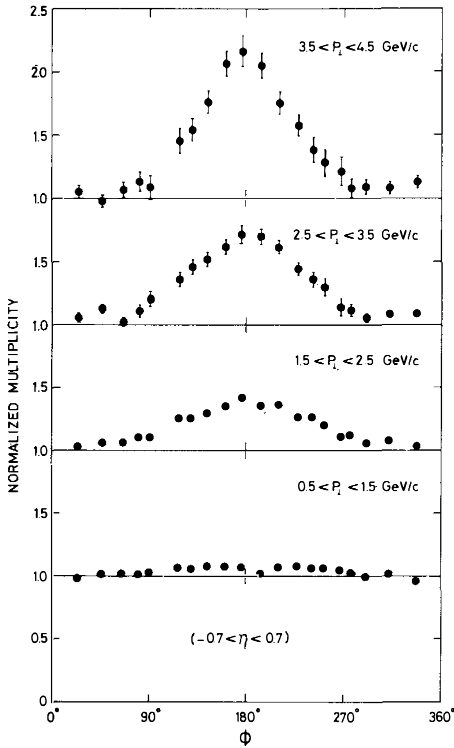

Fig. 4: Partial multiplicities as a function of c.m. azimuthal angle ϕ in the interval $-0.7 < \eta < 0.7$ at $\sqrt{s}$ = = 53 GeV. Data are normalized to the values for $0 \leq p_\perp \leq$ ≤ 0.5 GeV/c. The photon detector is at $\phi = 0^\circ$ and $\theta = 90^\circ$.

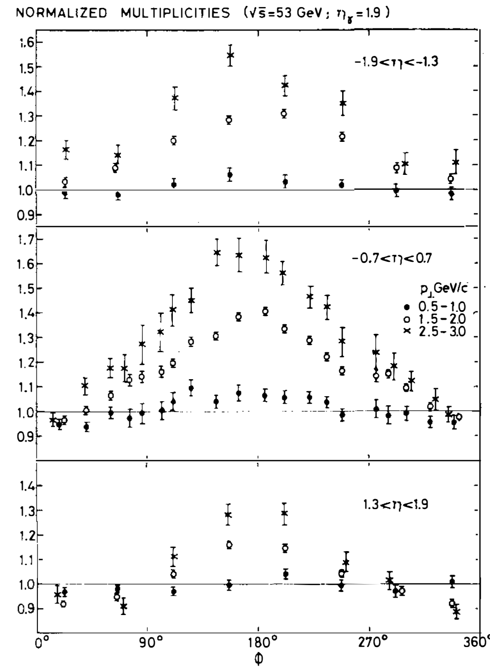

Fig. 5: Partial multiplicities as a function of c.m. azimuthal angle ϕ in three intervals of η at $\sqrt{s}$ = 53 GeV. Data are normalized to the values for $0 \leq p_\perp \leq 0.5$ GeV/c. The photon detector is at $\phi = 0^\circ$ and $\theta = 17.5^\circ$.

azimuthal hemisphere opposite the detected photon. The widths of the ϕ distributions are fairly broad as for the 90° data and roughly independent of the η region and of $p_\perp$.

The behaviour of the associate charged multiplicities hints that a large transverse momentum might be balanced mainly by particles produced over almost the entire azimuthal hemisphere opposite the photon direction. If this interpretation of the data is correct, then simple "back-to-back" scattering, as advanced by recent theoretical models[13] to explain phenomena involving large transverse momenta, is inadequate.

CORRELATIONS BETWEEN CHARGED PARTICLES AND A FORWARD NEGATIVE PARTICLE OR A FORWARD NEUTRON

Negatively charged particles produced at 0° were detected and momentum-analysed by the CERN-Roma magnetic spectrometer[8] (see Fig. 1). Particles entering the spectrometer were bent by a 2.5 m long septum magnet. Their trajectory was measured by four multiwire proportional chambers F_1, F_2, B_1, and B_2; their nature (π^-, K^-, or $\bar{p}$) was identified by four threshold Čerenkov counters $\check{C}_1$ to $\check{C}_4$. The trigger was provided by six scintillation counters S_1 to S_6. The solid angle covered by the spectrometer was $\Delta\Omega \simeq 4$ μsr, the momentum acceptance was $\Delta p/p \simeq \pm 12\%$, and the momentum resolution was about 1%.

In addition, neutrons emitted at 0° were detected by the calorimeter[10] shown in Fig. 1. This detector consisted of 40 scintillators, interspaced by 2 cm thick iron plates, viewed by a single photomultiplier. The first four iron plates, followed by a trigger counter P_1, were used as converter to localize the neutron interaction. A second trigger counter P_2 was placed at a depth of 12 cm of iron. A lead absorber ($\sim$ 5 radiation lengths thick) followed by a scintillation counter A was placed in front of the detector to reject γ-rays and charged particles. The solid angle covered by the calorimeter was about 5 μsr and the energy resolution ranged from ±35% at 5 GeV to ±10% at 30 GeV.

Both for negative particles and for neutrons, data were taken for y values larger than $y_{max} - 2$, i.e. in the fragmentation region.

The correlation function $R(\eta)$ for π^- at $\sqrt{s} = 53$ GeV is shown in Fig. 6a at three different values of the fractional momentum x ($x = 2p_L/\sqrt{s}$). For positive η values the data show, on top of a smooth continuum, a fairly wide bump centred at $\eta \simeq 3.7$ which decreases and finally disappears with increasing x. At large negative η values one notices a clear enhancement, again more pronounced at low x. Around the central region the smooth continuum shows a slope which is steeper at higher x; this behaviour may qualitatively be understood as an energy-momentum conservation effect which yields a negative correlation in the same hemisphere in which a very energetic particle is produced. The dashed lines in Fig. 6a show the results of a phase-space calculation by the Monte Carlo method, which support the above interpretation.

Figure 6b shows the correlation functions for K^- at $\sqrt{s} = 53$ GeV. For low values of x, the shape of the correlation of K^- is similar to that of π^- apart from the enhancement at large negative η. At high x, on the other hand, the bump at positive η values remains prominent, while for π^- it tends to disappear.

In Fig. 7, at the top, a comparison is shown between the inclusive correlation functions for π^-, K^-, and $\bar{p}$, at $x = 0.4$. The distribution $R(\eta)$ for $\bar{p}$ has a very similar shape to the one for K^-.

To understand better the features of the data for the different particles, the semi-inclusive correlation functions $R_n(\eta)$ have been measured. $R_n(\eta)$ is defined, as in Eq. (4), for subsets of events having a given value n of the total raw multiplicity. In Fig. 7b-d the π^-, K^-, and $\bar{p}$ data are shown divided into four classes of multiplicity. The corresponding η distributions, measured by the 4π-detector with the fully unbiased inelastic trigger, are shown in Fig. 7a to illustrate the shape of the denominator in Eq. (4). These distributions have been obtained by interpolating the data with a smooth curve and should be considered only as qualitative.

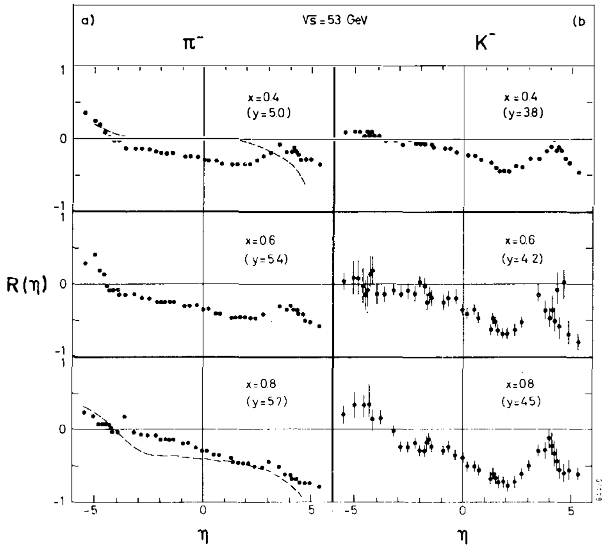

Fig. 6: Correlation functions R(η) at $\sqrt{s}$ = 53 GeV for π^- and K^-. Data are shown for three values of the fractional momentum x: x = 0.4, 0.6, and 0.8.

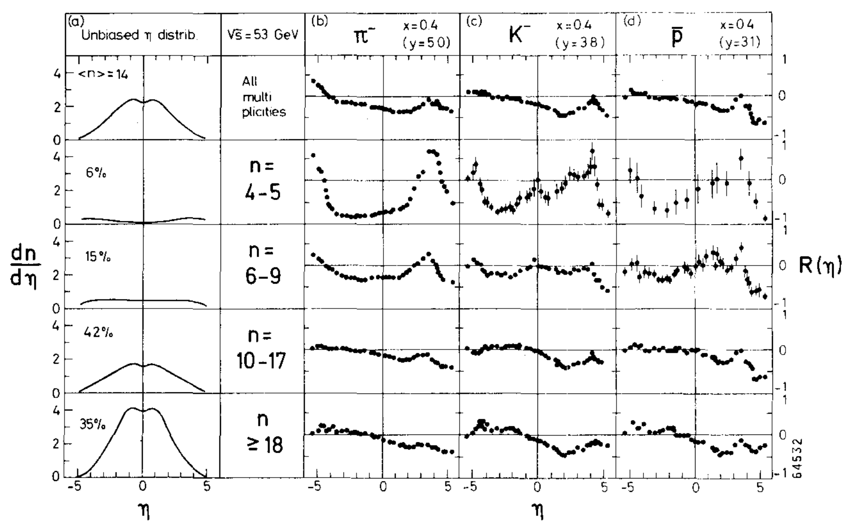

Fig. 7: Inclusive and semi-inclusive correlation functions R(η) at $\sqrt{s}$ = = 53 GeV for π^-, K^-, and $\bar{p}$, at x = 0.4. The unbiased η distributions are also shown for comparison. The variable n is the raw measured multiplicity.

The semi-inclusive π^- data (see Fig. 7b) show clearly that both the enhancement and the bump which are found in the inclusive correlation function are low-multiplicity phenomena. A similar behaviour is found in the neutron data. Figure 8 shows the inclusive and semi-inclusive correlation functions for neutrons at $\sqrt{s}$ = 53 GeV for three different values of x. A prominent feature in these data is the large bump at the lowest multiplicities, increasing with x.

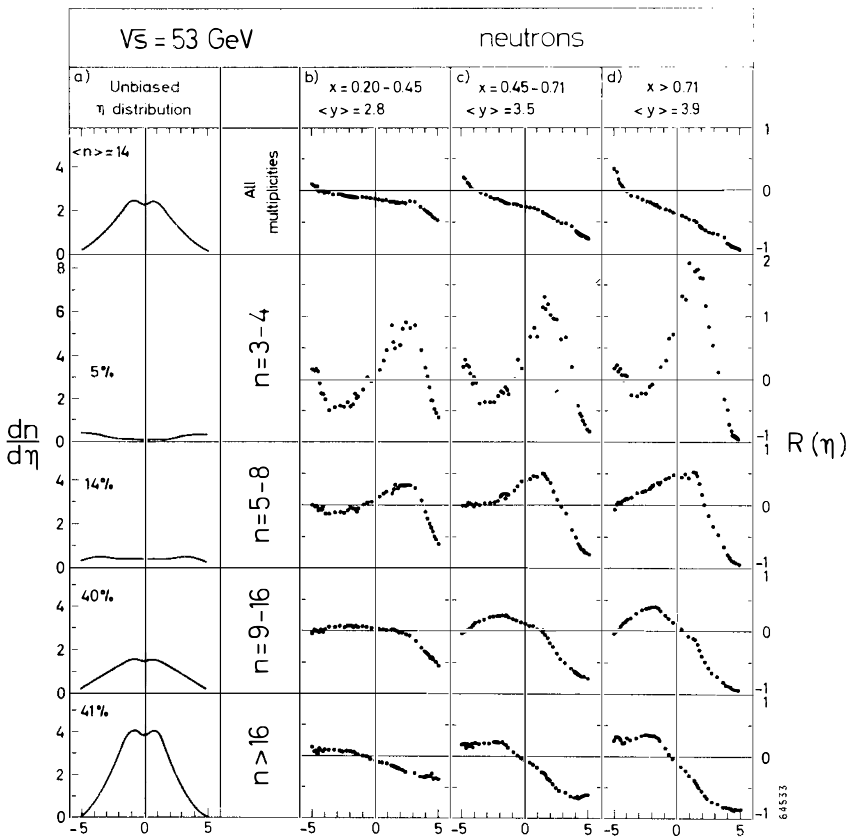

Fig. 8: Inclusive and semi-inclusive correlation functions R(η) at $\sqrt{s}$ = = 53 GeV for three x values of the detected neutron. The unbiased η distributions are also shown for comparison. The variable n is the raw measured multiplicity.

A simple dynamical interpretation of these facts is that, in the low-multiplicity events, both π^- and neutrons are produced in the fragmentation region in association with a cluster of other particles. One can then easily understand on the basis of kinematical arguments, the reason why these structures are more pronounced at lower x for π^- and at higher x for neutrons. In events in which a leading cluster (i.e. a cluster with baryonic number +1) is produced by the fragmentation of one of the incident protons, on the average the nucleon takes a high momentum, while the pions remain with lower momentum. In the limit of very low multiplicity, the production of a leading cluster coincides with the process of diffractive excitation of the nucleon.

The inclusive correlation functions for K^- and $\bar{p}$ show a bump at positive η, which is similar to the one of π^- and neutron. This feature suggests that in the fragmentation region K^- and $\bar{p}$ are also produced in association with a cluster of particles. However, the behaviour of the semi-inclusive correlation functions shows that the structure at positive η for K^- and $\bar{p}$, unlike that of π^- and neutrons, is not a low-multiplicity phenomenon and is due to a different production mechanism.

CONCLUSIONS

In events in which a photon of large transverse momentum is emitted at intermediate or large angles, a strong positive correlation is induced over a large region in the azimuthal hemisphere opposite the photon direction. It is therefore reasonable to conclude that the large $p_\perp$ value is balanced by particles produced over a wide η region and that a "back-to-back" picture alone is insufficient to explain the dynamics of the process.

When an energetic π^- or neutron is emitted in the forward direction, the strong correlations measured in the low multiplicity events show the presence of an important production of leading clusters in the fragmentation region. In addition, the behaviour of the correlation functions for K^- and $\bar{p}$ reflects a different production mechanism and indicates the presence of a cluster of charged secondaries accompanying these particles even in high multiplicity events.

REFERENCES AND FOOTNOTES

-1) S.R. Amendolia et al., Phys. Letters 48B, 359 (1974).

2) The members of the PSB Collaboration who have contributed to this experiment are: S.R. Amendolia, G. Bellettini, P.L. Braccini, C. Bradaschia, R. Castaldi, V. Cavasinni, C. Cerri, T. Del Prete, L. Foà, P. Giromini, P. Laurelli, A. Menzione, G. Paternoster, L. Ristori, M. Romano, G. Sanguinetti and M. Valdata for Pisa; G. Finocchiaro, P. Grannis, D. Green, H. Jöstlein, R. Kephart, D. Lloyd-Owen and R. Thun for Stony Brook.

3) The members of the CERN-Roma Collaboration who have contributed to this experiment are: U. Amaldi, W. Bartel, G. Cocconi, A.N. Diddens, Z. Dimčovski, R.W. Dobinson, P. Duinker, A.M. Thorndike, and A.M. Wetherell for CERN; A. Baroncelli and G. Matthiae for Roma.

4) The members of the DESY-Karlsruhe Collaboration who have contributed to this experiment are: W. Flauger for DESY; F. Mönnig for Karlsruhe.

5) S.R. Amendolia et al., Nuovo Cimento 17A, 735 (1973).
S.R. Amendolia et al., Proc. 1973 Int. Conf. on Instrumentation for High-Energy Physics, Frascati, 1973 (CNEN, Frascati, 1973), p. 391.

6) G. Finocchiaro et al., Phys. Letters 50B, 396 (1974).
G. Finocchiaro et al., Charged particle multiplicities associated with large transverse momentum photons at the ISR, to be published in Phys. Letters.

7) U. Amaldi et al., Correlations between a forward negative particle and the other charged particles produced in pp collisions at the ISR, to be published in Phys. Letters.

8) U. Amaldi et al., to be published.
Z. Dimčovski, CERN Internal Report NP 74-8, 17 October 1974.

9) U. Amaldi et al., Correlations between a forward neutron and the charged particles produced in pp collisions at the ISR, to be published in Phys. Letters.

10) J. Engler et al., Nuclear Instrum. Methods 106, 189 (1973).
V. Böhmer et al., Nuclear Instrum. Methods 122, 313 (1974).

11) H. Dibon et al., Phys. Letters 44B, 313 (1973).

12) R. Singer et al., Phys. Letters 49B, 481 (1974).

13) A recent review can be found in: S.D. Ellis, Proc. 17th Internat. Conf. on High-Energy Physics, London, 1974 (Rutherford Lab., Chilton, Didcot, 1974), p. V-23.

SEMINCLUSIVE CORRELATIONS AT THE ISR AND CLUSTER INTERPRETATION OF RESULTS

A. MENZIONE
Istituto Nazionale di Fisica
Nucleare, Pisa 56100 (Italy)

Abstract : Final results from the Pisa-StonyBrook ISR experiment on two-particle correlations at fixed charged multiplicity are shown. Positive, very short range correlations are found at all multiplicities. The data have been interpreted in the language of the independent cluster emission model. We show that the average cluster multiplicity $<k>$ depends smoothly on the energy and on the event multiplicity n. Scaling of $<k>$ as function of $n/<n>$ has also been found.

Résumé : Nous montrons les résultats definitives des mésures effectuées par le group Pisa-StonyBrook aux ISR sur les correlations entre deux particules chargées en fonction de la multiplicité de l'événement. Pour chaque valeur de la multiplicité nous obtenons des correlations à très courte portée qu'on peut bien interpreter avec un model à cluster. Nous montrons que la multiplicité moyenne des clusters varie doucement avec l'energie et avec la multiplicité et que une invariance d'echelle est valide si on presente les données en fonction de $n/<n>$.

INTRODUCTION

The study of inclusive correlation functions for an understanding of the behaviour of multiparticle production at high energy had been suggested already several years ago by many authors. First results on inclusive correlation (1) showing a broad positive peak of short range correlations, were suggesting of the creation of unstable resonant states between secondaries (clustering).

Furthermore two additional features of inelastic interactions have been also determined by experiments (2):

i) The existence of a diffractive component at low multiplicity ($\sim$20% of the overall production).

ii) The different y dependence of single-particle distributions at different event multiplicity.

These phenomena give origin to long range correlation effects which are leading in inclusive measurements and cannot be separated from the genuine dynamical short range effects.

In the following, the method applied in our experiment for the separation of these effects will be described and a quantitative measure of the short range clustering effect will be given. These results have been obtained by the study of the correlation functions at fixed charged multiplicity (seminclusive correlations).

In the last section the ideas of the independent cluster emission model are applied in order to determine the cluster size from the separate contribution of short range correlations.

THE EXPERIMENT

The Pisa-StonyBrook (*) experimental set-up has been described in detail elsewhere(3) and is skematically shown in fig. 1.

The features of the detector which are relevant to the present measurement are: a system of hodoscopes, structured in polar and azimuthal angles, and covering $\sim$90% of the full solid angle, is used to determine emission angles of charged secondaries. By requiring that at least one charged particle were emitted in the two emispheres downstream each beam, more than 95% of all inelastic proton-proton events are detected by the apparatus. The fast rate of data acquisition and the simplicity of the data reduction allowed to study the correlation function with very large statistics (10^8 entries in the two-body correlation matrix). Since the apparatus measures only angles and not momenta, the geometrical approximation to the rapidity $y \simeq \eta = -\ln \operatorname{tg}\theta/2$ has to be used.

(*) Members of the Pisa-StonyBrook collaboration are: S.R.Amendolia, G.Bellettini, L.Bosisio, P.L.Braccini, C.Bradaschia, R.Castaldi, T.Del Prete, G.Finocchiaro, L.Foà, P.Giromini, P.Grannis, D.Green, H.Jostlein, R.Kephart, P.Laurelli, A. Menzione, L.Ristori, G.Sangurinetti, R.Thun, and M.Valdata.

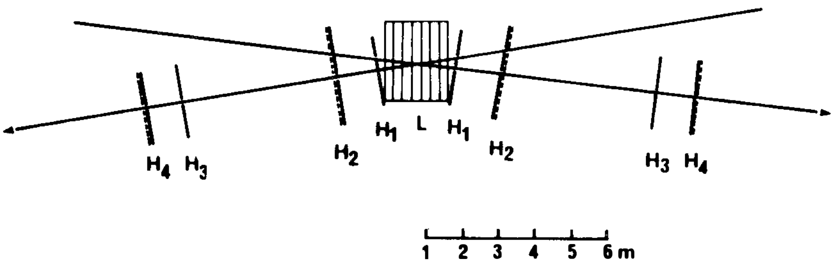

Fig. 1

Several sources of systematic errors have been taken into account and the corrections have been applied by making use of very detailed Montecarlo calculations. The most important correction had to account for the finite size of the counter elements, and for secondary interactions in the material of the vacuum pipes and in the apparatus itself (strong interactions, delta ray production and photon conversion). The overall correction resulting from these effects are summarized by a set of efficiency coefficients for each counter at given multiplicity and at given energy. The overall corrections are generally below 10%; the value of 25% is reached only at the highest multiplicities in the largest counters.

One should be aware of the fact that secondary interactions may simulate clustering effects. Being spurious clustering effects localized in narrow angular regions, the analysis has been made by excluding from the correlation matrix all the pairs of particles falling in the same azimuthal quadrant.

WHY SEMINCLUSIVENESS ?

Clustering effects are possibly an important feature of the inelastic, non-diffractive production at high energy. In order to gain a better insight into the problem we have focused our attention on correlations in the central region of the rapidity plot as a function of charged multiplicity. In this region ($y_{cm} = 0$) and for high enough multiplicities ($n > \langle n \rangle$) the contribution of the diffractive component can be neglected.

We give in the following the definitions of the relevant quantities together with their normalization properties: in full analogy with the inclusive single particle distribution,

$$\rho(y) = \frac{1}{\sigma_{in}} \frac{\partial\sigma}{\partial y} \qquad \int \rho(y) = \langle n \rangle \tag{1}$$

(σ_{in} is the inelastic cross-section) one can define the seminclusive distribution

$$\rho_n(y) = \frac{1}{\sigma_n} \frac{\partial\sigma_n}{\partial y} \qquad \int \rho_n(y) = n \tag{2}$$

where σ_n is now the topological cross-section. The inclusive correlation function in rapidity space is:

$$C(y_1,y_2) = \rho^{(2)}(y_1,y_2) - \rho(y_1)\rho(y_2) \; ; \quad \iint C(y_1,y_2) = \langle n(n-1) \rangle \tag{3}$$

with

$$\rho^{(2)}(y_1,y_2) = \frac{1}{\sigma_{in}} \frac{\partial\sigma}{\partial y_1 \partial y_2} \tag{4}$$

and the seminclusive correlations are defined similarly as:

$$C_n(y_1,y_2) = \rho_n^{(2)}(y_1,y_2) - \rho_n(y_1)\rho_n(y_2) \tag{5}$$

$$\iint C_n(y_1,y_2)\, dy_1\, dy_2 = -n \tag{6}$$

It is possible to express the inclusive correlation function (3) in terms of the complete set of the seminclusive ones (5), the expression being the following (ref 4) :

$$C(y_1,y_2) = \sum \frac{\sigma_n}{\sigma_{in}} C_n(y_1,y_2) + \sum (\rho_n(y_1) - \rho(y_1))(\rho_n(y_2) - \rho(y_2)) \tag{7}$$

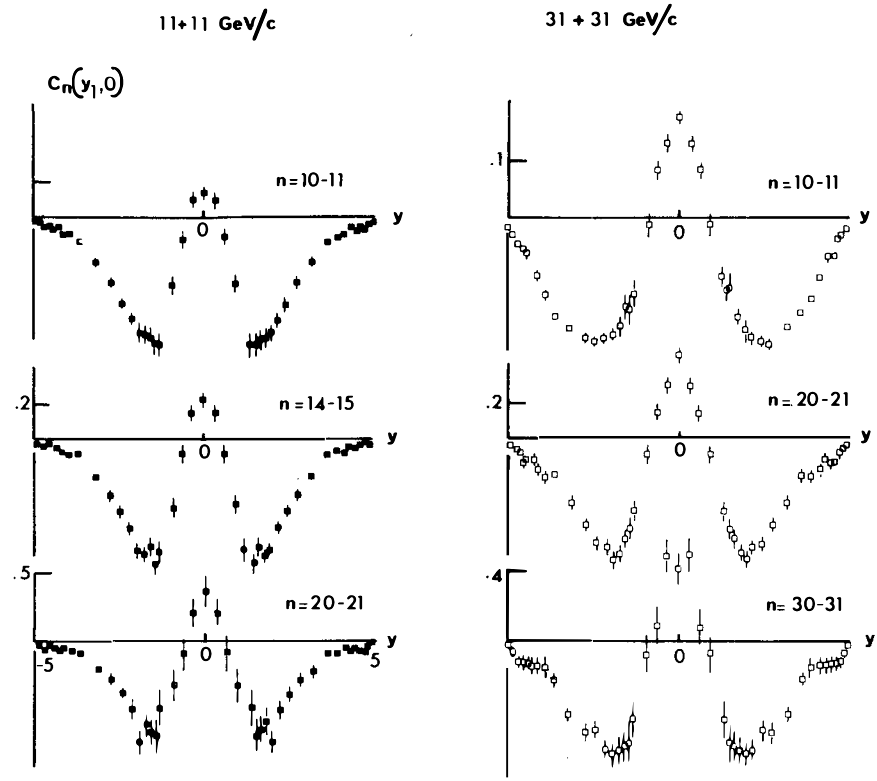

Fig. 2

The right hand side of expression (7) contains two terms : the first one is the sum of seminclusive correlations weighted on the multiplicity distribution; the second term is built with the differences between the inclusive single particle distributions and the seminclusive ones : such a term is independent of the double differential cross-section. This last term is strongly affected by experimental biases and it renders any direct comparison between experiments very difficult.

In fig. 2 we give the seminclusive correlation function at different multiplicities and energies as measured in our ISR experiment. In fig. 3 we show the decomposition of the inclusive correlation into the two terms appearing in the right-hand side of eq. 7 determined by means of inclusive and seminclusive single and two-particle distribution as measured in our experiment.

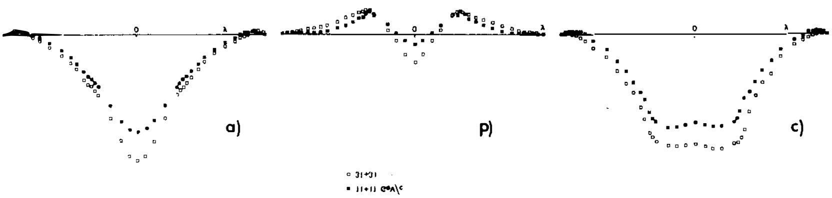

Fig. 3

By inspection of fig. 3 one learns the most important fact that the short-range peak displayed by seminclusive correlations is much narrower and much smaller than the bump displayed by the totally inclusive correlation function.

SEMINCLUSIVE CORRELATION ANALYSIS

In order to give a measure of the short- range correlation effect which is put in evidence by the series of peaks of fig. 2 we follow this simple line of arguments. By definition, in absence of any dinamical correlation, the correlation function would be given by:

$$C_n(y_1,y_2)\,|_{y_2=0} \propto -\rho_n(y_1) \qquad (8)$$

which is a negative smooth function, showing a minimum at $y_1=0$. We interpret the central peak seen in fig. 2 as due to short-range dynamical correlations standing in top of the above negative term. As it can be seen from the data, and as is confirmed by detailed fits, this peak is well represented by a gaussian distribution. Due to the normalization condition (6) stated above, the presence of the central dynamical peak will have to be compensated by a deeper negative part with respect to the no-correlation level. Our simplifing hypothesis is to assume that the negative contribution does not change in shape and remains proportional to $\rho(y_1)$ also in presence of short-range correlations:

Experimental corr. = Gaussian term + Norm. term

$$C_n(y_1,0) = C_n^*(y_1,0) - B_n\,\rho_n(y_1)$$

where $C_n^*(y_1,0) = C_n^*(0,0)\,\exp(-y_1^2/4\,\delta_n^2)$.
In this approach, one can try to fit the experimental correlation function at each multiplicity as a function of three parameters : $C_n^*(0,0)$, δ_n, B_n. All fits are rather good in the interval of multiplicity considered: the resulting values of χ^2 are between 40 and 120 for 43 experimental points. As an illustration of the plausibility criteria which have guided our analysis and which have been commented before, we show in fig. 4 some examples of the gaussian form of: $C_n(y_1,0)+B_n\,\rho_n(y_1)$.
The agreement with the data of such a simple hypothesis is indeed remarkable.

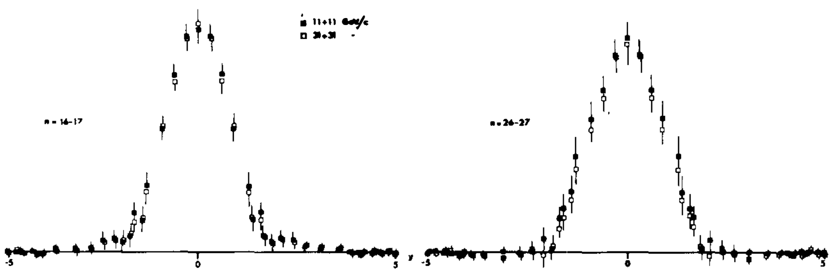

Fig. 4

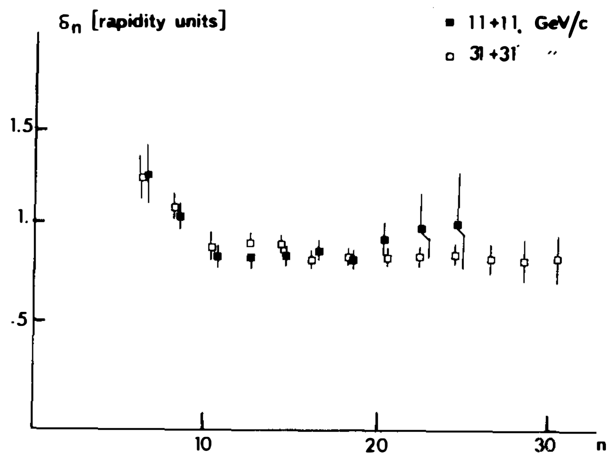

Fig. 5

For multiplicities higher than $<n>$, $\delta(n)$, as shown in fig.5 reaches a rather constant value, of the order of .85 rapidity units. Deviations from this value at low multiplicity may be understood as due to the presence of the diffractive component. B_n is found to be a multiplicity-dependent function, which will be discussed later in connection with the indipendent cluster emission model. An important increase of $C_n^*(0,0)$ with increasing multiplicity is observed at both energies (fig.6a), which is qualitatively similar to the behaviour of $\rho_n(0)$ (shown in fig.6b).

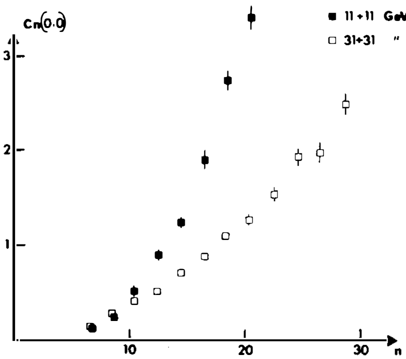

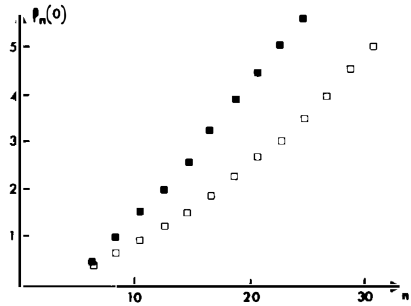

Fig. 6

INDIPENDENT CLUSTER EMISSION MODEL

This model describes the multiparticle production in terms of the uncorrelated production of a few clusters which decay isotropically in their c.m.s. into k charged hadrons. In the framework of this model it is possible to calculate the correlation function $C_n(y_1,y_2)$ at fixed multiplicity. The detailed calculation may be found in the literature (5). Let $\rho_n(y_1)$ be the probability of producing one particle at y_1. In order to determine, within the model, the joint probability for having a second particle at y_2 two different cases have to be considered. In the first case the second particle is originated in the decay of the same cluster and the two-particle distribution is simply given by the product of $\rho_n(y_1)$ times the rapidity distribution of the second particle (gaussian centered at y_1). Alternatively the second particle can come from the decay of a different cluster: the corresponding contribution to the correlation function results to be negative since clusters had been supposed to be uncorrelated. The result of the calculation is the following:

$$C_n(0,y_2)=\frac{<k(k-1)>}{<k>2\sqrt{\pi}\,\delta_n}\,\rho_n(0)\,e^{-y_2^2/4\delta_n} - \frac{1}{n}\left(1+\frac{<k(k-1)>}{<k>}\right)\rho_n(y_2)\,\rho_n(0)$$

This function consists of a positive gaussian term and of a negative one proportional to $\rho_n(y)$.

In addition to the cluster decay width δ, the factor : $<k(k-1)>/<k>$ is the physical quantity that can be determined by comparison with the data. This factor contains the average multiplicity $<k>$ and a quantity, $<k(k-1)>$, which is related to the dispersion of the same distribution. If the distribution is very narrow $<k(k-1)>/<k> \simeq <k>-1$. In the case of a Poisson distribution the same quantity is equal to <k>.

In order to evaluate <k(k-1)>/<k> as a function of n we have devided the experimentally determined values of $C^*_n(0,0)$ (fig 6a) by the corresponding values of $\rho_n(0)$ (fig 6b). The result (see fig 7) shows a smooth increase of the parameter with increasing multiplicity at both energies.

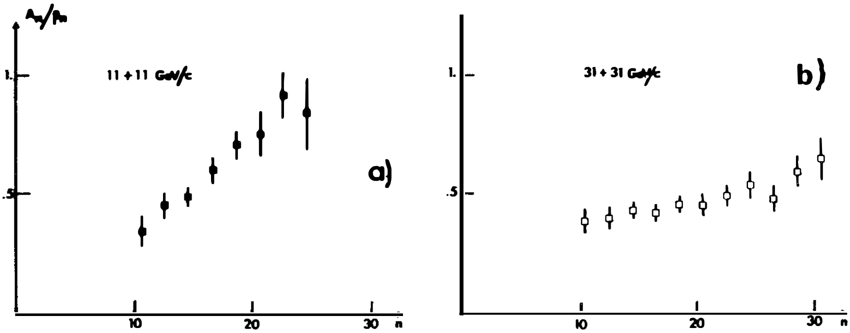

Fig. 7

A comparison between the data at the two different energies is also made by using as a variable the actual multiplicity scaled by its average value <n>, with the aim of comparing the different data at the same value of the density of particles in phase space (fig 8).

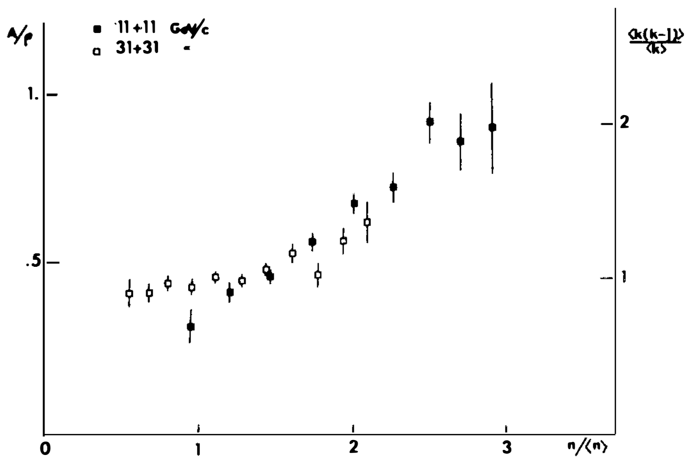

Fig. 8

One observes that the two sets of points fall rather well one in top of the other. A scale in terms of <k(k-1)>/<k> is also given. We conclude from this analysis that at n≃<n> the value of <k(k-1)>/<k> is 1.±.1 and increases to ∿1.6 at n=2<n>

Such a small value for the cluster multiplicity suggests the possibility that the production of well known meson resonances could play a dominant role for the generation of short-range correlations in high energy inelastic reaction.

In the following discussion the agreement between our correlation function and the analogous measurament of the A.C.M. collaboration was treated. Fig. 9 shows the comparison where the data are analyzed using as variable the difference of rapidities (y1-y2) and simulating the acceptances in angles and multiplicity of the A.C.M. experimental apparatus (6).

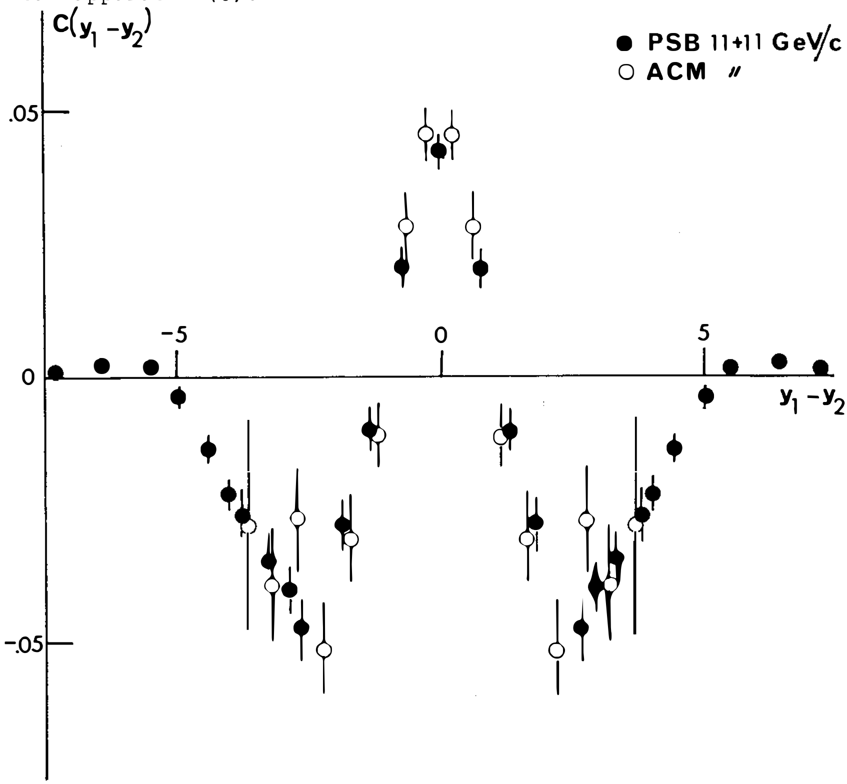

REFERENCES

1) S. R. Amendolia et al., Phys. Lett. 48B 1563 (1974)
   R. Singer et al. Phys. Lett. 49B 481 (1974)

2) M. G. Albrow et al. Phys. Lett. 44B 207 (1973)
   G. Bellettini, High Energy Collisions - 1973 StonyBrook
   L. Foà, Suppl. Journal de Physique 34 C1-317 (1973)

3) S. R. Amendolia et al., Nuovo Cimento 17A 735 (1973)

4) A. Białas, Proceedings IV International Symposium on Multiparticle Hadrodynamics, Pavia (1973)

5) E. Berger "Rapidity correlations at fixed multiplicity in cluster emission model", (cern/DPh II/Phis. 74-17).

6) K. Eggert et al. Nucl. Phys. (1975).

Multiparticle Production in Particle-Nucleus Collisions at High Energies

G. Berlad, A. Dar and G. Eilam

Physics Department, Technion - Israel
Institute of Technology, Haifa - Israel

Abstract. A simple model is proposed for multiparticle production in high energy particle-nucleus collisions. The production process factorizes into a product of nuclear properties and measured particle-particle collision properties. Most results are insensitive to nuclear structure details. Good agreement between experiment and theory is obtained. An important implication to high energy particle physics research is pointed out.

Résumé. On propose un modèle simple pour la production multiple dans les collisions particule-noyaux à hautes énergies. Le processus de production se factorise en un produit de propriétés nucléaires et de propriétés de collision particule-particule. La plupart des résultats sont indépendants des détails de structure nucléaire, et un bon accord avec l'expérience est obtenu. Une implication importante pour la physique des particules à hautes énergies est discutée en détail.

INTRODUCTION: Recent experiments[1] on multiparticle production in particle-nucleus collisions at high energies ($E_{lab} \equiv E > 10$ GeV) have revealed a number of interesting features such as:

(a) The multiplicity ratio

$$R_A \equiv \frac{\langle n\rangle_A}{\langle n\rangle} \tag{1}$$

where $\langle n\rangle_A$ and $\langle n\rangle$ are, respectively, the average charged multiplicity in particle-nucleus (shower particles only) and particle-particle collisions, increases only by a factor of about 2 from hydrogen to uranium (see Fig. 1), and exhibits no energy dependence.

(b) Koba-Nielsen-Olesen (KNO) scaling[2] is obeyed, i.e., the function

$$\psi_A \equiv \langle n\rangle_A \frac{\sigma_n^A}{\sigma_{in}^A} \tag{2}$$

depends only on $z \equiv n/\langle n\rangle_A$ (σ_n^A and σ_{in}^A are, respectively, the cross section for producing n charged particles and the total inelastic cross section in particle-nucleus collisions). ψ_A is almost indentical to ψ, measured in particle-particle collision (see Fig. 2).

(c) R_A for a fixed number N_h of heavy prongs (mostly protons) increases very slowly with N_h and is energy independent (see Fig. 3).

Although some existing models[3] are consistent with the data, they involve detailed assumptions that are hard to test regarding the propagation of hadrons through nuclear matter. In this letter we offer a simple model in which nuclear-structure details and properties measured in particle-particle collision factorize. The experimental facts (a), (b) and (c) are well reproduced; most results are insensitive to nuclear details. The underlying physical picture, if proven to be correct, has an important implication for particle physics research at high energies.

THE MODEL: The model is based on two observations:

Observation (1): Various quantities measured in particle-particle collisions, such as the average multiplicity, $<n>$, and the KNO scaling function ψ, are practically independent on the quantum numbers of the colliding particles[4].

Observation (2): The incident particle sees a nucleus that is Lorentz contracted to a narrow disk. Consequently, the "array" of i nucleons in the contracted nucleus that lie on the path of the projectile interact simultaneously with the projectile. The c.m. energy squared available for particle production in the particle-array collision is given by $s_i = 2imE$, (neglecting nuclear binding) where m is the nucleon mass. s_i is thus i times the center of mass energy squared in particle-nucleon collisions.

Motivated by the above observations we assume:

Assumption (1): When a high energy particle collides with an array of i nucleons the collision in the c.m. frame resembles a particle-particle collision at c.m. energy $\sqrt{s_i}$. In particular the probability to produce n charged particles, σ_n/σ_{in}, in an inelastic particle-array collision is

$$P_n(i,E) = P_n(1,iE) \quad , \tag{3}$$

and is hereafter denoted by $P_n(iE)$.

Assumption (2): Only those nucleons that lie within a cylinder of cross section σ along the projectile path will interact with the projectile.

According to assumption (1), information on particle-array collisions can be obtained from particle-particle collisions. In particular

$$P_n(iE) = \frac{1}{<n(iE)>} \psi\left(\frac{n}{<n(iE)>}\right) \quad . \tag{4}$$

According to assumption (2), the probability P(i,A) that the incident particle will encounter exactly i nucleons in a nucleus of A nucleons is calculated from low energy nuclear physics. For instance if the nuclear wave-function is a product of A identical nucleon wave functions, then the probability to find a given nucleon at impact parameter b is $\sigma T(b)/A$, where

$$T(b) = \int_{-\infty}^{\infty} dz\rho(b,z) \; ; \; \int d^2bT(b)=A. \tag{5}$$

ρ is the nuclear density.

Consequently,

$$P(i,A) = \frac{\int d^2b \binom{A}{i} \left(\frac{\sigma T}{A}\right)^i \left(1-\frac{\sigma T}{A}\right)^{A-i}}{\int d^2b \left[1-(1-\frac{\sigma T}{A})^A\right]} \tag{6}$$

Knowledge of P(i,A) enables us to predict multiparticle production in particle-nucleus collisions from data on particle-particle collisions:

(a) <u>The ratio R_A</u>: According to assumptions (1) and (2), the probability to produce n charged particles in particle-nucleus collision is given by:

$$P_n^A(E) \equiv \frac{\sigma_n^A}{\sigma_{in}^A} = \sum_{i=1}^{A} P(i,A)\, P_n(iE). \tag{7}$$

The average multiplicity in particle-particle collision is well described by[5]:

$$\langle n(E)\rangle \simeq C\, E^{1/4} \;, \tag{8}$$

thus Eqs. (7) and (8) yield

$$\langle n(E)\rangle_A \doteq \sum_n nP_n^A(E) = \langle n(E)\rangle \sum_{i=1}^{A} P(i,A) i^{1/4} \;, \tag{9}$$

or

$$R_A = \sum_{i=1}^{A} P(i,A)\, i^{1/4} \equiv \langle i^{1/4}\rangle_A \tag{10}$$

R_A is thus independent of E.

(b) <u>KNO scaling</u>: From Eqs. (2), (4) and (7) one writes:

$$\psi_A = \langle n(E)\rangle_A \sum_{i=1}^{A} P(i,A) \frac{1}{\langle n(iE)\rangle}\, \psi\left(\frac{n}{\langle n(iE)\rangle}\right) \tag{11}$$

and by using (8) and (10) one obtains

$$\psi_A = R_A \sum_{i=1}^{A} P(i,A) i^{-1/4} \psi(i^{-1/4} R_A Z). \tag{12}$$

R_A is energy independent, thus ψ_A obeys KNO scaling[6].

Since ψ_A scales, the scaled dispersion $D_A/\langle n\rangle_A$ (where $D_A \equiv \sqrt{\langle n^2\rangle_A - \langle n\rangle_A^2}$) is energy independent. In addition the following inequality is easily derived:

$$1 \lesssim \frac{D_A/\langle n\rangle_A}{D/\langle n\rangle} \lesssim \frac{\langle i\rangle_A^{1/2}}{R_A^2} \tag{13}$$

D is the dispersion measured in particle-particle collisions Note that these inequalities are independent of ψ .

(c) R_A as a function of N_h: Consider the situation where exactly N_p protons are knocked out from the nucleus[7]. According to our assumptions, $N_n = i-N_p$ neutrons $(0<N_n<A-Z)$ located in "array" i will accompany the N_p protons[8]. A derivation similar to that of Eqs. (6) and (10) then yields the energy independent relation:

$$R_A(N_p) = \frac{\sum_{i=N_p}^{A-Z+N_p} \binom{A-Z}{i-N_p} \int d^2b \left(\frac{\sigma T}{A}\right)^i \left(1-\frac{\sigma T}{A}\right)^{A-i} i^{1/4}}{\int d^2b \left(\frac{\sigma T}{A}\right)^{N_p} \left(1-\frac{\sigma T}{A}\right)^{Z-N_p}} \tag{14}$$

An independent particle model may be a poor approximation for heavy nuclei. Instead, if we assume that any number N_p of knocked out protons is accompanied on the average by $\frac{A-Z}{Z} N_p$ neutrons then

$$R_A(N_p) = \left(\frac{A}{Z} N_p\right)^{1/4} \tag{15}$$

COMPARISON WITH EXPERIMENT: In order to compare theory with experiment, we have represented the nucleus by a uniform sphere with a radius $r_o A^{1/3}$. For incident protons we have assumed [9]: $\beta = \sigma/2\pi r_o^2 = 1$, while for pions we have taken $\beta = .6$ since [10] $\sigma(\pi p)/\sigma(pp) \approx .6$.

In Fig. (1), Eq. (10) for R_A is compared with data for π-nucleus and p-nucleus as a function of A, and with p-emulsion data as a function of E. Good agreement between theory and experiment is obtained [11]. R_A is sensitive to β and to the assumed nuclear wave function. In Fig. (2), we compare Eq. (12) for ψ_A with data on π-Ne. Eq. (12) also describes well the measured ψ_A in p-emulsion [1f] [1j] (not presented here). ψ_A as predicted by (12) is practically A independent [12], (although a slight A dependence develops at high values of z) and is independent of β. The same holds also for $(D_A/\langle n_A\rangle/(D/\langle n\rangle)$ [13] (insert in Fig. (2)). Note that the bounds obtained in Eq (13) are rather strict. Eqs. (14) and (15) are compared with data on π-Ne and p-emulsion in Fig. 3; good agreement is found.

CONCLUSIONS: We have demonstrated that multiparticle production in high energy particle-particle and particle-nucleus collisions are successfully related by a simple model. Since $\langle i_A\rangle \sim A^{1/3}$, we find that the average effective energy for producing particles in particle-nucleus collisions is about $A^{1/3}$ larger than in particle-proton collisions. It implies that proton-nucleus collisions, and in particular nucleus-nucleus collisions (turning ISR into a heavy-ion colliding beams machine?) with the same energy per nucleon can take us beyond the kinematical thresholds for producing exotic massive particles such as intermediate vector bosons, heavy leptons and charmed particles.

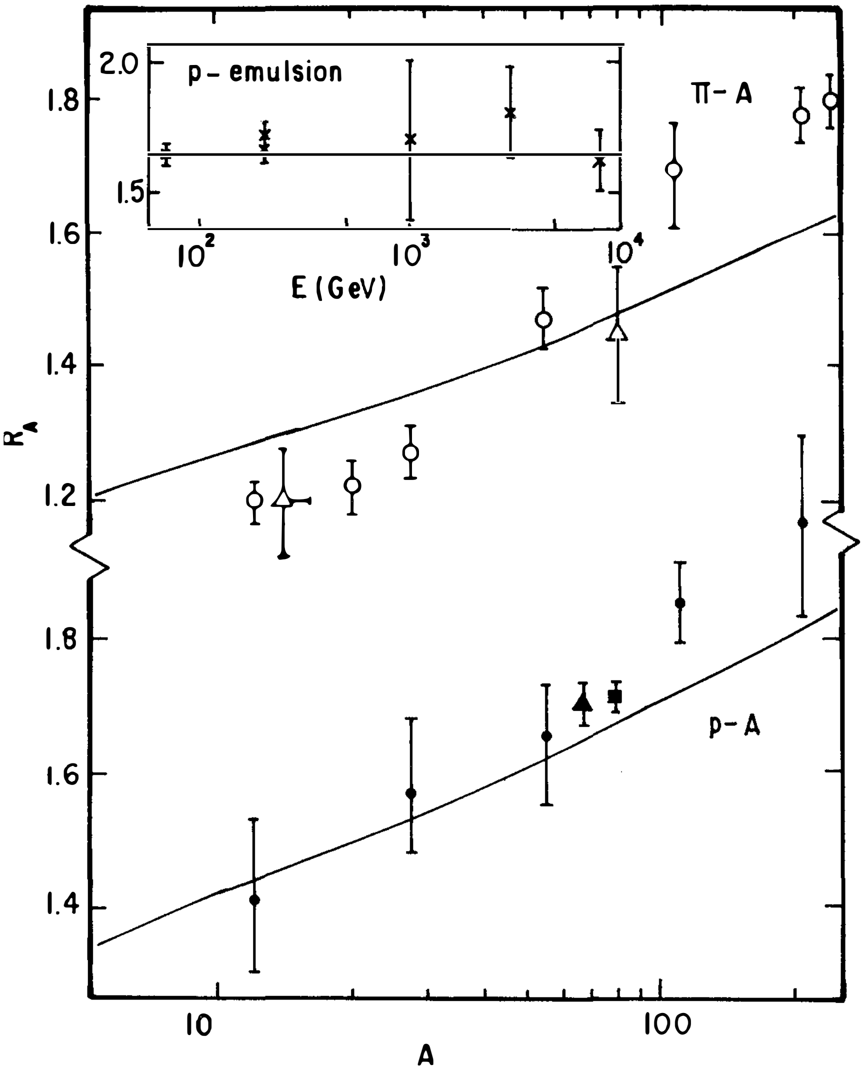

Fig. 1: R_A versus A for π-nucleus (circles: Ref. (1i), triangle: Ref. (1g)) and p-nucleus (circles: Ref. (1ℓ), triangles as compiled in Ref. (2e), square: Ref. (1k)). Insert: R_A for p-emulsion (A=67) versus $E=E_{lab}$, as compiled in Ref. (3e). The solid lines are the prediction of our model.

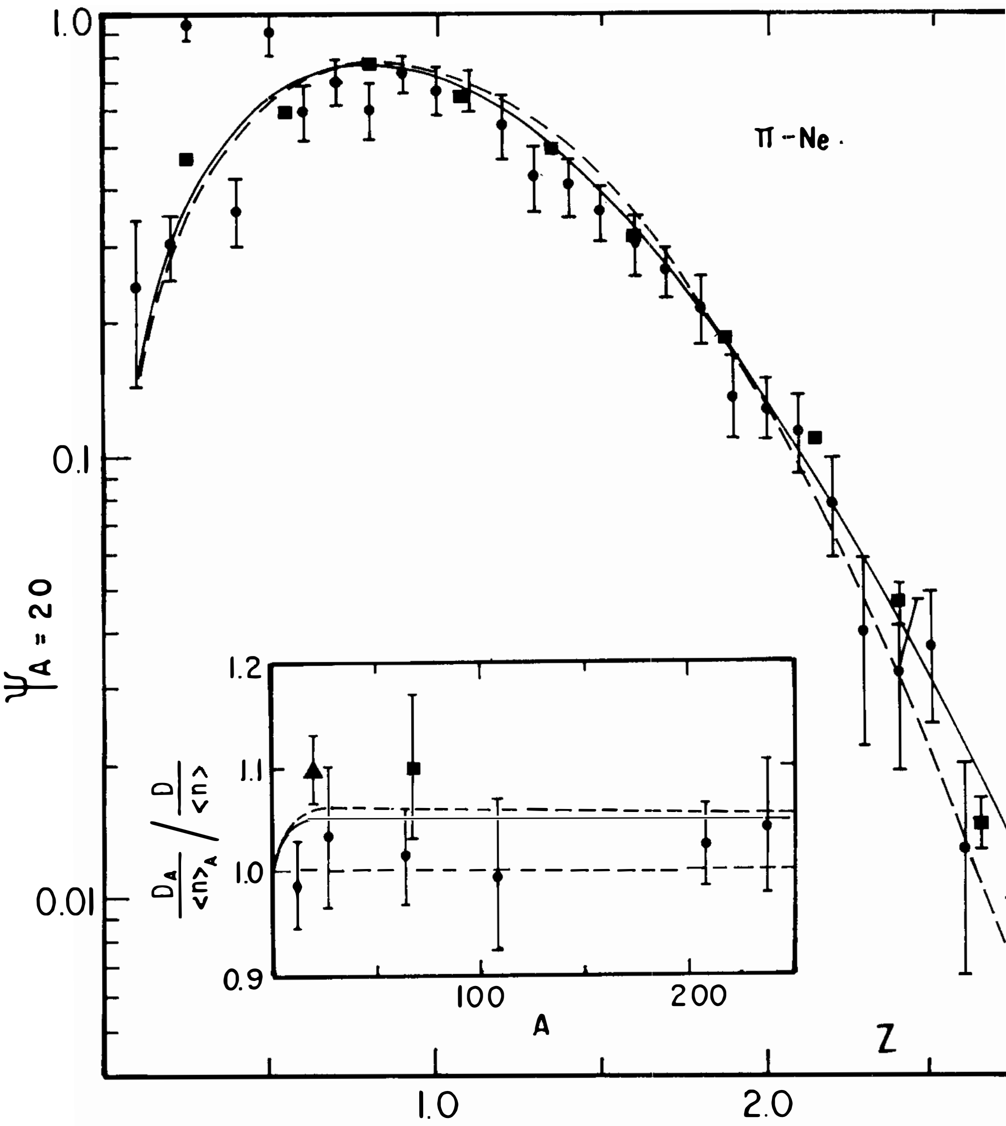

Fig. 2: ψ_A versus $z=n/\langle n\rangle_A$ for π-Ne. Data from Ref. (1g) (circles: 200 GeV, squares: 10.5 GeV). The solid line is the prediction of our model; the dashed line is the best fit for particle-particle collisions[2] Insert: $(D_A/\langle n\rangle_A)/(D/\langle n\rangle)$ versus A for π-and p-nucleus. Circles: Ref. (1i), triangle: Ref. (1g) square: Ref. (1b). The solid line is the prediction of our model, and the dashed lines are the predicted bounds.

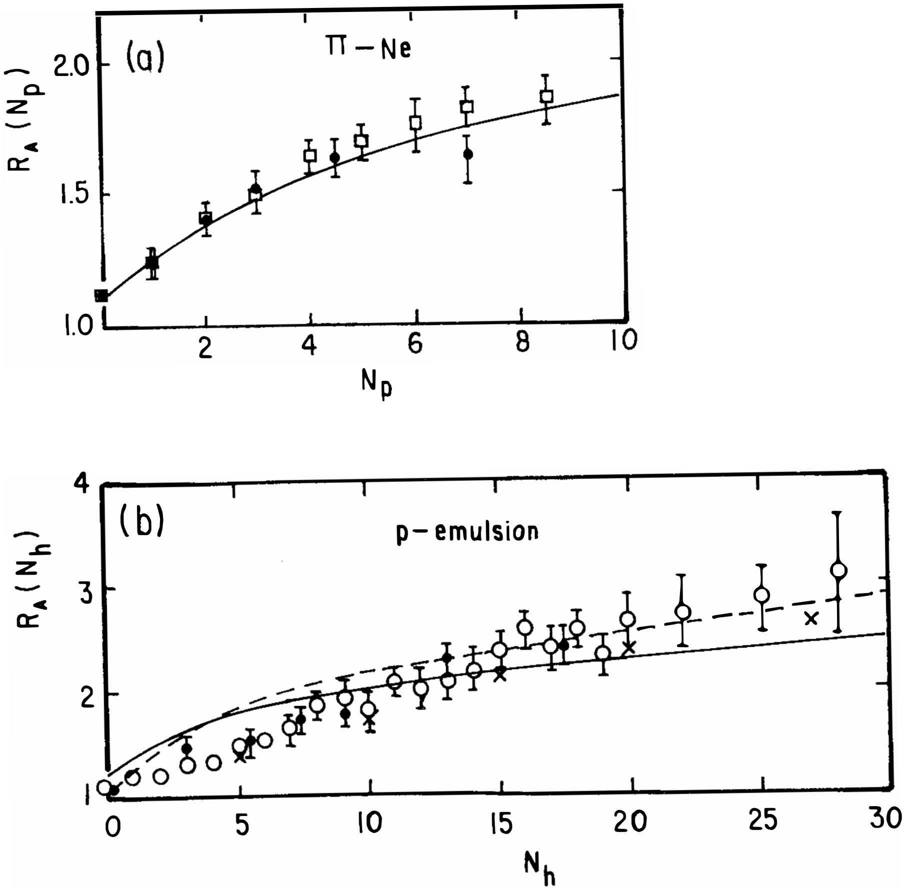

Fig. 3: (a) R_A versus the number of final protons for π-Ne. Data from Ref. (1g) (circles: 200 GeV squares: 10.5 GeV). (b) R_A versus the number of heavy trackes for p-emulsion. Solid Circles (300 GeV) and open circles (200 GeV): Ref. (1e), crosses (1000 GeV); Ref. (1). The solid lines are the predictions of Eq. (14), and the dashed line is the prediction of Eq. (15) ($N_p = 1.2N_h$).

References and Footnotes

1. a) J. Babecki et al. Phys. Lett. 47B 268 (1973).

   b) J. Hebert et al. Phys. Lett. 48B 467 (1974).

   c) A. Gurtu et al. Phys. Lett. 50B 391 (1974).

   d) R.E. Gibbs et al. Phys. Rev. D10 783 (1974).

   e) P.L. Jain et al. Phys. Rev. Lett. 33 660 (1974).

   f) J.W. Martin et al. Nuovo. Cim. 25A 447 (1975).

   g) J.R. Elliot et al. Phys. Rev. Lett. 34 607 (1975).

   h) V. Grishin et al. Yad. Fiz. 19 1364 (1974) Sov. J. Nucl. Phys. 19, 697 (1974).

   i) W. Busza et al. Phys. Rev. Lett. 34 836 (1975).

   j) M.I. Atanelishvili et al. ZhETF Pis. Red. 18 490 (1973) (JETP Lett. 18 288 (1973)).

   k) M.G. Antonova et al. Yad. Fiz. 19 1046 (1974) (Sov. J. Nucl. Phys. 19 536 (1974)).

   ℓ) P.R. Vishwanath, Bull Amer. Phys. Soc. 19 445 (1974) (see Ref. (1i)).

2. Z. Koba, H.B. Nielsen and P. Olesen, Nucl. Phys. B40 317 (1972); P. Slattery, Phys. Rev. Lett. 29 1624 (1972); Phys. Rev. D7 2073 (1973).

3. a) A. Dar and J. Vary, Phys. Rev.D6 2412 (1972).

   b) P.M. Fishbane and J.S. Trefil, Phys. Rev. D9 168 (1974).

   c) E.M. Friedlander, Nuovo Cimento Lett. 9 349 (1974).

   d) A. Bialas and W. Czyz, Phys. Lett. 51B 179 (1974).

   e) K. Gottfried, Phys. Rev. Lett. 32 957 (1974).

   f) B. Anderson and I. Otterlund, Preprint LUIP-CR-74-11 (1974).

4. F.T. Dao, Review Talk at the 1974 Meeting of the DPF of the APS, September 1974 (Fermilab-Conf.-74 98-EXP).

5. L.D. Landau, Izv. Akad. Nauk SSSR 17 51 (1953).

S.Z. Belenkij and L.D. Landau, Nuovo Cimento Suppl. 3 15 (1956).

P. Carruthers and Minh Duong-Van, Phys. Lett. 44B 507 (1973).

6. ψ_A is properly normalized as is clear from $\sum_{i=1}^{A} P(i,A)=1$ and from Eq. (10).

7. For emulsion we take $N_p \simeq 1.2 N_h$[14].

8. If $N_p=0$ then $N_n \neq 0$; in Eq. (14) the sum begins with i=1, and the denominator changes to

$$\int d^2b \left[\left(1-\frac{\sigma T}{A}\right)^{Z} - \left(1-\frac{\sigma T}{A}\right)^{A} \right]$$

9. If a nucleon is represented by a Gaussian with a radius r_o then the geometrical inelastic cross section for pp collisions is $\sigma_{in} = 2\pi r_o^2$.

10. A.N. Diddens, Proceeding of the XVI International Conference on High Energy Physics, London July 1974, Ed. by J.R. Smith (p.I-41).

11. Correlations among nucleons tend to increase R_A above our predictions for large A.

12. This fact is not surprising since the zero and first moments of ψ and ψ_A are equal (normalization) and the second moment is almost the same (see insert in Fig. (2)).

13. We have found that a Gaussian nuclear distribution does not change ψ_A and $D_A/\langle n\rangle_A$.

14. I. Otterlund, Invited talk given at the "Topical Meeting on High Energy Physics", Trieste, September 9, 1974. (LUIP - CR-74-12).

INDEPENDENT CLUSTER PRODUCTION AND THE KNO SCALING FUNCTION

E.H. de Groot
CERN, Geneva, Switzerland

Abstract: A single component independent cluster model, based on a certain smoothness property of the amplitudes involved, is presented. The KNO multiplicity distribution function, the momentum distribution of the leading particles and clusters, as well as the relations among them are deduced.

Résumé: Nous présentons un modèle de "clusters" indépendants à une composante, basé sur une certaine hypothèse de régularité des amplitudes de production. La fonction KNO pour la distribution en multiplicité, ainsi que le spectre d'impulsion de la particule entraînante, celui des "clusters", et les relations entre eux, sont déduits de ce modèle.

INTRODUCTION

In this contribution we try to give a comprehensive account of the unitary cluster model described elsewhere[1)], but without dealing explicitly with the problem of unitarity for which, together with some of the details and proofs, we refer to Ref. 1. The KNO multiplicity distribution which we find is specific for this model and is compared with the data in another paper[2)]. The leading-particle spectrum, as it appears in the following, expressed in terms of the KNO function, is of a more general nature and is extensively discussed and compared with the data in Benecke et al.[3)].

* * *

Consider the reaction $pp \to pp + X$, where X stands for any number of clusters. In case the number of clusters is equal to n we can always write the matrix element for this process as:

$$M_{2\to 2+n} = \left[(p_1+p_2)^2(p_1'+p_2')^2\right]^{\frac{1}{2}} T(p_1'p_2'|p_1p_2)\, f_n(p_1p_2p_1'p_2'k_1\ldots k_n) \ , \qquad (1)$$

with $f_0(p_1p_2p_1'p_2') \equiv 1$, and where $p_1p_2(p_1'p_2')$ are the initial (final) four momenta of the protons and $k_1\ldots k_2$ those of the clusters. Our conventions are such that ($đq \equiv d^3q/q_0$):

$$\sigma_{tot} = (2\pi)^3 \ \mathrm{Im}\ T(p_1p_2|p_1p_2) \ , \qquad (2)$$

$$\frac{d\sigma_{el}}{đp_1'đp_2'} = \frac{1}{4}(2\pi)^3|T(p_1'p_2'|p_1p_2)|^2 \underbrace{\pi(p_1'+p_2')^2\delta^4(p_1+p_2-p_1'-p_2')}_{R_{el}(p_1p_2p_1'p_2')} \ , \qquad (3)$$

$$\frac{d\sigma_{inel}}{đp_1'đp_2'} = \frac{1}{4}(2\pi)^3|T(p_1'p_2'|p_1p_2)|^2\ R_{inel}(p_1p_2p_1'p_2') \ , \qquad (4)$$

where

$$R_{inel} = \pi(p_1'+p_2')^2 \sum_{n=1}^{\infty} \int \prod_{i=1}^{n} đk_i\,|f_n(p_1p_2p_1'p_2'k_1\ldots k_n)|^2\delta^4\left(p_1+p_2-p_1'-p_2'-\sum_{\ell=1}^{n}k_\ell\right) \qquad (5)$$

Up till now our way of splitting off the leading-particle amplitude T from the cluster amplitudes f_n in Eq. (1) has been purely a matter of notation; but now we would like to give this a meaning. Let us suppose that the amplitude T appearing in Eq. (1), which is just the elastic amplitude if $p_1+p_2 = p_1'+p_2'$ due to the condition $f_0 = 1$, is changing smoothly in going from the inelastic case $(p_1+p_2 \neq p_1'+p_2')$ to the elastic case $(p_1+p_2 = p_1'+p_2')$, as one can regard T as an off-shell elastic amplitude. To be precise:

Written in the c.m.s. variables, $x_1 = 2p_{10}'/\sqrt{s}$, $x_2 = 2p_{20}'/\sqrt{s}$, $\vec{p}_{1T}$, $\vec{p}_{2T}$ and s, T is such that we can interchange the asymptotic limit $s \to \infty$ and the limit $x_1, x_2 \to 1$. (6)

As Eq. (1) is written in the form of a product of T and f_n, the condition (6) is still not very meaningful unless we introduce some smoothness condition in n on the f_n, but this we will deal with later.

Having assumed property (6) for the leading particle amplitude T we will now try to see what the function R_{inel} in Eq. (5) should look like. As we know that T will damp the transverse momenta of the leading particles severely and that the ratio $\sigma_{el}/\sigma_{inel}$ is asymptotically only weakly dependent on s, we can conclude, by comparing Eqs (3) and (4), that also the ratio $\int R_{el}(dx_1/x_1)(dx_2/x_2)/\int R_{inel}(dx_1/x_1)(dx_2/x_2)$ must be only weakly dependent on s (at most like some power of ln s asymptotically); as we can calculate $\int R_{el}(dx_1/x_1)(dx_2/x_2)$ from Eq. (3) and find it to be s independent we conclude that

$$\int R_{inel} \frac{dx_1}{x_1} \frac{dx_2}{x_2} \text{ is only weakly s dependent .} \tag{7}$$

The question now arises of how to construct a model for the f_n which actually does this. As an example we will take the Independent Emission Model (IEM), where we will keep the weights more or less arbitrary in order to fulfil condition (7):

$$|f_n(p_1 p_2 p_1' p_2' k_1 \ldots k_n)|^2 = a_n \lambda^n(s) \prod_{i=1}^{n} \frac{\exp\left(-k_{iT}^2/\langle k_T^2 \rangle\right)}{\pi \langle k_T^2 \rangle} \tag{8}$$

with $a_0 = 1$ as $f_0 \equiv 1$.

With regard to Eq. (8) we now come back to the point raised under Eq. (6): we could not have taken the same expression as in Eq. (8) for the $|f_n|^2$, but the r.h.s. multiplied by an arbitrary function of s, as this would have violated the condition $f_0 = 1$, or if we had done it only for $n \geq 1$ and not for $n = 0$ we would have introduced a highly non-smooth behaviour in going from the inelastic case ($n \geq 1$) to the elastic one ($n = 0$), contrary to the smoothness requirement indicated under Eq. (6).

Assuming expression (8) for the $|f_n|^2$ one can now calculate R_{inel} in Eq. (5) to be[1]:

$$R_{inel} \cong \frac{2}{\langle k_T^2 \rangle} \frac{(p_1'+p_2')^2}{Q^2} \int_0^\infty \frac{d\rho \; \rho}{[\Gamma(\rho+1)]^2} \left(\frac{Q^2}{s}\right)^\rho \phi(\rho,s) \,, \tag{9}$$

where $Q^2 = (p_1+p_2-p_1'-p_2')^2$ is the (missing mass)^2 to the protons, and $\phi(\rho,s)$ is defined by

$$a_n \lambda^n(s) = \frac{1}{\Gamma(n)} \int_0^\infty d\rho \; \rho^{n-1} \left(\frac{s}{\bar{\mu}^2}\right)^{-\rho} \phi(\rho,s) \,, \tag{10}$$

where $\bar{\mu}$ is the average transverse mass of a cluster.

The condition (7), i.e. that $\int R_{inel}(dx_1/x_1)(dx_2/x_2)$ is only weakly dependent on s, tells us now that $\phi(\rho,s)$ in Eqs (9) and (10) can itself only weakly depend on s. This, together with the fact that ϕ must be such as to produce a form like $a_n\lambda^n(s)$ in Eq. (10), leads then to powerful restrictions on $\lambda(s)$ and the a_n [1]:

$$\left.\begin{array}{l} \text{a)}\ \lambda(s) \underset{s\to\infty}{\simeq} [\ln(s/s_0)]^{-1} \\ \text{b) The } a_n \text{ are such that the series } \sum_{n=0}^{\infty} a_n x^n \text{ has a radius of convergence } R = 1. \end{array}\right\} \tag{11}$$

This result is quite similar to the one Białas and Kotański obtained, although in a completely different way, in their unitarization scheme for the IEM[4].

As a consequence of Eq. (11) $\phi(\rho,s)$ is of the form

$$\phi(\rho,s) \underset{\substack{s\to\infty \\ \rho>0}}{\simeq} \left(\frac{s_0}{\bar{\mu}^2}\right)^{\rho} \bar{\phi}(\rho \ln s) \quad , \tag{12}$$

where $\bar{\phi}$ varies at most as a power of its argument. So for practical purposes we can take it that ϕ is asymptotically of the form

$$\phi(\rho,s) \underset{\substack{s\to\infty \\ \rho>0}}{\simeq} C\left(\frac{s_0}{\bar{\mu}^2}\right)^{\rho} (\rho \ln s)^{r} \quad \text{for some } r \; . \tag{13}$$

Inserting this into Eq. (9) one obtains

$$R_{inel} \simeq \frac{2}{\langle k_T^2\rangle} C(\ln s)^r \frac{(p_1'+p_2')^2}{Q^2} \int_0^\infty \frac{d\rho\, \rho^{r+1}}{[\Gamma(\rho+1)]^2} \left(\frac{Q^2}{s}\right)^{\rho} \left(\frac{s_0}{\bar{\mu}^2}\right)^{\rho} \; . \tag{14}$$

Inserting this into Eq. (4) to obtain the leading-particle distribution one arrives at:

$$\frac{d\sigma_{inel}}{d p_1' d p_2'} = \frac{1}{2} (2\pi)^3 \frac{C}{\langle k_T^2\rangle} (\ln s)^r \left|T(p_1'p_2'|p_1p_2)\right|^2 \frac{(p_1'+p_2')^2}{Q^2} \int_0^\infty \frac{d\rho\, \rho^{r+1}}{[\Gamma(\rho+1)]^2} \left(\frac{Q^2}{s}\right)^{\rho} \left(\frac{s_0}{\bar{\mu}^2}\right)^{\rho} \; . \tag{15}$$

To get an idea of how this expression behaves, we will now assume that $T(p_1'p_2'|p_1p_2)$ only depends on the transverse variables or, in other words, that the longitudinal spectrum of the leading particles is solely determined by the clusters and the momentum which is carried away by these clusters.

As $(p_1'+p_2')^2 \simeq x_1x_2s$, if the final protons are in opposite hemispheres, and negligible otherwise and as $Q^2 \simeq s(1-x_1)(1-x_2)$, we can then perform the transverse integrations in Eq. (15) resulting in

$$\frac{d\sigma_{inel}}{dx_1dx_2} = D(\ln s)^r \int_0^\infty \frac{d\rho\, \rho^{r+1}}{[\Gamma(\rho+1)]^2} \left(\frac{s_0}{\bar{\mu}^2}\right)^{\rho} (1-x_1)^{\rho-1} (1-x_2)^{\rho-1} \tag{16}$$

with the condition that the protons are in opposite hemispheres (otherwise $d\sigma_{inel}/dx_1 dx_2 \simeq 0$). The constant D might, in principle, have a weak s dependence, stemming from the additional s dependence of T, but will be a constant at high energy if $\sigma_{el}/\sigma_{inel}$ is constant, at least in the Lippmann-Schwinger approach of Ref. 1, where T is essentially of the form

$$T \simeq (\ln s)^r \, e^{-(\ln s)^r p_{1T}'^2} \, e^{-(\ln s)^r p_{2T}'^2}$$

for small p_T' with $r \leq 2$ due to the Froissart theorem.

To obtain the one-proton distribution, we now integrate Eq. (16) over one of the protons:

$$\frac{d\sigma_{inel}}{dx} = D(\ln s)^r \int_0^\infty \frac{d\rho \; \rho^r}{[\Gamma(\rho+1)]^2} \left(\frac{s_0}{\bar{\mu}^2}\right)^\rho (1-x)^{\rho-1} , \tag{17}$$

which for $x \approx 1$ develops a peak of the form

$$\frac{d\sigma_{inel}}{dx} \underset{x\uparrow 1}{\simeq} D(\ln s)^r (1-x)^{-1} |\ln (1-x)|^{-(r+1)} \tag{18}$$

and is otherwise flat in x, which is at least in qualitative agreement with experiment. Integrating (17) once more we obtain the inelastic cross-section:

$$\sigma_{inel} = D(\ln s)^r \int_0^\infty \frac{d\rho \; \rho^{r-1}}{[\Gamma(\rho+1)]^2} \left(\frac{s_0}{\bar{\mu}^2}\right)^\rho . \tag{19}$$

To deduce the multiplicity distribution from this we remark, as is very easy to prove from Eq. (10), that in the KNO limit[5] ($n \to \infty$, $\ln s \to \infty$, $n/\ln s$ fixed) the parameter ρ, which we have been using up to now, is nothing but $\rho \simeq n/\ln s$. This then gives us in the KNO limit:

$$\sigma_n \simeq D \frac{n^{r-1}}{\left[\Gamma\left((n/\ln s)+1\right)\right]^2} \left(\frac{s_0}{\mu^2}\right)^{n/\ln s} \tag{20}$$

As one can calculate the average multiplicity from Eq. (20) to be

$$\langle n \rangle \simeq \rho_0 \ln s , \tag{21}$$

one obtains for the KNO function $\left[\psi(n/\langle n\rangle) \simeq \langle n\rangle \sigma_n/\sigma_{inel}\right]$

$$\psi(z) = A \frac{z^{r-1}}{\left[\Gamma(\rho_0 z+1)\right]^2} e^{-\alpha z}, \quad (\alpha = \rho_0 \ln \bar{\mu}^2/s_0) \tag{22}$$

which with four constants and the two normalizations

$$\int_0^\infty \psi(z)\, dz = \int_0^\infty z\psi(z)\, dz = 2$$

leaves us with only two constants, for example ρ_0 and r. With $\rho_0 = 1$ and $r = 2$ formula (22) produces an excellent fit[2] to the data. Such a fit would then imply that all cross-sections would go like $(\ln s)^2$ (as $r = 2$), while the average cluster multiplicity would be ln s. For completeness we now give the distribution (17) as an integral over the KNO function ψ of Eq. (22), an expression which is in fact more general than in this model (see Ref. 3, also for the experimental comparison):

$$\frac{1}{\sigma_{inel}} \frac{d\sigma_{inel}}{dx} = \frac{1}{\rho_0} \int_0^\infty d\rho\ \rho\ \psi\left(\frac{\rho}{\rho_0}\right) (1-x)^{\rho-1} \tag{23}$$

and if one calculates the one-cluster distribution one obtains a similar result:

$$\frac{1}{\sigma_{inel}} \frac{d\sigma_{inel}}{dx} = \frac{1}{x\rho_0} \int_0^\infty d\rho\ \rho\ \psi\left(\frac{\rho}{\rho_0}\right) (1-x)^{\rho}\ , \tag{24}$$

and, in general,

$$\left(\frac{1}{\sigma_{inel}} \frac{d\sigma_{inel}}{dx}\right)_{\text{leading particle}} = \frac{x}{1-x} \left(\frac{1}{\sigma_{inel}} \frac{d\sigma_{inel}}{dx}\right)_{\text{clusters}} \tag{25}$$

REFERENCES

1) E.H. de Groot and Theo W. Ruijgrok, A unitary model for independent cluster production, CERN preprint TH.2018 (in preparation).

2) E.H. de Groot, The multiplicity distribution in a unitary uncorrelated cluster model, Phys. Letters (in press).

3) J. Benecke, A. Białas and E.H. de Groot, Max Planck Institute, preprint MPI-PAE/PTh 10/75.

4) A. Białas and A. Kotański, Acta Phys. Polon. B4, 659 (1973).

5) Z. Koba, H.B. Nielsen and P. Olesen, Nuclear Phys. B40, 317 (1972)

FINAL STATE CHARACTERISTICS OF CENTRAL pp COLLISIONS AT 28.5 GeV/c.

P. SCHÜBELIN

Brookhaven National Laboratory
Upton, New York 11973 (USA)

A B S T R A C T

Results are presented from an experiment of inelastic central pp collisions at 28.5 GeV/c observed by the Multiparticle Argo Spectrometer System (MASS). Characteristics of final states are given as a function of transverse momentum to a forward proton or π^+ meson over a considerable range of the allowed phase space (.3 GeV/c < $P_\perp$ < 2 GeV/c, 1.3 GeV < MM < 6.5 GeV).

Resumé

Des résultats d'une expérience de diffusion inélastique pp à 28.5 GeV/c obtenus avec le "Multiparticle Argo Spectrometer System" (MASS) sont donnés. Les characteristiques des états finaux sont presentés comme fonction du moment de transfer d'un proton ou pion vers l'avant couvrant un interval considérable de l'espace de phase permis (0.3 GeV/c < $P_\perp$ < 2 GeV/c, 1.3 GeV < MM < 6.5 GeV).

INTRODUCTION

The possible existence of hadron constituents has been one of the most fascinating ideas in recent years[1,2]. It has been triggered by a surprisingly large cross section found in deep inelastic ep scattering[3]. The interest in such ideas has been heightened by the much larger probability of producing large transverse momentum particles in hadron-hadron collisions[4] than might have been expected from a simple extrapolation of low transverse momentum data. We believe the key to verification and further advancement of such ideas lies in the study of detailed properties of multiparticle final states where at least one outgoing particle carries a substantial fraction of the incident momentum transverse to the beam direction (we call these collisions central). In hadron-hadron collisions, such interactions represent a small fraction of the total cross-section, e.g. $< 10^{-3}$ at 30 GeV/c. For this reason alone high statistics experiments in this regime can not be performed in a bubble chamber. A fast detector measuring and identifying all particles in the final state seems to be exceedingly costly and difficult to conceive and build, but an electronic detector measuring all charged particles at a ten thousand times higher interaction rate and a hundred times higher recording rate than the bubble chamber will already provide access to a hitherto virgin field of particle physics and enhance our knowledge and understanding of central collisions.

The first successful effort to overcome existing limitations in experimental techniques for studying charged particle final states in bubble chamber like detail is the Multiparticle Argo Spectrometer System, MASS[5]. It can be described as an "all-electronic bubble chamber" triggered by one or two mass-identified charged particles emitted into specifiable regions of phase space. The question arises to the energy at which such a comprehensive study of central collisions should be started. Even though the highest energy presently available seems most promising and attractive, we have chosen to carry out the first such study at 30 GeV/c in order to obtain a higher success probability and to create a data sample that can be used as reference and pivot for later high energy studies. A third reason lies in the possibility of gathering specific ideas and notions based on observations in the 30 GeV/c energy range which can later be pursued at higher energies with less specific, more dedicated means. A last reason stems from the fact that at the time of conception and construction of MASS, 30 GeV/c was the top energy and anything higher would have meant delay. How our study fits into the present overall picture of large transverse momentum and large $X_{\perp} = \frac{2P_{\perp}}{\sqrt{s}}$ investigations can be seen from Fig. 1. In contrast to most - in some cases all - the other experiments, the data taken by MASS can investigate - among other items - the following questions and areas:

1. Relations between the characteristics of a trigger proton or pion and the average charged multiplicity.
2. Relations between available energy and average number of charged particles.
3. Charged multiplicity probability distributions for different missing mass and four-momentum transfer to a trigger proton (multiplicity scaling).
4. Study of $pp\pi^+\pi^-$, $pp\pi^+\pi^+\pi^-\pi^-$, $pn\pi^+$ and $pp\pi^o$ final states over considerable range of $P_{\perp}$ to a forward proton.
5. Study of inclusive π^- spectra over considerable range of $P_{\perp}$ to a forward proton.
6. Comparison between ep and pp deep inelastic scattering.

EXPERIMENTAL RESULTS

We have measured the reactions

$$p_1 + p_2 \rightarrow p_3 + MM \quad (1)$$

and

$$p_1 + p_2 \rightarrow \pi^+ + MM \quad (2)$$

at 28.5 GeV/c. People involved in the experiment are listed in Table I. A Peyrou-plot for the trigger particle illustrates where the data lie in phase space (Fig. 2).

The data have been taken at the Brookhaven AGS by the Multiparticle Argo Spectrometer System (MASS) which consists of the High Momentum Spectrometer (HMS), the Low Momentum Spectrometer (LMS), the Vertex Spectrometer (VS)[6], the PDP9 local computer, the fast two-way data link to a CDC 6600 computer and the off-line analysis chain. A schematic of the floor equipment is shown in Fig. 3, a birds eye view of the same in Fig. 4. The characteristics of the system are given in Table II. The HMS and/or the LMS have been used to trigger the system, the VS[6] and the pattern recognition code PITRACK[7] to count and momentum analyze the charged particles contained in MM. On the average, 83% of all charged particles in the final state are detected. At this efficiency level corrections for the undetected particles when evaluating the charged multiplicity can be made rather easily by using charge conservation. The spark chambers of the VS are shown in Fig. 5, a typical 10 prong event as reconstructed by PITRACK in Fig. 6. Fig. 7 shows a display of the event with the largest transverse momentum to p_3 taken by MASS.

A. Multiplicity Studies

In Fig. 8 we show the average charged multiplicity $\bar{n}_{CH}$ (includes trigger particle) as a function of transverse momentum of p_3 and π^+ for constant MM[8,9]. The following characteristics appear: In reaction (1) and apparently (2) as well, $\bar{n}_{CH}$ rises by $\sim .6$ charged particles for MM > 2 GeV, the location of the rise moves towards smaller $P_\perp$ values for intervals of higher average MM, being located at $P_\perp \sim .85$ GeV/c for $\overline{MM} = 5.5$ GeV. When plotting $\bar{n}_{CH}$ vs $|t_{13}|$, the four momentum transfer to p_3 for data of reaction (1), we observe the rise for all MM bins in approximately the same place, namely at $|t_{13}| \sim 2\ (\text{GeV}/c)^2$. In order to compare reactions (1) and (2) we display

$\Delta = \bar{n}_{CH}(p_3) - \bar{n}_{CH}(\pi^+)$ vs $P_\perp$ (Fig. 9). We note that the difference Δ amounts to 1.1 particles. This can be qualitatively understood from the fact that MM contains one baryon in reaction (1) and two baryons in reaction (2).

We can study the dependence of $\bar{n}_{CH}$ on the available energy (MM) for reactions (1) and (2) both below and above the rise in multiplicity (Fig. 10). All 4 data sets are compatible with a linear dependency with slope $= .65 \pm .01$ GeV^{-1}.

For some time now, people have plotted $\bar{n}_{CH} \cdot P_{n_{CH}}$ versus $n_{CH}/\bar{n}_{CH}$[10] for different values of s integrating over t and MM, marvelling that all of the data from 50 GeV/c to 300 GeV/c fall on a universal curve[11] (KNO scaling). If instead of n_{CH} one uses $(n_{CH} - \alpha)$[12], scaling is observed down to energies of 5.5 GeV/c and $\alpha = + 0.9$. We can pursue this exploratory line of plotting data and do it at fixed s for various bins in MM and $|t|$[13]. For given intervals, data with different missing mass ranging from MM = 1.67 GeV to MM = 5.25 GeV and MM = 2.61 GeV to MM = 6.07 GeV, fall on top of each other (Fig. 11). The constant α turns out to be -0.7 which throws a heavy shadow onto the interpretation of α being the average number of unfragmented leading particles[14]. Data in different t intervals have different widths of the multiplicity scaling curve: From low $|t|$ ($|t| < 2$ (GeV/c)^2) to high $|t|$ ($|t| > 3$ (GeV/c)^2) the scaling curve shrinks by 10% (Fig. 12). We also observe that $P_{n_{CH}}$ vs MM shows the same functional form for low and high $|t|$ but is displaced by .75 GeV in MM (Fig. 13). The 2 prongs are an exception.

B. Exclusive Studies

Using standard kinematic mass hypothesis fitting techniques, we were able to isolate a data sample of the reaction

$$p_1 + p_2 \rightarrow p_3 + p_4 + \pi^+ + \pi^- \qquad (3)$$

It has the following features at $P_{3\perp} \sim 1$ GeV/c:[15] In events where the π^+ and p_4 form a Δ^{++} (1238), one sees a low effective mass enhancement of the

$p_4\pi^+\pi^-$ system, probably the $N^*(1688)$ (Fig. 14). Even though the $N^*(1688)$ is produced peripherally, its decay product, the Δ^{++}, is observed at considerable four-momentum transfer (Fig. 15). At higher effective mass of $p_4\pi^+\pi^-$ ($M > 1.9$ GeV) the π^- balances most ($\sim$ 80%) of the transverse momentum of the trigger proton p_3 while the four momentum transfer to the Δ^{++} is small (Fig. 15). In events where the π^+ or the π^+ and π^- do not resonate with p_4, one observes the pions emerging from the central region and all 3 particles (p_4, π^+, π^-) balance $P_{3\perp}$ $\sim$ equally. We conclude that in one quarter of the events of reaction (3) a π^- balances a dominant fraction of $P_{3\perp}$ while in the other events, balancing is done more democratically. In reaction

$$p_1 + p_2 \rightarrow p_3 + p_4 + \pi^+ + \pi^+ + \pi^- + \pi^- \tag{4}$$

we do not observe any significant fraction of events where a single pion balances a large portion of $P_{3\perp}$. We have also isolated data samples of the reactions

$$p_1 + p_2 \rightarrow p_3 + p_4 + \pi^0 \tag{5}$$

and

$$p_1 + p_2 \rightarrow p_3 + n_4 + \pi^+ \tag{6}$$

In events of reaction (5)[16] we observe a very strong peak at $\sim$ 1.6 GeV in the effective mass system $p_3\pi^0$ (Fig. 16) which contains $\sim$ 50% of all our events. When we plot the mass region below 2 GeV in 40 MeV bins we see indication of separation into two structures, possibly the N^* (1520) and N^* (1688) (Fig. 17). These low mass events are characterized by a fairly large four momentum transfer $|t_{13}|$ to p_3 ranging from $\sim$ .8 (GeV/c)^2 to $\sim$ 1.6 (GeV/c)^2. $|t_{24}|$ to p_4, which is also the t to the excited system $p_3\pi^0$ is much lower, the depletion at small values of $|t_{24}|$ possibly due to an experimental bias (Fig. 18). The reason may be the preferentially transverse decay of the peripherally produced excited system, a behavior we have already encountered in some events of reaction (3). In events of reaction (6)[16] we observe projectile excitation as well but not in the I = 1/2 state as in reaction (5) but rather in the I = 3/2 state. Looking at the effective mass distribution of the $p_3\pi^+$ system we observe a significant bump at ~ 1.9 GeV, possibly the $\Delta(1950)$ (Fig. 19). It is produced very peripherally as can be seen from the very steep four-momentum transfer distribution t_{24} to the recoil neutron n_4 which is approximately equal to the four-momentum transfer to the $\Delta(1950)$ (Fig. 20).

C. Inclusive Studies

We have studied π^- momentum spectra as a function of $P_{3\perp}$ in events of reaction (1)[17]. It seems to be informative to look at the momentum components of negative pions in the scattering plane (the plane containing p_1 and p_3) and normal to the scattering plane:[18] In the first case, momentum balancing plays an important role, in the latter it does not. In the scattering plane normal to the beam direction (x direction) we observe the shape of the momentum spectrum of the π^-'s to remain unchanged (Fig. 21) (with the exception of 4 prongs) while the center of the distribution moves to larger values with increasing $P_{3\perp}$ (Fig. 22). This leads us to the conclusion - with the exception of the 4 prongs - that all particles tend to balance transverse momentum of the trigger particle equally; in some of the 4 prongs, one pion receives a larger transverse kick than the other particles. We came to the same conclusion for events of reaction (3).

Normal to the scattering plane (y direction) there is no momentum component of the trigger proton to be balanced. We observe the shape of the P_y distribution unchanged as $P_{3\perp}$ increases from .4 GeV/c to 1.6 GeV/c (Fig. 23), the central values being zero for all data samples. The shape of P_y is also approximately independent of MM over its entire range. This means that the momentum component of π^-'s normal to the scattering plane is constant even though the collisions among the 2 protons becomes more and more central and the inelasticity varies. Closely related to the above discussion is the correlation between $(P_\perp)^{\pi^-}$ and $(P_\parallel)^{\pi^-}$ or $(X_\parallel)^{\pi^-}$, the so-called sea gull effect[19]. We can study it as a function of $P_{3\perp}$ (Fig. 24). The behavior observed can be understood from the previously shown dependence of $P_x^{\pi^-}$ and $P_y^{\pi^-}$ on $P_{3\perp}$.

D. Comparison with Electroproduction

A comparison between lepton-proton[20,21] and proton-proton collisions is very instructive because we know in the first case (A) one vertex being elastic, a condition not necessarily true in the latter case (B).

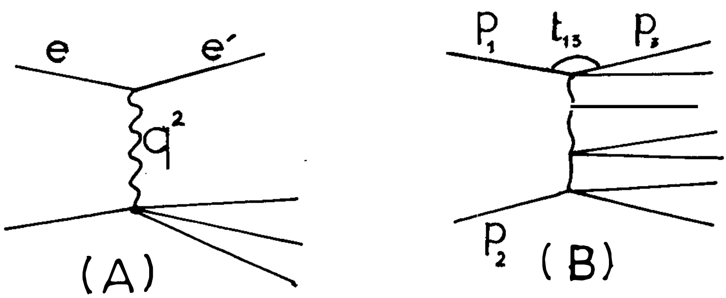

A comparison of the 2 classes of reactions with respect to their multiplicity dependence on $P_\perp$ and q^2 is shown in Fig. 25 and Fig. 26. We observe different behavior in ep and pp data when plotted versus q^2 - if you believe Cornell - while there is not sufficient overlap in the data when plotted versus transverse momentum (the electron data have been taken at 7 GeV/c and 11.5 GeV/c). When we analyze our data of reaction (1) in the same way electroproduction data are usually analyzed by transforming into the rest system of MM, we can look at φ-(azimuthal angle with respect to the direction of MM) X- and $P_\perp$-distributions[22]. We observe that in all these distributions the functional dependencies from electroproduction also describe our data for X^{π^-} between 0 and .6, the coefficients in the functions being the same or near those from electroproduction.

INTERPRETATION OF RESULTS

It may be possible to expand and generalize certain notions obtained from the study of exclusive channels to the much larger sample of general multiparticle final states, to explain the features. In our data we have seen that for small t_{13}, $0.2 < |t_{13}| \lesssim .5\ (\mathrm{GeV}/c)^2$ in reactions (4), (5) and (6) there is predominantly no projectile excitation going on because the transverse kick to p_3 coming from a peripherally produced Δ is too small while from e.g. a $N^*(1520)$ or $N^*(1688)$ it is too large to enter the acceptance. We are therefore restricted to the detection of target fragmentation processes, producing the well known large cross section excited states like the Δ etc. When we move into the second regime with $|t_{13}|$ between .5 and $\sim 2\ (\mathrm{GeV}/c)^2$, some of the trigger protons - as we have seen from the exclusive data samples - are decay products of $N^*(1520)$'s, $N^*(1688)$'s and $\Delta(1950)$'s which are themselves produced rather peripherally. Often these excited states of the projectile proton have a π^o meson among their decay products. The presence of such π^o's associated with the projectile proton causes us to "miscalculate" the missing mass in the sense that not all of it is available to produce particles. The average multiplicity for constant MM is therefore depressed with the occurrence of such π^o's. We now move into the third regime the $|t_{13}|$ region around 2 $(\mathrm{GeV}/c)^2$. The disappearance of forward protons with $|t_{13}| \sim 2\ (\mathrm{GeV}/c)^2$ being associated with N^*'s causes the p_3 vertex to turn elastic within a relatively narrow $|t_{13}|$ margin. This causes $\bar{n}_{CH}$ for constant MM to rise rapidly due to the fact that MM is more and more often fully available for particle production. Beyond this regime, $|t_{13}| > 2\ (\mathrm{GeV}/c)^2$, $\bar{n}_{CH}$ saturates and we seem to deal almost exclusively with target fragmentation and/or particles produced along the multiperipheral chain but no production at the p_3 vertex. A similar condition prevails in data of reaction (2). Whenever projectile excitation into a I = 1/2 state occurs and we trigger on the charged decay product π^+, our missing mass MM includes a neutron which will never contribute to $\bar{n}_{CH}$. The absence of such projectile excitation does not enforce any more the presence of a neutral baryon and the resulting average charged multiplicity can be expected to be higher.

From our study of inclusive π^- meson spectra we learn that in the 30 GeV/c energy range there is no clear indication of fireball production in central collisions while hard scattering models are consistent with the data.

A last finding is the close similarity of distributions of deep inelastic ep scattering where the interaction process is described in terms of hard photon-hadron scattering and pp central collisions, where it is not clear what mediates the interaction.

CONCLUSION

We have demonstrated at BNL energies that all-electronic equipment can produce bubble chamber-like information in a field of low cross section physics, i.e. central collisions. In exploring the final state characteristics of 30 GeV/c pp interactions over a large range of transverse momentum to one proton, interesting features of central collisions have been discovered and the stage has been set for a similar exploration at considerably higher energies.[23]

REFERENCES

1. J.D. Bjorken and E.A. Paschos, Phys. Rev. 185, 1975 (1969).
2. R.P. Feynman, Photo-Hadron Interactions, W.A. Benjamin, New York, (1972).
3. M.J. Breidenbach, J.I. Friedman, H.W. Kendall, E.D. Bloom, D.H. Coward, H. De Staebler, J. Dues, L.W. Mo and R.E. Taylor, Phys. Rev. Lett. 23, 935 (1969).
4. F.W. Büsser, L. Camilleri, L. Di Lello, G. Gladding, A. Placci, B.G. Pope, A.M. Smith, J.K. Yoh, E. Zavattini, B.J. Blumenfeld, L.M. Lederman, R.L. Cool, L. Litt and S.L. Segler, Phys. Letters 46B, 471 (1973); M. Banner, J.L. Hamel, J.P. Parmsart, A.V. Stirling, J. Teiger, H. Zaccone, J. Zsemberg, G. Bassompierre, M. Croissiaux, J. Gresser, R. Morand, M.L. Leidinger, M. Schneegans, Phys. Letters 44B, 537 (1973). B. Alper, H. Boggild, G. Jarlskog, G. Lynch, J.M. Weiss, P. Booth, L.J. Carroll, J.N. Jackson, M. Prentice, G. von Dardel, L. Jonsson, G. Damgaard, K.H. Hansen, E. Lohse, F. Bulos, L. Leistam, A. Klovning, E. Lillithun, B. Duff, F. Heymann and D. Quarrie, Phys. Letters 44B, 521 (1973).
5. E.W. Anderson, G.B. Collins, G.P. Fisher, E. Lazarus, K.M. Moy, A. Ramanauskas, P. Schübelin, R. Siemann, A.M. Thorndike, F. Turkot, L. von Lindern, T.S. Clifford, J.R. Ficenec, D.R. Gilbert, W.N. Schreiner, B.C. Stringfellow, W.P. Trower, A.R. Erwin, L.J. Gutay, E. Harvey, N.C. Hien, A. Laasanen, G.P. Larson, M. O'Neill, W. Selove, K. Stanfield and R.B. Willmann, Nucl. Instr. and Meth. 122, 587 (1974).
6. J.R. Ficenec, B.C. Stringfellow, G.B. Collins, A. Ramanauskas, P. Schübelin and F. Turkot, Nucl. Inst. and Meth. 113, 535 (1973).
7. D.R. Gilbert, W.N. Schreiner, W.P. Trower and P. Schübelin, Nucl. Instr. and Meth. 116, 501 (1974).
8. A. Ramanauskas, E.W. Anderson, G.P. Fisher, N.C. Hien, E. Lazarus, K.M. Moy, P. Schübelin, A.M. Thorndike, F. Turkot, L. von Lindern, T.S.

Clifford, G.B. Collins, J.R. Ficenec, D.R. Gilbert, W.N. Schreiner, B.C. Stringfellow, W.P. Trower, A.R. Erwin, G.P. Larson, L.J. Gutay, A. Laasanen, K. Stanfield, R.B. Willmann, E. Harvey and W. Selove, Phys. Rev. Letters 31, 1371 (1973).

9. E.W. Anderson, T.S. Clifford, G.P. Fisher, G.P. Larson, E. Lazarus, K.M. Moy, F. Turkot, P. Schübelin, W.N. Schreiner, L. von Lindern, L.J. Gutay, A. Laasanen, G.B. Collins, J.R. Ficenec, D.R. Gilbert, B.C. Stringfellow and W.P. Trower, Phys. Rev. Letters 34, 294 (1975).

10. Z. Koba, H.B. Nielsen and P. Olesen, Nucl. Phys. B40, 317 (1972).

11. P. Slattery, Phys. Rev. Letters 29, 1627 (1972).

12. A.K. Wroblewski, Acta Phys. Pol. B4, 857 (1973).

13. E. Lazarus, K.M. Moy, P. Schübelin, F. Turkot, T.S. Clifford, J.R. Ficenec, W.N. Schreiner, W.P. Trower, A.R. Erwin and G.P. Larson, Phys. Rev. Letters 33, 1239 (1974).

14. A. Buras, J. Dias de Deus and R. Mølller, Phys. Letters 47B, 251 (1973).

15. E.W. Anderson, J.R. Ficenec , D.R. Gilbert, L.J. Gutay, A. Laasanen, A. Ramanauskas, P. Schübelin and F. Turkot, Lettere al Nuovo Cimento 11, 491 (1974).

16. E. Lazarus, W.N. Schreiner, P. Schübelin, F. Turkot, C. Ezell and L.J. Gutay. To be published.

17. T.S. Clifford, E. Lazarus, G.P. Larson, W.N. Schreiner, P. Schübelin, F. Turkot and L. von Lindern. Submitted to Phys. Rev. Letters (Feb. 1975).

18. S.D. Ellis and R. Thun. Invited talk presented at the IXth Recontre de Moriond, March 1974. Preprint TH. 1874-CERN.

19. e.g. See the review by M. Deutschmann, Amsterdam International Conference on Elementary Particles 1971, p. 190.

20. V. Eckardt, H. G. Gebauer, P. Joos, H. Meyer, B. Naroska, D. Notz, W.J. Podolsky, G. Wolf, S. Geller, H. Dan, G. Drews, D. Grenbel, W. Meincke, N. Nagel and E. Rahe, Nucl. Phys. B55, 45 (1973).

21. P.H. Garbincius, K. Berkelman, B. Gibbard, J.S. Klinger, P. Wanderer and A.J. Sadoff, Phys. Rev. Letters 32, 328 (1974).

22. E.W. Anderson, T.S. Clifford, W.N. Schreiner, P. Schübelin, F. Turkot, L.J. Gutay, G.B. Collins, J.R. Ficenec and B.C. Stringfellow. To be published.

23. In our opinion a vertex detector to be used in the 100 - 500 GeV/c range should be very similar to the VS in MASS but contain improvements in three major areas:

    1. Lower mass of the detector to reduce unwanted interactions.
    2. Capability of withstanding beam rates of a few million particles per second.
    3. Readout of 2 coordinates (x and y) from the same wire.

    We are in the process of building a prototype cylindrical proportional chamber at BNL which will meet these improvements: 2 coordinate read-out is accomplished by means of the current ratio method with resolution $\Delta\ell/\ell \lesssim .5\%$ and chamber mass is .025 g/cm^2 in the active area.

Table I

Participants of AGS #396

Brookhaven National Laboratory	E.W. Anderson	Iowa State University
	G.B. Collins	Virginia Polytechnic Institute and State University
	G.P. Fisher	R & D Associates, California
	N.C. Hien	T.J. Watson Research Center, I.B.M.
	E. Lazarus	Singer-Kearfott Company, New Jersey
	K.M. Moy	Seton Hall University
	A. Ramanauskas	Deceased
	P. Schübelin	
	R. Siemann	Cornell University
	A.M. Thorndike	
	F. Turkot	Fermi National Accelerator Laborator
	L. von Lindern	Max Planck Institute for Psychiatry, Munich, Germany
Virginia Polytechnic Institute and State University	T.S. Clifford	Brookhaven National Laboratory Applied Math. Dept.
	J.R. Ficenec	
	D.R. Gilbert	University of Toronto
	W.N. Schreiner	Brookhaven National Laboratory
	B.C. Stringfellow	CERN
	W.P. Trower	
University of Wisconsin	A.R. Erwin	
	G.P. Larson	
Purdue University	L.J. Gutay	
	A. Laasanen	
	K. Stanfield	
	R.B. Willmann	
University of Pennsylvania	E. Harvey	University of Wisconsin
	M. O'Neill	Computer Sciences Corporation, Maryla
	W. Selove	

Table II - MASS Characteristics

Spectrometer	HMS	LMS	VS
Solid Angle (horizontal x vertical) (mr^2)	33 x 10	180 x 47	4700 x 1750
Momentum Acceptance δp at Incident Momentum of 28.5 GeV/c (GeV/c)	5 -- 28.5	.6 - 28.5	.08 - 28.5
Resolution Δθ (mr)	± .2	± 1.0	± 4 (forward) ± 11 (side)
Resolution Δp/p (%)	± 1/3 (p = 20 GeV/c)	± 1 (p = 2 GeV/c)	± 2 (forward) ± 10 (side) (p = 1 GeV/c)
Mass Identification	π,p	π,p	None
Maximum Tracking Capability	1	2	14
Chamber Readout	Core	Magnetostriction	Shielded Magnetostriction
Data Rate (events/.6s burst	120	60	12*
CDC-6600 Track Reconstruction Time (s)	.02	.03	1.5
Movement Time (hrs.)	4	.75	not movable

*Limited by the capacity of the Data Handler.

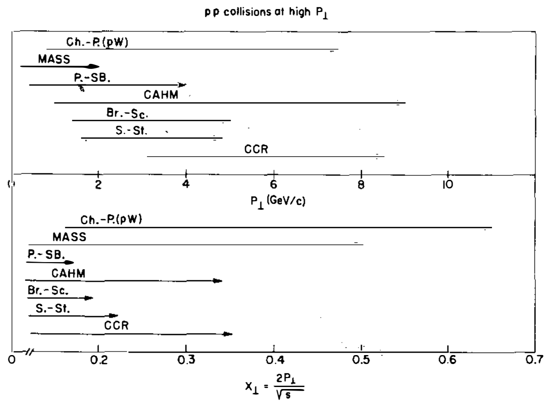

FIG. 1. THE RANGE IN $P_\perp$ AND $X_\perp = \frac{2P_\perp}{\sqrt{s}}$ OF SEVEN EXPERIMENTS EXPLORING CENTRAL COLLISIONS IS SHOWN. THE CHICAGO-PRINCETON EXPERIMENT (CH.-P.) AT FNAL MADE USE OF A TUNGSTEN TARGET. THE MULTIPARTICLE ARGO SPECTROMETER SYSTEM (MASS) STUDIED pp INTERACTIONS AT BNL. ALL THE OTHER EXPERIMENTS INVESTIGATED pp COLLISIONS AT THE CERN ISR: PISA-STONY BROOK (P.-SB.), CERN-AACHEN-HAMBURG-MUNICH (CAHM); THE BRITISH-SCANDINAVIAN COLLABORATION (BR.-SC.), SACLAY-STRASBOURG (S.-ST.) AND CERN-COLUMBIA-ROCKEFELLER (CCR).

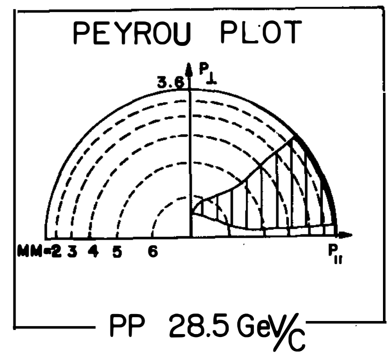

FIG. 2. PROTONS (p_3) HAVE BEEN TRIGGERED UPON WITHIN THE SHADED AREA OF THE PEYROU PLOT.

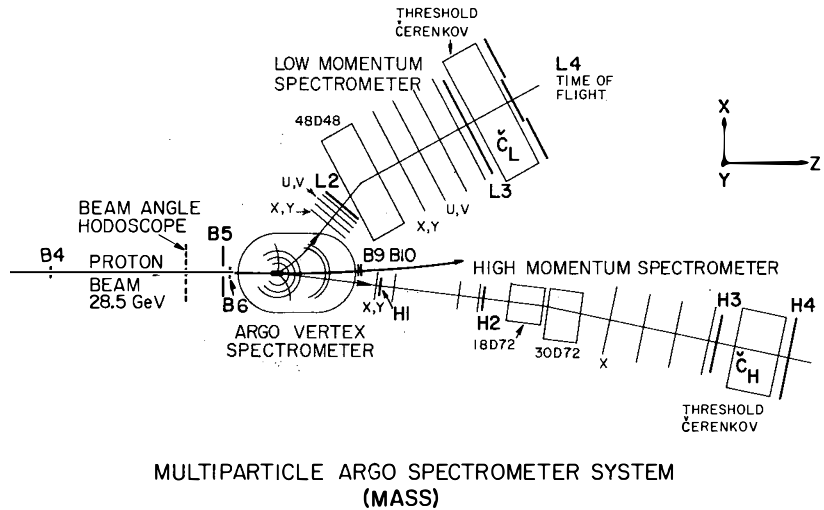

FIG. 3. SCHEMATIC OF MASS. THE DISTANCE FROM THE TARGET TO H4 IS 23m. THE DISTANCE FROM THE TARGET TO L4 IS 12.5 m.

FIG. 4. TOP VIEW, LOOKING DOWNSTREAM, OF MASS: IN THE FOREGROUND THE UPSTREAM END OF THE CABLE SUSPENSION BRIDGE, TO THE LEFT THE LMS, TO THE RIGHT THE HMS, IN THE RIGHT FOREGOUND THE ARGO MAGNET AND DOWNSTREAM OF THE LMS THE ELECTRONICS AND COMPUTER TRAILERS.

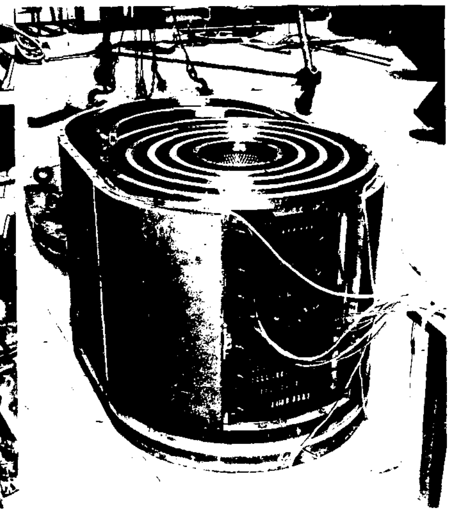

FIG. 5. TOP VIEW OF SEVEN OF THE NINE VS CHAMBERS. THE TWO CHAMBERS NOT SHOWN ARE LOCATED OUTSIDE THE FULL-ROUND AND HALF-ROUND CHAMBERS RESPECTIVELY. HV AND SIGNAL CABLE CONNECTIONS ARE MADE THROUGH THE UPSTREAM AND LEFT SIDE CUT-OUTS IN THE CHAMBER HOUSING.

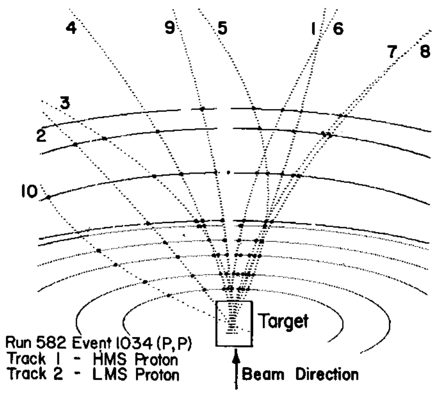

FIG. 6. TOP VIEW AFTER ROTATION AND MAGNIFICATION OF THE VS DIGITIZINGS (HEAVY BLACK DOTS) AND THE FITRACK SOLUTION FOR THIS 10 PRONG EVENT, SELECTED AMONG OTHER 10 PRONG EVENTS IN A RANDOM WAY.

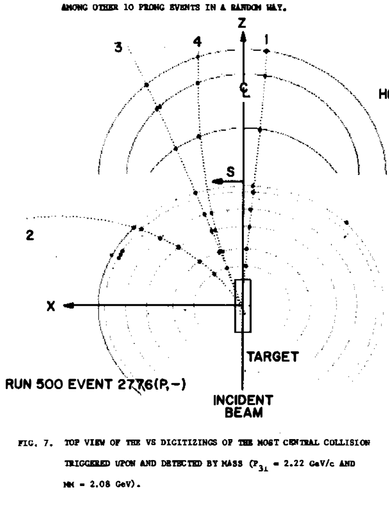

FIG. 7. TOP VIEW OF THE VS DIGITIZINGS OF THE MOST CENTRAL COLLISION TRIGGERED UPON AND DETECTED BY MASS ($P_{3\perp}$ = 2.22 GeV/c AND MM = 2.08 GeV).

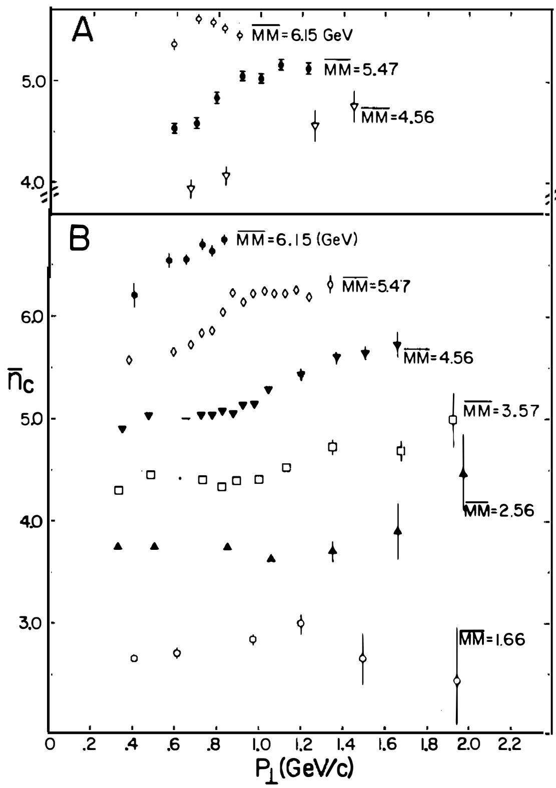

FIG. 8. A. CHARGED PARTICLE MULTIPLICITY $\bar{n}_{CH}(\pi^+)$ vs $P_\perp$ OF A FORWARD π^+ MESON IN THE REACTION $p_1 + p_2 \rightarrow \pi^+ + MM$.

B. CHARGED PARTICLE MULTIPLICITY $\bar{n}_{CH}(p)$ vs $P_\perp$ OF A FORWARD PROTON IN THE REACTION $p_1 + p_2 \rightarrow p_3 + MM$.

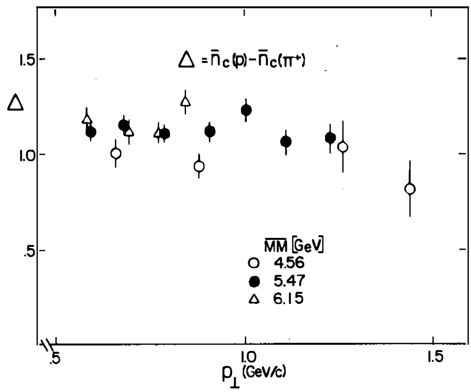

FIG. 9. DIFFERENCE $\Delta = \bar{n}_{CH}(p) - \bar{n}_{CH}(\pi^+)$ vs $P_\perp$ FOR THREE INTERVALS OF MM.

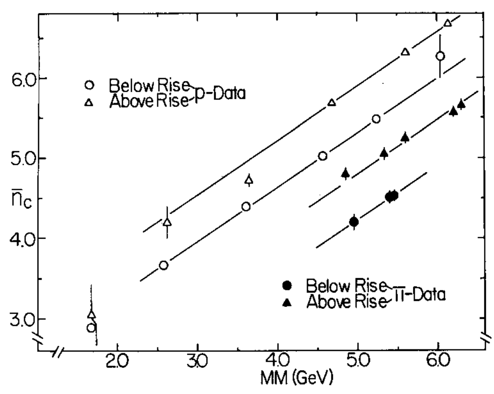

FIG. 10. MM DEPENDENCE OF $\bar{n}_{CH}(p)$ AND $\bar{n}_{CH}(\pi^+)$ BEFORE AND AFTER THE RISE IN MULTIPLICITY WITH $P_\perp$. ALL FOUR DATA SETS ARE COMPATIBLE WITH A COMMON SLOPE OF .65 ± .01 GeV^{-1}. FROM THE INTERCEPT DIFFERENCES WE DETERMINE THE AVERAGE VALUE OF THE RISE $\Delta\bar{n}_{CH}$ = .58 ± .05 AND THE AVERAGE PROTON-PION MULTIPLICITY DIFFERENCE Δ = 1.08 ± .05.

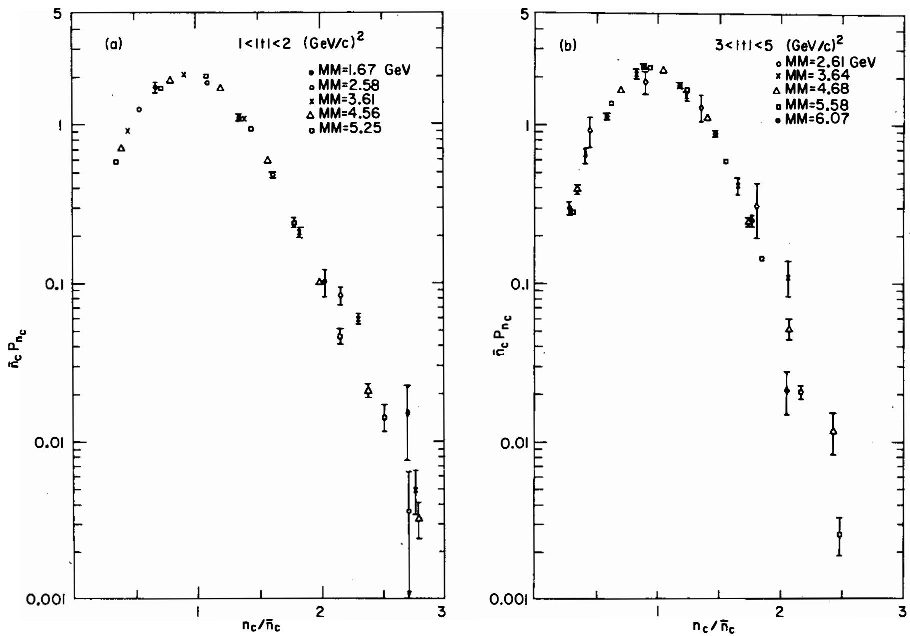

FIG. 11. MULTIPLICITY SCALING PLOTS FOR LOW (a) AND HIGH (b) FOUR-MOMENTUM TRANSFER t TO p_3.

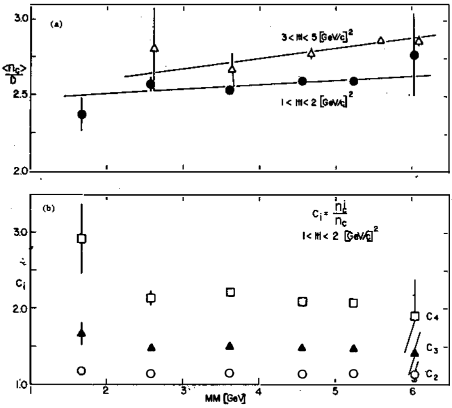

FIG. 12. DEVIATIONS FROM EXACT MULTIPLICITY SCALING IN MM

a. $\frac{\bar{n}_{CH}}{D}$ vs MM FOR LOW AND HIGH |t| (D = DISPERSION). THE LINES FITTED TO THE DATA ARE $\bar{n}_{CH}/D = (0.03 \pm 0.04)$ MM $+ 2.45 \pm .06$ FOR THE LOW |t| REGION AND $\bar{n}_{CH}/D = (0.07 \pm 0.03)$ MM $+ 2.46 \pm .16$ FOR THE HIGH |t| REGION.

b. THE NORMALIZED HIGHER MOMENTS vs MM.

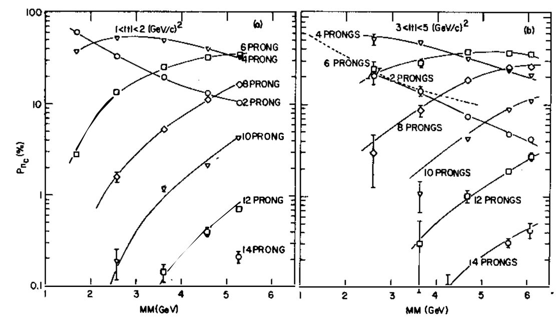

FIG. 13. PRONG NUMBER PROBABILITIES $P_{n_{CH}}$ vs MM FOR LOW AND HIGH |t| REGIONS. THE HAND DRAWN CURVES (EXCEPTING THE 2-PRONG CASE) WERE OBTAINED BY SUPERIMPOSING THE HIGH |t| DATA ON THE LOW |t| DATA WITH A SHIFT IN MM OF + 0.75 GeV. THE DOTTED LINE IS THE 2 PRONG CURVE OBTAINED FROM THE LOW |t| DATA.

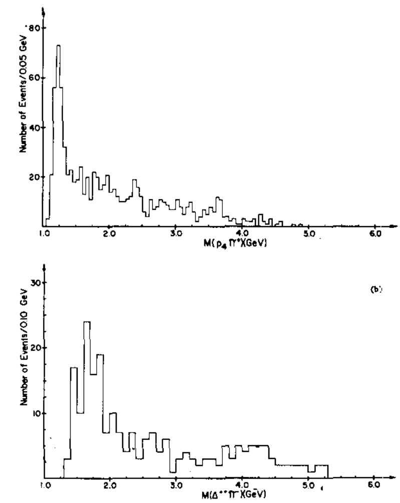

FIG. 14. a. THE EFFECTIVE MASS DISTRIBUTION OF THE $p_4\pi^+$ SYSTEM.

b. THE EFFECTIVE MASS DISTRIBUTION OF THE $\Delta^{++}\pi^-$ SYSTEM.

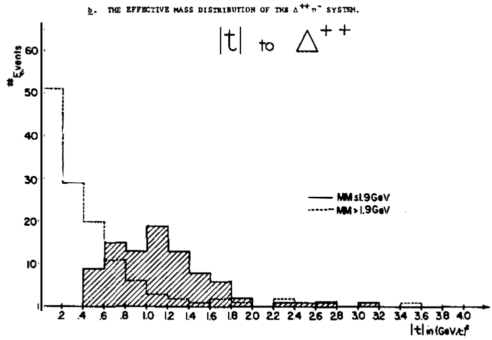

FIG. 15. FOUR MOMENTUM TRANSFER $|t|$ TO Δ^{++}. THE SOLID LINE REPRESENTS Δ^{++} EVENTS WITH $M(p_4\pi^+\pi^-) \leq 1.9$ GeV, THE DASHED LINE REPRESENTS Δ^{++} EVENTS WITH $M(p_4\pi^+\pi^-) > 1.9$ GeV.

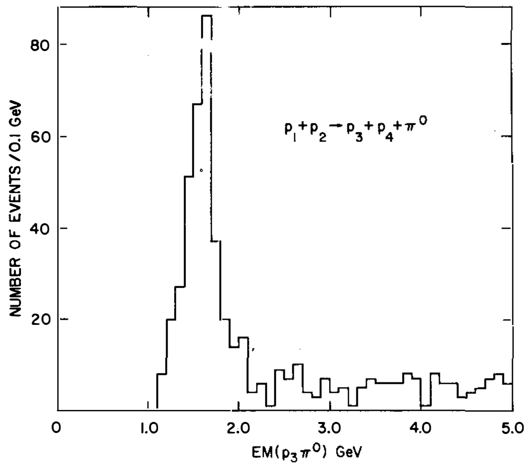

FIG. 16. EFFECTIVE MASS DISTRIBUTION OF THE $p_3\pi^0$ SYSTEM IN THE REACTION $p_1 + p_2 \rightarrow p_3 + p_4 + \pi^0$.

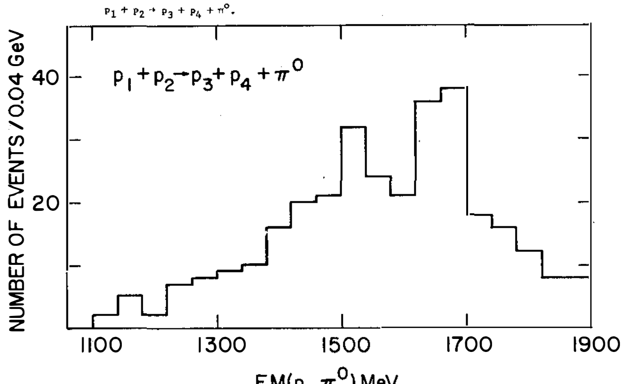

FIG. 17. SAME AS FIG. 16 BUT FINER BINNING.

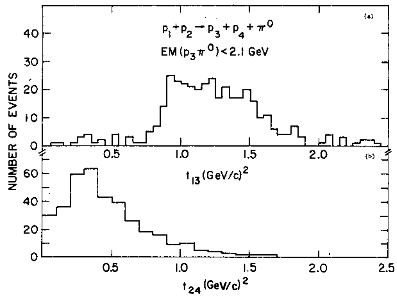

FIG. 18. a. FOUR-MOMENTUM TRANSFER t_{13} TO p_3 FOR EVENTS WITH THE EFFECTIVE MASS OF THE $p_3\pi^0$ SYSTEM LESS THAN 2.1 GeV.

b. FOUR-MOMENTUM TRANSFER t_{24} TO p_4 (AND THEREFORE ALSO TO THE SYSTEM $p_3\pi^0$) FOR THE SAME EVENTS AS a.

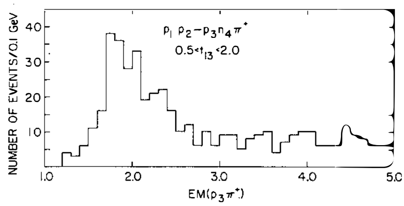

FIG. 19. EFFECTIVE MASS DISTRIBUTION OF THE $p_3\pi^+$ SYSTEM IN THE REACTION $p_1 + p_2 \rightarrow p_3 + n_4 + \pi^+$.

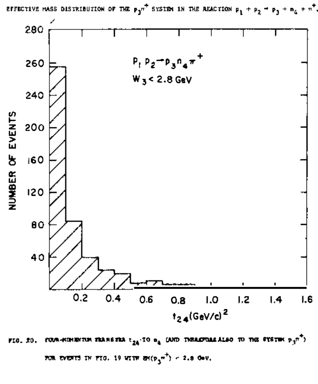

FIG. 20. FOUR-MOMENTUM TRANSFER t_{24} TO n_4 (AND THEREFORE ALSO TO THE SYSTEM $p_3\pi^+$) FOR EVENTS IN FIG. 19 WITH $EM(p_3\pi^+) < 2.8$ GeV.

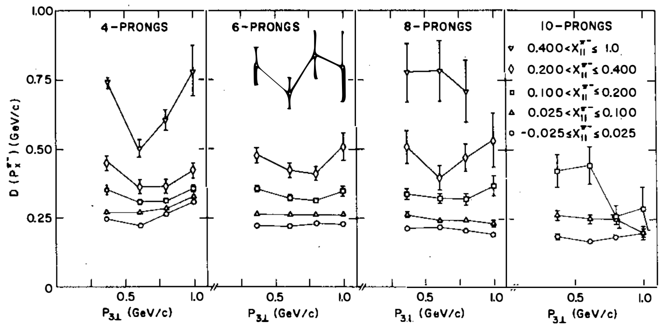

FIG. 21. DISPERSION OF P_x DISTRIBUTION FOR π^-'s FOR FOUR DIFFERENT MULTIPLICITIES AND FIVE DIFFERENT $x_{\parallel}^{\pi^-}$ BINS vs THE TRANSVERSE MOMENTUM OF P_3.

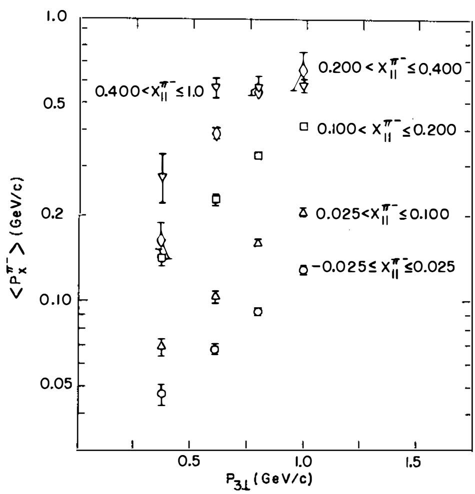

FIG. 22. AVERAGE VALUE OF P_x FOR π^-'s vs $P_{3\perp}$ FOR FIVE DIFFERENT $x_{\parallel}^{\pi^-}$ INTERVALS.

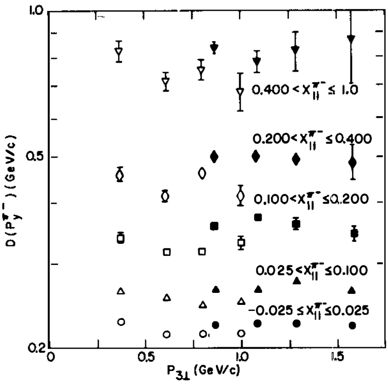

FIG. 23. DISPERSION OF P_y DISTRIBUTION FOR π^-'s vs $P_{3\perp}$ FOR FIVE DIFFERENT INTERVALS OF $X_{\parallel}^{\pi^-}$. OPEN SYMBOLS REPRESENT DATA BELOW THE RISE IN MULTIPLICITY, SOLID SYMBOLS DATA ABOVE THE RISE IN MULTIPLICITY.

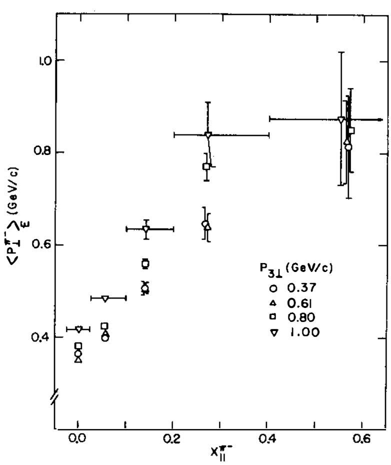

FIG. 24. THE SEA GULL EFFECT ($P_{\perp}^{\pi^-}$ vs $X_{\parallel}^{\pi^-}$) FOR FOUR DIFFERENT INTERVALS OF $P_{3\perp}$.

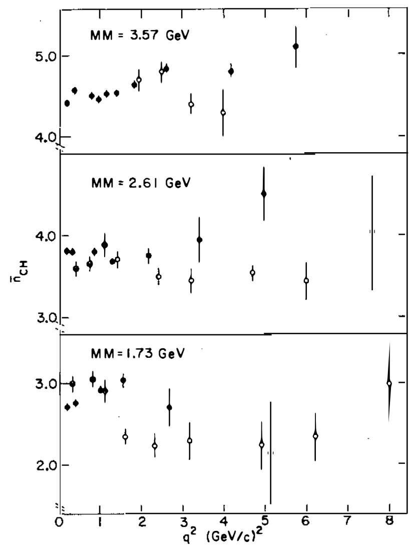

FIG. 25. ep AND pp AVERAGE CHRAGED MULTIPLICITIES vs q^2 ($q^2 \equiv t_{13}$) FOR 3 DIFFERENT INTERVALS OF MM. $\bar{n}_{CH}$ INCLUDES e'. OPEN CROSSED CIRCLES REPRESENT ep DATA FROM A DESY STREAMER CHAMBER EXPERIMENT,[20] OPEN CIRCLES ARE ep DATA FROM A SCINTILLATION COUNTER EXPERIMENT AT CORNELL[21] (MULTIPLICITY CORRECTIONS AMOUNT TO 46% IN THIS EXPERIMENT) AND THE SOLID SYMBOLS ARE THE pp DATA FROM MASS.

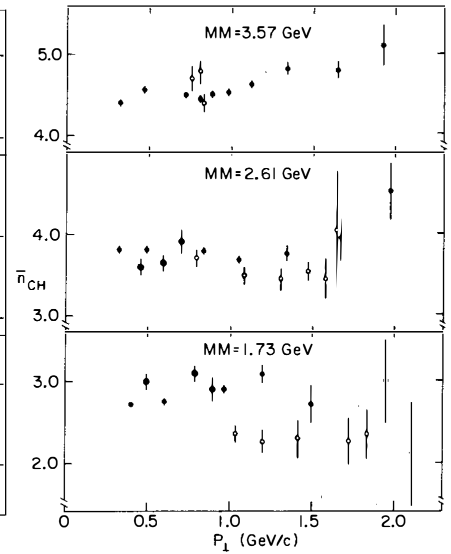

FIG. 26. ep AND pp AVERAGE CHARGED MULTIPLICITIES vs $P_\perp$ FOR THREE DIFFERENT INTERVALS OF MM FOR THE SAME DATA AS FIG. 25. THE LOWER BEAM ENERGY (7.0 GeV/c AND 11.5 GeV/c) IN THE ep DATA LIMITS THEIR RANGE IN $P_\perp$ IN A WAY THAT THERE ARE NO DATA AVAILABLE WHERE THE pp MULTIPLICITY RISES.

MESON SPECTROSCOPY WITH THE OMEGA SPECTROMETER

L. Mandelli

CERN, Geneva - I.N.F.N., Milan

Abstract: A short summary of the Omega experimental program is given. Expected results in the field of boson resonances are discussed and some preliminary data shown.

Résumé: Un bref résumé du programme expérimental de l'Oméga est donné. Les résultats attendus dans l'étude des résonances bosoniques sont discutés et quelques résultats préliminaires sont montrés.

1. THE SPECTROMETER

Before to expose the experimental program developed with the Omega spectrometer at CERN and to discuss some preliminary results, it is useful to give a very brief technical description of the spectrometer itself. The interested reader will find more details in ref. 1.

Omega is essentially constitued by a superconducting dipole magnet, generating a 14 m^3 magnetic volume and a spark chamber system placed inside it. The pole diameter is 3 m and the gab between the poles is 1.5 m.

The charged tracks detector is placed inside the magnetic volume, and it is constituted by eight spark chamber modules (10 gaps each) placed in front of the target and perpendicular to the beam, and eight smaller modules (8 gaps each) placed on each side of the target and parallel to the beam to detect slow large angle tracks. The target (30 or 60 cm H_2/D_2) is placed inside the magnetic field. All sparks chambers are read-out by four stereo pairs of plumbicon cameras, and sparks coordinates are stored on magnetic tape with all relevant electronic information.

Caracteristic constants of the acquisition system are listed in table I.

TABLE I.

Data acquisition dead time	20 ms
Max. data raking rate	15 ev/b (400 ms flat top)
Spark chamber memory	1 μs
Maximum tolerated beam intensity	5 10^5 part./burst
Accuracy on spark location σ_y	500 μm
Spark resolution	1.5 cm
$\Delta p/p$ at 10 GeV/c	0.8%
Caracteristic data processing time (CPU 7600 CDC)	200 ms/ev.

A relevant number of permanent facilities have been built by different groups around Omega, allowing a great variety of different triggers:

(a) multiparticle atmospheric pressure Cerenkov ($\sim$ 43 m^3) placed downstream Omega (π from K, p between 2.8 - 9.8 GeV/c);

(b) high pressure Cerenkov (π, K from P between 5 and 10 GeV/c);

(c) M.W.P.C. H's to trigger on multiplicity and/or correlations;

(d) five (200 x 20 cm) scintillators to measure T.O.F. of slow particles ($\delta t \simeq 500$ ps);

(e) array of scintillation counters to detect and measure recoiling neutrons.

The beam is an unseparated beam ranging from 3.0 to 19.0 GeV/c. Incident particles are flagged by three Cerenkov counters, their momentum is determined to 0.3% and their angle to 0.2 mrad by a system of five M.W.P.C. H's (11 planes).

The highest sensitivity can be reached for processes initiated by a high intensity incident flux (π^-'s or p's), a good trigger acceptance and a cross section which just saturates the data acquisition system.

For example, a trigger on a process having 500 μb total cross section and an acceptance of 50%, allows to collect 400 ev/μb · day. reliability of the system included.

The basic data processing package is constituted by an automatic pattern recognition and a geometry reconstruction program (ROMEO). The typical CPU processing time is of the order of 200 ms/event (CDC 7600).

2. THE EXPERIMENTAL PROGRAM

After one and a half years of effective operation, Omega has collected data for many different experiments. All experiments aim to investigate strong interactions, but while some of them are more oriented to the study of rare dynamic processes, some others are primarily motivated by the study of meson resonances.

In table II all experiments which took data up to April 1975 are listed according to the preceding and to some extent arbitrary subdivision. In the following I will briefly comment on the resonances study program and on the expected results from each experiment.

TABLE II

A) Dynamic oriented experiments

Triggered Reaction (*)	P_i	Exp. sensitivity	Collaboration	Comment
1) $\pi^\pm p \to \underline{\pi^\pm \pi^+} n$	3.2 GeV/c	≥ 1000 ev/μb	CERN, Saclay	To determine T=0,2 ππ scattering length at threshold ($M_{\pi\pi} \lesssim .4$ GeV)
2) $\pi^- p \to \underline{\Lambda^0_F} K^{*0}$ $\pi^+ p \to \underline{\Lambda^0_F} K^{*++}$	8.0 GeV/c 12.0 GeV/c	≥ 1000 ev/μb ≥ 100 ev/μb	CERN, ETH, Karlsruhe, Freiburg, Saclay,	To study hyperon exchange processes and exotic search
3) $\pi^\pm p \to \underline{p_F} X^\pm$	9.0 and 12.0 GeV/c	≥ 1000 ev/μb	CERN, Collège de Fr. Ec. Polyt. Orsay	To study backward scattering processes

B) Spectroscopy oriented experiments

1) $\pi^- p \to X^- \underline{p}$ $\hookrightarrow \pi^-\pi^0$ $\pi^+\pi^-\pi^-$ $\pi^+\pi^-\pi^-\pi^0$ etc.	12 GeV/c	200 ev/μb	Bari, Bonn, CERN, Daresbury, Liverpool, Milan	Study of the missing mass to the proton with detection of all charged final states $1.4 \leq M_X \leq 2.3$ GeV
2) $\pi^- p \to X^0 \underline{n}$ $\hookrightarrow \pi^+\pi^-$ $\pi^+\pi^-\pi^0$ $\pi^-\pi^-\pi^+\pi^+$ etc.	12 GeV/c and 15 GeV/c	250 ev/μb	Birmingham, Rutherford Lab., Tel-Aviv, Westfield College	To study neutral missing mass with detection of charged final states $1.2 \leq M_X \leq 2.2$ GeV
3) $K^+ p \to (\underline{\bar{\Lambda}, K^-, p^-}) X$	12 GeV/c	200 ev/μb	Glasgow, Saclay	To study $\bar{\Lambda}N$, K^+K^- spectra ./.

(*) In each reaction the triggering particles are underlined.

Table II (Cont'd)

Triggered Reaction (*)	P_i	Exp. sensitivity	Collaboration	Comments
4) $\pi^- p \to (\underline{K^-,\bar{p}})X$	10 GeV/c and 16 GeV/c	2000 ev/μb 1000 ev/μb	Bari, Bonn, CERN, Daresbury, Liverpool, Milan, Purdue, Vienna,	To detect rare decays of mesons in $K\bar{K}$, $K\bar{K}\pi$, $N\bar{N}$, $N\bar{N}\pi$ etc.
$(\underline{K}^+)X$		2000 ev/μb		Study of K^* in hypercharge exchange reactions.
5) $K^-p \to \underline{K}^o\pi^+\pi^-n$	10 GeV/c	250 ev/μb	Aachen, CERN, ETH	To study non-diffractive K^* production
6) $\pi^-p \to D\bar{D}N$ ↳ $\underline{K}\pi$, $\underline{K}\pi\pi$	19 GeV/c	1000 ev/μb in high multiplicity channels (6prongs)	"Omega Groups"	To detect charm anticharm production. D is assumed to decay into $K\pi$ or $K\pi\pi$, giving rise to a high p_t K^-.

(*) In each reaction the triggering particles are underlined.

It is evident from the list of table II that a considerable part of the experimental program has been dedicated to experiments aiming to improve our knowledge of the meson systems.

In my mind, this is justified by a number of open questions in meson spectroscopy to which Omega may contribute to give an answer:

(a) is our understanding of SU_3 breaking (coming from the study of 0^-, 1^- and 2^+ nonets) extensible to other nonets?

Omega with its large acceptance for detection and particles identification and with the possibility of reaching high sensitivity, may hope to complete the existing information on some not so well known nonet (like 3^- and 0^+) and to discover still heavier members.

(b) Can the natural spin-parity effects (A_1, A_3, Q and L) be interpreted as resonances or are they pure kinematic effects?

The high statistic which Omega may collect on exclusive channels, will make possible refined P.W.A. on old and new meson systems: 3π, $K\bar{K}\pi$ etc. Parallel investigation on non-diffractive channels (charge exchange and hypercharge exchange) will give complementary essential information.

(c) Do towers of resonances (daughters) systematically exist. Below resonances lying on the leading trajectory?

Only a few examples are known up to now (S^*, δ, ε(?), K(?), ρ'(?), ρ'' and E). High statistic on exclusive channels and refined analysis may contribute with new information to answer to this question.

(d) Which is the meaning of the new discovered particles? Are they some kind of meson predicted by various theories (coulored, charmed mesons etc)? Do exotic mesons exist?

Omega is a unique device for the detection of rare multiparticle reactions, and this property allows an exciting exploratory search (see experiments A2 and B6 in table II) of such new effects.

Experiments B1 and B2 of table II, originally motivated by the CERN missing mass results aim to study boson resonances decaying mainly into pions, to clarify the situation in the R and S region.

Preliminary results on the $n\pi^+\pi^-$ system, have been presented at the 17th International Conference on High Energy Physics[2] based on 20% of the data, from which appears a confirmation of $J^P = 3^-$ for the g meson and a possible indication of a structure in the Y_0^8 moment at $M \simeq 2.0$ GeV. If confirmed, this would establish the 4^+ Regge recorrency on the ρ trajectory.

When the analysis of both experiments will be completed, the comparative study of channels like $\pi^+\pi^-$, $\pi^-\pi^o$, $\pi^+\pi^-\pi^-$, $\pi^+\pi^-\pi^o$, $\pi^+\pi^+\pi^-\pi^-$, $\pi^+\pi^-\pi^-\pi^o$ etc. will bring refreshing information on S=O states with a mass between 1.4 and 2.2 GeV where many different spin parity states are predicted by the quark model[3].

Complementary information on mesons with $S = \pm 1$ will be obtained by the analysis of experiments B4 and B5 via the study of the non-diffractive reactions:

$$K^- p \rightarrow n K^o \pi^+ \pi^- \tag{1}$$

and

$$\pi^- p \rightarrow (\Lambda^o, \Sigma^o) K^+ \pi^- \quad . \tag{2}$$

Fig. 1 shows the preliminary $K^+\pi^-$ raw mass spectrum obtained from reaction (1) on 10% of the data during the data taking.

Heavy isosinglet states strongly coupled to the $K\bar{K}$ system (like ϕ,f') are investigated in experiment B3, when produced opposite to pK^+ in the reaction

$$K^+ p \rightarrow (PK^+) K^+ K^- \quad . \tag{3}$$

Reactions in which a kaon-antikaon or a barion-antibarion pair is produced are particularly unexplored above a few GeV/c incident momentum.

More simple spectrometers like the CERN-Munich and the Argonne Effective Mass Spectrometer (EMS) have studied reactions giving rise to two charged tracks.

However, these spectrometers have a rather poor acceptance at high effective masses in contrast to the one obtained with the Omega spectrometer. This feature makes of Omega a competitive device to study high effective masses of two-body systems. Furthermore, its large solid angle charge tracks detection makes feasible the study of more complicated systems like $K^+K^-\pi^-$, $P\bar{P}\pi^-$ etc. Study of the K^+K^-, K^oK^- and $K^+K^-\pi^-$ systems is possible in the experiment B4 via the study of the reactions:

$$\pi^- p \rightarrow n K^+ K^- \tag{4}$$

and

$$\pi^- p \rightarrow p K^+ K^- \pi^- \tag{5}$$

$$\pi^- p \rightarrow p K^- K^o \tag{6}$$

20% of the data have being processed during the data taking and the K^+K^- and $K^+K^-\pi^-$ raw mass spectra are shown in figs 2 and 3.

In the K^+K^- system, clear structures are present around 1.30 and 1.70 GeV, which can be interpreted as due to the production of f^o, A_2^o and g meson. Above them a small peak may be present around 2 GeV and could be produced by the 4^+ recurrence of the ρ trajectory as previously mentioned.

Final statistics will prove or disprove its existence, but it is worth to note that analysis of the same reaction at 18.8 GeV/c by the CERN-Munich group[4] presents, if not a structure in the mass spectrum, a rapid variation of Y_o^7 moment, which can be interpreted as due to the interference of the g meson (3^-) with a 4^+ wave.

At threshold, the K^+K^- spectrum of fig. 2, shows structures which does not seem easy to interpret as due to S^* and ϕ production. A narrow peak is present at $M \simeq 1085$ GeV. Acceptance corrections are however necessary before to draw any physics conclusion.

The $K^+K^-\pi^-$ system is dominated by a broad structure centered around M = 1.640 GeV, (fig. 2) and which include the A_3 ($\pi^- f^o \to \pi^- K^+ K^-$) as well as some other effect since the $K^* K^-$ decay is present.

A partial wave analysis will illuminate on the diffractive nature of the structure.

Also interesting to note that the F1 meson (M = 1540 GeV) does not seem produced in reaction (5) in contradiction with lower energy and lower statistic data[5].

The $\bar{N}N$ system could be interesting to detect heavy low spin resonances. Formation experiments have given however inconclusive results.

The $p\bar{p}$ system produced by incident pions has been extensively studied by the CERN-Munich group[6] in the reaction:

$$\pi^- p \to N_s \, p\bar{p} \quad . \tag{7}$$

It shows the remarkable property of being produced predominantly via one pion exchange, of not presenting any "narrow" resonance but only a rapid variation of the $p\bar{p}$ angular distribution.

The pure T = 1 $\bar{p}n$ system is being studied in experiment B1 and B4 in the reaction:

$$\pi^- p \to p_s \, (\bar{p}n) \tag{8}$$

where the $\bar{p}$ is flagged by the downstream Cerenkov counter. A preliminary analysis from experiment B1[7] shows for the $\bar{p}n$ system, properties similar to the $p\bar{p}$.

No narrow structures are found and the symmetry of the angular distribution is coherent with a pure one-pion exchange process.

Much higher statistic (X10) will be available from experiment B4. In the same experiment, the study of the reaction

$$\pi^- p \to pp\bar{p}\pi^- \qquad (9)$$

will allow to extend the analysis to the $\bar{p}p\pi^-$, $\Delta^o\bar{p}$, $\overline{\Delta^{++}p}$ systems, whyle the strange counterpart can be looked at in experiment B3 in the system $\bar{\Lambda}N$.

I am convinced that when such large amount of data will be analysed it will bring to an improved knowledge of the meson systems.

REFERENCES

(1) O. Gildemeister et al., Proc. Int. Conf. on Instrumentation for High Energy Physics Frascati, 1973, p. 669.

(2) 17th International Conf. on High Energy Physics London, 1974, paper 38 and p. II-35 of the Proceedings.

(3) G. Ascoli et al., Phys. Rev. Letters 20 (1968) 1411.

(4) W. Männer et al., Invited talk at EMS 1974 and Proceedings of 17th Int. Conf. on High Energy Physics London, 1974, p. II-35.

(5) Aderholz et al., Nucl. Phys. B11 (1969) 259.

(6) G. Grayer et al., Phys. Letters 39B (1974) 563.
B. Hyams et al., Nucl. Phys. B 73 (1974) 202.

(7) Proceedings of the 17th International Conf. on High Energy Physics London, 1974, p. II-45 and paper 75.

FIGURE CAPTIONS

Fig. 1 (a) $K^+ \pi^-$ effective mass for 4484 events (10% total) from reaction $\pi^- p \to (\Lambda^0, \Sigma^0)\, K^+ \pi^-$ at 10 GeV/c.

(b) As (a) but high mass region only.

Fig. 2 K^+K^- effective mass from 5995 events (20% total) from reaction $\pi^- p \to u\, K^+K^-$ at 10 GeV/c.

Fig. 3 $K^+K^-\pi^-$ effective mass from 4767 (20% total) from reaction $\pi^- p \to p\, K^+K^-\pi^-$ at 10 GeV/c.

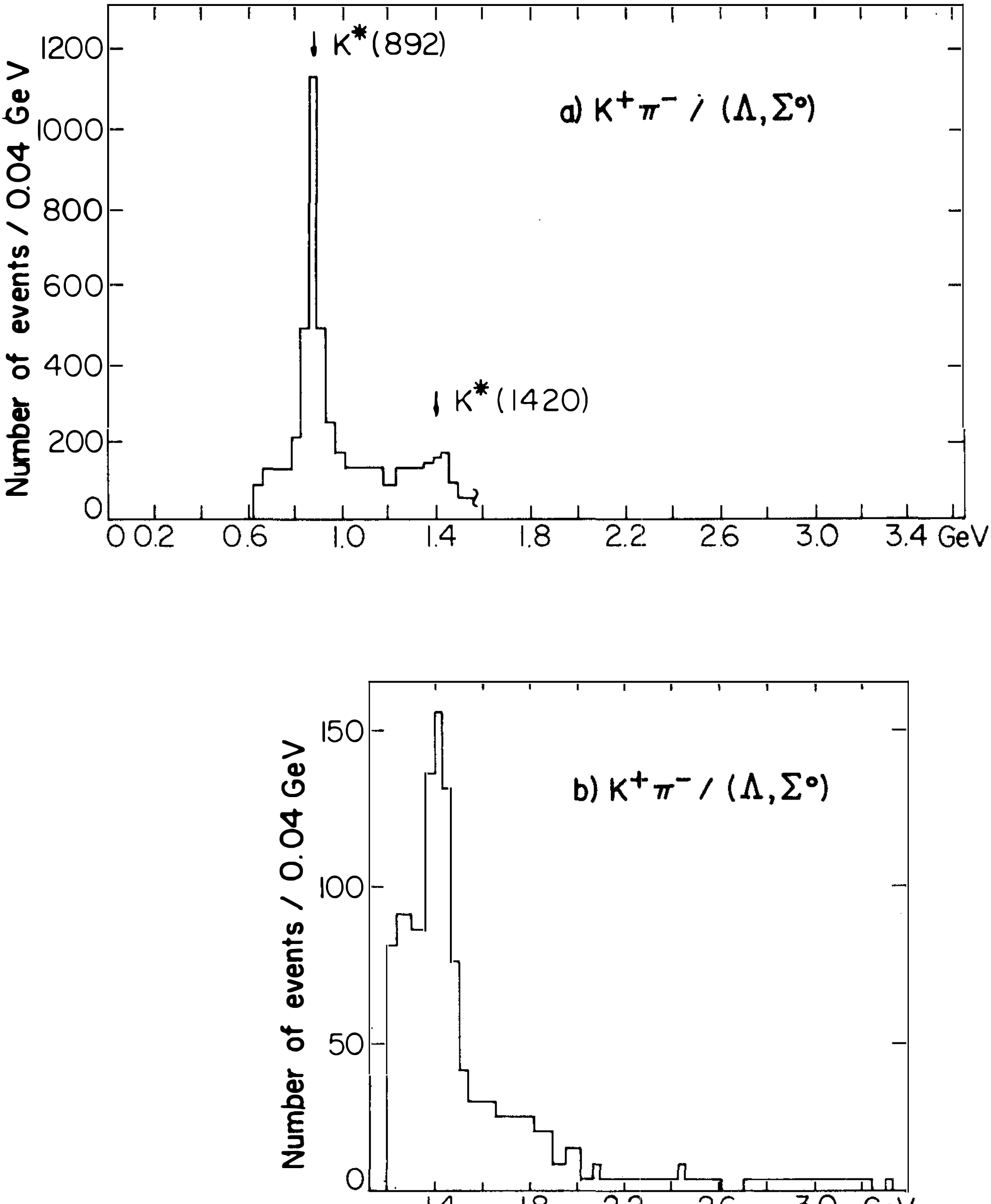

EFFECTIVE MASS$(K^+\pi^-)$ fig. 1

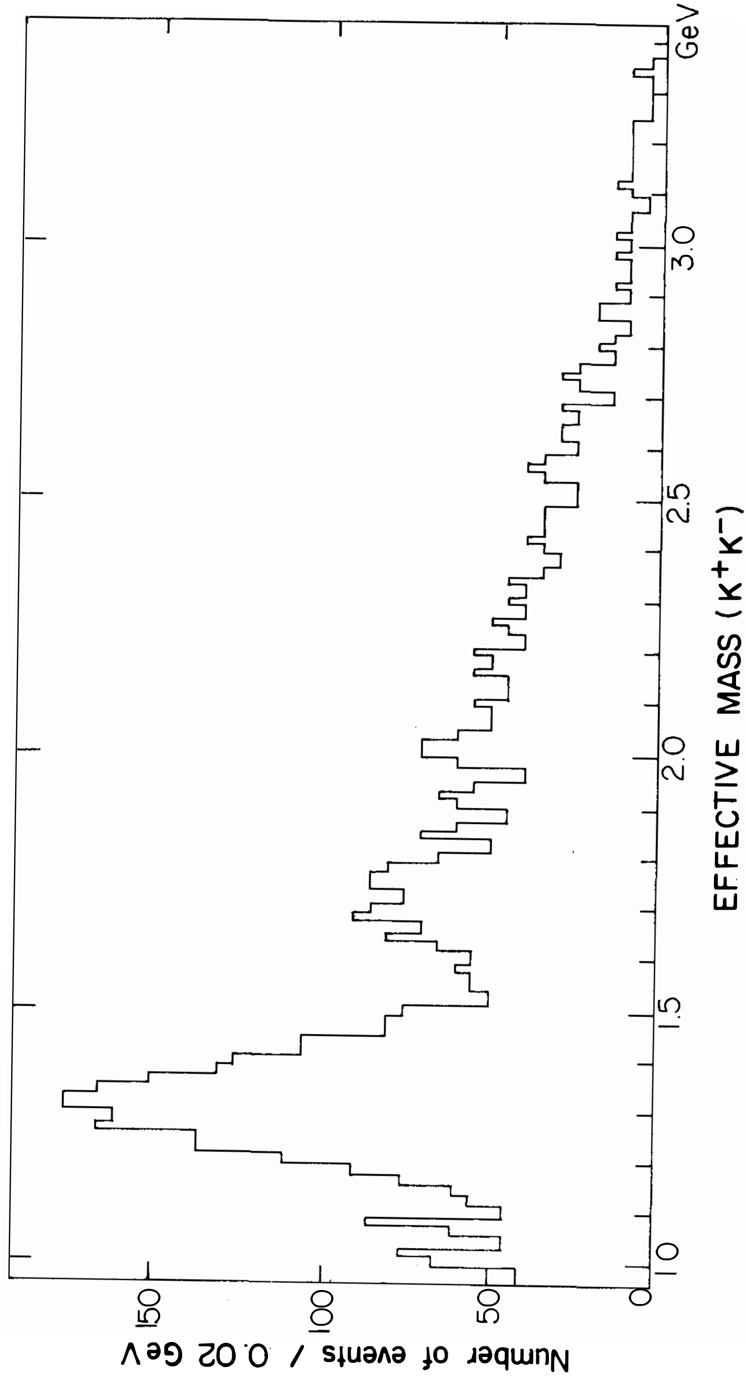

0
50
100
150
Number of events / 0.02 GeV
1.0
1.5
2.0
2.5
3.0
GeV
EFFECTIVE MASS (K+K−)

fig. 2

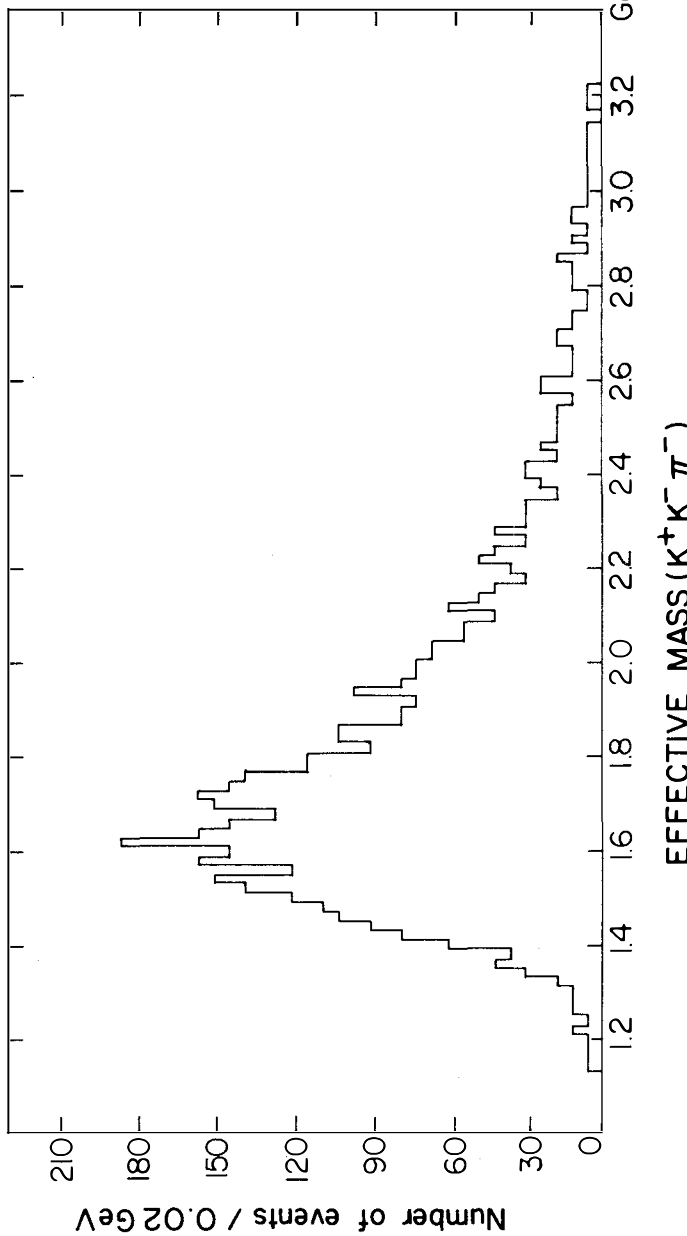

Number of events / 0.02 GeV
EFFECTIVE MASS ($K^+K^-\pi^-$)
GeV
0
30
60
90
120
150
180
210
1.2
1.4
1.6
1.8
2.0
2.2
2.4
2.6
2.8
3.0
3.2

fig. 3

LOCAL COMPENSATION OF QUANTUM NUMBERS AND

SHADOW SCATTERING

A. KRZYWICKI

Laboratoire de Physique Théorique et Particules Elémentaires, Orsay

Abstract : This paper contains a theoretical discussion of the hypothesis of local compensation of quantum numbers and of the implications of this local compensation for the shadow scattering of hadrons.

Résumé : Cet article contient une discussion théorique de l'hypothèse de compensation locale des nombres quantiques et de ses implications pour la diffraction hadronique.

1. Preamble.

Last year progress was made in our understanding of some of the basic features of hadronic diffraction. This progress was made possible by the accumulation of data on production processes. In turn, the resulting theoretical ideas about the relation between production processes and diffractive scattering led to interesting experimental research.

From a simple and general hypothesis about fluctuations of quantum number densities in inelastic final states, called local compensation of quantum numbers (LCQN), one can deduce among others[1-4]:

a. The asymptotic decline of charge exchange in shadow scattering.

b. The shrinking with increasing energy of the forward diffraction peak.

The above statements agree with the widespread folklore concerning the pomeron. However, the dynamical origin of these features of the pomeron has never been really understood. They were, at best, derived from very specific models. On the other hand, a model independent investigation helps to distinguish the important from the secondary. One also finds that certain results are more general than might be expected from experience with models.

The purpose of the present paper is to review the results obtained assuming local compensation of quantum numbers. I shall consistently employ the methods and the terminology developed in the papers by Don Weingarten and myself. I shall also take this opportunity to include here some of my unpublished results and suggestions*. I shall limit myself to theoretical considerations and I shall not attempt to evaluate the experimental evidence in favour of local compensation. In particular, I shall not discuss the very interesting results obtained by the Saclay group[5] (pp collisions at 69 GeV/c) and by the Rochester-Michigan collaboration[6] (pp collisions at 100 and 400 GeV/c).

---

* In particular those from my preliminary draft "Multiparticle production and Regge trajectory parameters" (October 1974).

2. Local compensation of quantum numbers (LCQN).

Local compensation of quantum numbers can be abstracted from various models of multiparticle production, including most versions of the multiperipheral model. An explicit discussion of this idea appeared for the first time, to my knowledge, in a paper by Hagedorn and Ranft[7] and in the context of the thermodynamical model. The possibility of stating this hypothesis independently of any specific model was emphasized in my Marseille talk[8], where some empirical evidence in favour of local compensation was also reviewed. Soon after, Don Weingarten and myself[1] were able to prove that local compensation of electric charge implies a power fall with energy of the charge exchange component of the inelastic overlap function. Ref. 1 contains the first precise formulation of the hypothesis of local compensation. It turned out later on, that a slightly different although physically equivalent formulation, due to Don Weingarten, is technically more convenient. It was used in refs. 3 and 4 and will be used in this paper too.

Consider a multiple production event and let $Z_Q(y)$ denote the transfer across the rapidity y of some additive quantum number Q. Since $Z_Q(y)$ varies randomly from event to event, it can be regarded as a realization of a random function* $\zeta_Q(y)$. The probability that $\zeta_Q(y) = Z_Q(y)$ will be written $P[\zeta_Q(y) = Z_Q(y)]$; in general the symbol P(A) will denote the probability of the event A.

The hypothetical local (in rapidity space) compensation of Q involves the following two basic postulates:

(i) Stationary fluctuations in phase space: The moment functions $< \zeta_Q(y_1) \ldots \zeta_Q(y_n) >$ become independent of the total available rapidity interval Y ($\approx \ln(s)$), for Y large enough.

Lorentz invariance implies that the moment functions, at large enough Y,

---

*An excellent discussion of the theory of random functions and of its applications can be found in a book by Stratonovich[9]. The reader of this book discovers with surprise that many results and concepts painfully elaborated by high energy physicists have been known for many years by people working on the theory of stochastic point processes.

depend only on the rapidity differences y_i-y_j.* Consequently, $\zeta_Q(y)$ can be regarded as a stationary random function if one adopts the idealized viewpoint neglecting phase space boundary effects.

(ii) Cluster decomposition:

$$< \zeta_Q(y_1) \dots \zeta_Q(y_n) > = < \zeta_Q(y_{i_1}) \dots \zeta_Q(y_{i_k}) > < \zeta_Q(y_{i_{k+1}}) \dots \zeta_Q(y_{i_n}) >$$

provided

$$\min \left(|y_{i_j} - y_{i_{j'}}| \; ; \; 1 \le j \le k, \; k < j' \le n \right) \qquad \gg \quad \lambda_Q$$

Here λ_Q is a correlation length, independent of Y.

It is obvious that LCQN is far more general than the popular cluster emission models. However, the independent production of clusters with Q=0 is the simplest model where Q is locally compensated.

The intuitive meaning of LCQN is very simple. A secondary S with $Q=Q_S$ is surrounded by a collection of particles of total $Q= -Q_S$, contained in a region of rapidity space whose average length eventually becomes independent of the collision energy (instead of continuously growing as $Y \to \infty$; it grows like $Y^{\frac{1}{2}}$ when Q's of secondaries are distributed at random). Furthermore, the manner in which the Q of S is compensated by the Q's of the neighbours of S does not depend on what happens far away in rapidity. When the incident particles have $Q \neq 0$, the conditions (i)-(ii) imply that Q_{target} (resp. Q_{beam}) is carried away by one or a few target (resp. beam) fragmentation secondaries. We recognize the well known leading particle effect.

It will be shown in the following that if Q is locally compensated, the ratio of the moduli of shadow scattering amplitudes, respectively with and without Q exchange, falls like a power of the collision energy.

3. LCQN and shadow scattering : a heuristic discussion.

Consider a two-body reaction involving exchange of the quantum number Q :

$$a(Q=0) + b(Q=0) \quad \Rightarrow \quad c(Q= -\Delta) + d(Q= +\Delta) \tag{1}$$

---

*A random function $\zeta(y)$ is called stationary if the moment functions $< \zeta(y_1) \dots \zeta(y_n) >$ depend on y_i-y_j, $i,j = 1,\dots,n$, only.

We shall inquire whether the process (1) can proceed via an intermediate multiparticle state X:

$$a(Q=0) + b(Q=0) \Rightarrow X \Rightarrow c(Q=-\Delta) + d(Q=+\Delta) \qquad (2)$$

We assume, of course, that Q is locally compensated in the state X. This means that X is characterized by some order at the microscopic level (rapidity distances $\leqslant \lambda_Q$) and by a disorder at the macroscopic level (rapidity distances $\gg \lambda_Q$). It turns out, on the other hand, that a macroscopic order in X is necessary if one requires the two steps in (2) to be probable. However, the probability of a macroscopic order in X falls exponentially with Y when $Y \to \infty$. Once one has realized this point, one has understood the implications of LCQN for shadow scattering.

For example[1,10], let Q be the electric charge and let $\Delta = +1$. Consider first the reaction $a(Q=0) + b(Q=0) \Rightarrow X$. We partition the secondaries belonging to X into zones with total charge zero :

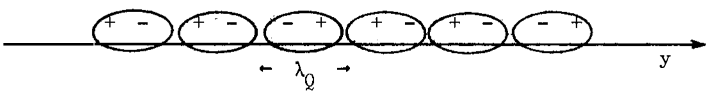

The rapidity space extensions of these zones are $\approx \lambda_Q$ and their "dipole moments" point equally likely to the left (like this: + −) and to the right (like that: − +). Furthermore, simplifying slightly, we assume that the "dipole moments" of different zones are uncorrelated.

Second, consider the reaction $c(Q=-1) + d(Q=+1) \Rightarrow X$. Now, we make a different partition of the secondaries belonging to X :

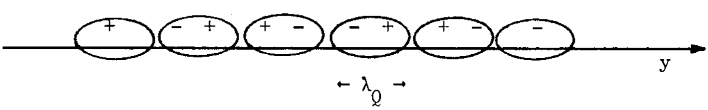

There are two charged groups of fragmentation secondaries carrying respectively the charge of $c(Q=-1)$ and that of $d(Q=+1)$. The remaining secondaries are partitioned into neutral zones as before. Again the rapidity extensions of zones are of the order of λ_Q and the "dipole moments" of the neutral zones are chaotic.

When one requires that the two partitions just described are simultaneously probable, one finds that all the "dipole moments" in the first (second) drawing should point to the left (right). The probability of such a macroscopically ordered configuration is $(\frac{1}{2})^{Y/\lambda_Q}$ (since Y/λ_Q is roughly the number of neutral zones) and therefore tends exponentially to zero when $Y \to \infty$. The argument of this section is obviously not rigorous, since various fluctuation effects are neglected, but it gives a good intuitive idea of the physical origin of results obtained using more abstract techniques.

4. Exchange of transverse momentum.

We consider in this section the elastic scattering a + b → a + b at a small angle $\theta \approx 2(-t/s)^{\frac{1}{2}} << 1$; s and t are the conventional Mandelstam variables and we work in cms. The relevant scattering amplitude is denoted by $T_\theta(ab \to ab)$. We obtain from unitarity

$$\mathrm{Im}\, T_\theta(ab \to ab) = \sum_X T(ab \to X)\; T^*(ab \to R_\theta X) \tag{3}$$

where R_θ is a rotation by the angle θ in the plane of the collision a + b → a + b. The summation is over all possible intermediate states. However, in the following we shall use the approximation where all states X are multiparticle states satisfying LCQN by assumption. In other words we shall investigate the properties of the inelastic overlap function[11]. After a simple algebra one obtains from (3)

$$\left|\mathrm{Im}\, T_\theta(ab \to ab)/\mathrm{Im}\, T_0(ab \to ab)\right| \le \sum_X \left[P(ab \to X)\; P(ab \to R_\theta X)\right]^{\frac{1}{2}} \tag{4}$$

A state X is partly determined by the corresponding function $Z_T(y)$; we use here the subscript "T" for "transverse momentum" instead of "Q" used in the preceding section. With the help of the Cauchy-Schwarz inequality one obtains from (4):

$$\left|\mathrm{Im}\, T_\theta(ab \to ab)/\mathrm{Im}\, T_0(ab \to ab)\right| \le \tag{5}$$

$$\int d[Z_T(y)] \left\{ P[\zeta_T(y) = Z_T(y)]\; P[\zeta_T(y) = R_\theta Z_T(y)] \right\}^{\frac{1}{2}}$$

The transformation properties of $Z_T(y)$ under R_θ are easily found. The momentum of the j^{th} secondary transforms as follows

$$\begin{aligned} R_\theta q_{jT} &= q_{jT}\cos\theta + q_{jL}\sin\theta \approx q_{jT} + (2q_{jL}/\sqrt{s})\sqrt{-t} \\ R_\theta q_{jL} &= -\, q_{jT}\sin\theta + q_{jL}\cos\theta \approx q_{jL} \end{aligned} \tag{6}$$

Therefore, in the central region one has approximately

$$R_\theta Z_T(y) \approx Z_T(y) - \sqrt{-t} \tag{7}$$

We have taken into account the energy-momentum consrvation constraint

$$\sum_{\text{left movers}} 2q_{jL}/\sqrt{s} = -1 \tag{8}$$

Notice that the sum above is almost saturated by the momenta of fragmentation secondaries. It can be shown that the error in (7) is irrelevant for our results. We rewrite (5) using (7) :

$$|\mathrm{Im}\ T_\theta(ab \to ab)/T_o(ab \to ab)| \le \tag{9}$$

$$\int d[Z_T(y)]\ \{P[\zeta_T(y) = Z_T(y)]\ P[\zeta_T(y) = Z_T(y) - \sqrt{-t}]\}^{\frac{1}{2}}$$

The integration is over all possible functions $Z_T(y)$. The mismatch between the two factors in the integrand is responsible for the energy dependence of the integral.

The random function $\zeta_T(y)$ can be expanded in Fourier series

$$\zeta_T(y) = Y^{-\frac{1}{2}} \sum_j \eta_{Tj}\ \exp(2\pi ijy/Y) \tag{10}$$

and one can consider the functional integration in (9) as an integration over all possible values of the random variables η_{Tj}. However, the transformation $\zeta_T(y) \to \zeta_T(y) - \sqrt{-t}$ affects the zero frequency mode of $\zeta_T(y)$ only : The energy dependence of the integral in (9) results mostly, if not enirely, from the integration with respect to η_{To}. Therefore, one expects to get a good bound after eliminating from (9), using the Cauchy-Schwarz inequality, the integrations with respect to all non-zero frequency modes:

$$|\mathrm{Im}\ T_\theta(ab \to ab)/\mathrm{Im}\ T_o(ab \to ab)| \le \tag{11}$$

$$\int du\ \{P(\eta_{To} = u)\ P(\eta_{To} = u - \sqrt{-t}Y)\ \}^{\frac{1}{2}}$$

Let us insert the identity

$$P(\eta_{To} = u) \equiv e^{-gu^2}[\ e^{gu^2} P(\eta_{To} = u)] \tag{12}$$

into (10) and let us use again the Cauchy-Schwarz inequality ($g > 0$ is, as yet, an arbitrary parameter) to get

$$|\mathrm{Im}\ T_\theta(ab \to ab)/\mathrm{Im}\ T_o(ab \to ab)| \le \tag{13}$$

$$\{\int du\ \exp[\ -\tfrac{1}{2}gu^2 - \tfrac{1}{2}g(u - \sqrt{-t}Y)^2]\ \exp(gu^2)\ P(\eta_{To} = u)\}^{\frac{1}{2}} \times$$

$$\times\ \{\int du\ \exp[\ -\tfrac{1}{2}gu^2 - \tfrac{1}{2}g(u - \sqrt{-t}Y)^2]\ \exp[g(u - \sqrt{-t}Y)^2]\ P(\eta_{To} = u - \sqrt{-t}Y)\}^{\frac{1}{2}}$$

Transforming the integration variable in the second integral $u \to -u + (-tY)^{\frac{1}{2}}$ and taking into account the symmetry of the problem

$$P(\eta_{To} = u) = P(\eta_{To} = -u) \tag{14}$$

one finds that the second factor on the right side of (13) is identical to the first one. An easy calculation yields

$$|\mathrm{Im}\ T_\theta(ab \to ab)/\mathrm{Im}\ T_0(ab \to ab)| \leq \qquad (15)$$

$$e^{\frac{1}{2}gtY} \int du\ e^{ug\sqrt{-tY}}\ P(\eta_{To} = u)$$

In general, it is not guaranteed that the integral on the right side of (15) exists. Define the moments

$$\mu_n = \langle \eta_{To}^n \rangle \qquad (16)$$

For symmetry reasons $\mu_{2n+1} = 0$ (cf. eq. (14)). We supplement LCQN by assuming that

$$\limsup_{n \to \infty} (\mu_n/n!)^{1/n} = O(Y^{-\frac{1}{2}}) \qquad (17)$$

Now, the integral in (15) is meaningful for $-tg <$ const and the characteristic function

$$\Pi(p) = \int du\ e^{iup}\ P(\eta_{To} = u) \qquad (18)$$

is analytic for $|p| < \mathrm{const} \times Y^{\frac{1}{2}}$. The cumulants $\varkappa_n$ of η_{To} are defined by the series expansion

$$\ln \Pi(p) = \sum_n (\varkappa_n/n!)\ (ip)^n \qquad (19)$$

Until now we have not made any use of LCQN. This hypothesis implies the following behaviour of the cumulants $\varkappa_n$:

$$\varkappa_n = Y^{-\frac{1}{2}n + 1}\ \tilde{\varkappa}_n \qquad (20)$$

where $\tilde{\varkappa}_n$ are finite (or zero) in the limit $Y \to \infty$. One way of seeing that this follows from LCQN is to introduce the correlation functions B_n according to the standard recipe

$$\langle \zeta_T(y_1)\zeta_T(y_2)\rangle = B_2(y_1 - y_2)\ , \qquad (21)$$

$$\langle \zeta_T(y_1)\zeta_T(y_2)\zeta_T(y_3)\zeta_T(y_4) \rangle = B_2(y_1 - y_2)B_2(y_3 - y_4) + B_2(y_1 - y_3) \times B_2(y_2 - y_4) + B_2(y_1 - y_4)B_2(y_2 - y_3) + B_4(y_1 - y_2, y_1 - y_3, y_1 - y_4)$$

....

....

According to LCQN the function B_n vanishes if at least one of its arguments becomes much larger than the characteristic distance. With the help of the obvious equation

$$\eta_{To} = Y^{-\frac{1}{2}} \int_{-Y/2}^{Y/2} dy\ \zeta_T(y) \qquad (22)$$

one easily verifies the validity of (20) ($\tilde{\varkappa}_n$ equals B_n integrated with res-

-pect to all its arguments). We now combine (15),(18),(19) and (20):

$$|\mathrm{Im}\, T_\theta(ab \to ab)/\mathrm{Im}\, T_o(ab \to ab)| \underset{\substack{Y \to \infty \\ t \text{ fixed}}}{\leq} \exp\{ Y [\tfrac{1}{2}gt + \sum_{\substack{\text{even} \\ n}} (\tilde{\varkappa}_n/n!)\, (g\sqrt{-t})^n] \} \tag{23}$$

The limit $Y \to \infty$ is indicated, because our considerations implicitly involve the assumption that Y is very large (for example the effect of phase space boundaries is ignored; cf. the formulation of LCQN). The series in the exponent is a formal series unless the coefficients $\tilde{\varkappa}_n$ satisfy a condition analogous to (17). The next step is to minimize the right side of (23) with respect to g , keeping t fixed. At this "best" $g = g_o(t)$ the exponent in (23) is certainly negative since $\tilde{\varkappa}_2 = \varkappa_2 > 0$. Hence

$$|\mathrm{Im}\, T_\theta(ab \to ab)/\mathrm{Im}\, T_o(ab \to ab)| \underset{\substack{Y \to \infty \\ t \text{ fixed}}}{\leq} \exp[Y\gamma(t)] \tag{24}$$

with

$$\gamma(t) = \min_g \{ \tfrac{1}{2}tg + \sum_{\substack{\text{even} \\ n}} (\tilde{\varkappa}_n/n!)\, (g\sqrt{-t})^n \} < 0 \tag{25}$$

If instead of keeping t fixed , one takes the limit $-tY \to \infty$, $|t|^{1+\epsilon}Y \to 0$, g_o can be explicitly calculated : $g_o = 1/2\varkappa_2$. Therefore

$$|\mathrm{Im}\, T_\theta(ab \to ab)/\mathrm{Im}\, T_o(ab \to ab)| \underset{\substack{-tY \to \infty \\ |t|^{1+\epsilon} Y \to 0}}{\leq} \exp(Yt/8\varkappa_2) \tag{26}$$

Eq. (26) implies a lower bound for the Pomeron slope:

$$\alpha_P' \geq 1/8\varkappa_2 \tag{27}$$

Notice that the higher order cumulants do not appear in (26). It can be shown that when one takes the limits indicated in eq. (26) the regularity condition (17) becomes superfluous.

Kubar-André, Le Bellac and Meunier[12] were recently able to give explicit and physically non-trivial examples of models which saturate the bound (27). It means that this bound cannot be improved without making additional hypotheses.

5. Charge exchange.

Consider a reaction involving the exchange of electric charge E:

$$a(E=0) + b(E=0) \Rightarrow c(E=-1) + d(E=+1) \tag{28}$$

The formalism of the preceding section has the advantage of being directly applicable to the case of exchange of a discrete quantum number. In analogy to the eq. (4) of sect. 4 we have now

$$|\mathrm{Im}\, T_\theta(ab \to cd)| / |\mathrm{Im}\, T_0(ab \to ab)\ \mathrm{Im}\, T_0(cd \to cd)|^{\frac{1}{2}} \leq \sum_X \{P(ab \to X)\ P(cd \to R_\theta X)\}^{\frac{1}{2}} \tag{29}$$

With each event $a + b \to X$, we associate the following two functions:

$Z_T(y)$ = the transverse momentum transfer across y (as in sect. 4)

$Z_E(y)$ = the electric charge transfer across y

The corresponding quantities for the reaction $c + d \to R_\theta X$ are respectively denoted by $Z'_T(y)$ and $Z'_E(y)$. One easily verifies that

$$\begin{aligned} Z'_T(y) &\approx Z_T(y) - \sqrt{-t} \\ Z'_E(y) &\approx Z_E(y) - 1 \end{aligned} \tag{30}$$

The zero-frequency amplitudes of $Z_T(y)$ and $Z_E(y)$ are respectively denoted by η_{To} and η_{Eo}. We introduce the bivariate characteristic function

$$\Pi(p,q) = \int du\, dw\, e^{ipu + iqw}\, P(\eta_{To} = u,\ \eta_{Eo} = w) \tag{31}$$

which in turn is used to define the bivariate cumulants of (η_{To}, η_{Eo}) :

$$\ln \Pi(p,q) = \sum_{n\, m} (\varkappa_{nm}/n!m!)\ (ip)^n\ (iq)^m \tag{32}$$

In close analogy to the results of the preceding section one finds

$$|\mathrm{Im}\, T_\theta(ab \to cd)| / |\mathrm{Im}\, T_0(ab \to ab)\ \mathrm{Im}\, T_0(cd \to cd)|^{\frac{1}{2}} \underset{\substack{Y \to \infty \\ t \text{ fixed}}}{\leq} e^{Y\gamma(t)} \tag{33}$$

where

$$\gamma(t) = \min_{g\, h} \{ \tfrac{1}{2}tg - \tfrac{1}{2}h + \sum_{\substack{\text{even} \\ n\, m}} (\tilde{\varkappa}_{nm}/n!m!)\ (g\sqrt{-t})^n\ h^m \} < 0 \tag{34}$$

The reduced cumulants $\tilde{\varkappa}_{nm}$ are defined by the equation

$$\varkappa_{nm} = Y^{-(n+m)/2\ +1}\ \tilde{\varkappa}_{nm} \tag{35}$$

The coefficients $\tilde{\varkappa}_{nm}$ with $n \neq 0$, $m \neq 0$ measure the correlation between fluctuations of charge and transverse momentum transfers. Again $\gamma(t) < 0$ because $\Pi(p,q)$ is convex along the imaginary axes in the neighbourhood of the point $p = q = 0$.

Eq. (33) is a bound on the charge exchange component of the inelastic overlap function. One can try to identify the expansion in powers of s of $T_\theta(ab \to cd)$ with the Regge expansion. This is a very natural hypothesis if one adopts a perturbative approach to unitarity, considering the "typical" inelastic states (those which do not involve "abnormally" large rapidity gaps; cf. ref. 1) as the driving force producing the dominant Regge singularities. With this assumption eq. (33) becomes equivalent to the bound

$$\alpha_{CEX}(t) \leq 1 + \gamma(t) \tag{36}$$

where $\alpha_{CEX}(t)$ represents the $\rho - A_2$ trajectory.

As pointed out by Weingarten[13] and confirmed by a more recent analysis[14] there is evidence for the smallness of higher order cumulants of multiplicity distributions. It is very plausible that the coefficients $\tilde{\kappa}_{nm}$, which are very similar objects, exhibit an analogous behaviour. If $\tilde{\kappa}_{nm}$ decrease very rapidly with increasing order, the "best" g and h are approximately given by $g_o \approx 1/2\tilde{\kappa}_{2o}$ and $h_o \approx 1/2\tilde{\kappa}_{o2}$. Thus

$$\gamma(t) \approx - 1/8\tilde{\kappa}_{o2} + t/8\tilde{\kappa}_{2o} - t\tilde{\kappa}_{22}/64(\tilde{\kappa}_{o2}\tilde{\kappa}_{2o})^2 + \ldots \tag{37}$$

In particular, at t=0 and neglecting higher order terms

$$\alpha_{CEX}(t) \leq 1 - 1/8\tilde{\kappa}_{o2} \tag{38}$$

Experimentally, $B_{o2}(y-y') = \langle \zeta_E(y)\zeta_E(y') \rangle$ is well approximated by the expression $B_{o2}(0)\exp(-|y-y'|/\lambda_E)$ with both $B_{o2}(0)$ and λ_E being close to unity. With this input eq. (38) yields $\alpha_{CEX}(0) \leq 0.94$. One is thus led to suspect that the bound (36) is far from being saturated. Perhaps the higher order $\tilde{\kappa}_{nm}$ are important? This cannot be excluded, but is somewhat in variance with what we know about multiplicity cumulants. And also, as pointed out by Grassberger and Miettinen[15], the Cauchy-Schwarz inequality used in deriving the bound would then be far from saturation.

Experience with models indicates that in order to get a realistic $\alpha_{CEX}(t)$ one needs information about phases of the inelastic amplitudes. The importance of phases is also suggested by the difficulty with extending the arguments of this paper to treat the exchange of a multiplicative quantum number, like G-parity. On the other hand, as is well known, the observed intercept of ω is close to that of ρ.

At this point I would like to remark that one should clearly distinguish between the following two questions:

(1) Can one, at least qualitatively, understand the asymptotic features of the Pomeron starting from the observable features of multiple production?

(2) Can one further extend the arguments used to answer the preceding question, so as to actually calculate the parameters of Regge singularities?

The aim of refs. 1-4 was to give a partial and hopefully affirmative answer to the question (1). The answer to the question (2) is presumably negative.

Even if the bound (36) is not saturated, one feature of the function $\gamma(t)$ is likely to be shared by the Regge function $\alpha_{CEX}(t)$: the curvature of $\gamma(t)$ is related to the deviation from Gaussian of the charge and transverse momentum transfer fluctuations. I believe that the observed smallness of the higher order multiplicity cumulants and the observed small curvature of Regge trajectories are closely related phenomena.

The idea of short range order in the structure of inclusive spectra appeared first as an abstraction from the multiperipheral model. This model is also a prototype of LCQN. Therefore one might suspect that the topics reviewed in this paper are merely other aspects of the short range order hypothesis. This would be a mistake. Local compensation of quantum numbers is compatible with the presence of certain long range correlations in the inclusive spectra.

References.

1. A.Krzywicki and D.Weingarten, Phys. Lett. B50 (1974) 265.
2. P.Grassberger, Ch.Michael and H.Miettinen, Phys. Lett. B52 (1974) 60.
3. A.Krzywicki, Nucl. Phys. B86 (1975) 296.
4. D.Weingarten, Rochester preprint UR-505, COO-3065-96 (1974).
5. J.Derré et al., French-Soviet Collaboration, presented at the 17th Int. Conf. on High Energy Physics (London, July 1974).
6. C.Bromberg et al., Rochester-Michigan Collaboration, private communication.
7. R.Hagedorn and J.Ranft, Nuovo Cim. Suppl. 6 (1968) 169.
8. A.Krzywicki, "Cluster oriented approach to multiparticle production" Proc. of the "Colloque sur la Physique Hadronique aux Energies des ISR", (Marseille, November 1973).
9. R.L.Stratonovich, "Topics in the theory of random noise", Gordon & Breach (London).
10. R.Peccei, Phys. Lett. B51 (1974) 274.
11. L.Van Hove, Rev. Mod. Phys. 36 (1964) 655.
12. J.Kubar-André,M.Le Bellac and J.L.Meunier, Nice preprint N TH 75/3
13. D.Weingarten, Nucl. Phys. B70 (1974) 501.
14. E.DeWolf,J.J.Dumont and F.Verbeure, Brussels preprint IIHE-74.3
15. P.Grassberger and K.Miettinen, CERN preprint TH-1979

IMPACT PARAMETER STRUCTURE OF MULTI-BODY PROCESSES

C. Michael

Department of Applied Mathematics and

Theoretical Physics,

University of Liverpool, U.K.

ABSTRACT

Estimates of the impact parameter structure of many body production processes can be obtained from exclusive data on the transverse momentum distribution. Applications have been made to diffraction dissociation, proton anti-proton annihilation and n-body final states in K^-p interactions.

Résumé

Des estimations de la structure en paramètre d'impact des processus de production multiple peuvent être obtenues à partir de données exclusives en impulsion transverse. Des applications ont été faites à la dissociation diffractive, à l'annihilation proton anti-proton et aux états finaux dans les interactions K^-p.

Impact parameter is conjugate to transverse momentum, so that experimental information on the transverse momentum distributions allows, via the uncertainty principle of quantum mechanics, bounds to be put on the average impact parameter. Such lower limits (of the form $\langle b^2 \rangle > \langle p_\perp^2 \rangle^{-1}$) will be close to saturation provided (i) the dependence on $p_\perp$ is gaussian (ii) the phase variation of the amplitude with p_+ is less rapid than the dependence on the modulus. Such lower limits have been extended to many body production reactions [1]. A simplified version of such an extension is to identify [2] $p_\perp$ as the transverse momentum transfer between hemispheres. In practice it is found that the limits derived for the overall (average) impact parameter b_L from the experimental data on the $p_\perp$ distributions are about one half of the expected values. This difference is to be ascribed mainly to the unobservable phase variations. If these phase effects are similar in all reactions, then the relative impact parameter limits can be used to compare the relative impact parameter structure of different reactions.

Some applications are (i) to the diffraction dissociation region of phase space for $pp \to pp\pi^+\pi^-$ from 7 to 200 GeV/c, where the lower limits b_L are found [3] to be $\sim$ 0.5 fm and larger than the limits for similar non-diffractive events. This implies that diffraction dissociation is at least as peripheral as elastic scattering. (which has $\bar{b} \sim 0.6$ fm).

(ii) to a comparison [2] of $\bar{p}p \to n\pi$ with $\bar{p}p \to \bar{p}p(n-2)\pi$ at 4.6 and 9.1 GeV/c. The lower limits b_L are found to be consistently smaller for the annihilation channels than for non-annihilations. This is in conflict with the simple identification of $\bar{p}p$ annihilation to mesons as accounting for the sole difference between $\bar{p}p$ and pp interactions, since the latter difference is known to be very peripheral ($\sim$ 1.2 fm) from data on $\bar{p}p$ and pp elastic scattering.

(iii) to a comparison [4] of various n-body channels in K^-p interactions at 10 and 16 GeV/c. When careful account is taken of large angle effects, the lower limits show a systematic decrease with increasing n. It is harder to translate this to a result on the average impact parameters for increasing n since the phase corrections might become relatively stronger or weaker as n varies.

References

1. B. R. Webber, Phys. Letters 49B, 474 (1974).
2. Liverpool - Stockholm Collaboration (private communication).
3. B. R. Webber et al, Cavendish preprint HEP 75/5 (1975).
4. M. Counihan (private communication).

HELICITY STRUCTURE OF THE TRIPLE-REGGE FORMULA

N. Sakai* and J. Uschersohn**

Rutherford Laboratory, Chilton, Didcot, OXON, England

*Address after September 1975: Department of Physics, Tohoku University Sendai, 980 Japan.

**On leave of absence from the Department of Theoretical Physics, University of Lund

Abstract : The triple-Regge vertex depends in general on five variables: besides the squared Reggeon masses t, t_1 and t_2 there are two others ϕ_1 and ϕ_2 which give information on the helicity structure of the states X in the exclusive reactions $a + b \rightarrow c + X$. Together with t, they give also the spin content of X.

We show how to obtain the functional dependence of the triple-Regge vertex on its arguments using experimental data on the density matrix elements for the exclusive reactions and summing over the reactions.

We show that all three limits i.e. the triple-Regge, the helicity-pole and the combined limit are obtainable in this way, but only the triple-Regge limit carries full information on the spin and helicity structure of the states X.

We find that if the triple-Regge vertex depends only on t, t_1 and t_2 then the t-channel helicity is conserved in $a + b \rightarrow c + X$. On the other hand, we show that only a flat trajectory is allowed if the s-channel helicity is conserved for all states X which are dual to it.

The full account of the contribution is published in Nucl. Phys. B92 (1975) 507.

HADRONIC INTERACTIONS IN BAG MODELS

EUAN J. SQUIRES
Department of Mathematics
University of Durham
Durham, U.K.

Abstract : We consider how the interaction between two hadrons can be evaluated if the hadrons are made of non-interacting quarks confined by a boundary condition.

Résumé : Nous examinons comment l'interaction entre deux hadrons peut être évaluée si les hadrons sont faits de quarks sans interaction soumis à une condition aux limites.

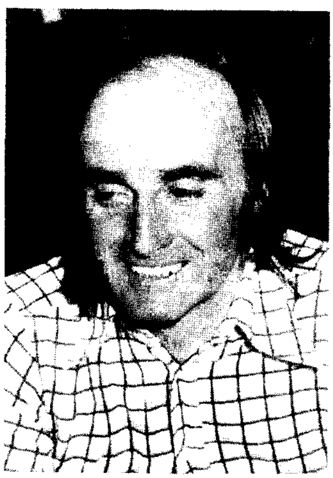

HADRONIC INTERACTIONS IN BAG MODELS

In the old-fashioned quark model the quarks are assumed to be strongly interacting particles, their mutual interactions being responsible for the binding of quarks to form hadrons. The interaction between these hadrons is then due to the quark-quark interactions and by quark counting a satisfactory qualitative description of hadron interactions is obtained. This scheme however is incompatible with the evidence from deep inelastic probes which suggests that the quarks behave as non-interacting point particles.

In "bag" models[1)], on the other hand, the quarks do not have strong interactions, so there is no difficulty in seeing them as free point objects. In this case the strong interactions between hadrons arise from the boundary conditions. In principle these interactions involve no free parameters so if we can calculate them we have a crucial test of the model. In this note we attempt such a calculation and discuss some of the difficulties which arise.

We restrict ourselves at first to one-dimension bags. Here it is easy to see the interaction of two bags by following what happens when they collide[2)]. In fig. 1, at $t = t_1$, we have two identical bags moving towards each other with velocities $-v_o$ and $+v_o$ respectively. At $t = 0$ these bags collide. What happens then can be determined from the conditions that the lengths measured along $(t \pm x)$ remain constant[1)]. Clearly this leads uniquely to the situation shown in fig. 1 up to $t = 2a\ (1 + v_o)^{-1}$. At this time there is an ambiguity[2)]; the bags could stick together and oscillate - perhaps to part at a later time. We ignore this possibility and let the bags move apart as shown. Note that in our case of idential bags it is not determined whether the bags have in fact passed through each other or whether they have bounced back. However if we draw a corresponding figure for bags of different lengths it becomes clear that they do in fact move through each other. This is important in what follows.

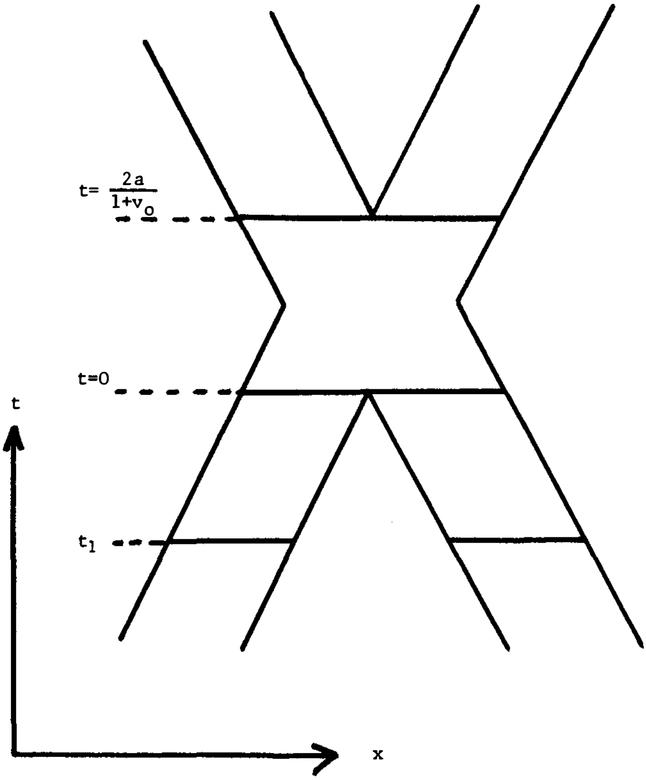

Fig. 1 : Showing a collision between two one-dimensional bags.

Inspection of fig. 1 shows that the time taken for the bags to move through each other is less than it would be if they had not interacted - thus we have an attractive interaction between them. Unfortunately we do not know how to attach an unambiguous meaning to the 'position' of either bag in the time interval $0 < t < 2a(1+v_o)^{-1}$ so we cannot calculate the velocity of the bags as a function of time. However, from the time taken we can calculate any average of the inverse of the relative velocity, i.e.

$$\frac{2a}{1+v_o} = \int_{-a}^{+a} \frac{dx}{2v} \qquad (1)$$

where 2v is the relative velocity.

To use this to calculate an average of the interaction potential V, we put

$$\frac{1}{2}\frac{M}{2}(2v)^2 = \frac{1}{2}\frac{M}{2}(2v_o)^2 + V \qquad (2)$$

where M is the nucleon mass.

Then

$$\frac{2a}{1+v_o} = \int_{-a}^{+a} \frac{dx}{(4v_o^{\,2} + \frac{4V}{M})^{\frac{1}{2}}} \qquad (3)$$

The potential is seen to be velocity dependant (of course we should only consider small v_o in this non-relativistic treatment). In the limit of low velocity

$$4a = M^{\frac{1}{2}} \int_{-a}^{+a} \frac{dx}{V^{\frac{1}{2}}} \qquad (4)$$

Thus, if we assume that V is a square well, we obtain a depth of 0.25M. In three dimensions we actually need a square well potential with a depth about one-fifth of this. However we are sufficiently close to encourage further effort.

To try to be more realistic we note the following obvious defects of this calculation:

(A) Since we intend to use the potential V in a Schrödinger equation we have a curious mixture of <u>classical</u> bags and <u>quantum mechanics</u>.

(B) We have worked only in one space dimension.

(C) A square well potential is probably unrealistic.

(D) We have ignored spin and isotopic spin. In particular the basic bag model[3)] does not distinguish between a Δ and a nucleon - how can it therefore hope to get the deuteron right?

We treat these points in turn.

A. Ideally we need a consistent quantum-mechanical treatment of the whole system but we do not know how to give this. We can easily see that a purely 'classical' treatment is inadequate. To do this we must consider the bag equations in more detail than was necessary above.

We assume the bag contains complex fields which satisfy

$$\frac{\partial^2 \phi}{\partial x^2} - \frac{\partial^2 \phi}{\partial t^2} = 0 \tag{5}$$

inside the bag;

$$\phi = 0 \tag{6}$$

and $$N \quad \left|\frac{\partial \phi}{\partial x}\right|^2 - \left|\frac{\partial \phi}{\partial t}\right|^2 = 2B \tag{7}$$

on the surface of the bag. Here N is the number of fields ('quarks') in the hadron, i.e. for a nucleon N=3. Presumably these are three different 'colours' in a coloured quark scheme but this is irrelevant here. For each field we take the ground state solution

$$\phi = \frac{e^{ikt}\,(e^{ikx} + e^{-ikx})}{(2a)^{\frac{1}{2}}} \tag{8}$$

where $k = \frac{\pi}{a}$. This corresponds to a bag with fixed ends at $x = \pm\, ^a/_2$, and we have normalised to one particle for each field. Using the non-linear boundary condition (7) we find

$$a = \left[\frac{2\pi N}{B}\right]^{1/2} \tag{9}$$

The mass of the bag is given by

$$\begin{aligned} M &= 2\ Ba \\ &= 2\ (2\pi\, B)^{1/2}\ N^{1/2} \end{aligned} \tag{10}$$

If we take M as the nucleon mass and N-3 we determine the bag constant and the value of a. This is the classical nucleon bag. We can also put six quarks into a bag (all in the ground state) and calculate the "classical deuteron". It has binding energy given by

$$
\begin{aligned}
V_o &\equiv 2M_3 - M_6 \\
&= M(2 - 2^{1/2}) \simeq 0.59M\,. \qquad (11)
\end{aligned}
$$

Apart from the fact that this has too large a binding energy, it is a bad approximation to the deuteron since it represents a state where the two nucleons have effectively zero separation whereas we know that the true deuteron wave function spreads out over a distance larger than the range of nuclear forces. We have endeavoured to allow for this by finding an effective potential and solving a Schrödinger equation. One could of course object to a treatment in which we solve two three-body problems classically and then obtain a solution to the six-body problem by solving a two-body Schrödinger equation. One reason why this might not be too bad an approximation is that there is not likely to be much excitation into two (or more) body states which are not colour singlets; the mechanism that prevents hadrons splitting into coloured objects will presumably be operative here[1].

B. In principle the calculation which we have done for one-dimensional bags could be done for three dimensions. Indeed we can consider the scattering at different impact parameters and thereby evaluate V as a function of separation. We are attempting to do this calculation but have not made any significant progress.

One exact thing which can be said is that if we regard a as the diameter of the nucleons and consider zero impact parameter then the fig. 1 holds up to $t = \frac{2a}{2(1+v_o)}$ even in three dimensions. This follows since the points on the spheres opposite to the point of impact cannot know about the collision till they intersect the light-cone passing through the collision point. In the zero velocity limit, apart from the perturbation due to the collision, no parts of the nucleons away from the line of centres will have come into contact. It is therefore intuitively unlikely that we can regard this time as the half-way point of the collision (as it is in one-dimension) and we therefore guess that (4) gives an overestimate for the depth of the potential.

The calculation leading to the binding energy of the classical six quark system, i.e. eq.(11), can easily be done in three dimensions. Using the results of ref.[3] for spinor quarks we find

$$V_o = M(2 - 2^{3/4}) \doteq 0.32M \tag{12}$$

Since this is smaller than the value given in (11) it appears that going from one to three dimensions takes us in the right direction.

C. We speculate that the classical binding energy gives a good approximation to the depth of the potential at zero separation (x = o). Then we know two things about the potential and can determine something about its shape. To this end we put

$$V(x) = V_o(1 - \frac{x}{a})^{2p}, \quad 0 < x < a. \tag{13}$$

We use the three-dimensional value (eq.12) for V_o and substitute in (4). This gives

$$\lambda\ (2 - 2^{3/4}) = \frac{1}{4(1-p)^2} \tag{14}$$

where λ (> 1) allows for the fact that the one-dimensional calculation of the 'average' overestimate its depth. If we put $\lambda = 1$ we obtain p = ·12. This gives a deuteron binding energy of 125MeV; or, to obtain the correct answer we need a potential reduced by a factor about 1/5.

To see the effect of changing λ we suppose that the "average" of the potential is reduced by the same factor as the 'central' potential in going from one to three dimensions, i.e. by the factor $\frac{0.32}{0.59}$. This leads to p = 0.35 and a binding energy of 70 MeV. The average potential would need reducing by a factor about two to obtain the correct answer.

D. To study this problem we need a model for the difference between the Δ and the N. The simplest possibility is to assume a small, spin-and/or isotopic-spin-dependent interaction between the quarks. For example if we take an interaction potential A $(\sigma_1.\sigma_2 + \tau_1.\tau_2)$, assumed constant over a distance of the order of the deuteron radius, and fit A to the N-Δ mass difference, we find that the deuteron binding energy decreases by 30 MeV. By changing the form of the spin dependance we can easily increase or decrease this value and in any case this calculation presumably overestimates its effect since the quarks in the deuteron are further apart than in the N and Δ.

Conclusion.

There are many uncertainties but grounds for hoping that if we really understand the problem we might obtain the right result.

Many of the considerations in this article are the result of discussions with Mr. G.T.Fairley[4].

References.

1. A.Chodos, R.L.Jaffe, K.Johnson, C.B.Thorn and V.F.Weisskopf, Phys. Rev. 9. 3471 (1974.
2. T.T.Wu, B.M.McCoy and H.Cheng, Phys. Rev. 9. 3495 (1974).
3. A.Chodos, R.L.Jaffe, K.Johnson and C.B.Thorn, Phys. Rev. 10, 2599 (1974).
4. G.T.Fairley and E.J.Squires, "The Deuteron in a Bag Model of Hadrons", University of Durham Preprint, 1975.

DOES IT MATTER THAT THE A_1 DOES NOT EXIST ?

G.L. KANE
Physics Department
University of Michigan
Ann Arbor, Michigan 48104

Abstract : In this talk I review some arguments for expecting axial vector mesons (especially the A_1) to exist, summarize the (now rather compelling) evidence that the A_1 does not exist, and discuss what some consequences might be for the quark model, for chiral symmetry, and several other areas of particle physics.

Résumé : Dans cet exposé, je rappelle quelques arguments pour l'existence des mésons axiaux (spécialement le A_1), présente l'évidence que le A_1 n'existe pas et discute les différentes conséquences possibles pour le modèle des quarks, la symétrie chirale et plusieurs autres domaines de la physique des particules.

It is a fruitful and basic part of the lore of high energy physics that particle states are associated with interactions. This view has its origins in the identity of photon exchange with electromagnetic interactions, and in Yukawa's pion.

It now appears that this is not the situation for axial vector currents. The main axial vector state, the A_1, which would naively be expected, seems not to exist experimentally.

In this talk I want to : 1) briefly review the reasons for expecting certain axial vector states to exist (chiral symmetry, quark model, exchange degeneracy,...), 2) summarize the (now rather compelling) evidence against the existence of the A_1, 3) tentatively explore some implications of the absence of the A_1 for sum rules, the quark model, ν reactions, etc. 4) comment briefly on SU(3) related axial vector states (Q,D,H).

1. REASONS FOR EXPECTING AXIAL VECTOR PARTICLES

a) At a qualitative level, we see evidence of vector interactions, such as the electromagnetic current, the weak vector current and CVC, and large exchange contributions of the appropriate quantum numbers in hadron two body reactions.

And, we have vector particles $\rho,\omega,\phi,\ldots$

Similarly, for the axial vector we have the weak axial vector current and PCAC. It is certainly justifiable to expect axial vector meson states.

b) Chiral Symmetry Clearly nature shows evidence for some sort of chiral symmetry. It is reasonable to expect some implications for the spectrum of vector and axial vector mesons, and presumably some sort of symmetry in the particle spectra. The accepted answer since 1967 has been in terms of the Weinberg sum rules,

$$\int_0^\infty \left[\rho_V(m^2) - \rho_A(m^2)\right] dm^2/m^2 = f_\pi^2$$

$$\int_0^\infty \left[\rho_V(m^2) - \rho_A(m^2)\right] dm^2 = 0$$

The ρ_V and ρ_A are the vector and axial vector spectral functions, and f_π is the pion decay amplitude, present because the axial current is not conserved. Single particle states appear as $\delta(m^2 - m_R^2)$ in the spectral functions. States of definite J^P and isospin are projected out. If these are saturated with ρ and an A_1, one gets $m_{A1} \simeq \sqrt{2}m_\rho$. This corresponds to the mass of the $\pi\rho$ enhancement observed in diffractive $\pi N \to (3\pi)N$ reactions. Thus the theory and data appeared to coincide and the naive expectations appeared fulfilled. I will return below to questions of interpreting the sum rules when axial vector states do not exist.

c) Quark model In the quark model the L = 0 $q\bar{q}$ mesons with S = 0,1 are π and ρ (concentrating on isovectors). With L = 1 one has the B (which exists) with S = 0 and A_2, A_1, and $J^{PC} = 0^{++}$ states with S = 1. Thus here we not only expect A_1, it is somewhat hard to imagine the quark model without it.

d) Exchange degeneracy Consider $\pi^+\rho^+$ scattering, with the ρ having helicity zero in the s-channel. Then only unnatural parity, odd G exchanges will contribute to leading order in s. Since this is an exotic channel it is necessary by the usual arguments of duality to have real partial wave amplitudes. The contribution of π exchange, while real for $t \simeq 0$, will not give real partial wave amplitudes because of its Regge phase. Thus an exchange degenerate exchange with the quantum numbers of the A_1 or the H is expected if these assumptions are approximately correct. There may not be a clean way to decide whether the A_1 must be degenerate with the π in some meson-meson reactions ; if the H does not exist the A_1 is needed, but that may not be a fair argument. If the A_1 is required by the quark model and not by exchange degeneracy, it may be significant.

In any case, an A_1 state is required by the spectrum of dual models (see P. Frampton, Phys. Rev. Lett. 34, 840 (1975)).

2. SUMMARY OF EXPERIMENTAL EVIDENCE (Historical order)

a) Diffractive reactions In diffractive $\pi^{\pm}p \to (3\pi)^{\pm}p$ there is a "bump" in $m_{3\pi}$. In the absence of further information one could assume a resonance. Very early the resonance interpretation was questioned since one could reproduce data with Deck model calculations and especially with Reggeized ones. (Berger, 1968). Chew and Pigniotti suggested that duality implied a resonance even if the Deck model were appropriate, but that is not right because the production amplitude is real while the duality argument applies to the imaginary part of an amplitude.

With the completion of the Illinois partial wave analysis of the 3π system (Ascoli and collaborators), in about 1971 serious doubt was cast on the possibility of a resonance interpretation. They found (Fig. 1) a nice resonant behavior for the A_2, but no apparent phase shift variation for the A_1 partial wave with $m_{3\pi}$. Clearly no simple resonance was present.

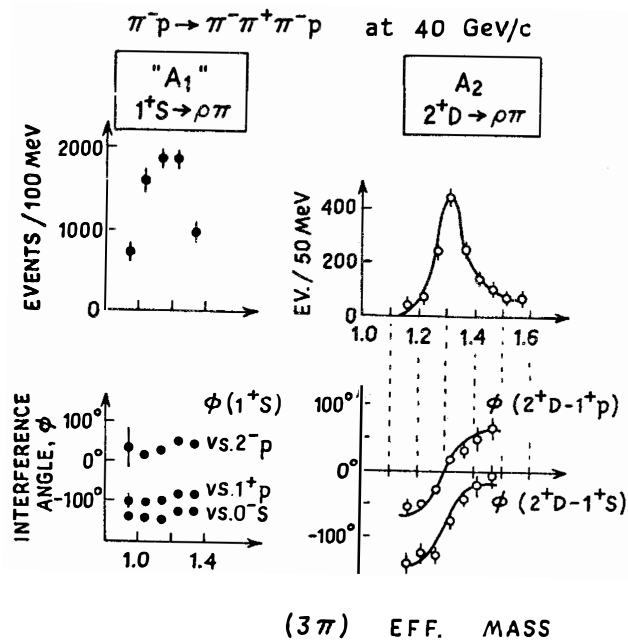

Fig. 1. From the partial wave analysis of Ascoli et al. showing the "A_1" and A_2 partial waves and the relative "A_1" - A_2 phase.

Because of the complicated production dynamics, however, it is not ruled out from the diffractive partial wave analysis that extensive interference with background could mask a resonance. Bowler and Game (Oxford preprint) produced such a model, requiring that $M_{A1} = M_{A2}$ to hide the A_1. In practice, I think an analysis of $\pi\eta$, $k\bar{k}$, $\pi\rho$ modes including t dependence eliminates that interpretation, but the following analysis of non-diffractive production does even better so we turn to it.

b) Non-diffractive production If $A_1 \to \rho\pi$ then it must be possible to produce A_1 as in Fig. 2

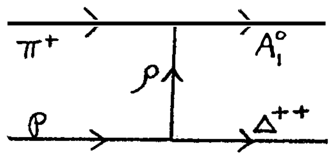

Experimentally this is measured, and now even a partial wave analysis of the 3π system has been performed. The data is from the LBL 7 GeV/c $\pi^+ p \to (3\pi)^\circ \Delta^{++}$ experiment. Fig. 3 shows a mass plot from that experiment, with a clear η, ω, A_2 and with very little room for an A_1. Fig. 4 shows the 1^+ partial wave from the recent analysis of Wagner, Tabak, and Chew. These authors conclude $\sigma(A_1) < 2\mu b$. They find a resonant behavior for the A_2, helping confirm the general validity of these phase shift analyses. They do not have enough 1^+ events to do a real phase shift analysis of the 1^+ partial wave, but the data are consistent with a constant phase shift.

To evaluate the meaning of the above cross section limit we need an estimate of the expected A_1 cross section if the A_1 is real. It is easy to obtain this for Fig. 2. The coupling size and structure at the lower vertex is known from other reactions. At the upper vertex the overall size is determined by the A_1 width (chosen as 150 MeV by Wagner et al. above, so we have used this number). The relative amount of s/d wave coupling can be fixed at pure s-wave or by the SU(6) relation $2(F_1/F_o)_{A1} = 1 + (F_o/F_1)_B$ without much effect on the numbers. Absorption must be included somehow or the final estimates will be too big.

I then expect (presumably accurate to a factor of two or better)

$$\sigma(A_1) \sim 30\ \mu b$$

more than an order of magnitude above the experimental upper limit. Thus, I interpret the data to imply the nonexistence of an A_1 resonance with a width

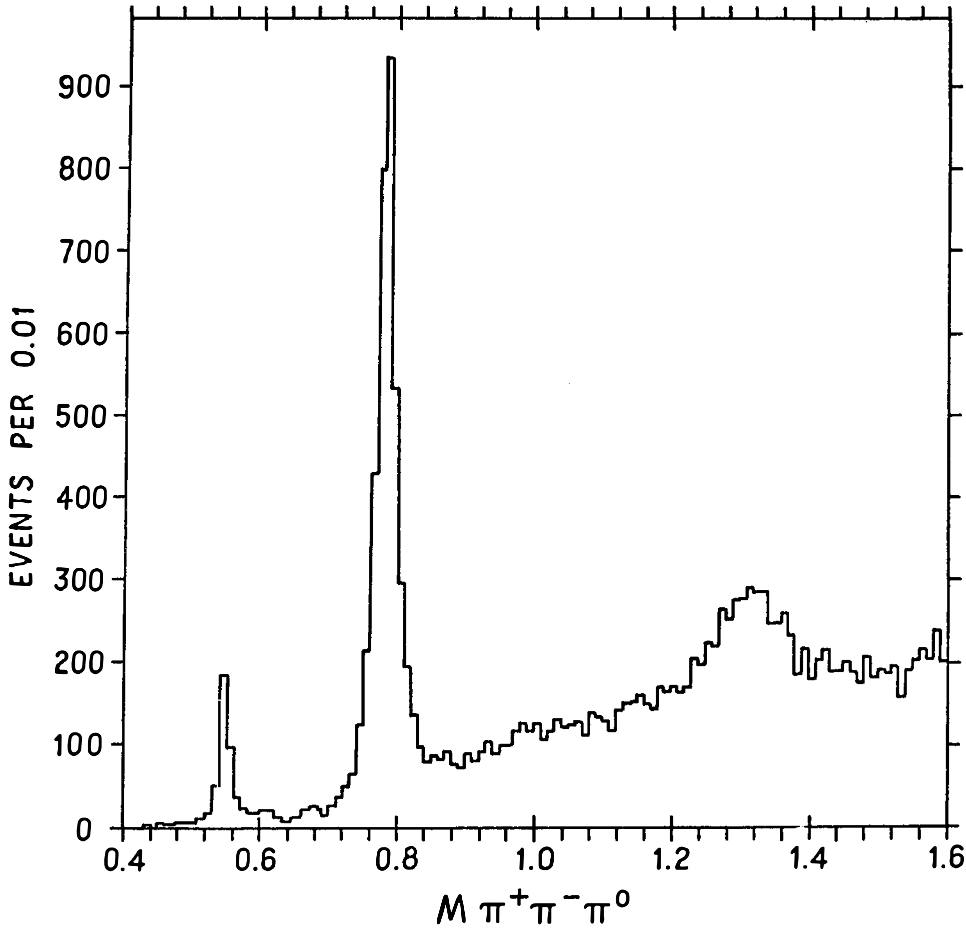

Fig. 3. $\pi^+\pi^-\pi^\circ$ Mass spectrum, showing an A_2 but no A_1 in charge exchange production.

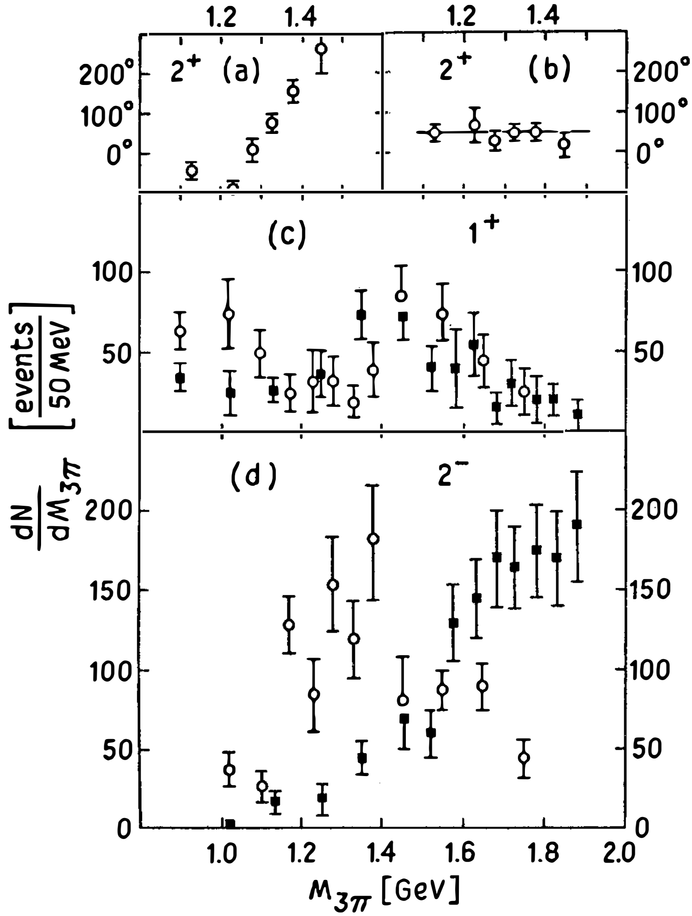

Fig. 4. From Wagner, Tabak and Chew. Shows results of partial wave analysis of 3π system in non-diffractive production. Note part (C) showing number of events that can be associated with an "A_1" resonance.

small compared to its mass and a mass less than about 1800 MeV.

[Aside. My estimate above assumes conventional behavior of amplitudes as functions of s,t. There is an earlier attempt which has been made by Fox and Hey to produce smaller estimates. I do not think it is a valid attempt, but I should mention it for completeness. Basically, they use a current conservation argument due to Kisslinger for vector exchange to introduce an extra factor of t at a meson vertex where mass changes. This then reduces cross section sizes, and they predict $\sigma(A_1)$ = 12 μb for this experiment ; that is surely a lower limit for any estimate. In fact, I think that experimentally the data on B production by ω exchange rules out such a t dependence. Perhaps, the Q crossover also does. Theoretically there is also a compelling argument against their factor, from duality. If such a factor were present,then $\pi^+A_1^\circ \to \pi^+A_1^\circ$ where the A_1 has $\lambda_s = 0$, by an s-channel ρ pole, would have a normal Legendre function forward peak while the ρ exchange u-channel process would have a forward dip from the ad hoc factor of t, so the two views would be qualitatively different, violating duality.]

To summarize : the strongest evidence against the existence of an A_1 resonance is the nondiffractive production data and partial wave analysis. It is consistent with the phase shift analysis of the diffractive data. If the experiments are correct, they have shown that the A_1 is absent with a sensitivity at least one (and perhaps two) order of magnitude below the expected cross section.

Where else can one look to check ? In specific reactions within the next year or so it will be good to check both

$$\pi^- p \to A_1^\circ\, n \text{ (forward)}$$

which can be done in the ANL TST bubble chamber and in the MSU-OSU-ANL $\pi^- p \to (\pi\pi\pi)^\circ n$ experiment at 6 GeV/c, which has preliminary data showing no A_1 signal (M. Abolins, private communication), and

$$\pi^+ p \to pA_1^+ \quad \text{(backward)}$$

which will have results expected from an ANL experiment at 8 GeV/c and particularly an LBL experiment at 4 GeV/c. Confirming that an A_1 is also absent in these reactions will be important in providing confidence that the situation is clear. Photoproduction should also provide a clear place to look eventually.

3. IMPLICATIONS OF THE ABSENCE OF A_1

Considering the importance of the A_1 for several areas of particle physics, its absence presumably has significant implications. We do not know what these implications are. The best we can do so far are some simple observations.

a) Exchanges in 2-body reactions Since exchanges in two-body hadron reactions are associated with particle states, we could look for consistency there. There is, so far, no unequivocal evidence for exchanges with A_1 quantum numbers. The main characteristics of such exchanges would be unnatural parity, and s-channel helicity non-flip at an NN vertex. Various places to look include

(i) in $\pi N \to \rho N$ find a sizeable $\rho^{\circ\circ}_{++}\, d\sigma/dt$ where ρ is the density matrix element for s-channel helicity o for the ρ, which picks out unnatural parity exchange, and the ++ refers to nucleon helicity non-flip.

(ii) in $\pi N \to$ (s-wave $\pi\pi$)N observe significant polarization. This was once reported by Sonderegger et al. but has not been confirmed.

(iii) in a reaction like $0^- 1/2^+ \to 1^- 1/2^+$ or $\gamma N \to \pi N$ the left-right asymmetry on a polarized target and the recoil nucleon polarization will be identical in magnitude if no A_1-like exchange is present.

(iv) the total cross section difference $\sigma_T(++) - \sigma_T(+-)$ for longitudinally polarized proton beams and targets is proportional to the contribution with A_1 quantum numbers.

In the related (but not equivalent) situation of strange particle exchange, Field and collaborators have observed evidence for a small contribution which would under certains assumptions have the quantum numbers of the strange partner of the A_1 (see also section 4).

b) Quark model Presumably the first thing to try for the quark model is to modify mass predictions from their standard values to put the A_1 at a very high mass. It is not easy. One could write

$$M^2 = M_o^2 + M_1^2\, \vec{s}_q \cdot \vec{s}_{\bar{q}} - M_2^2\, \vec{S} \cdot \vec{L}$$

The eigenvalues of $\vec{s}_q . \vec{s}_{\bar{q}}$ are 1/4 for S = 1 and -3/4 for S = 0 (π,B). The eigenvalues of $\vec{S} \cdot \vec{L}$ go as 1,0,-1,-2 for A_2, B, A_1, and 0^+ states. Presumably the A_2 and B masses can be put in. That leaves one free mass. Note the sum rules

$$M_{A1}^2 + M_{A2}^2 - 2M_B^2 = 8M_1^2$$

$$M_o^2 = M_{A1}^2 + (M_{A1}^2 - M_{A2}^2)/2$$

Since M_1^2 is presumably constrained to give the π-ρ splitting too, it cannot allow M_{A1}^2 to get very large, from the first of these. The second tells us that if we wish the scalar meson states in the mass range below the A_2 to have anything to do with quark model 0^+ states than $M_{A1} < M_{A2}$. So far I have not seen any way the quark model spectroscopy can function without an A_1. It is not easy to see how constituent quark models can survive the absence of an A_1 without basic modification.

c) ν Reactions

It is important to note that for exclusive ν reactions the situation is just as has always been naively expected, with the data behaving as if there were a particle dominated axial vector form factor, of the expected strength. The absence of an A_1 does not seem to affect this situation.

Presumably where we should expect an effect is in comparing the processes

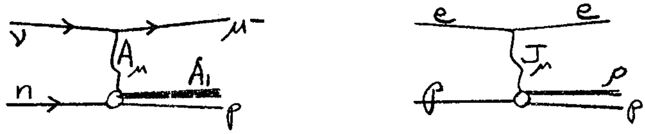

where the ρ production will occur and the A_1 production not. It will be instructive to study the way in which the axial vector current materializes in these processes.

d) Sum Rules

With J. Krisch and M.S. Chen (details will be published separately), I have looked at the Chiral Symmetry sum rules in some detail to see if any hints appear as to how to interpret things. At least, we can make some measure of how bad local saturation with particle states seems to be.

Basically, one can proceed by noting that if sum rules are not saturated by single particle states, the integrands can be written in terms of scattering amplitudes. Essentially,

$$\delta(M^2 - M_A^2) \sim \text{Im} \frac{M\Gamma}{M^2 - M_A^2 - iM\Gamma} \sim \sin^2 \delta_{1+}$$

For example, it could have been that the $\pi\rho$ amplitude had a large imaginary part over a large range in $M_{\pi\rho}$ and so the vector and axial vector sum rules were comparably saturated in the low mass region.

In fact, we can estimate the phase δ_{1^+} from the Illinois analysis. The experiment measures the relative $A_1 - A_2$ phase. The part of the phase due to the production mechanism is approximately the same for A_1 and for A_2, because

(i) By comparison with charge exchange reactions, one can see that isoscalar and consequently even signature exchanges dominate

(ii) The two processes are observed to have similar energy dependence

$$\sigma(A1) \sim P_L^{-0.4\pm0.06}, \quad \sigma(A2) \sim P_L^{-0.51\pm.05}$$

(iii) Whenever an even signature amplitude has a power behavior s^γ it has a phase $e^{-i\pi\gamma/2}$ by crossing and analyticity.

Thus the observed relative $\pi\rho$ phase can be interpreted as due to $\pi\rho$ scattering in the 1^+ and 2^+ partial waves, with the 1^+ phase shift constant at about 20°.

A compact way to summarize the results for sum rules is by defining f_ρ and f_A by

$$\langle\rho|V_\mu|0\rangle = f_\rho \epsilon_\mu^\rho, \quad \langle 3\pi(1^+)|A_\mu|0\rangle = f_A \epsilon_\mu^A$$

and using the sum rules to evaluate f_A, f_ρ. Then one expects $f_A/f_\rho = 1$ if saturation by particles occurs, while we find $f_A/f_\rho \simeq 1/3$. The sum rule contributions go as f^2.

The Chiral Symmetry is not locally satisfied. The V, A currents do not manifiest themselves in similar ways in the sum rules. If the sum rules are satisfied, it is in a way which is not symmetric as far as the low energy parts are concerned.

4. OTHER AXIAL VECTOR STATES

Let us briefly consider what other (I=0 and I=1/2) axial vector states might exist.

For the strange particle (named Q) states there is currently evidence which implies at least one state is present, but the total evidence is sufficiently inconsistent so that one does not know what to conclude. Q enhancements have been observed in $\pi^- p \rightarrow (K\pi\pi)^\circ \Lambda$ (BNL experiment), in $\bar{p}p$ annihilations, in backward reactions. But a recent CERN charge exchange experiment (Otter et al., CERN/D.Ph.II/Phys. 74-10) has not observed any clear signal in $K^- p \rightarrow (K\pi\pi)^\circ n$. No inconsistency is implied ; e.g., perhaps $Q \rightarrow K^* \pi$ and $Q \not\rightarrow \rho K$ so only K^* and not ρ exchange will produce Q's. Such a result would imply some subtle SU(3) relations. The situation is not easily interpreted.

Another possible 1^+ state is the D meson, with $M_D = 1290$ MeV, $\Gamma_D = 30$ MeV, and $K\bar{K}\pi$ and $\eta\pi\pi$ decays. There is no doubt of a D signal in several experiments. It has I=0, G = +, so it would have to be in an SU(3) multiplet with the A_1 (not the B). Indeed, it has been advanced as an argument for the A_1 to exist that the D does (assuming the D really has $J^P = 1^+$).

I think the answer to this argument is in terms of the notion of "Accidental Particles" introduced by Dashen and myself. Basically, the idea is that some particles (e.g. $\pi, \rho, N, \Delta, \ldots$) will exist for "fundamental" reasons (e.g., the quark model or bootstrap, or whatever). Once these exist, strong forces act between them, and occasionally rearrange the density of states in some channels, producing a resonance, an "accidental particle". Averaged over 200-300 MeV there is no net increase in the number of states because the rise of the phase shift through $\pi/2$ is compensated by a decrease back to zero. The deuteron is a very good example of this. One then expects because of SU(3) breaking in the basic multiplets that the accidental particles will not generally come in complete SU(3) multiplets. For example, the deuteron is bound by the strong long range π exchange force, while the forces due to heavier K, η exchanges are not strong enough to bind the other members of a deuteron multiplet. Probably for hadrons the main forces are strongly coupled inelastic channels.

Consider the axial vector isoscalar state D and H(G = -1) from this point of view. For the D (ignoring strange particle and baryon channels) one has πA_2, ηf, $\rho\rho$, $\omega\omega$ channels coupled, and $\pi A_2 \rightarrow f\eta$, $\pi A_2 \rightarrow \rho\rho$, $\rho\rho \rightarrow \omega\omega$ are all strongly coupled by π exchange. On the other hand, for the H only $\pi\rho$ and $\eta\omega$ are coupled and they are not coupled by a long range π exchange force. Thus, it is much more probable that the D should exist as a result of the strong interactions than that H should, and that is what is observed. If this viewpoint is basically correct then the existence of the D does not have implications for the A_1.

SUMMARY

The evidence is now convincing that no A_1 (axial vector) state exists experimentally, at levels of sensitivity one-two orders of magnitude better than what is expected. This certainly has serious implications for our interpretation of hadrons and their interactions, but it is rather unclear what these implications are. The physical interpretation of Chiral Symmetry will have to change, and the constituent quark model will require serious modification if it is to remain a valid approach.

REFERENCES

S. Weinberg, Phys. Rev. Lett. 18, 507 (1967)

Yu. M. Antipov *et al.*, Nuc. Phys. B63, 141 (1973), 153 (1973)

E.L. Berger, Phys. Rev. 166, 1525 (1968)

G. Ascoli *et al.*, Phys. Rev. D8, 3894 (1973)

G.L. KANE, Quasi-two Body Reactions and Properties of Resonances, ANL Symposium on Resonance Production, March 1974.

M.G. Bowler and M.A.V. Game, Oxford Preprint

F. Wagner, M. Tabak and D.M. Chew, LBL-3395, submitted to Phys. Lett.

G.C. Fox and A.J.G. Hey, Nuc. Phys. B56, 386 (1973)

R. Dashen and G.L. Kane, Phys. Rev. 11D, 136 (1975)

R. Field *et al.*, Phys. Rev. D6, 1863 (1972)

M.S. Chen, J. Krisch and G.L. Kane, in preparation.

A STATIONARY PHASE APPROACH TO HIGH ENERGY HADRONIC SCATTERING*

H. FRIED

Brown University, Providence, R.I. 02912

and

H. MORENO

Centro de Investigación del IPN

Apartado Postal 14-740; México 14, D.F.

In this note we will consider high energy hadronic scattering as described by a simplified theory involving nucleons ψ, neutral vector mesons W_μ and scalar pions π interacting via a Lagrangian density L':

$$L' = -ig\overline{\psi}\gamma_\mu W_\mu \psi - \frac{1}{2}\lambda\pi W_\mu W^\mu$$

g and λ are coupling constants and the metric is such that $W_\mu W_\mu = \vec{W}^2 - W_o^2$.

We will see how in the high energy limit one may expect several simple features to emerge and how a nice relationship between elastic and inelastic scattering can be established. All this will be possible due to the use of the stationary phase technique of approximation to some of the general expressions that will be derived.

All the time-ordered Green's functions of the theory may be obtained by functional derivation of the time-ordered generating functional

$$Z(j,k_\mu,\eta,\overline{\eta}) = <(e^{i\int\left[j\pi+k\cdot W+\overline{\eta}\psi+\overline{\psi}\eta\right]})_+>$$

One can prove that the form of Z for the case at hand is

$$<S>Z = \exp\{i\int\overline{\eta}G\left[-i\frac{\delta}{\delta k}\right]\eta + \mathrm{Tr}\,\ln\,(1+g\gamma\cdot\frac{\delta}{\delta k}S_c)\}\ .$$

$$\cdot \exp\left\{ i/2 \int k \cdot \bar{\Delta}_c \left[-i \frac{\delta}{\delta j} \right] k - \frac{1}{2} \mathrm{Tr}\, \ell n \left(1 - i\lambda \frac{\delta}{\delta j} \Delta_c\right) \right\} \cdot$$

$$\cdot \exp\left\{ i/2 \int j\, D_c\, j \right\}$$

where

$$G[A] = S_c \, (1 + ig\gamma \cdot A\, S_c)^{-1}$$

$$\bar{\Delta}_c[\pi] = \Delta_c \, (1 + \lambda \pi \Delta_c)^{-1}$$

S_c, $\delta_{\mu\nu}\,\Delta_c$ and D_c are the free-field nucleon, vector meson and pion propagators, respectively. $G[A]$ and $\bar{\Delta}_c[\pi]$ are the nucleon and vector meson propagators in the presence of arbitrary external c-number sources A and π. $\langle S \rangle$ is the normalizing vacuum to vacuum amplitude.

Considering now only graphs of the following type for elastic nucleon-nucleon scattering:

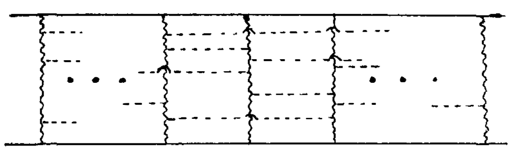

= nucleon line

= neutral vector meson line

= pion line

and approximating the nucleon propagators by Bloch-Nordsieck[1] (no-recoil) Green's functions one may easily arrive to the eikonal representation of the amplitude[2]

$$T(s,t) = \frac{is}{2m^2} \int d^2b\ e^{i\vec{q}\cdot\vec{b}}\ (1 - e^{i\chi(\vec{b},s)})$$

with m = mass of nucleon

$$s = -(p_1 + p_2)^2$$

$$t = -(p_1 - p_1')^2 = -\vec{q}^{\,2} < 0$$

$|\vec{b}|$ = impact parameter of collision

$$p_1 + p_2 = p_1' + p_2'$$

and

$$e^{i\chi} = \exp\left(-i/2 \int \frac{\delta}{\delta\pi} D_c \frac{\delta}{\delta\pi}\right) \exp\left(ig^2 \int F_1 \bar{\Delta}_c(\pi) F_2\right)\Big|_{\pi=0}$$

where

$$F^{\mu}_{1,2}(x) = p^{\mu}_{1,2} \int_{-\infty}^{\infty} d\xi\ \delta(x - z_{1,2} + \xi p_{1,2})$$

z_1 and z_2 are any two points along the two lines of motion of the nucleons, so that $\vec{b} = (\vec{z}_1 - \vec{z}_2)_\perp$.

In terms of T the elastic differential cross section is

$$\frac{d\sigma_{e\ell}}{dt} = \frac{m^4}{\pi s^2} |T|^2$$

The optical theorem states

$$\sigma_T = \frac{4m^2}{s} \text{ Im } T(s,t=0) = 2 \text{ Re} \int d^2b \; (1 - e^{i\chi})$$

where σ_T = total cross section.

One very easily finds the elastic cross section $\sigma_{e\ell}$:

$$\sigma_{e\ell} = \int d^2b \; |1 - e^{i\chi}|^2$$

Hence, by unitarity

$$\sigma_T = \sigma_{e\ell} + \sigma_{in}$$

where σ_{in} = inelastic cross section; so that

$$\sigma_{in} = \int d^2b \; (1 - e^{-2\rho})$$

$$\rho = \text{Im } \chi .$$

One can also prove that the inelastic pion production in the region where all the meson momenta are small (pionization region) compared to the nucleon momenta (so that the approximation of the nucleon propagators by Bloch-Nordsieck forms is still good) is given by[3]

$$\sigma_n = \frac{1}{n!} \int d^2b \; \left(i \frac{\delta}{\delta \pi'} D_+ \frac{\delta}{\delta \pi}\right)^n e^{F^+[\pi']} e^{F[\pi]} \Big|_{\pi'=\pi=0}$$

where σ_n is the total inelastic cross section for the production of n pions; D_+ = on mass shell pion propagator; and

$$e^{F[\pi]} = e^{-i/2\int \frac{\delta}{\delta\pi} D_c \frac{\delta}{\delta\pi}} e^{ig^2\int F_1\bar{\Delta}_c[\pi]F_2}$$

So that

$$e^{F[\pi]}\Big|_{\pi=0} = e^{i\chi}$$

One can introduce now the so-called particle partition function defined by

$$\sigma_{in}(z) = \sum_{n=1}^{\infty} z^n\sigma_n$$

which is seen to be

$$\sigma_{in}(z) = \int d^2b \left(e^{iz\int \frac{\delta}{\delta\pi'} D_+ \frac{\delta}{\delta\pi}} -1\right) e^{F[\pi]} e^{F^+[\pi']}\Big|_{\pi=\pi'=0}$$

We now make use of the folbwing identity:[4]

$$c_{\pm}e^{-1/2\ \mathrm{Tr}\ln B} e^{\pm i/2\int jB^{-1}j} = \int d[\chi]\ e^{i\int j\chi \mp i/2\int \chi B\chi}$$

To represent

$$e^{F[\pi]} = c_+^{-1} e^{-1/2\mathrm{Tr}\ln D_c} \int d[\phi] e^{-i/2\int\phi K\phi} e^{\int\phi \frac{\delta}{\delta\pi}} e^{F[\pi]}$$

where

$$KD_c = 1$$

$$F[\pi] = ig^2 \int F_1 \bar{\Delta}_c[\pi] F_2$$

Changing the functional integration from ϕ to $\phi' = \phi - \pi$ and using the identity once more one arrives to:

$$e^{F[\pi]} = (c_+c_-)^{-1} e^{-1/2 \mathrm{Tr}\ln D_c}\, e^{-1/2 \mathrm{Tr}\ln K} \int d[\phi]\, d[\alpha]\, e^{i\int \alpha(\phi-\pi)} \cdot$$

$$\cdot\, e^{i/2\int \alpha D_c \alpha}\, e^{F[\phi]}$$

We can also use the complex conjugate to represent $e^{F^+[\pi']}$. As π and π' appear only linearly one can easily find:

$$e^{iz\int \frac{\delta}{\delta\pi'} D_+ \frac{\delta}{\delta\pi}}\, e^{F^+[\pi']} e^{F[\pi]}\Big|_{\pi=\pi'=0} =$$

$$= |c_+|^{-2}\, e^{-1/2 \mathrm{Tr}\ln D_c}\, e^{-1/2\ \mathrm{Tr}\ln D_{\bar{c}}} \cdot$$

$$\cdot \int d[\phi]\, d[\chi]\, e^{F[\phi]} e^{F^+[\chi]} e^{-i/2\int \phi K \phi}\, e^{iz\int (\chi K) D_+ (K\phi)} \cdot$$

$$\cdot\, e^{i/2\int \chi K \chi}$$

In order to arrive to this form one uses the fact that $KD_+ = 0$. So far no approximations have been made, apart from the basic ones leading to eikonal forms.

At this point we use physical intuition. Since ϕ and χ in the last equation represent c-number pion fields under which the vector mesons propagate we will assume that at high energies, when many particles are produced on the average, the functional integration is dominated by some semiclassical value(s) of the pion fields. Naturally this is the source of the idea that a stationary phase approximation is appropriate.

Following this idea we define:

$$G[\phi] \equiv iz \int (\chi K)\, D_+(K\phi) - i/2 \int \phi K \phi + F[\phi] =$$

$$= G[\phi_o] + \frac{\delta G}{\delta \phi_o} (\phi-\phi_o) + \frac{1}{2} (\phi-\phi_o) \frac{\delta^2 G}{\delta\phi_o \delta\phi_o} (\phi-\phi_o) + \ldots.$$

The stationary phase condition reads:

$$\left.\frac{\delta G}{\delta \phi}\right|_{\phi_o} = 0 = iz \int (\chi K)\, D_+ K - iK\phi_o + \left.\frac{\delta F}{\delta \phi_o}\right|_{\phi=\phi_o}$$

Since χ and ϕ are pion fields we will take for granted that they are solutions of second order differential equations; so that they possess at most simple poles on the mass shell. If so; the action of D_+K on (χK) is zero and the stationary phase condition reads:

$$K\phi_c = -i \left.\frac{\delta F}{\delta \phi}\right|_{\phi=\phi_o}$$

Hence ϕ_o is independent of z.

One can now use the functional integral identity to integrate on ϕ, and repeating the stationary phase approximation on χ one arrives finally to

$$e^{iz\int \frac{\delta}{\delta\pi'} D_+ \frac{\delta}{\delta\pi}} e^{F^+[\pi']} e^{F[\pi]} \doteq |e^{\tau[\phi_o]}|^2 \, e^{iz\int (\phi_o^+ K) D_+ (K\phi_o)}$$

where

$$\tau[\phi_o] = F[\phi_o] - i/2\int \phi_o K\phi_o - 1/2 \, \mathrm{Tr}\, \ell n \, (1+iD_c \frac{\delta^2 F}{\delta\phi_o \delta\phi_o})$$

Moreover if z=0 it is clear that $\tau[\phi_o] = i\chi$ in the stationary phase approximation; and for z=1 unitarity imposes the condition

$$2\rho = i \int (\phi_o^* K) \; D_+ \; (K\phi_o)$$

So that we have derived

$$\sigma_{in}(z) = \int d^2b \; e^{-2\rho}(e^{2z\rho} - 1)$$

and this equation we expect to be true independently of what ρ is. We may go one step further and conjecture that the equation should be true regardless of the specific field-theoretic model we used to find it. We see several interesting features emerge:

1) The final equation provides a link between elastic and inelastic processes in a unitary-preserving fashion. As a matter of fact if the elastic scattering at high energies is purely imaginary ρ is the only quantity determining both elastic and inelastic scattering.

2) The final equation is of the same form as that provided by the simplest unitary models of Aviv, Blankenbecler and Sugar;[5] where the basic mechanism is the exchange of a complicated object

between the colliding particles accompanied by (at most) one single pion emission.

We can expect thus that at high energies this will be the predominating mechanism and more complicated processes, such as the emission of more than one pion from every chain, to be merely small corrections at asymptotic energies.

We hope to investigate further consequences of the stationary phase approximation in the near future, as well as rigorous conditions for its validity.

In the meantime, since its predictions in this simple case are in accord with what physical intuition indicates, we believe that it is a good approximation technique at high energies.

One of us (H.M) is grateful to Prof. TRAN THANH VAN for his warm hospitality at the Rencontre and to the Secretaria de Comunicaciones Y Transportes of Mexico for Travel Support.

REFERENCES

1.- F. Bloch and A. Nordsieck; Phys. Rev. 52, 54 (1937).

2.- H.M. Fried; Functional Methods and Models in Quantum Field Theory. MIT Press (1972). (See in particular Chapter 9).

3.- H.M. Fried, Nuclear Physics B73, 93 (1974).

4.- H.M. Fried, Functional Methods and Models in Quantum Field Theory. MIT Press (1972). (See Appendix K)

5.- R. Aviv, R.L. Sugar and R. Blankenbecler, Phys. Rev. D5, 3252 (1972).

IMPACT PARAMETER REPRESENTATION
WITHOUT HIGH-ENERGY, SMALL-ANGLE LIMITATION

by

M.M. ISLAM

Service de Physique Théorique
Centre d'Etudes Nucléaires de Saclay
BP n°2 - 91190 Gif-sur-Yvette
France

and

Department of Physics
University of Connecticut
Storrs, Connecticut, U.S.A.

Abstract

Using Watson-Sommerfeld transform the impact parameter representation of the scattering amplitude is shown to be valid for all physical energies and scattering angles. It is also shown how the direct channel Regge poles enter in the impact parameter amplitude.

1. Introduction

Phenomenologically it has become clear that the impact parameter or Fourier-Bessel (FB) representation provides us an effective tool to explore high-energy scattering. This has been well reflected at this meeting by the fact that several speakers have used the impact parameter description in connection with their work. The traditional derivations of this representation based on using approximate Schrödinger wave functions, modifying propagators in Born series expansion, and summing infinite sets of Feynman diagrams[1,2] indicate that the representation can be used only for high-energy small-angle scattering. So from phenomenological point of view it is of considerable interest to us to find out whether the representation can be extended to high-energy large-angle scattering, and thus furnish information on hadronic interactions at small distances.

Of course, in discussing the FB representation of the scattering amplitude a dynamical question has to be faced by us ; namely -How do the energy levels of the interacting system (that is, the bound states and resonances occurring in various partial waves) must enter in the FB amplitude ? Since the theory of complex angular momentum tells us that these energy levels are represented by Regge poles, so the question becomes : How do Regge poles enter in the construction of the FB amplitude ?

We now attempt to find answers to the questions raised above.[3]

2. FB representation from Watson-Sommerfeld transform

We first show how a FB representation can be derived without any approximation from the partial wave expansion :

$$T(s,y) = \frac{W}{p} \sum_{n=0}^{\infty} (2n+1)\, P_n(1-2y^2)\, a_n(s) \tag{2.1}$$

In Eq.(2.1) we have used the variable $y = \sin\frac{\theta}{2}$ instead of $z = \cos\theta$ ($z = 1-2y^2$). The physical region corresponds to $s = W^2$ greater than threshold and $0 \leq y \leq 1$ ($0 \leq \theta \leq \pi$). Using the formula

$$P_n(1-2y^2)\, \theta(1-y) = \int_0^{\infty} \beta\, d\beta\, J_o(\beta y)\, \frac{J_{2n+1}(\beta)}{\beta} \tag{2.2}$$

in Eq.(2.1), we obtain immediately the FB representation :

$$T(s,y) = \frac{W}{2p} \int_0^{\infty} \beta\, d\beta\, J_o(\beta y)\, h_1(s,\beta) \quad , \quad (0 \leq y < 1) \tag{2.3}$$

where

$$h_1(s,\beta) = 2 \sum_{n=0}^{\infty} (2n+1)\, \frac{J_{2n+1}(\beta)}{\beta}\, a_n(s) \tag{2.4a}$$

$$= \frac{2p}{W} \int_0^{1} y\, dy\, J_o(\beta y)\, T(s,y) \tag{2.4b}$$

The FB integral (2.3) with the FB amplitude (2.4) reproduces the scattering amplitude exactly for $0 \leq y < 1$, and in fact is the result of Cottingham and Peierls[4]. However, the representation (2.3) is very non-unique[5]. This can be seen simply by adding to $h_1(s,\beta)$ another term $h_2(s,\beta)$ of the form

$$h_2(s,\beta) = \int_1^{\infty} y'\, dy'\, J_o(\beta y')\, \lambda(s,y')$$

where $\lambda(s,y)$ is arbitrary. The new FB amplitude will reproduce the same scattering amplitude for $y < 1$ since

$$\int_0^{\infty} \beta\, d\beta\, J_o(\beta y)\, h_2(s,\beta) = \int_1^{\infty} dy'\, \delta(y-y')\, \lambda(s,y') = 0$$

Uniqueness of the FB amplitude is of course essential, if the FB representation is to be physically meaningful. So we examine now how an exact unique FB representation can be established.

The above non-uniqueness of the FB amplitude occurs because we started from the partial wave expansion, and did not specify the scattering amplitude in the unphysical region $1 < y < \infty$ ($-1 > z > -\infty$). Had we required $h_2(s,\beta)$

to be such that its FB transform not only vanished for $0 \leq y < 1$, but also reproduced the correct scattering amplitude for $1 < y < \infty$, then it would have been uniquely fixed. To determine $h_2(s,\beta)$ we therefore need to specify $T(s,y)$ in the unphysical region. We do this by Watson-Sommerfeld transform[6] which defines the scattering amplitude in the whole range $-\infty < z < -1$:

$$T(s,y) = -\frac{1}{2\pi i} \frac{W}{p} \int_C d\ell \, a(\ell,s)(2\ell+1) P_\ell(2y^2-1) \frac{\pi}{\sin\pi\ell} . \quad (2.5)$$

Clearly, if we had a FB representation of $P_\ell(2y^2-1)$ for $\infty > y > 1$ and $\mathrm{Re}\,\ell > -1$, then we could insert it in Eq. (2.5) and write $T(s,y)$ in the form

$$T(s,y) = \frac{W}{2p} \int_0^\infty \beta \, d\beta \, J_0(\beta y) \, h_2(s,\beta) \quad ; \quad (\infty > y > 1) \quad (2.6)$$

$h_2(s,\beta)$ would then be determined automatically as a contour integral over $a(\ell,s)$.

There is, however, mathematical difficulty in carrying out the above program. To see this simply, let us suppose a direct channel Regge pole exists, so that for large y $T(s,y)$ behaves as $y^{2\alpha(s)}$. To reproduce this asymptotic power behavior, $h_2(s,\beta)$ in (2.6) has to be highly singular at $\beta = 0$ $(h_2(s,\beta) \sim \beta^{-2(\alpha+1)})$. But if $h_2(s,\beta)$ is too singular, then the FB integral (2.6) does not exist. The way around this difficulty is to consider $h_2(s,\beta)$ as a distribution, such that when its FB transform is taken, it reproduces the scattering amplitude $T(s,y)$ given by the Watson-Sommerfeld transform[7].

Once $h_2(s,\beta)$ is obtained, we can combine Eqs. (2.3) and (2.6) to write our final result as

$$T(s,y) = \frac{W}{2p} \int_0^\infty \beta \, d\beta \, J_0(\beta y) \, h(s,\beta) \quad (2.7)$$

for $\infty > y \geq 0$, where

$$h(s,\beta) = h_1(s,\beta) + h_2(s,\beta) \quad (2.8)$$

Equation (2.7) provides an exact unique FB representation. The part $h_1(s,\beta)$ of the FB amplitude determines the scattering amplitude in the physical region $(0 \le y < 1)$ while the part $h_2(s,\beta)$ determines it in the unphysical region $(1 < y < \infty)$. It is the determination of $h_2(s,\beta)$ [3] that has removed the non-uniqueness of the FB amplitude.

3. Direct-channel Regge pole contribution to the FB amplitude

We examine now how the ℓ-plane analyticity properties of the partial wave amplitude $a(\ell,s)$ enter in the FB amplitude $h(s,\beta)$. For this purpose, let us express $h_1(s,\beta)$ given by Eq.(2.4a) as a contour integral in the complex ℓ-plane :

$$h_1(s,\beta) = -2 \sum_{n=0}^{\infty} (2n+1) \frac{J_{2n+1}(\beta)}{\beta} \frac{1}{2\pi i} \int_C d\ell \frac{a(\ell,s)(2\ell+1)}{(\ell-n)(\ell+n+1)} \quad ; \qquad (3.1)$$

that this indeed coincides with (2.4a) can be checked by simply collapsing the contour on the real axis. The advantage of writing h_1 in the above form is that displacing the contour C away from the real axis exposes the poles and cuts of $a(\ell,s)$, and contribution from any singularity of $a(\ell,s)$ to $h_1(s,\beta)$ can be explicitly obtained. Thus a Regge pole term $r(s)/(\ell-\alpha(s))$ in $a(\ell,s)$ gives the following contribution to $h_1(s,\beta)$:

$$h_1^R(s,\beta) = -2 \sum_{n=0}^{\infty} (2n+1) \frac{J_{2n+1}(\beta)}{\beta} \frac{r(s)\ (2\alpha+1)}{(\alpha-n)(\alpha+n+1)} \quad . \qquad (3.2)$$

The FB amplitude $h_2(s,\beta)$ can also be expressed as an integral of $a(\ell,s)$ in the ℓ-plane over the contour C. So contributions from singularities of $a(\ell,s)$ to $h_2(s,\beta)$ are obtained as for $h_1(s,\beta)$ by simply displacing the contour C .

4. Concluding remarks

From eq.(2.7) we conclude that an exact unique FB representation exists valid for all physical energies and scattering angles $(0 \le \theta \le \pi)$. The basic assumption we have put in is that the partial wave amplitude is analytic around the positive real axis in the ℓ-plane (in other words, we have the Watson-Sommerfeld transform). This assumption is now on a firm footing [6]. So we may regard the impact parameter representation as an exact tool no longer limited by any high-energy, small-angle approximation.

One may wonder why we feel as a tool the impact parameter representation will provide us insights into the phenomenology of hadronic interactions. The obvious reason of course is that at high energies we expect optical description and geometrical features to emerge as indeed exhibited by the ISR data on pp elastic scattering, and such ideas are best expressed by the impact parameter language[8].

I like to add one further reason using the Coulomb scattering as an illustration. Here we notice the small b behavior determining the bound states and also controlling the high-energy behavior in t-channel[5,9], so that we have schematically

Regge pole
phenomenology

bound states
in s-channel

high-energy behavior
in t-channel

small b behavior
in s-channel

In contrast to Regge poles, it is the impact parameter amplitude that retains the knowledge of 1/r dependence of the Coulomb interaction through its small b behavior. It is likely that in other cases also the FB amplitude provides more basic insight.

Acknowledgement

The author wishes to thank his colleagues in Saclay for the warm hospitality extended to him.

References

[1] - "Lectures in Theoretical Physics", edited by A.O. Barut and W.E. Brittin (Colorado University Press, 1972), vol.XIV A .

[2] - H.M. Fried, "Functional Methods and Models in Quantum Field Theory" (MIT Press, 1972).

[3] - For mathematical details and a more comprehensive treatment, see M.M. Islam, Saclay preprint DPh-T. 74/97 (1974).

[4] - W.N. Cottingham and R.F. Peierls, Phys. Rev. 137, B 147 (1965) ; T. Adachi and T. Kotani, Prog. Theor. Phys. Suppl. (Extra n°) p.316 (1965).

[5] - M.M. Islam, in "Lectures in Theoretical Physics", edited by A.O. Barut and W.E. Brittin (Gordon and Breach, 1968), vol.X B, p.97.

[6] - P.D.B. Collins and E.J. Squires, "Regge Poles in Particle Physics" (Springer Tracts in Modern Physics, 1968), vol.45.

[7] - Using subtracted dispersion relation in the momentum transfer variable t, Kupsch and Stamatescu (Nuovo Cimento 15A, 663 (1973)) have also concluded that the FB amplitude has to be a distribution at the origin.

[8] - Proceedings of the Eighth and the Ninth Rencontre de Moriond, edited by J. Tran Thanh Van.

[9] - E. Brézin, C. Itzykson and J. Zinn-Justin, Phys. Rev. D1, 2349 (1970) ; M. Lévy and J. Sucher, Phys. Rev. D2, 1716 (1970).

HOW TO LEARN ABOUT HADRON DYNAMICS FROM AN UNDERLYING QUARK-GLUON FIELD THEORY

GLENNYS R. FARRAR
California Institute of Technology
Pasadena, California 91125 (USA)

Abstract: A solution is proposed to the problem of how physics can be abstracted from a fundamental quark-gluon field theory for hadrons, without having solved the problem of confinement.

Résumé: On propose une solution au problème qui consiste à extraire certaines propriétés physiques des hadrons d'une théorie des champs fondamentale des quarks et des gluons sans avoir à résoudre le problème du confinement.

HOW TO LEARN ABOUT HADRON DYNAMICS FROM AN UNDERLYING QUARK-GLUON FIELD THEORY

There is ample evidence that the quark model has something to do with nature, as shown by the success of its predictions for current algebra, hadron spectroscopy and the large t behavior of form factors. However, the problem of actually constructing a theory which has fundamental quark and gluon fields, and yet insures that only hadrons are observed, remains unsolved. Evidently, promiscuous use of low-order perturbation theory to learn about hadron dynamics is a mistake, since that neglects the complicated coherent processes that necessarily are present and responsible for confinement. A question thus presents itself: Can we formulate a prescription as to when perturbation theory may be legitimately used? That is, is there a class of phenomena in which the physics responsible for confinement does not modify beyond recognition the results of low-order perturbation theory?

I wish to present a possible answer, or partial answer, to that question. However, it must be stressed that without having solved the problem of confinement, the validity of my proposal cannot be proved theoretically. From a theoretical standpoint, the important issues therefore are its self-consistency, reasonableness, and attractiveness. Experiment is the best test of its validity.

In order to be specific I will choose what seems to me to be the most likely candidate for a correct field theory of the hadrons - a non-abelian Yang-Mills theory of quarks and vector gluons with an exact SU(3) color symmetry. This theory possesses the desirable feature that the effective quark-gluon coupling vanishes logarithmically as the momenta-squared of the quarks and gluon become large and spacelike. Furthermore, the interaction of very soft gluons is so singular that it is conceivable that an infrared catastrophe insures confinement. I will go further and imagine that the quark-gluon coupling is small even for momentum transfers (q^2) of the order of 1 GeV^2, and is only effectively large if very soft processes are occurring[1)].

Thus we should expect that perturbation theory would be a useful tool for studying processes that selectively probe regimes of small coupling, for instance large momentum transfer scattering (inclusive or exclusive), or reactions necessarily involving quarks of very dissimilar momenta, such as massive lepton pair production (e.g., $pp \to \ell^+\ell^- + X$) or the propagation of fast secondaries through nuclear material. In what follows I will discuss each of these in turn, facing the issue of when binding effects "factorize" and do not significantly modify the perturbation theory results, and when they are crucial. An application of perturbation theory which I will not discuss is to the dynamics of bound states of very heavy quarks. For instance it has been conjectured that, assuming the ψ is a $c\bar{c}$ bound state, its relative narrowness is due to a decrease in the quark gluon coupling as the quark mass increases[2]. Although similar in spirit, that is not the same as the assumption of importance to us.

Let us begin, as a simple illustration, with the pion form factor at large q^2 which is written in terms of Bethe-Salpeter wave functions as:

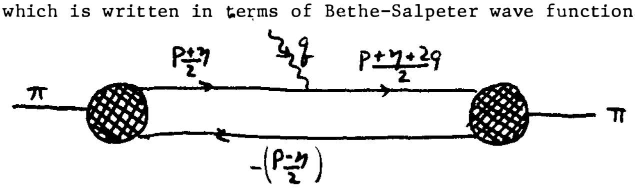

Since $p^2 = (p+q)^2 = m_\pi^2$, at least one of $(\frac{p+\eta}{2})^2$, $(\frac{p-\eta}{2})^2$ or $(\frac{p+\eta+2q}{2})^2$ is of order q^2. In general the Bethe-Salpeter wave functions are not computable, nor will they be until we have solved the problem of confinement. They must therefore be taken to be unknown functions. However, the wave function for those very improbable configurations in which one of the quarks has an invariant mass much larger than any natural length scale <u>is</u> computable from perturbation theory. Let us introduce some terminology: the "normal" part of the wave function is that part in which the quarks have finite momenta-squared, of the order of some characteristic hadronic mass scale such as m_ρ^2; the "exceptional" part of the wave function involves at least one quark whose momentum-squared is very large on that scale. In terms of infinite momentum wave functions, the normal part has both constituents carrying a finite fraction x, $0 < x < 1$, of the total momentum and having limited transverse momentum; the exceptional part involves either large transverse momenta or x not in the range $0 < x < 1$. Given the normal wave function ψ_N, [] the exceptional part ψ_E [] can be computed from perturbation theory:

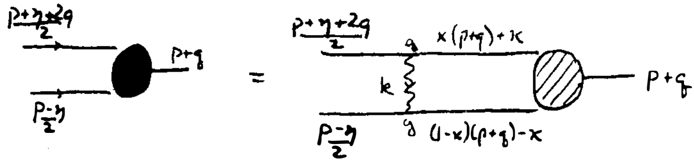

If $\eta \sim xp$ so that $(\frac{p+\eta+2q}{2})^2 \sim q^2$, then $k^2 \sim q^2$ so that our ansatz of g being small applies. As mentioned above, this procedure can only be proved to be legitimate when detailed information on the properties of ψ_N at large distances is known. The necessary conditions on ψ_N are discussed in detail in Ref. 3.

Thus the calculation of the large q^2 pion form factor amounts to evaluating:

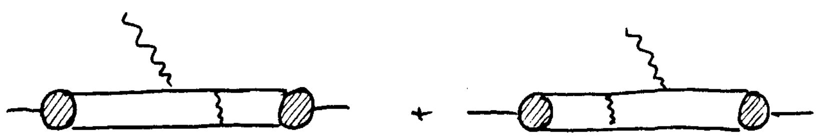

The q^2 dependence is completely determined, independent of details of the normal wave functions. One finds modulo logarithms[4)] $1/q^2$ for the pion, and for the proton $G_E(q^2) \sim G_M(q^2) \sim \frac{1}{q^4}$, consistent with experiment as discussed in Ref. 3. In fact, this prediction of the power with which the leading form factor decreases is not specific to the choice of a non-abelian gauge theory; it is the same in any renormalizable field theory with small coupling constant for $q^2 > 1\ \mathrm{GeV}^2$. However the result that G_E/G_M scales, as appears to be the case experimentally, follows only in a theory with vector gluons[3)].

In the form factor examples, binding simply generates the normal wave function and makes no serious modification to the power law, assuming the wave function is reasonably well behaved. However, if we wish to discuss hadron-hadron scattering the problem is somewhat more complex. Shown below are two possible lowest order diagrams for pp → pp scattering:

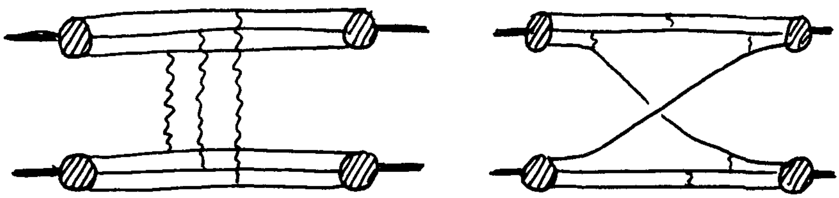

Only gluons carrying large q^2 are shown, and all wave functions shown are "normal." As pointed out by Landshoff[5)], the three-gluon exchange diagram is dominated by the configuration in which each gluon carries almost exactly one third of the total momentum transfer, and gives an asymptotic (large s, θ_{cm} fixed) behavior $\frac{d\sigma}{dt}(pp \to pp) \sim \frac{g^{12}}{s^8} f_1(\theta)$. All diagrams involving at least one $q\bar{q}$ pair in the t channel[6)], such as the one on the right above, give $\frac{d\sigma}{dt}(pp \to pp) \sim \frac{g^{20}}{s^{10}} f_2(\theta)$. If the effects of binding can be ignored here, so that perturbation theory can be used, we would expect that the three gluon exchange diagram would dominate. Experimentally that is clearly not the case. The ratio of theory to experiment with three gluon exchange varies by nearly three orders of magnitude between θ_{cm} of 30° and 90°[7)]. Furthermore a simple fit to the energy dependence suggests $s^{-9.7 \pm 0.5}$ [8)].

What is the explanation for this? I propose that it is simple. Binding modifies our field theory diagrams in precisely one way - it replaces free quarks, antiquarks, and gluons by hadrons in each physical channel, as required by dispersion theory. If that can be accomplished without additional large momentum transfers, then the field theory result for that diagram is unmodified. If not, then I argue that the diagram as written does not contribute and the additional large momentum transfer interactions necessary to give physical particles in the s,t and u channels must be explicitly included. We have no evidence of the existence of hadrons which consist exclusively of "hard" glue (epoxyons), at least for masses less than about 2 GeV^2. In fact, the narrowness of the ψ, if it is a $c\bar{c}$ state, can be "explained" as due to the absence of any vector epoxyon through which it could mix with a $u\bar{u}$, $d\bar{d}$ or $s\bar{s}$ state and hence to ordinary hadrons. The reason that such states appear not to bind or at least couple very weakly to ordinary hadrons is in this approach an unexplained mystery of the confinement mechanism, which while nice to understand, need not be understood in order to analyze large $p_\perp$ scattering [9].

I propose then that the expected confinement mechanism eliminates Landshoff's diagram, at least at present values of t, leaving those with at least $q\bar{q}$ or qqq in each channel[10]. It is easily seen that all remaining allowed diagrams give the asymptotic behavior[3] (modulo logarithms)

$$\frac{d\sigma}{dt} \sim s^{2-n} f(\theta) \quad , \tag{1}$$

where n is the total number of elementary fields in the initial and final states, including photons, leptons and quarks (e.g., for pp scattering n = 12). This is the same result obtained by dimensional analysis if $s^{-1/2}$ is the only length scale in the problem[3,11]. Equation (1) can be generalized to 2 → N scattering such as $\pi N \to \pi\pi N$ and scattering of hadrons with non-zero orbital angular momentum. When applied to eh → eh or $e^+e^- \to h\bar{h}$ one obtains for the spin averaged form factor

$$F_h(t) \sim \frac{1}{t^{n_h - 1}} \; , \tag{2}$$

where n_h is the minimum number of elementary fields in hadron h.

These dimensional scaling laws are in good agreement with available data[3]. Nonetheless it is very difficult over the measured ranges of s and t to experimentally rule out modified exponentials, etc. A more stringent test of the validity of this use of perturbation theory, which also specifically checks whether the non-abelian color gauge theory is the correct underlying field theory, is the angular dependence of large s and t elastic scattering. While the scaling behavior, eq. (1), is independent of the details of the normal wave function, the angular dependence in general is not. However, it is often the case that the quark scattering amplitude is sharply peaked at the configuration in which the momenta of the hadrons are evenly shared by their constituents, e.g., in which the q and $\bar{q}$ of a pion each carry half the pion momentum[12]. If that is generally true, then the angular dependence of high energy wide angle elastic scattering will be insensitive to details of the normal wave functions and thus computable[13].

The analysis of large $p_\perp$ inclusive scattering is more difficult than for elastic scattering because the minimal quark scattering diagrams are not so easily identified. Some of the possible diagrams for $pp \to \pi + X$ are shown below.

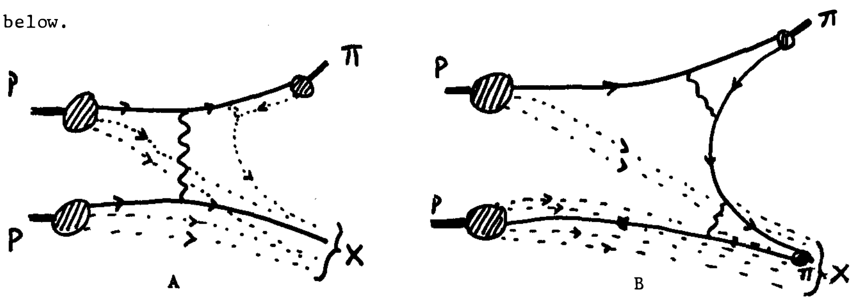

Quark, antiquark and gluon lines which are involved in the large momentum transfer are solid; "spectator" lines are dotted. Call M the amplitude for the minimal high $p_\perp$ scattering; then $E d\sigma/d^3p \sim \frac{1}{s^2}|M|^2$. Direct computation[3] shows that $M \sim \sqrt{s}^{\,4-n}$, where n is the number of quarks and antiquarks in the minimal large $p_\perp$ scattering. In diagram (A) $qq \to qq$ is the minimal large $p_\perp$ scattering so that $n = 4$ and $M \sim g^2$, giving $E d\sigma/d^3p \sim g^4/p_\perp^4\ f(\theta,x)$[14]; in diagram (B) which has $q\bar{q} \to \pi\pi$ as the minimal process, $M \sim g^4/s$ so that $E d\sigma/d^3p \sim g^8/p_\perp^8\ f(\theta,x)$. Naive application of perturbation theory without considering the effects of binding indicates that the $qq \to qq$ subprocess (diagram (A)) should dominate. It is certainly not dominant experimentally[15].

This can be qualitatively accounted for by requiring physical hadrons in each channel. In particular the t channel in case (A) can be shown to require a gluon carrying a large fraction of the t channel momentum. While it is well known that roughly half a proton's momentum is carried by glue, there is no evidence that any individual gluon carries a substantial fraction of the momentum. In fact, the absence of excited baryons with the additional degrees of freedom implied by "valence glue" is evidence that known hadrons do not contain fast gluons. (This is not surprising in view of the absence of other exotic states such as $q\bar{q}q\bar{q}$. The more natural expectation is for the gluon distribution to resemble that of antiquarks, which is only non-negligible at very small momenta. If we assume that intermediate states in the s,t and u channels which require a gluon to carry an asymptotically finite fraction of the momentum are not physically allowed, then $qq \to qq$ is not a possible minimal subprocess and $Ed\sigma/d^3p$ falls faster than $p_\perp^{-4}$. Whether $p_\perp^{-8}$ is the leading allowed power is not yet known. A detailed analysis of the energy, angle, and particle species dependence of inclusive scattering data is underway[13)] which will provide additional tests of these ideas.

We have assumed above that the elementary quark-gluon coupling is inherently small unless very soft processes are occurring, and have seen that we thereby obtain a reasonable picture of large $p_\perp$ scattering. Presumably low $p_\perp$ strong interactions are due to the multiple soft interactions of quark and antiquark constituents of hadrons which have small relative momenta and large effective couplings. Quarks which have large relative momenta may be assumed to interact very weakly. Thus any hadronic process which selectively involves fast quarks should be amenable to analysis. Two examples are the nuclear size (A) dependence of large $p_\perp$ or $p_\parallel$ inclusive scattering and massive lepton pair production in high energy hadron-hadron collisions.

From our analysis of large $p_\perp$ scattering we have learned that it is well described as resulting from a few hard scatterings of constituents, rather than multiple soft scatterings. Thus to obtain a hadron of large $|P_{cm}|$

requires a q or $\bar{q}$ from each initial hadron which has cm momentum $\geq |P_{cm}|$. Similarly to create a lepton pair of large invariant mass $\sqrt{Q^2}$ at rest in the cm, requires a q and $\bar{q}$ of cm momentum $\sqrt{Q^2}/2$. Thus if $|P_{cm}|$ and $\sqrt{Q^2}/2$ are large, the quarks and antiquarks involved will interact only very weakly with the rest of the hadronic material. Thus in each case we expect an A dependence which is A^1 (no shadowing) rather than the $A^{2/3}$ (shadowing) which is seen at low $|P_{cm}|$ or low $\sqrt{Q^2}/2$. The value of $|P_{cm}|$ or $\sqrt{Q^2}/2$ at which the A^1 dependence takes over can be estimated as follows[16]: If the incident particle is a proton of cm momentum P, consider its three fast valence quarks. These three bare quarks may be written as a superposition of baryons, e.g., p and N^* (plus higher states which we will truncate) by cleverly arranging their phases. As they propagate their relative phases change, since they have different masses. After a distance z, the relative phase is

$$\phi_{N^*} - \phi_p = \left[\frac{m_{N^*}^2}{P} - \frac{m_p^2}{P}\right] z \quad .$$

When the relative phase becomes large, say > 1 radian, the three fast quarks have evolved into a state which no longer looks like three bare quarks but instead looks like hadrons. That is, the three fast quarks have grown a "tail" of quarks, antiquarks and glue with which they can interact hadronically. Thus if P is such that in a distance z, $\phi_{N^*} - \phi_p < 1$, the fast quarks will interact very weakly (usually not at all) within that distance z. The diameter in the cm of a nucleus of atomic number A is $D \approx A^{1/3}/m_\pi P$. Hence requiring $|\Delta\phi| < 1$ for $z < D$ gives

$$[P/1.3 > A^{1/3}/m_\pi P] \quad . \tag{3}$$

For typical nuclei $A^{1/3} \sim 4$ so $P \approx 6$ GeV/c. Since the valence quarks in a proton typically carry 1/6 - 1/3 of the momentum, we may deduce that quarks having $P^q_{cm} > 1$-2 GeV/c will not be shadowed. Thus processes involving lepton pairs with $\sqrt{Q^2}/2 > 1$-2 GeV or pions of $|P_{cm}| > 1$-3 GeV/c will have no shadowing. The latter has been observed experimentally two ways: Cronin et al.[17], measure the A dependence, parameterized by $A^{n(p_\perp)}$ of the inclusive cross section for π's produced at 90° in the cm and $\sqrt{s} \approx 23$ GeV. Their results for $n(p_\perp)$ are shown in Fig. 1.

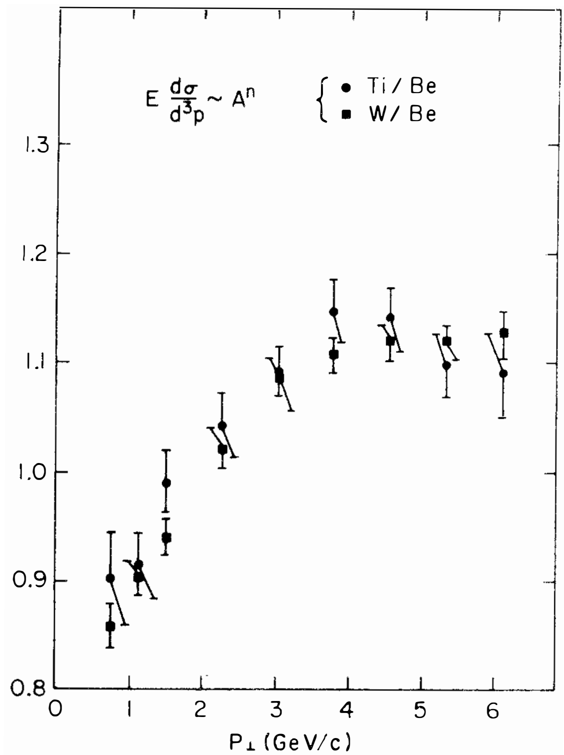

Fig. 1: The A dependence of high $p_\perp$ pion production at $p_{lab} = 300$ GeV/c and $\theta_{cm} = 90°$ taken from Ref. 17.

The qualitative agreement with our result is remarkable. However our discussion does not explain why $n(p_\perp)$ should become larger than 1, as is observed. Possible reasons for this are discussed in Ref. 16. The second observation is that the multiplicity of particles produced forward in the cm in p-nucleus collisions is independent of A[18], as expected from our argument but far from obvious in conventional Glauber models[19]. No measurement has been made of the A dependence of $pp \rightarrow \mu^+\mu^- + X$.

We can use our analysis of quark propagation through nuclear matter to decide when the Drell-Yan model[20] for massive lepton pair production is applicable. In that model the virtual photon is produced by the annihilation of a q from one initial hadron with a $\bar{q}$ from the other:

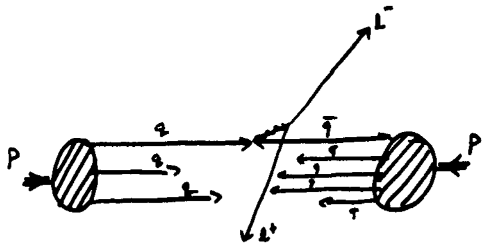

The cross section is:

$$\frac{d}{dQ^2 d\xi} = \frac{4\pi\alpha^2}{3Q^4}\left(\frac{1}{x_A+x_B}\right)\left\{\frac{4}{9}\, x_A u_A(x_A) x_B \bar{u}_B(x_B) + \frac{1}{9}\,(u \leftrightarrow d) + \underbrace{\frac{1}{9}\,(u \leftrightarrow s)}_{\text{negligible}} + \text{c.c.}\right\}$$

where $\xi = \frac{2Q_{\parallel}}{\sqrt{s}}$ and $x_A = \frac{1}{2}\left[\xi + \sqrt{\xi^2 + 4Q^2/s}\right]$, $x_B = x_A - \xi$. The $u_A(x)$ is the probability of finding an up quark in hadron A with fraction x of the momentum, etc. Taking eq. (3) with $A^{1/3} = 1$, gives $P^q_{min} \approx .5$-1 GeV. Thus if both $x_A \sqrt{s}/2$ and $x_B \sqrt{s}/2$ are > 1/2 - 1 GeV, the distributions u(x), $\bar{u}(x)$, d(x) and $\bar{d}(x)$ will be just those which are measured in electron and neutrino deep inelastic scattering. Consequently the theory makes a definite prediction if the q and $\bar{q}$ distributions are known. Fig. 2 shows such a prediction (solid line) for $pp \to \mu^+\mu^- + X$ based on a particular (reasonable) guess for the antiquark distributions[21], assuming there are three colors of quarks. Also shown (circles) is the data of Christenson et al.[22], which they extracted from $p + U \to \mu^+\mu^- + X$, assuming essentially that the cross section scales as $A^{2/3}$. The triangles show that data "renormalized" by using the $A^{n(\sqrt{Q^2})}$ dependence from Cronin et al.[17], (Fig. 1) for $\sqrt{Q^2} = 2p_\perp < 4$ GeV and n = 1 for $\sqrt{Q^2} > 4$ GeV. In addition the dotted line shows their data with the new resonances removed[23] and renormalized by the correct A dependence. The prediction of the theory is within about a factor of three of the experiment, which is within the range of the theoretical and experimental uncertainties.

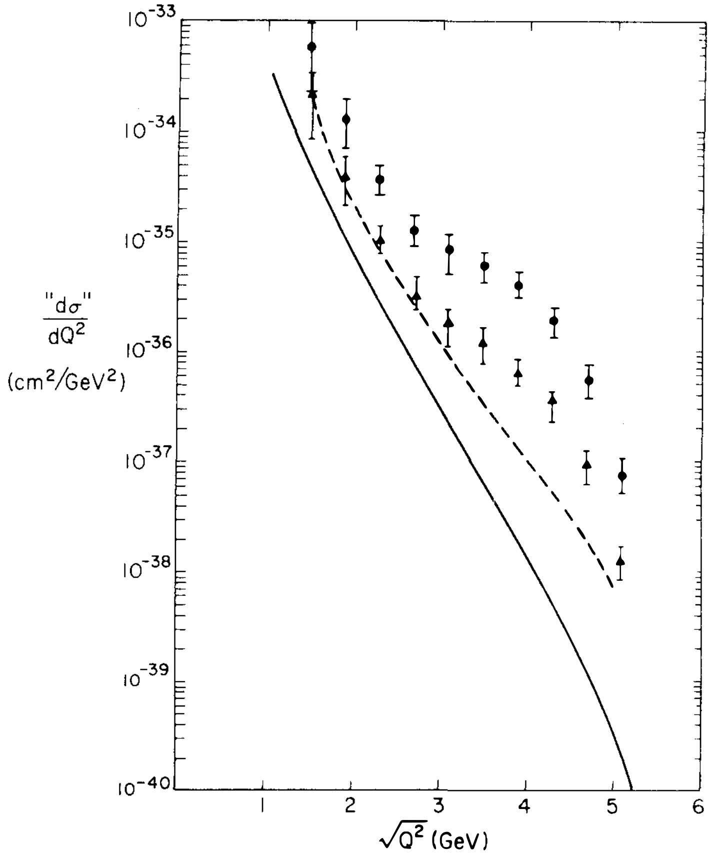

Fig. 2. The cross section (folded with experimental cuts) for $pp \to \mu^+\mu^- + X$ as a function of the $\mu^+\mu^-$ invariant mass, $\sqrt{Q^2}$, at $P_{lab} = 28.5$ GeV/c.

To summarize, I have attempted to present here a unified description of several hadronic phenomena. The basic assumption is that only confinement and other soft interactions involve a large effective quark gluon coupling constant. I have proposed that in large $p_\perp$ inclusive and exclusive scattering low order perturbation theory should give a correct description of the energy and angle dependence of cross sections, with the effect of confinement being to eliminate the contribution of all diagrams which have fast gluons in any physical channel. Theoretical predictions for angular dependences, except in ep $\to$ ep, are not yet available for comparison with the data. Exclusive scattering is in good agreement with the predicted energy dependence. A complete analysis of inclusive scattering $p_\perp$ dependence is not yet available, however absence of a $p_\perp^{-4}$ falloff is evidence in favor of these ideas on the role of confinement. Further evidence of the fundamentally small strength of quark-gluon coupling is the absence of shadowing in large $p_\perp$ hadron production from nuclei and the A-independence of the multiplicity of forward produced pions. The qualitative agreement of theory and experiment for $pp \to \mu^+\mu^- + X$, when account is taken of the expected A dependence, is an encouraging indication of the consistency of all of these ideas. The most crucial missing tests of the validity of using perturbation theory as we propose are: 1) angular distributions for exclusive scattering must be predicted and compared with data; 2) data on the pion form factor at larger t and $\pi p \to \pi p$ at larger s and t is needed to check the energy scaling behavior of eq. (1); 3) $\bar{p}p \to \ell^+\ell^- + X$ and the A dependence of $pA \to \ell^+\ell^- + X$ should be measured. In addition, a complete theoretical analysis of inclusive high $p_\perp$ scattering and further experimental exploration of it are of great importance.

These ideas presented here have evolved over the past two years as a result of collaborations and conversations with a number of people to whom I am indebted. They include S. J. Brodsky, R. P. Feynman, M. Gell-Mann, A. Schwimmer and C. C. Wu.

References

1. This ansatz has been made by a number of people. In particular H. Fritzsch and P. Minkowski, Nucl. Phys. B76, 365 (1974) showed that $g^2/4\pi \lesssim 1/3$ is consistent with scaling at SLAC.
2. E. ., T. Appelquist and H. D. Politzer, Phys. Rev. Lett. 34, 43 (1974).
3. S. J. Brodsky and G. R. Farrar, Phys. Rev. Lett. 31, 1153 (1973) and Phys. Rev. D, to be published.
4. If the wave function is sufficiently convergent there is very weak logarithmic variation due to the q^2 dependence of the coupling g:

$$g^2(q^2)/4\pi = \left[\frac{g^2(M^2)/4\pi}{1 + g^2/16\pi^2\, b\, \ell n\, (q^2/M^2)}\right].$$

M^2 is a mass at which $g^2(M^2)/4\pi$ is already small (we are assuming $M^2 \approx 1\ \mathrm{GeV}^2$). In addition there is a factor $[\ell n\ (q^2/m^2)]^{n-1}$, where n is the number of constituents, which comes from the integrations over the mass of the n-1 far-off shell quarks.
5. P. V. Landshoff, Cambridge preprint DAMTP 73/36.
6. These are not the only diagrams giving s^{-10}, some gluon exchange diagrams give the same behavior. See Ref. 3.
7. G. R. Farrar and C.-C. Wu, Nucl. Phys. B85, 50 (1975).
8. P. V. Landshoff and J. C. Polkinghorne, Phys. Lett. 44B, 293 (1973).
9. Apparently in the MIT bag model the lowest lying epoxyons have quite large mass. R. Jaffe, private communication.
10. That only quark interchange, and not gluon exchange, contributes to large angle scattering was originally proposed by R. Blankenbecler, S. J. Brodsky and J. F. Gunion, Phys. Lett. 39B, 649 (1972) and Phys. Rev. D8, 187 (1973). They used a phenomenological model for exceptional hadron wave functions, rather than quark gluon perturbation theory as we do here and in Ref. 3.
11. V. Matveev, R. Muradyan and A. Tavkhelidze, Lett. Nuovo Cim. 7, 719 (1973).

12. C.-C. Wu and G. R. Farrar, unpublished.

13. This is presently under investigation in collaboration with R. D. Field.

14. S. Berman, J. D. Bjorken and J. Kogut, Phys. Rev. D4, 2381 (1971).

15. For example, F. W. Busser et al., Phys. Lett. 46B, 471 (1973) and J. W. Cronin et al., Phys. Rev. Lett. 31, 1426 (1973).

16. G. R. Farrar, Phys. Lett. B56, to be published.

17. J. W. Cronin et al., Proc. of the XVII International Conf. on High Energy Physics, London, 1974.

18. B. Busza et al., Phys. Rev. Lett. 34, 836 (1975); J. R. Elliott et al., Phys. Rev. Lett. 34, 607 (1975); P. L. Jain et al., Phys. Rev. Lett. 33, 660 (1974).

19. See, e.g., K. Gottfried, Proc. of the 2nd Int. Conf. on Elementary Particles, Aix-en-Provence, 1973. It is possible in the framework of conventional hadronic models to explain this: O. V. Kancheli, JETP Lett. (Sov. Phys.) 18, (1973) and A. Schwimmer, Nucl. Phys. B, to be published.

20. S. D. Drell and T. M. Yan, Phys. Rev. Lett. 25, 316 (1970).

21. G. R. Farrar, Nucl. Phys. B77, 429 (1974).

22. J. H. Christenson et al., Phys. Rev. Lett. 25, 1523 (1970) and Phys. Rev. D8, 2016 (1973).

23. L. M. Lederman, private communication.

CONCLUSIONS FOR THE X^{th} MORIOND ON THE PHENOMENOLOGY OF HADRONIC STRUCTURE

A. Yokosawa
Argonne National Laboratory
High Energy Physics Division
Argonne, Illinois 60439
(U. S. A.)

Introduction

The easy part of the conclusion of this Conference would be to make general remarks; the Conference was well organized and a very successful one. Discussion leaders kept the program well on time and allowed fairly generous time for discussion after each talk. Many impressive experimental data were presented. It seems that experimentalists are moving fast and theorists are having a hard time catching up with them. Remarkably, most of the Conference participants managed daily full-time physics and full-time skiing.

The difficult part of the conclusion would be to answer the question "Do we learn something definite from these massive experimental data?", to compare one theoretical talk with another related talk, and to settle the issue.

What I am going to present here is a summary of talks given; it is obviously impossible to cover all of the talks (about 50), but I will review some of them.

Diffractive-Scattering Data from ISR

We review the experimental data presented by P. Strolin, C. Broll, and G. Goggi covering the following reactions:

$$pp \to (p\pi^+\pi^-)\, X \qquad \text{SDE + DDE}$$

$$pp \to (p\pi^+\pi^-)\, p \qquad \text{SDE}$$

$$pp \to (p\pi^+\pi^-)(p\pi^+\pi^-) \qquad \text{DDE}$$

$$pp \to p(n\pi^+)$$

Important results include an evidence for double-diffractive dissociation and a test of Pomeron factorization; (the quantitative prediction is

$$\frac{d\sigma}{dt}(p_1x_2) / \frac{d\sigma}{dt}(p_1p_2) = \frac{d\sigma}{dt}(x_1x_2) / \frac{d\sigma}{dt}(x_1p_2).$$

From the previous reaction,

$$D = \frac{DDE}{1/2\ SDE + DDE} = 12 \pm 2.5\% .$$

From FNAL and ISR data, we also have

$$D = \frac{1/2\ SDE}{EL + 1/2\,SDE} = 13.5\% ,$$

which is in good agreement with the above value; this is consistent with the fact that the Pomeron is factorizable.

A typical mass plot of $M(p\pi^+\pi^-)$ is shown in Fig. 1, and we observe two distinct peaks. The Breit-Wigner fits to the data give $M_1 = 1500 \pm 8$ MeV with $\Gamma_1 = 150 \pm 50$ and $M_2 = 1678 \pm 4$MeV with $\Gamma_2 = 148 \pm 16$; they are consistent with $N^*(1520)$ and $N^*(1688)$, respectively. The differential

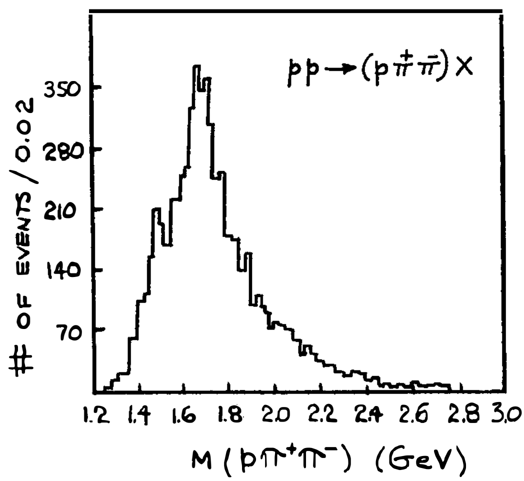

Figure 1

cross sections for different mass regions are shown in Fig. 2; notice

Figure 2

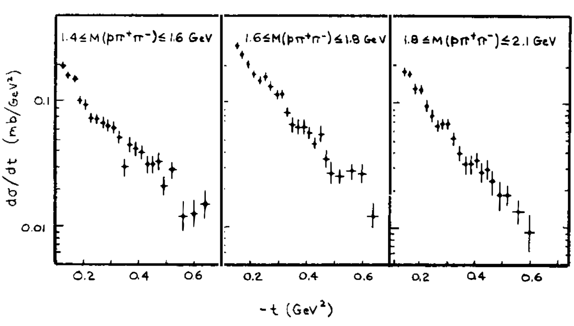

a break near $|t| = 0.2$ for $1.4 < M(p\pi^+\pi^-) < 1.6$ GeV. Cross sections for the $pp \to (p\pi^+\pi^-)\,p$ reaction are shown in Fig. 3, and the slope is $p_{lab}^{-0.64}$

Figure 3

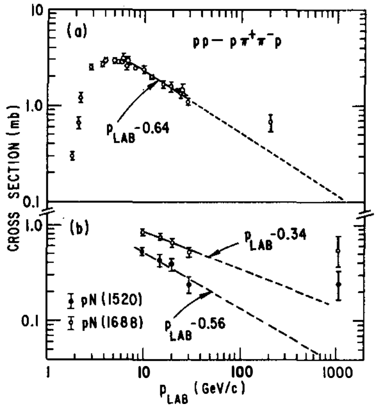

The slopes for pN(1520) and pN(1688) are less steep and -0.56 and -0.34, respectively.

In the $(n\pi^+)$ system, resonance excitation is clearly observed in the backward Jackson hemisphere, but nothing in the forward hemisphere, as shown in Fig. 4. The differential cross section for this system has a clear break near $|t| = 0.3$ (see Fig. 5). Both the $p(n\pi^+)$ and $p(p\pi^+\pi^-)$ processes are dominantly peripheral and have similar slopes, slightly smaller than the elastic slope.

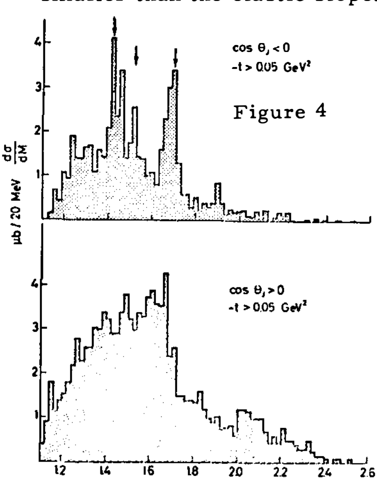

Figure 4

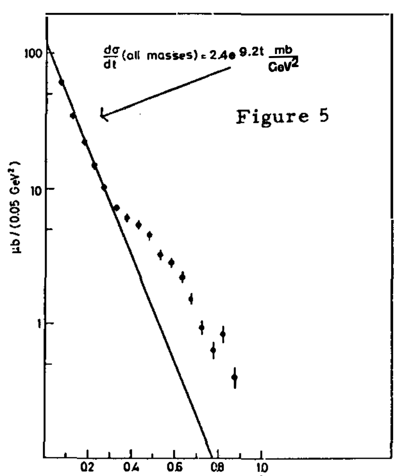

Figure 5

The cross section for double-diffractive dissociation (predicted) is shown in Fig. 6, together with other cross sections. The mass spectra is shown in Fig. 7, and we observe structures at 1.4 and 1.7 GeV. The

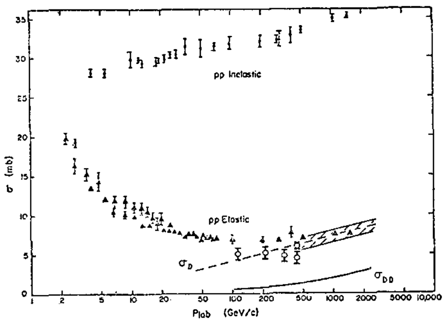

Figure 6

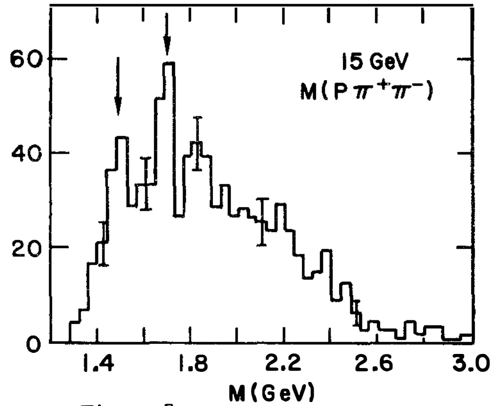

Figure 7

differential cross section is shown in Fig. 8. The slopes for the dN/dt (all) and dN/dt(1470 + any) are 3.6 and 5.8 respectively.

Exponential slopes of the above reactions are compared in Fig. 9.

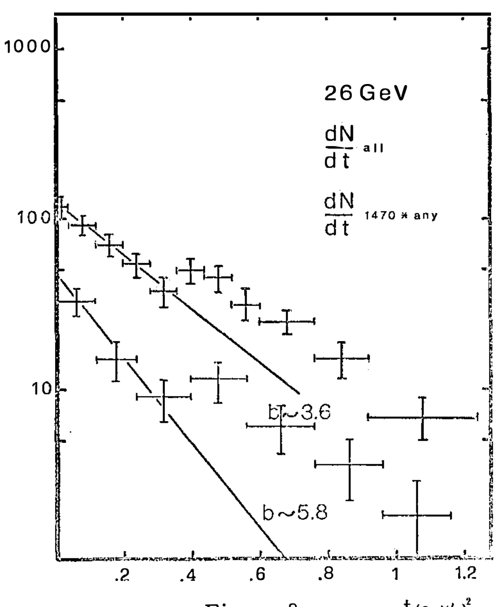

Figure 8

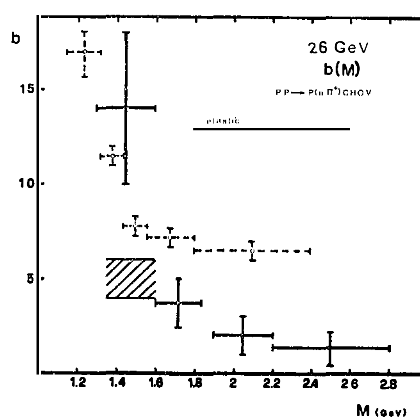

Figure 9

Elastic-Scattering Data at ISR Energies

It was nice to see final results on large-angle pp elastic scattering at ISR energies, p_{ISR} = 11, 15, 26, and 31 GeV (by E. Nagg). The dip position and the second-maximum cross section with respect to energy were finalized. Typical data at p_{ISR} = 23 GeV are shown in Fig. 10.

Figure 10

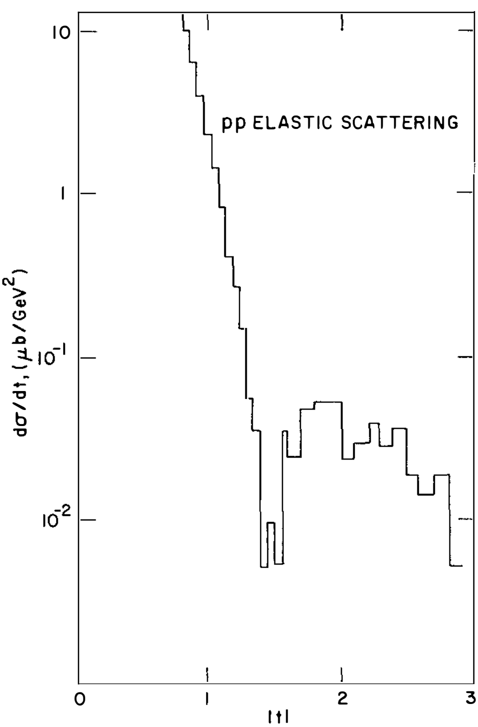

The dip position moves to smaller $|t|$, and the second-maximum cross section increases as p_{ISR} increases, as shown below.

Energy	$\sqrt{s}$ = 23 GeV	$\sqrt{s}$ = 62 GeV
Dip Position	1.45 ± 0.02	1.31 ± 0.05
Second Maximum ($\mu b/GeV^2$)	0.05 ± 0.008	0.066± 0.013

This new fact is in agreement with geometrical scaling, but there remains a question if the scaling works at the forward region, where the statistical rrors are much smaller.

Results of cross-section measurements in elastic scattering at 50, 100, and 140 GeV/c in the region of $0.02<|t|<0.8\ (\mathrm{GeV/c})^2$ were presented (by D. Cutts). Experiments were carried out using a FNAL Single-Arm Facility. Differential cross sections for $\pi^{\pm}p$, $K^{\pm}p$, pp, and $\bar{p}p$ reactions were fitted to $d\sigma/dt = A(e^{Bt+Ct^2})$ and the energy dependence of these coefficients was discussed. Total cross sections together with σ_{inel} and σ_{el} for the above reactions are shown in Fig. 11 and 12. One of their results I would like to quote here is: K^+p elastic slope increases by $\sim 13\%$, $\sigma_{tot}^{\pm K^+p}$ increases by 8%, $\sigma_{inel}^{\pm K^+p}$ increases by $\sim 9\%$, but $\sigma_{el}^{K^+p} \approx$ const.

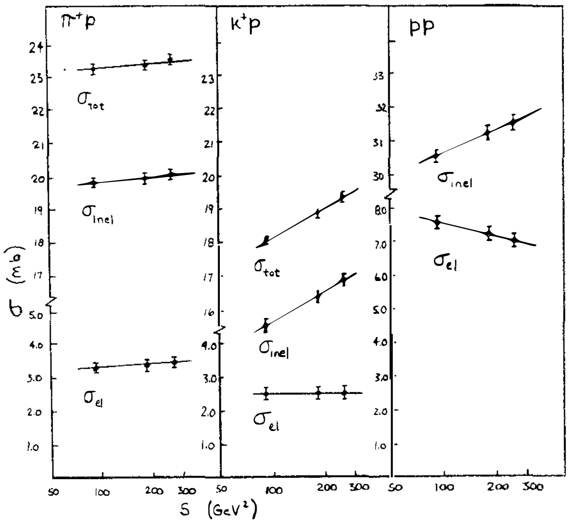

Figure 11

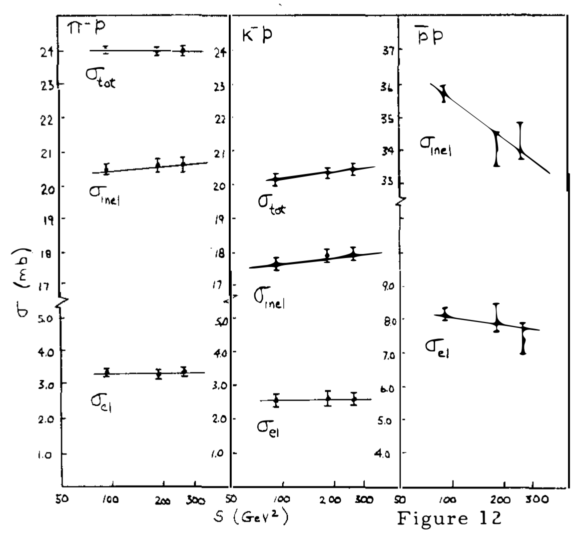

Figure 12

S. Olsen discussed diffractive dissociation of high-energy protons in p-d interactions with a deuterium gas jet; pd → dX and pd → pd at 50 to 400 GeV/c. Slopes of differential cross sections are steeper for the low-mass data. The slope behavior is similar for protons and neutrons. He observed no sign of turnover at small $|t|$ in the differential cross section of the pd $\rightarrow$ dX reaction.

Results of pn $\rightarrow$ pX data at FNAL energy were presented by(F. Sannes). The motivation of the measurement was to sort out Triple-Regge couplings. When these are compared with ISR pp $\rightarrow$ nX data, there is a factor-of-10 difference and we hope that such difference can be clarified soon. It was concluded that the Triple-Regge model works if one can include enough terms.

Correlation Experiments at ISR

P. Darriulat discussed a study of two-particle angular correlations in pp collisions, pp $\rightarrow \pi^{0}$ + ---, detected by the streamer chamber and the shower detector. The angular distribution of charged particles triggered with π^{0} is shown in Fig. 13. The bulk of excess particles is observed in the opposite hemisphere if $\Delta\Phi > \sim 140^{\circ}$ but in the same hemisphere if $\Delta\phi < \sim 30^{\circ}$.

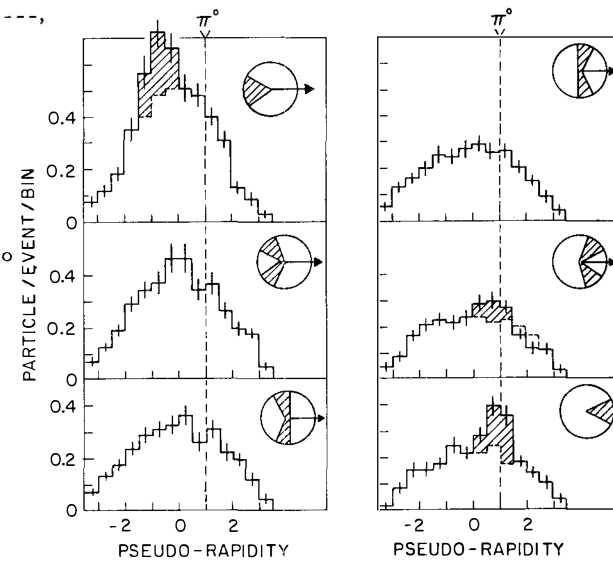

Figure 13

R. Stroynowski reported measurement of large-transverse-momentum positive particles at angular range of $9^{\circ} < \theta^{*} < 21^{\circ}$ at $\sqrt{S}$ = 52.5 GeV using the Split-Field Magnet Facility. The proportional wire chambers used in this experiment cover large solid angles, allowing fully inclusive triggers and good resolution, $\Delta p_T/p_T \approx 1\%$ at 3 GeV/c. Invariant cross-section distributions as a function of transverse momentum at (a) fixed values of $x = 2p^{*}_{L} / \sqrt{S}$ and (b) fixed c.m. angle θ^{*} are shown in Fig. 14. The slope

B, given in $E d^3\sigma/dp^3 = A\,C^{-Bp_T}$, varies from 3.65 to 4.96 in the p_T range of 1.3 to 4.9 for the above-mentioned angular range. At fixed angles, the invariant cross section can be approximated by $E d^3\sigma/dp^3 = A \exp(-Bp_T)$. The slope of the distributions decreases with increasing θ^* from $B = 4.9 \pm 0.1$ for $\theta^* = 10.2^\circ$ to $B = 3.4 \pm 0.1$ for $\theta^* = 20.8^\circ$.

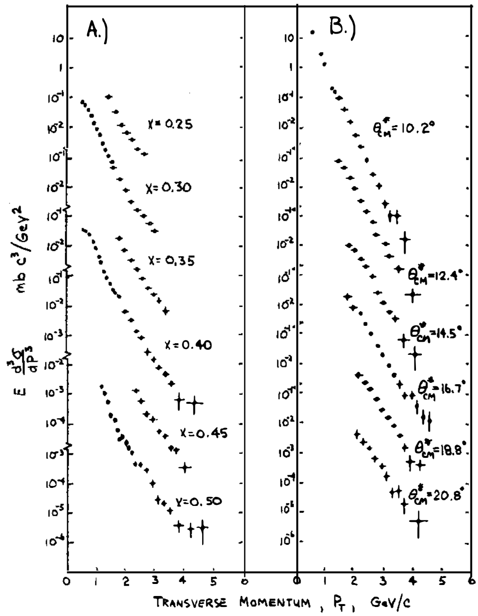

Figure 14

Correlations between charged particles and one momentum-analyzed forward particle at the ISR were discussed. A neutron detector was located at forward 0°. The correlation function is given in Fig. 15. We observe

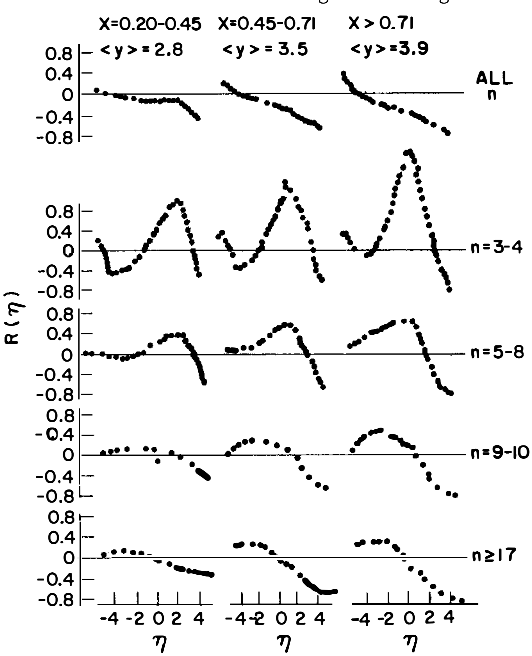

Figure 15

that the cluster effect disappears completely at higher n (R. Castaldi)

Experimental Data From Brookhaven

Multiplicity at large-transverse momentum was discussed by P. Schubelin. Many tracks detected by the cylindrical chambers are demonstrated in Fig. 16.

Total charged multiplicity is plotted against p_T for $pp \to \pi^+ + MM$ (two nucleons) and $pp \to p + MM$ (one nucleon) reactions as shown in Fig. 17. We observe the same shape but different level for these two reactions. Note that a rise takes place at $p_T \approx 0.6$.

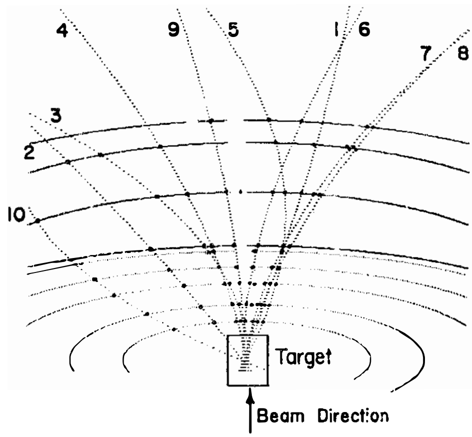

Figure 16

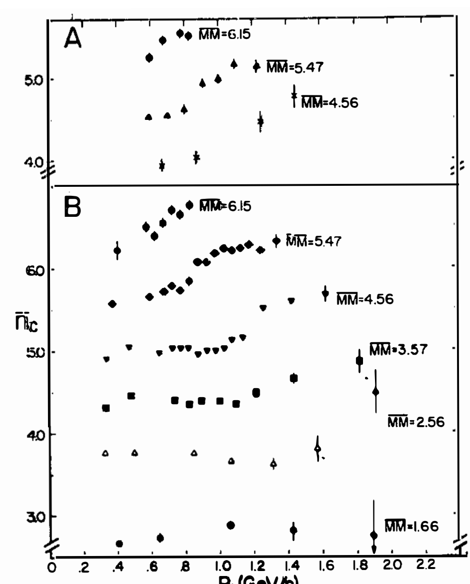

Figure 17

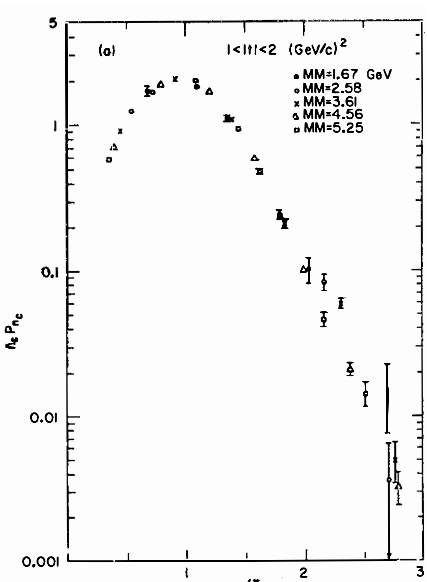

Figure 18

Fig. 18 shows $\bar{n}_c p_{nc}$ with respect to $n_c/\bar{n}_c$ for different values of MM in the region of $1<|t|<2\,(\mathrm{GeV/c})^2$, and the results may be compared with the prediction of KNO scaling. Comparing this data with one for $3<|t|<5\,(\mathrm{GeV/c})^2$, we see a shrinkage in the curve, narrowed by 10% in the large $|t|$ data. The dispersion of p_Y distribution for π^-'s is shown in Fig. 19.

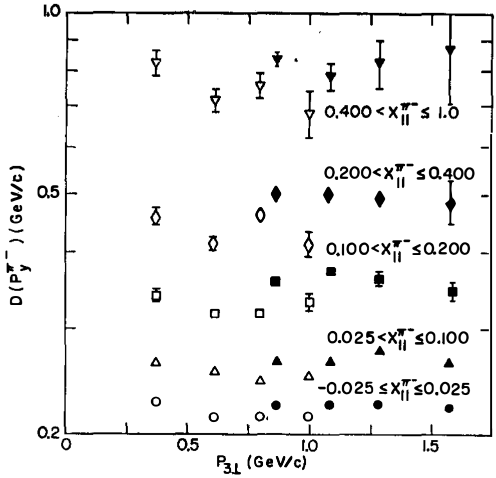

Figure 19

The flat curve can be interpreted as evidence against the fireball idea.

Theoretical Talks and Phenomenology at High Energies

Because it is difficult to fit ISR data to the old multiperipheral model, J. Ball presented a "consistent" MP model in which 700 data points were fitted. He used nine parameters and obtained $\chi^2 = 1000$. From the interpretation of the results of fit, he concluded that much more theoretical improvement was needed.

LeBellac discussed transverse-momentum correlations and also presented an improved version of the multiperipheral model. Krzywicki discussed local compensation of transverse momenta. It was not clear to me how well the model explains the data. Savit's talk on high-energy scattering as a critical phenomenon is a stimulating one, and it is interesting to compare his talk with Amati's talk covering the energy region in which the critical phenomenon takes place.

There were several theoretical talks on geometrical scaling. We are still left with the question of whether the model explains pp scattering.

Capella presented Regge-calculus phenomenology (Triple-Pomeron formula with signs given by Gribov) of elastic forward scattering. He made a five-parameter fit to total cross sections of pp, Kp, and πp. A typical fit is shown in Fig. 20. From $\Delta\sigma_T(\pi p)$, he obtained $\alpha_\rho = 0.57$ and $\alpha_{\omega,\rho} = 0.4$ for $\Delta\sigma_T(pp)$ and $\Delta\sigma_T(Kp)$ data, respectively. Based upon this work, he pointed out a possibility of a 100% exchange-degeneracy breaking.

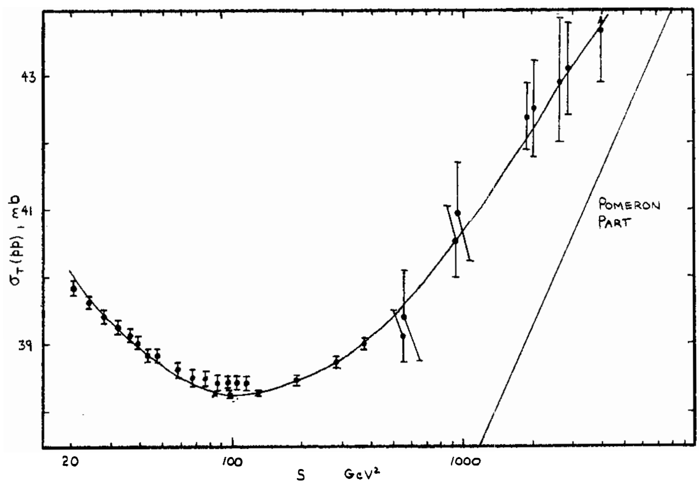

Figure 20

B. Schrempp described her work on "Is Large-Angle Exclusive Scattering Controlled by the Hadron Radius?" The analysis of her guideline is a dual peripheral model. The comparison of the model's prediction with experimental data is well demonstrated in the reactions $\pi^- p \to \pi^0 n$ and $\pi^+ p \to \eta \Delta^{++}(1236)$. Notice that large-angle pp data plotted against P_T oscillate regularly around a straight line, as shown in Fig. 21. The same 90° data are replotted by using the $d\sigma/dt/$(slope) as shown in Fig. 22. An eyeball fit gives $1 + \cos(RP_T + \phi)$ with $2\pi/R \approx 1.7$ GeV/c; then $R \approx 0.73$ fermi.

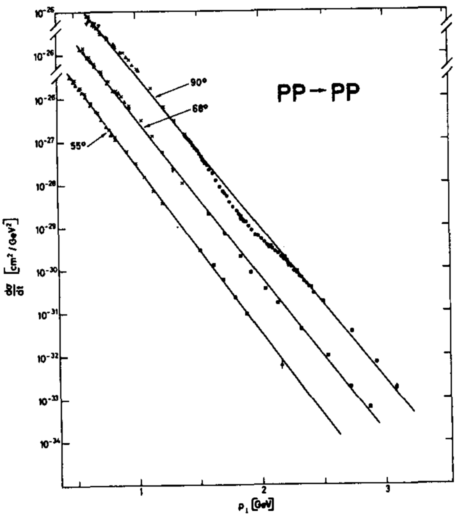

I would like to quote the summary given by one of our discussion leaders, A. Bialas

"None of those models works perfectly, too many corrections are made, and too many parameters are used, without much thought in fitting to the data. Thus, the models are suspicious."

Figure 21

Figure 22

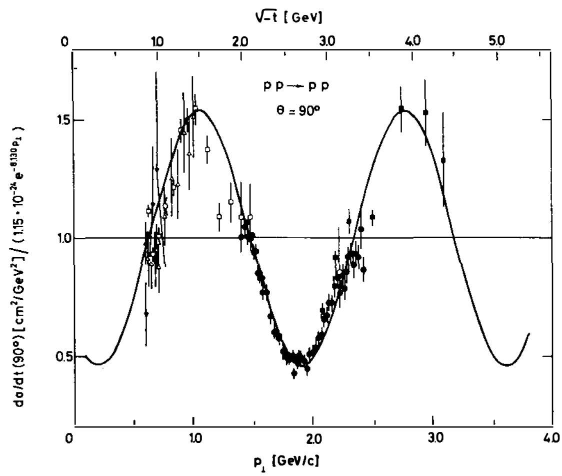

Experimental Results from CERN PS

A. Lundby presented results on large-angle scattering. Figure 23 shows π^-p elastic scattering at 6.2 GeV/c. Together with the earlier 5.0-GeV/c data, he discussed the validity of Ericson fluctuations. His $\bar{p}p$

elastic-scattering data at 6.2 GeV/c show much less structure than the one in πp, and the cross section ($\sim$10 nb) near $\theta_{cm} \simeq 90^{o}$ is much higher than had been theoretically predicted. His group is going to accumulate more statistics in the backward region of the same reaction in order to confirm the existence of a sharp slope.

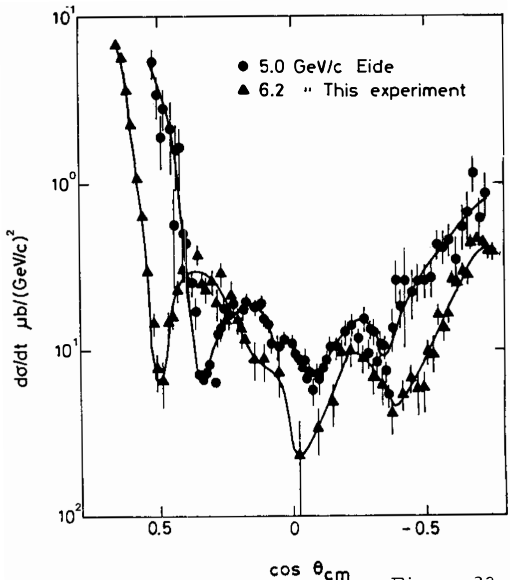

Figure 23

He also presented the results of $K^- p \to \pi^- \Sigma^+$ and $\pi^- p \to K^+ \Sigma^+$ at $|t| < 0.3$, and the difference in the slope is less than 10%.

L. Mandelli discussed meson spectroscopy at Omega covering many reactions in πp and Kp system. Indications of a few new resonances (1085 MeV in $KK^- n$, etc.) were pointed out.

Hyper-charge exchange reactions in $K^- p$ at 4.2 GeV/c were presented (by R. Hemingway). The results of high-accuracy experiments clearly revealed the shapes of the cross sections. Some of the reactions are shown in Fig. 24. The results are summarized as follows:

Reaction	Differential Cross Section	Polarization
$K^- p \to \Lambda \pi^{o}$	Break at $t' \sim -0.3$ Large backward peak	+0.7
$K^- p \to \Lambda \eta$	Deep dip at $t' \sim -0.3$ small backward peak	zero
$K^- p \to \Lambda \eta'$	No structure	+0.4
$K^- p \to \Lambda \omega$	Turnover at $\|t'\| \sim 0$ large backward peak	+0.5
$K^- p \to \Lambda \phi$	No structure	-0.6

More complicated processes in $K^- p$ reactions with final states of

$\pi^- Y_{1385}$, $\omega^o \Lambda_{1520}$, etc, were discussed by W. Van der Walle.

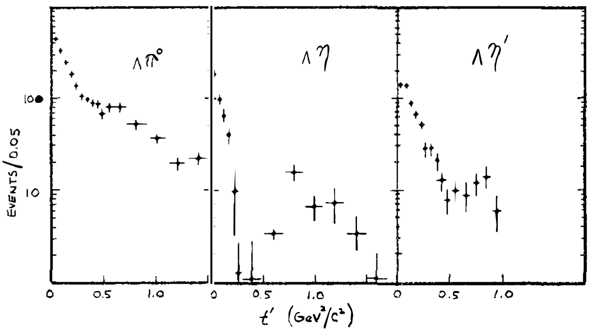

Figure 24

ψ -Particle Production

We heard an interesting result of a ψ photoproduction experiment at FNAL by J. Peoples. The experimental setup was originally made to look for heavy leptons, but was quite adequate for the following reactions:

$$\gamma + Be \rightarrow \mu^+ \mu^- X$$

$$n + Be \rightarrow \mu^+ \mu^- X.$$

The aim was to find out whether ψ is some kind of hadron. His impressive results with 60 events of ψ particles are shown in Fig. 25. The cross section is given by

$$B_{\mu\mu} \cdot \sigma_{\gamma\psi} = 16 \cdot 10^{-33} cm^2.$$

This cross section is typical of hadrons in photoproduction. We may rule out the new particle as being a neutral intermediate boson. The angular

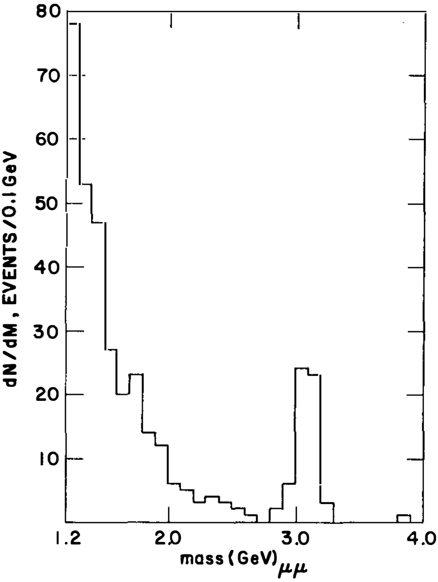

Figure 25

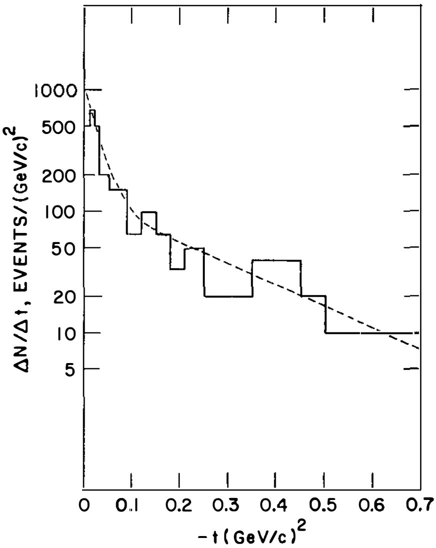

Figure 26

distributions is shown in Fig. 26. If the production is coherent, we expect $d\sigma/dt = c\, e^{+bt}$, and the data yield b = 40 at small $|t|$ region.

Leptons produced at large p_T from ISR were discussed by M. Banner. Single electron production is shown in Fig. 27. He observed nine events of e^+e^- with mass $\sim$3000 MeV, and $\sigma B = 5 \cdot 10^{-23} \pm 2$, which is 50 to 100 times larger than the cross section produced

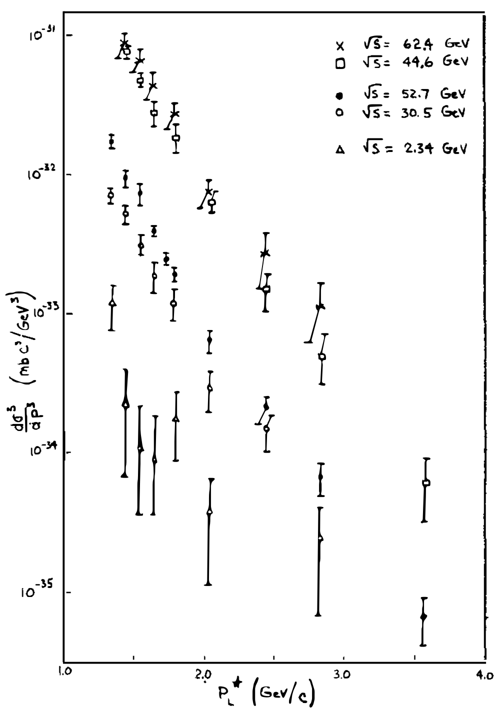

Figure 27

by a similar experiment at Brookhaven National Laboratory (S. Ting, et al).

np Charge-Exchange Reaction at FNAL

Preliminary results of np charge-exchange scattering at Fermilab were discussed by M. Abolins. The existing data of this reaction have been interpreted in terms of the $I = 1$ $|t|$-channel exchange by π, ρ, and A_2 poles. The aim of the experiment at higher energies is to find out the energy dependence of forward-region cross sections and to determine whether the remarkable forward peak is persistent at the Fermilab energy region. Preliminary results indicate that the reaction at high energies seems to be dominated by ρ and A_2 exchanges.

Theoretical Talks and Phenomenology at Low Energies

G. Kane thoroughly discussed the evidence against the existence of A_1. Yet, it seems difficult to draw a definite conclusion at this time. There is also the question of what the theoretical consequences would be. A. Dar made an enthusiastic talk on high-energy collisions between nuclei, pointing out that these studies are linked to many other fields. He even stressed the acceleration of heavy ions at ISR and Fermilab energies. It is true that the interest in high-energy heavy ions has recently been growing rapidly.

R. Worden presented his new "almost complete" amplitude analyses for inelastic scattering, such as $K^-p \to \omega\Lambda$, $\pi^+p \to K^+Y^*$, and $\pi^+p \to \rho^on$. Does he have a better chance of succeeding than those doing amplitude analyses for elastic processes? Derivative relations for the helicity amplitudes (given by F. Schrempp) are interesting and should be very useful in the future amplitude analyses.

A. P. Contogouris presented a general way of doing amplitude analyses from a set of incomplete data, using dispersion relations to relate real and imaginary parts, thus reducing by a factor of two the number of unknown quantities. The method was applied to several two-body nondiffractive reactions and led to some understanding of the t structure of the amplitudes.

I discussed measurements of p-p scattering amplitudes being made by using polarized beams and polarized targets. Note that the measurements are unique to the Argonne ZGS.

Finally, I would like to thank Tran for this very successful and enjoyable conference.

MORIOND PROCEEDINGS

N° 1	First Rencontre de Moriond : 2 vol.	(1966)
N° 2	Second Rencontre de Moriond : 2 vol.	(1967)
N° 3	Third Rencontre de Moriond : 2 vol.	(1968)
N° 4	Fourth Rencontre de Moriond : 1 vol.	(1969)
N° 5	Fifth Rencontre de Moriond : 1 vol.	(1970)
N° 6	Electromagnetic and Weak Interactions	(1971)
N° 7	High-Energy Phenomenology	(1971)
N° 8	Two Body Collisions	(1972)
N° 9	Multiparticle phenomena and inclusive reactions	(1972)
N° 10	Electromagnetic and Weak Interactions	(1973)
N° 11	The Pomeron	(1973)
N° 12	High energy hadronic physics	(1974)
N° 13	High energy leptonic physics	(1974)
N° 14	Phenomenology of Hadronic Structure	(1975)
N° 15	Charm, Color and the J/ψ	(1975)

All orders should be sent to.

Rencontre de Moriond
Laboratoire de Physique Théorique et Particules Élémentaires
Bâtiment 211 - Université de Paris-Sud
91405 ORSAY (France)
Tél. 928.59.87

12 HIGH ENERGY HADRONIC INTERACTIONS

CONTENTS

13 HIGH ENERGY LEPTONIC INTERACTIONS

Proceedings of the second session of the Ninth Rencontre de Moriond
3-15 March 1974

CONTENTS

14 PHENOMENOLOGY OF HADRONIC STRUCTURE

CONTENTS

First Session

I - DIFFRACTION AND ELASTIC SCATTERING

G. Goggi, Single and double diffraction dissociation at FNAL and ISR energies ; **P. Strolin,** Diffractive production of the $p\pi^+\pi^-$ system at the ISR ; **S.L. Olsen,** Coherent diffraction dissociation of protons on deuterium at high energies ; **G. Goggi,** Preliminary results on double diffraction dissociation ; **E. Nagy,** Experimental results on large angle elastic pp scattering at the CERN ISR ; **A. Capella,** Elastic scattering in the Reggeon calculus at ISR energies ; **C.E. De Tar,** How can we trust the Reggeon calculus ? ; **R. Savit,** High energy scattering as a critical phenomena ; **J.S. Ball,** Seft consistent diffraction in the multiperipheral model ; **U. Maor,** Comments on the systematics of Pomeron exchange reactions ; **P. Kroll,** Geometrical scaling in proton scattering ; **A. Martin,** Does the Pomeron obey geometrical scaling ? ; **N.G. Antoniou,** Effects of the inclusive dipole Pomeron to exclusive processes.

II - TWO BODY SCATTERING

A. Yokosawa, pp scattering amplitude measurements with polarized beam and polarized targets at 2 to 6 GeV/c ; **A. Contogouris,** The structure of amplitudes of two-body reactions ; **F. Schrempp,** Towards a solution for the helicity dependence of scattering amplitudes ; **B. Schrempp,** Geometrical versus constituent interpretation of large angle exclusive scattering.

III - MULTIPARTICLE PRODUCTION

F. Sannes, Inclusive cross sections for $p+n \rightarrow p+X$ between 50 and 400 GeV ; **G. Jarlskog,** Results on inclusive charged particle production in the central region at the CERN ISR ; **R. Castaldi,** Measurements on two-particle correlations at the CERN ISR ; **A. Menzione,** Semi-inclusive correlations at the CERN ISR and cluster interpretation of results ; **A. Dar,** Multiparticle production in particle-nucleus collisions at high energies ; **E.H. de Groot,** Independent cluster production and the KNO scaling function ; **P. Schubelin,** Final state characteristics of central pp collisions at 28.5 GeV/c ; **L. Mandelli,** Meson spectroscopy with the Omega spectrometer ; **A. Krzywicki,** Local compensation of quantum number and shadow scattering ; **C. Michael,** Impact parameter structure of multi-body processes; **N. Sakai,** Helicity structure of the triple Regge formula.

IV - MISCELLANEOUS

E.J. Squires, Hadronic interactions in bag models ; **G.L. Kane,** Does it matter that the A1 does not exist ? ; **H. Moreno,** A stationary phase approach to high energy hadronic scattering ; **M.M. Islam,** Impact parameter representation without high energy, small-angle limitation ; **G.R. Farrar,** How to learn about hadron dynamics from an underlying quark-gluon field theory.

V. - CONCLUSIONS

A. Yokosawa, Conclusions and outlook.

Achevé d'imprimer le 14 juillet 1975
sur les presses de l'Imprimerie Laboureur et Cie - Paris
113, rue Oberkampf, 75011 Paris
Dépôt légal n° 8183